Influence of electrostatics upon electrospray with the intention of application to colloid thrusters

Ryan, Charles N.

Influence of electrostatics upon electrospray with the intention of application to Colloid Thrusters

Charles N. Ryan

Submitted to the Department of Engineering Queen Mary, University of London in partial fulfillment of the requirements for the degree of Doctor of Philosophy in Engineering

Abstract

A thorough experimental and theoretical characterization of the effect of electrostatics on the electrospray process, focusing particularly on the flow rate sensitivity to the applied potential difference (voltage), has been completed.

The flow rate and current increase linearly with the applied voltage within cone-jet mode. The effect of geometry on the flow rate to voltage relationship is sensitive to two parameters – the hydraulic resistance and the variation of the electric pressure sensitivity to external geometry. A theoretical and FEM model based on the calculation of the electric field provides an explanation of the geometry variation. This allows for an estimation of the change of flow rate with voltage, under any geometrical circumstance.

For the first time the effect of voltage on flow rate across enhanced dripping, pulsed and multi-jet electrospray regimes are outlined. With the exception of enhanced dripping, a linear increase is noticed within most regimes, and is geometrically sensitive. Also at the onset of cone-jet mode a drop in flow rate occurred.

The variation of flow rate with voltage can be applied to colloid thrusters to vary the performance. Using the theory outlined in this thesis, an estimate of the flow rate change for a colloid thruster is described, along with its associated performance variation.

The effect of voltage on current in cone-jet mode electrospray is detailed, with a similar geometric dependence as the flow rate to voltage relationship established. It is also sensitive to various other parameters, including nominal flow rate.
The stability island of cone-jet mode electrospray is explored, and its relationship to the variation of electric field with voltage is outlined. The effect of emitter and electrode geometry on cone-jet onset voltage and cone-jet voltage range is outlined.

Acknowledgements

I must acknowledge my office friends, who have kept my spirits up over the years – Andrew Sheldon, Ke Wang, Mike Micci, Siobash Dhuree, Zhikai Tang, you have been a great help, and good company. Also many thanks to the various technicians, especially Roger Nelson, who have managed to make my incomprehensible designs. Thanks also to the SEMS office staff – Jonathon Hills, Catherine Jones, amongst many. Cheers!

I was lucky enough to work for three months at Emdot Ltd, as spin off of the engineering department at QM. I greatly enjoyed my time there, and would like to thank Mark Shepherd, Mark Paine, Richard Marsden, and Gareth Neal for putting up with me.

Dr Kate Smith –thanks for introducing me to the world of electrospray, being a friend and colleague, and for putting up with my never ending questions! I am deeply grateful.

I owe a great debt of gratitude to my supervisor Professor John Stark. Without your careful and deliberated input I would not have made it. This thesis is infused with your considerable enthusiasm and knowledge.

Finally I would like to thank my family - my dad, mum, sisters - and friends; you have been a great help through the marathon of a sprint that is a PhD.

Contents

List of Figures

Nomenclature

Units are those most commonly used in this thesis.

a	Twice the distance between the hyperbolic focus and the flat surface, m
A_1	Corrective term of order unity
$B_{i,p}$	Bernstein basis function
c_{pulsed}	y-intercept of $Q(V)$ relationship in pulsed mode, $nL \cdot s^{-1}$
c_Q	y-intercept of $Q(V)$ relationship in cone-jet mode, $nL \cdot s^{-1}$
$d_{droplet}$	Diameter of droplet, m
d_{jet}	Diameter of jet, m
E_{apex}	Electric field at emitter meniscus apex, $V \cdot m^{-1}$
E_L	Laplace electric field, $V \cdot m^{-1}$
E_{Max}	Maximum electric field at emitter tip, $V \cdot m^{-1}$
E_P	Poisson electric field (with space charge), $V \cdot m^{-1}$
E_r	Radial electric field within cone, $V \cdot m^{-1}$
$f(\varepsilon_r)$	Empirical permittivity function
f_i	Modelled values
g_0	Gravitational acceleration on earth, 9.8 $m \cdot s^{-2}$
$G(E)$	Reduction in free energy due to the electric field, eV
h	Planck's constant, 6.626068 $\cdot 10^{-34}$ $m^2 \cdot kg \cdot s^{-1}$
I	Current, nA
I_{on}	Cone-jet mode onset current, $nL \cdot s^{-1}$
I_s	Surface current, A
I_{sp}	Specific impulse, s
j_0	Surface current density, $A \cdot m^{-2}$
k	Boltzmann's constant, 1.380 $\cdot 10^{-23}$ $J \cdot K^{-1}$
K	Electrical conductivity, $S \cdot m^{-1}$
L	Length of pipe, m
$\overline{L}$	Average length of the emitter, m
$\dot{m}$	Mass flow rate, $Kg \cdot s^{-1}$
m/e	Mass to charge ratio of emitted droplets, $Kg \cdot C^{-1}$
m_I	Change of current with voltage in cone-jet mode, $nA \cdot kV^{-1}$
m_{pulsed}	Change of flow rate with voltage in pulsed mode, $nL \cdot s^{-1} \cdot kV^{-1}$
m_{pe}	Change of electric pressure with voltage in cone-jet mode, $Pa \cdot V^{-1}$
m_{MJ}	Change of flow rate with voltage in multi-jet mode, $nL \cdot s^{-1} \cdot kV^{-1}$
m_Q	Change of flow rate with voltage in cone-jet mode, $nL \cdot s^{-1} \cdot kV^{-1}$
$\overline{M}$	Average mass of the emitter, kg
n	$I(Q)$ relationship exponent
P_D	Driving fluid pressure, Pa
P_E	Electric pressure at emitter tip, Pa

$\vec{P}_n$	Vectors representing points, (n = 1, 2, . . . , n)
Q	Flow rate, nL·s^{-1}
$Q_{1/2}$	Legendre polynomial of order 1/2
Q_{jump}	Drop in flow rate from pulsed to cone-jet mode, nL·s^{-1}
$q_{\max}$	Rayleigh charge limit, C
Q_{max}	Maximum periodic flow rate in enhanced dripping mode, nL·s^{-1}
Q_{min}	Minimum theoretical flow rate, nL·s^{-1}
Q_{nom}	Nominal flow rate, nL·s^{-1}
Q_{on}	Cone-jet mode onset flow rate, nL·s^{-1}
r^*	Relaxation length, m
r_a	Meniscus apex radius, m
r_e	Emitter external radius, μm
r_i	Calculated internal radius of emitter, μm
R_1, R_2	principal radii of curvature, m
R_b	Base radius of Taylor cone, m
R_i	Internal radius of flow rate measurement tubing, m
R_T	Total hydraulic resistance of fluidic system, N·s·m^{-5}
s	Running parameter
SS_{err}	Sum of squared errors
SS_{tot}	Total sum of squares
T	Thrust, N
u	Cone fluid velocity, m·s^{-1}
v_e	Exhaust velocity, m·s^{-1}
V_{AT}	Total acceleration voltage, V
V_{acc}	Total acceleration voltage, V
V_{on}	Cone-jet mode onset voltage, kV
V_{ext}	Cone-jet mode extinction voltage, kV
$V_{hysteresis}$	Difference between V_{on} and V_{ext}, kV
V_{range}	Cone-jet mode voltage range, V
w	Parameter defining the apex radius of curvature
$\overline{y}$	Mean of the observed data
y_i	Observed y - values
z_0	Emitter tip to extractor distance, mm

α	Cone semi angle, degrees
α_T	Taylor's angle, degrees
ΔG	Free energy of solvation, eV
ΔP	Change in pressure along fluid line, Pa
ΔQ	Change of flow rate due to voltage before cone-jet mode, nL·s^{-1}
ΔQ_{hyp}	Hypothetical change of flow rate with voltage in pulsed mode, nL·s^{-1}
ε_r	Relative electrical permittivity
ε_0	Permittivity of free space, 8.854 ·10^{-12} F·m^{-1}
η	Voltage efficiency factor

γ	Interfacial surface tension, $N \cdot m^{-1}$
κ	Surface curvature, m^{-1}
κ	Ratio between the apex electric field and the applied voltage, m^{-1}
Λ_m	Molar conductivity at infinite dilution [$S \cdot m^2 \cdot mol^{-1}$]
μ	Dynamic fluid viscosity, $N \cdot s \cdot m^{-2}$
ξ, η, φ	Coordinates in the prolate spheroidal coordinate system
ρ	Density of liquid, $Kg \cdot m^{-1}$
ρ_s	Surface charge density, $C \cdot m^{-2}$
σ	Standard deviation
τ_{res}	Hydrodynamic residence time, s
τ_{rel}	Electrical relaxation time, s
ϕ_0	Potential difference between the emitter and the plate electrode, V
Φ	Electric potential, V
∇^2	Laplace operator

Chapter 1

1. Introduction

If a sufficiently large electric field is applied at the interface of a conductive liquid and an insulator, the conductive liquid forms a cone like shape, with a jet emanating from the apex of the cone. Due to axisymmetric varicose wave instabilities[1] on its surface, the jet subsequently breaks down into a monodisperse spray that consists of micro to nano-metre sized charged droplets.

This method of creating ultra-fine charged droplets, commonly called cone-jet electrospray, has developed into a widely employed experimental technique, particularly within electrospray mass spectrometry (ESMS)[2,3], whilst the very closely related technique of electrospinning has experienced exponential growth[4].

Another application of the electrospray technique experiencing resurgence is that of electrospray colloid thrusters. These apply the electrospray technique to produce micro levels of thrust. The reasons for this revival are varied, but revolve around the growth of a nano-satellite market with a corresponding micro-propulsion demand, the discovery of room temperature ionic liquids, and the ready availability of electrospray technology as the ESMS method has grown in popularity. Currently the development has moved on to the point that within a few years LISA Pathfinder should be the first of many spacecraft to use colloid thrusters[5], although there is considerable competition from the closely related Field Emission Electric Propulsion (FEEP)[6].

1.1. Thesis objectives

Although the electrospray technique is used extensively the theoretical understanding is only partially complete[7,8]. One subject lacking in theoretical depth is the effect of electrostatic parameters on current and flow rate. The effect of voltage, and more

specifically electric field (that encompasses the effect of geometry), are often put to one side in an attempt to simplify the complex electrospray physics. But recent pioneering work at Queen Mary, University of London has outlined that the voltage that is applied to create a Taylor cone can have a considerable effect on the on the flow rate and current[9,10]. The strength of the relationship would seem to be related to the geometry of the emitter, suggesting that the effect may be electric field based.

The effect of the applied potential difference on the flow rate through the emitter is the principal investigation of this doctoral thesis. This is investigated across the four major modes of electrospray – enhanced dripping, pulsed, cone-jet and multi-jet modes. It is shown that the geometry has considerable effect on the flow rate-voltage relationship (regardless of mode), and the experimental results inspire a simple theoretical and modeling analysis of the change in flow rate with voltage.

1.2. Thesis structure

The following thesis consists of seven chapters, the first being this introduction.

Chapter 2 presents a comprehensive literature review, composed of two main sections. The first concentrates on the current level of knowledge about the electrospray process, particularly focusing on the electrostatics and various other phenomena that are applied in the following chapters. The second section looks into the recent findings of a substantial effect of voltage on the flow rate and current in cone-jet mode electrospray, investigated in detail at Queen Mary, University of London[10]. Discussed are the applications of this effect, including colloid thruster performance modulation and nano-electrospray.

Chapter 3 details the experimental apparatus used for the experiments completed as part of this research effort. The experimental equipment is based around the application of the highly accurate flow rate measurement device used during previous studies[10].

Chapter 4 discusses the change of flow rate with voltage solely within the cone-jet mode of operation. Presented is a detailed analysis of the effect of various geometric parameters on the magnitude of the flow rate to voltage relationship, some of which has been published in a peer reviewed journal[11]. The magnitude variation of the $Q(V)$ effect with geometry is explained, with both a theoretical and simulated explanation provided. The application of this effect to colloid thruster performance modulation is also postulated upon, following on from previous studies[12].

Chapter 5 introduces the notion of the cone-jet mode of operation being a relative stability island compared to the surrounding electrospray modes. It investigates the interrelationships found experimentally of emitter outer diameter and flow rate on the stability of cone-jet mode electrospray.
As various different geometric changes were systematically investigated, a large data set of cone-jet mode onset voltage sensitivity to geometry was collected. These are discussed in chapter 5, and compared to theoretical and simulated results, with the simulation method the same as applied by previous studies[13]. Chapter 5 goes on to investigate the effect of geometry on the cone-jet mode voltage range.
The last section of chapter 5 discusses the change of current with voltage in cone-jet mode electrospray. The $I(V)$ relationship is shown to have a complex dependence on various parameters, including flow rate and geometry.

Chapter 6 discusses the change of flow rate with applied voltage across the other three main electrospray modes - enhanced dripping, pulsed and multi-jet modes. The relationship to geometric parameters is again discussed, and any changes in flow rate from one mode to the next are investigated. The total flow rate increase due to voltage, up to cone-jet mode is illustrated. The implications of the flow rate increase up to cone-jet mode on the performance modulation of colloid thrusters are also discussed.

Finally chapter 7 summarises the findings presented, and provides some recommendations for future studies.

Chapter 2

2. Theoretical aspects of electrospray and the influence of voltage

2.1. Introduction to electrospray

Electrospray is a process that allows the production of micron sized charged droplets and ions from the tip of a macro-sized emitter, by the application of an electric field. Within cone-jet mode electrospray, a moderately conductive liquid emerging from the end of an emitter experiences a severe electrohydrodynamic effect thanks to a large applied potential difference between the emitter and an extractor electrode, forming a cone like protrusion at the emitter tip (see Figure 2.1). At the apex of the cone-like structure the fluid accelerates and a fluid jet considerably smaller than the emitter forms. This small jet breaks up into charged particles with diameters ranging from hundreds of micrometres to nanometres (the size varies with the fluid properties). The charge of the particles depends on the potential difference applied. If the extractor electrode is at a positive potential relative to the emitter, the particles are negatively charged. Alternatively, if the electrode is at a negative potential relative to the emitter, then the particles produced are positively charged.

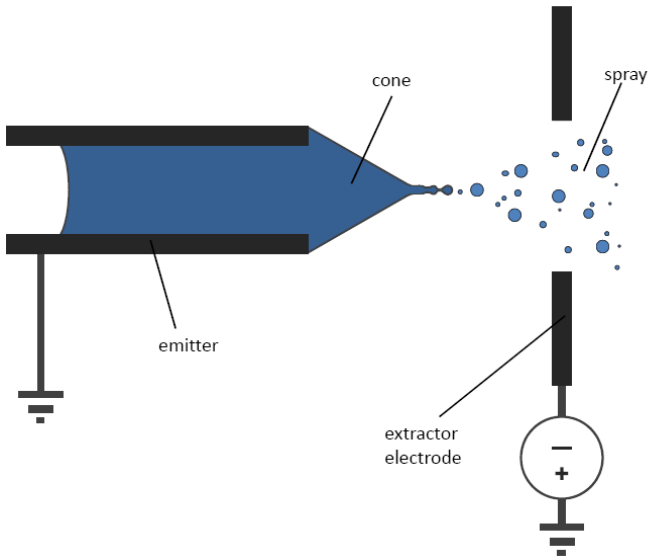

Figure 2.1. The cone-jet mode electrospray phenomena.

The technique provides a simple method to produce tiny drops from a relatively large emitter. It can be applied to various fields of engineering, including spray painting, mass spectrometry (by deflecting the charged droplets in an electric field), the creation of tissue scaffolds (by electrospraying biomolecules), electrospinning (wherein the jet does not break up), and colloid electrospray thrusters (a type of very low thrust spacecraft propulsion).

First investigated experimentally by Zeleny[14], with subsequent investigations by Taylor[15], interest in electrospray has though fluctuated, mostly due to difficulties with getting applications from the lab bench to the market. A resurgence in interest in the last 25 years resulted from the discovery of Electrospray Mass Spectroscopy (ESMS), a technique employing electrospray to ionise and consequently analyse large biomolecules[2,3]. This procedure is still common with over 1500 articles/year produced within ESMS literature.

There have been considerable hurdles hampering applications to other areas. Particularly the low flow rates needed to establish cone-jet mode electrospray, and to produce the fine charged droplets, is coupled with a low production rate, and make actual application

difficult (with the exception of ESMS which does not require a high production rate). It is particularly severe for applications needing droplets at the smallest scale, for example drug inhalation and nanoparticle synthesis[16].
Also exacerbating the issues with the application of the process is that theoretically electrospray is incompletely understood[7]. There is a lack of theoretical provision for under what circumstances the cone-like structure is stable, and what parameters affect the emitted flow rate and current, amongst other issues.

What follows is a brief review which outlines the current electrospray theory and analysis that is relevant to the experimental studies completed.

In the second part of this review (from Section 2.4), the effect of the applied potential difference (voltage) between the emitter and the extractor electrode on the flow rate and the current in cone-jet mode electrospray is reviewed separately, as this forms the main experimental investigation of this thesis.

2.2. Modes of electrospray

As well as the cone-jet mode of electrospray illustrated in Figure 2.1, there are various other modes of electrospray that typically occur. These can be grouped by their geometry, and the charged droplet size produced[17-19]. Here, two groups are identified; the first group emits relatively large fluid fragments, called an enhanced dripping regime. The second group emits microdroplets from a cone like electrohydrodynamic protrusion (as in Figure 2.1). The two groups occur at differing electric field intensities, with generally smaller particles emitted at higher electric fields.

2.2.1. The first group – the enhanced dripping regime

At low electric field intensities (a smaller applied potential difference between the emitter and extractor electrode) and flow rates, liquid leaves the emitter in a dripping fashion[19-21]. This is illustrated in Figure 2.2. As the electric field increases the drops become more frequent and generally smaller[21,22]. The reduction in droplet volume occurs as the effective electromechanical surface tension decreases with rising electric field strength[21,23]. Even with this decrease in size, the primary droplets created remain relatively large, approximately the size of the capillary diameter[19].

The enhanced dripping regime has a maximum flow rate limit, above which a large jet is produced with a radius of the order of the emitter diameter (analogous to liquid from a tap). Below this limit the process is dependent on various conditions, including flow rate, fluid viscosity, and capillary diameter[19]. The creation of secondary droplets is especially dependent upon these conditions. For example, a liquid thread can be created between droplet and capillary, which breaks up into satellite droplets, with the thread length, and consequently the number of satellites dependent on various parameters[21]. Alternatively a thread-like jet can form at the tip of the droplet, again breaking up into finer droplets[19]. In general though these progeny only consist of a small fraction of the fluid fragments created.

A subset of the dripping regime is microdripping, wherein a cone-like shape forms at the emitter tip, and droplets break from at its apex. This is similar to cone-jet mode (described in the next Section), except it occurs irregularly and the charged droplets created are considerably larger. Its occurrence seem very dependent on experimental conditions; for example emitter wettability and conductivity[19].

Another mode that produces large droplets is the ‘spindle’ mode. It is characterized by long thick jet-like structures emanating from the emitter, with these ‘spindles’ breaking off sporadically. Spindle mode occurs at higher voltages than dripping, although it is only evident under some conditions[24]. At yet higher voltages, multiple spindles can occur at once.

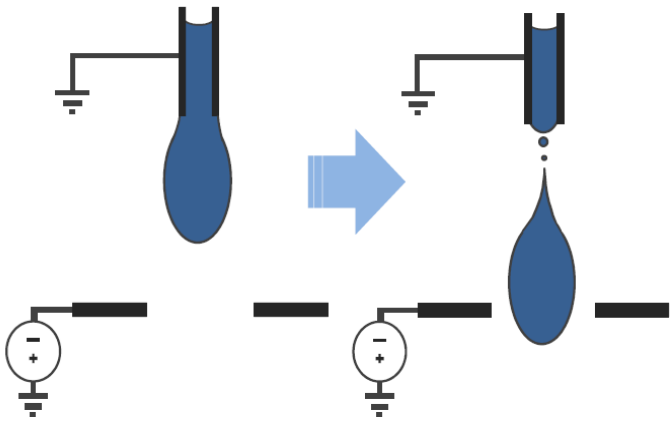

Figure 2.2. The enhanced dripping regime forms a droplet of the size of the emitter.

2.2.2. Second group –electrohydrodynamic jetting

Pulsed cone-jet regime

At higher electric field strengths than the enhanced dripping regime, intermittent cone like apices are formed; this has been defined as a pulsating cone-jet regime[19,25]. The pulsation of the Taylor cone has been attributed to an imbalance between the electrostatic and capillary pressure at the liquid surface[26]. The charge accumulates on the liquid surface, with a resulting tangential stress leading to a deformation of the liquid[27]. At a certain point the Coulombic repulsion is large enough to overcome the capillary forces, and the charge is emitted in the form of a jet at the emitter tip. Once all the charge is emitted the cone cannot be supported and collapses, with the liquid reverting into an approximately spherical shape. These four cyclic phases would seem to occur over similar time frames[27], and are illustrated in Figure 2.3.

Various subsets within the pulsed regime have been described, with the two major groups being axial mode I and II[26,28]. Axial mode I is characterized by large regular peaks in current at a frequency or the order of 10's of Hertz, with a higher frequency oscillation within these peaks[26]. There is a clear interval between these relatively large peaks, with

this time interval decreasing as voltage is increased, until only high frequency pulses are evident. At this point the mode is defined as axial mode II, with a current frequency of the order of 1kHz. The frequency of these pulsations increases with applied voltage, and is very dependent on fluid and emitter parameters[28].

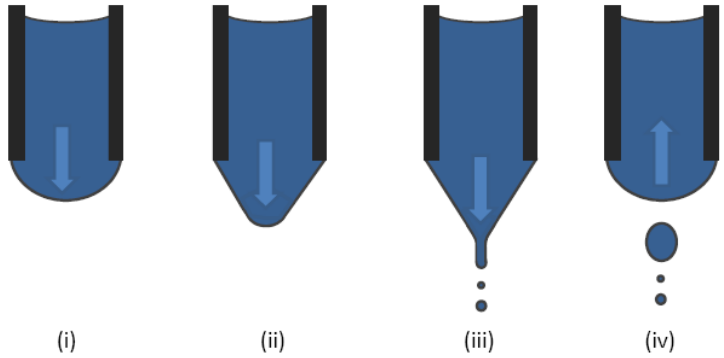

Figure 2.3. The four phases of pulsed cone-jet mode electrospray (extractor electrode not shown). (i) Liquid accumulates at the emitter tip in a spherical shape; (ii) As more charge in the liquid reaches the tip, a cone-like structure begins to form; (iii) Maxwell stresses overcome the surface tension and the liquid is emitted in a jet; (iv) The cone collapses and the liquid retreats.

Stable cone-jet mode

If a moderately charged liquid drips from the emitter when no voltage is applied, then it is likely that a stable cone-jet regime is possible at higher field intensities[20]. This regime occurs at electric field intensities greater than those at which the pulsed cone-jet regime takes place, with the change from pulsating to stable cone -jet occurring at an 'onset voltage', described in Section 2.3.2. A protrusion analogous to a Taylor cone[15] is formed at the tip of the emitter, with a jet at the apex of the cone – see Figure 2.4. This jet breaks up under the influence of varicose (as shown in Figure 2.1) and/or non-axisymmetric kink instabilities[29].

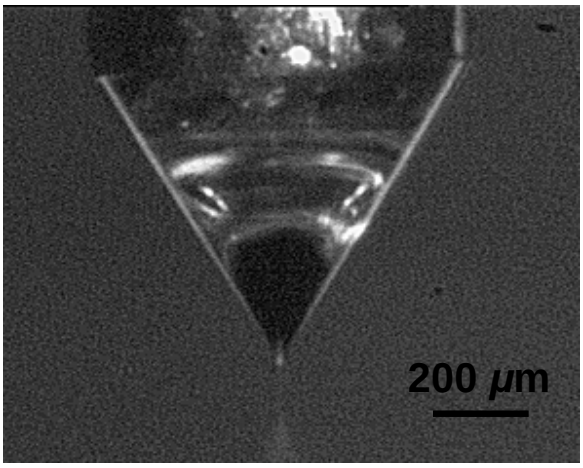

Figure 2.4. Stable cone-jet electrospray. From the top the emitter is visible, followed by the cone, jet, and spray break-up. Shown schematically in Figure 2.1.

The stable cone-jet mode of electrospray is the most studied and utilised regime. It is a simple method to produce a quasi-monodisperse spray of fine charged droplets, with the mono-dispersity induced by the Coulombic repulsion of the initial charged droplets preventing coalescence[16]. It offers control of output parameters by the variation of certain properties, at least to the first order[30]. For example by increasing the fluid conductivity the mean droplet size decreases, producing very fine droplets from a relatively large emitter needle[19].

Theoretically, Taylor provided an analysis where under specific circumstances the electrostatic and capillary pressures are in equilibrium[15]. This results in a cone with a straight generatrix and cone half-angle of 49.3 degrees, as described in Section 2.3.1. In reality the cone-jet appearance can vary greatly, from a convex cone with a small jet to a convex cone with a large diameter jet.

Stable multi-jet mode

When the electric field (applied potential difference) is increased further, the cone bifurcates and two cones form at the emitter tip, with a jet emanating from each. Each

cone-jet points away from the emitter axis[19,31], probably due to self repulsion. This has been described as the multi-jet regime, as shown in Figure 2.5. Further increases in electric field result in more cone-jet protrusions, with normally three, five then possibly six cone-jets at the tip[10], with each a further subset of the multi-jet mode. Each increase in cone number is coupled with a large increase in current. The flow rates and applied voltages for which each multi-jet mode subset is stable are considerably more limited than cone-jet mode, and for this reason few applications have been found for this particular regime[16].

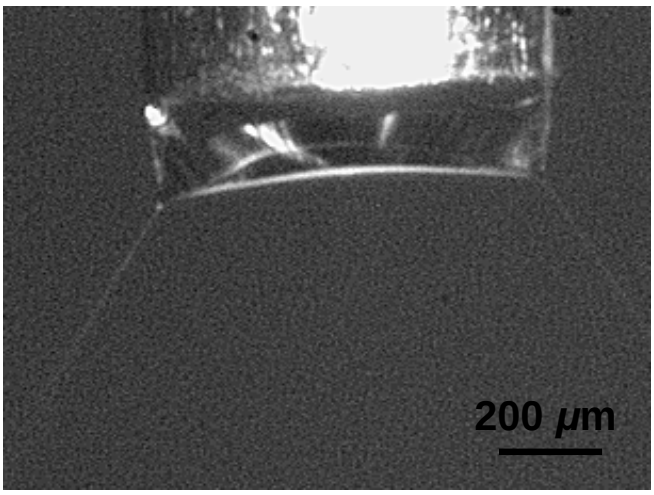

Figure 2.5. The two cone multi-jet electrospray mode. Visible from top is the emitter, two short divergent cones, and two jets.

For the remainder of this thesis, we will consider four simplified regimes. Firstly an enhanced dripping regime where large drops of the size of the emitter are emitted, elongated by the electric field. At higher applied voltages an unstable cone-jet is taken as evidence for the pulsed regime, with the cone apex and jet breaking off intermittently. At even higher applied voltages the situation switches to the stable cone-jet mode, with the current approximately doubling. Lastly at even higher voltages the multi-jet regime occurs, with two or more cones at the tip of the emitter, and another rise in current.

2.3. Theoretical aspects of electrospray

The most studied electrospray regime is the steady cone-jet mode[7]. Consequently most theoretical aspects of electrospray outlined below are confined within this region.

2.3.1. The Taylor cone

In an electrospray system, as a potential difference is applied between the emitter and the extractor electrode charged molecules in the fluid at the emitter tip will attempt to move towards the surface of the drop. This results in the fluid feeling an attractive force towards the counter electrode.

The pressure from the application of the potential difference is a result of the Maxwell stress tensor, which once tangential forces are ignored (i.e. a perfect conductor case) is[15];

$$P_E = \frac{\varepsilon_0}{2} E_n^2 . \tag{2.1}$$

ε_0 is the permittivity of free space, whilst E_n is the electric field normal to the fluid surface. The surface tension pressure of the liquid is;

$$P_{st} = \gamma\left(\frac{1}{R_1} + \frac{1}{R_2}\right) \tag{2.2}$$

where R_1 and R_2 are the principal (maximum and minimum) radii of curvature (with $1/R$ the curvature, κ), and γ is the surface tension of the fluid.

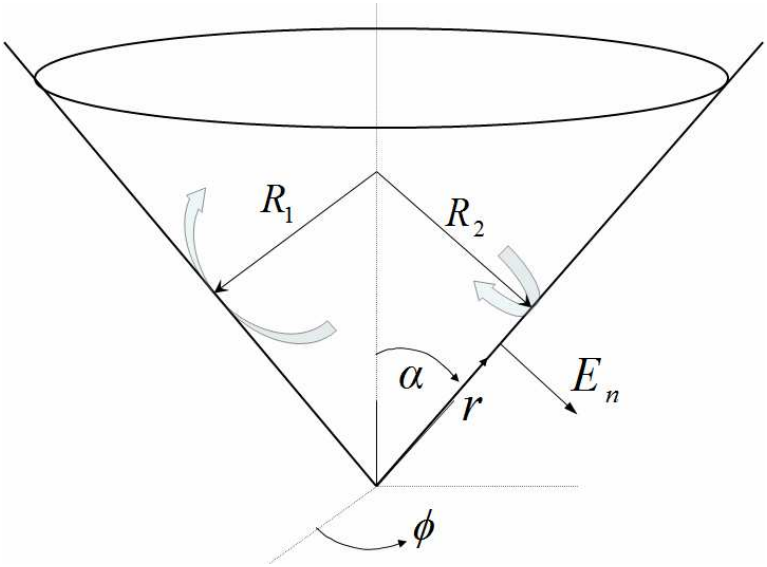

Figure 2.6. The coordinates of the fluid 'Taylor' cone.

From Figure 2.6, for a cone R_1 is equal to infinity as it is along the cone generatrix, whilst $R_2 = r\tan\alpha$. Assuming there are no other forces involved, then by combining equations (2.1) and (2.2), the normal electric field is[15]

$$E_n = \sqrt{\frac{2\gamma}{\varepsilon_0 r\tan\alpha}}. \tag{2.3}$$

The electric potential can be calculated from the Laplace equation, $\nabla^2\Phi = 0$. In spherical coordinates, and with the cone assumed to axisymmetric (hence $\frac{\partial}{\partial\phi} = 0$), the Laplace equation is[32];

$$\frac{1}{r^2}\frac{\partial}{\partial r}\left(r^2\frac{\partial\Phi}{\partial r}\right) + \frac{1}{r^2\sin\alpha}\frac{\partial}{\partial\alpha}\left(\sin\alpha\frac{\partial\Phi}{\partial\alpha}\right) = 0. \tag{2.4}$$

This is solved to give two solutions involving Legendre polynomials P_v and Q_v, of the first and second kind respectively[33];

$$\begin{aligned}\Phi_1 &= A_1 P_v(\cos\alpha) r^v \\ \Phi_2 &= A_2 Q_v(\cos\alpha) r^v .\end{aligned} \tag{2.5}$$

Consequently the normal electric field is given by;

$$E_n = -\frac{1}{r}\left(\frac{\partial \Phi}{\partial r}\right) = -\left(A_1 \frac{\partial P_v}{\partial \cos\alpha} + A_2 \frac{\partial Q_v}{\partial \cos\alpha}\right)\frac{\sin\alpha}{r^{1-v}}. \quad (2.6)$$

For the normal fields of equations (2.3) and (2.6) to be equal then v = ½, and the potential is;

$$\Phi = A_1 P_{1/2}(\cos\alpha) r^{1/2} + A_2 Q_{1/2}(\cos\alpha) r^{1/2}. \quad (2.7)$$

The two Legendre functions have singularities, for P_v at α = 180 degrees, and for Q_v at α = 0 degrees, and as the solution outside of the cone is needed, $P_{1/2}$ is removed by setting A_1 to 0. Hence the potential is

$$\Phi = A_2 r^{1/2} Q_{1/2}(\cos\alpha). \quad (2.8)$$

For the surface to be equipotential and independent of r, the solution must be

$$Q_{1/2}(\cos\alpha) = 0 \text{ with } \Phi = 0. \quad (2.9)$$

Figure 2.7 shows how the Legendre polynomial $Q_{1/2}$ varies with alpha, the angle of the cone apex. It is clear that for the cone to be equipotential the cone semi-angle must be equal to 49.29°, a result first resolved by G. I. Taylor[15].

The plot uses the identity[34]

$$Q_{1/2}(x) = K\left(\frac{1+x}{2}\right) - 2E\left(\frac{1+x}{2}\right) \quad (2.10)$$

where K and E are complete elliptic integrals of the first and second kind, respectively, and are calculated numerically using MatLab.

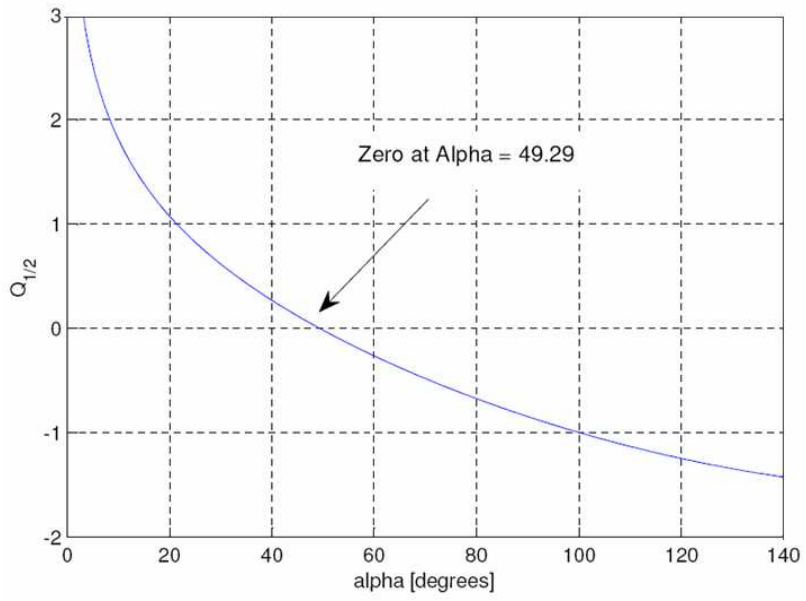

Figure 2.7. Variation of the Legendre polynomial with alpha.

This is a remarkable result - that for an equipotential case with no jet emanating from the tip of the cone, the cone has a specific half-angle that can be defined theoretically. This angle was verified photographically by Taylor[15], with a more detailed investigation completed using liquid metals[35,36].

A significant issue regarding Taylor's model is it assumes a perfectly conducting liquid. In some cases, when spraying a liquid metal this might be a valid assumption, but often the liquid sprayed has a low conductivity. Taylor's solution provides an initial understanding of why a cone shape is formed, and even for low conductivity liquids, may still be valid when the charge relaxation time is less than the hydrodynamic time (see Section 2.3.3). For many liquids this occurs over the majority of the cone, and consequently the cone shape is formed.

Taylor's solution also assumes that the potential is applied on a specifically shaped electrode; Taylor himself tested the analytical result using one cone like electrode, and a second electrode representing a Legendre function[15].

2.3.2. Apex electric field and cone-jet onset voltage

A Taylor cone does not immediately form at the tip of the emitter until the voltage is high enough for the process to be stable. Before this 'onset voltage' is reached, the spray pulses as an intermittent cone forms, and then collapses as too much charge is emitted as droplets to sustain the cone shape, as illustrated in Figure 2.3. As the voltage is increased further the stable cone-jet mode electrospray is formed, as shown in Figure 2.4 and illustrated in Figure 2.1. The cone-jet mode onset voltage is defined as the potential difference between the emitter and extractor electrode at which the cone-jet mode electrospray is a constant and stable phenomenon. It can be estimated from the combination of a theoretical electric field calculation, and equation (2.3)[37].

The electric field at the apex of an emitter with a cone like protrusion can be estimated from a solution of the Laplace equation in prolate spheroidal coordinates[32];

$$\nabla^2\Phi = \frac{1}{a^2\left(\xi^2-\eta^2\right)}\left\{\frac{\partial}{\partial\xi}\left[\left(\sigma^2-1\right)\frac{\partial\Phi}{\partial\xi}\right]+\frac{\partial}{\partial\eta}\left[\left(1-\eta^2\right)\frac{\partial\Phi}{\partial\eta}\right]\right\}+\frac{1}{a^2\left(\xi^2-1\right)\left(1-\eta^2\right)}\frac{\partial^2\Phi}{\partial\phi^2}=0 \quad (2.11)$$

where the coordinate system has been defined as[38];

$$\begin{aligned} x &= a/2\sqrt{\left(\xi^2-1\right)\left(1-\eta^2\right)}\cos\phi \\ y &= a/2\sqrt{\left(\xi^2-1\right)\left(1-\eta^2\right)}\sin\phi\ . \\ z &= a/2\,\xi\eta \end{aligned} \quad (2.12)$$

Surfaces having constant values of ξ or η are confocal ellipses and hyperbolae rotated around the major axis, respectively, whilst *a* is twice the distance between the hyperbolic focus and the flat surface. This geometry results in the emitter being modelled as a hyperbolic surface opposite a flat electrode, as shown in Figure 2.8. F_1 and F_2 are the foci of the hyperbola, and r_1 and r_2 are the distances from the foci to a point on the hyperbola. η_0 is the hyperbolic emitter surface.

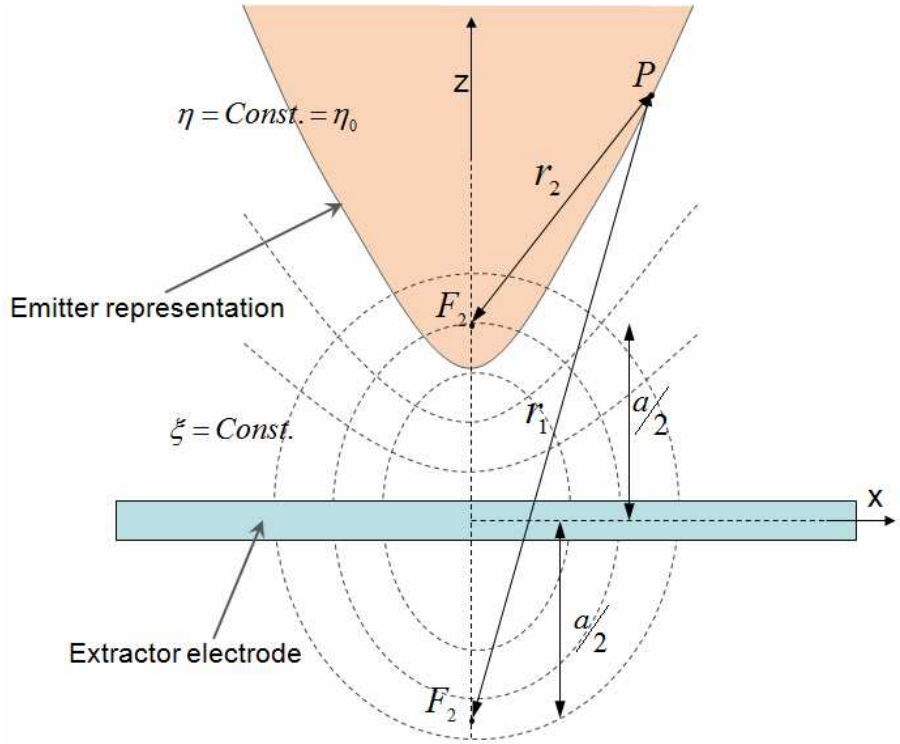

Figure 2.8. Illustration of the prolate-spheroidal coordinates and tip geometry.

If the potential is assumed to have a constant value on one prolate spheroid plane $\eta = \eta_0$, then the solution will depend on η alone[34]. Consequently equation (2.11) is simplified to;

$$\frac{\partial}{\partial \eta}\left[\left(1-\eta^2\right)\frac{\partial \Phi}{\partial \eta}\right] = 0\,. \tag{2.13}$$

Which, with boundary conditions $\Phi(\eta_0) = \Phi_0$ and $\Phi(0) = 0$, integrates to[34]

$$\begin{aligned} \int d\Phi &= C\int \frac{1}{\left(1-\eta^2\right)} d\eta \\ \Phi &= C_1 \arctan h\eta + C_2 \\ \Phi &= \Phi_0 \frac{\arctan h\eta}{\arctan h\eta_0} \end{aligned} \tag{2.14}$$

where arctanh is the inverse hyperbolic tangent, with $\operatorname{arctanh}(\eta) = \frac{1}{2}\ln\left(\frac{1+\eta}{1-\eta}\right)$.

The electric field at the tip of the approximated hyperbolic emitter is

$$E_T = -\left(\frac{\partial \Phi}{\partial z}\right)_T = -\left(\frac{\partial \Phi}{\partial \eta}\frac{\partial \eta}{\partial z}\right)_T = -\left(\frac{\partial \Phi}{\partial \eta}\Big/\frac{\partial z}{\partial \eta}\right)_T = -\left(\frac{\partial \Phi}{\partial \eta}\Big/\left(\frac{a}{2}\right)\right)_T$$
$$E_T = -\frac{2\Phi_0}{a\left(1-\eta_0^2\right)\arctan h^{-1}\eta_0} \tag{2.15}$$

a and η_0 now need to be converted into Cartesian coordinates. From Figure 2.8, the relationship between the η and the z coordinate is;

$$\eta = \frac{r_1 - r_2}{a}$$
$$a\eta = \sqrt{R^2 + \left(z + \frac{a}{2}\right)^2} - \sqrt{R^2 + \left(z - \frac{a}{2}\right)^2}, \tag{2.16}$$

where R is the cylindrical radius, $R = x^2 + y^2$. Rearranging for z gives[34];

$$z = \eta\sqrt{\frac{a^2}{4} + \frac{R^2}{1-\eta^2}}. \tag{2.17}$$

The radius of curvature is calculated from

$$r_e = \frac{\left(1 + \left(z''(R)\right)^2\right)^{3/2}}{z''(R)}. \tag{2.18}$$

Which produces an equation for r_e;

$$r_e = \frac{\left(1 + R\eta\left(\frac{a^2}{4}\left\{1-\eta^2\right\} + R^2\right)\right)^{3/2}}{\frac{\eta}{1-\eta^2}\left(\frac{a^2}{4} + \frac{R^2}{1-\eta^2}\right)^{-1/2}\left(1 - \frac{R^2}{1-\eta^2}\left\{\frac{a^2}{4} + \frac{R^2}{1-\eta^2}\right\}^3\right)}. \tag{2.19}$$

The tip to plane distance results from equation (2.17) with $R = 0$ and $\eta = \eta_0$

$$z_0 = \frac{a}{2}\eta_0. \tag{2.20}$$

Rearranging the previous two equations, with $R = 0$, results in:

$$a = 2z_0\sqrt{1+r_e/z_0}\,, \quad \eta_0 = \frac{1}{\sqrt{1+r_e/z_0}}\,. \tag{2.21a, b}$$

Substituting Equations (2.21) (a) and (b) into equation (2.15) gives;

$$E_T = -\frac{2\Phi_0}{2z_0\sqrt{1+\frac{r_e}{z_0}}\left(1-\frac{1}{1+r_e/z_0}\right)\arctan h^{-1}\left[\frac{1}{\sqrt{1+r_e/z_0}}\right]}\,. \tag{2.22}$$

Following considerable rearrangement it is found;

$$E_T = -\frac{2\Phi_0\sqrt{1+r_e/z_0}}{r_e\ln\left[\frac{r_e+2z_0+2\sqrt{z_0(z_0+r_e)}}{r_e}\right]}\,. \tag{2.23}$$

Equation (2.23) has been described previously, derived using similar methods[34,39-41]. Related equations have also been found[42].

In the case when $z_0 >> r_e$, the equation may be approximated by

$$E_T = -\frac{2\Phi_0}{r_e\ln(4z_0/r_e)} \tag{2.24}$$

with the result being the most commonly applied equation[37,43]. Jones and Thong also derived equation (2.24) using the method of images procedure, assuming a line of charges perpendicular to a flat plate[44].

Equation (2.23) can be equated to the Taylor cone electric field (equation (2.3)), which with the cone-jet onset voltage V_{on} taken to be the applied potential difference Φ_0 gives;

$$V_{on} = \left[\frac{2\gamma\, r_e\cos\alpha}{\varepsilon_0}\right]^{1/2}\frac{\ln\left(\frac{r_e+2z_0+2\sqrt{z_0\left(z_0+r_e\right)}}{r_e}\right)}{2\left(1+r_e/z_0\right)^{1/2}}\,. \tag{2.25}$$

Alternatively using the simpler version of the electric field

$$V_{on} = A_1\left[\frac{2\gamma r_e \cos\alpha}{\varepsilon_0}\right]^{1/2} \ln\left(4z_0/r_e\right), \tag{2.26}$$

where A_1 is a corrective term of order unity, a result of the variation of the constant of the electric field equation when differing methods of derivation are used[37].

The use of equation (2.26) should be limited to situations that resemble the theoretical geometry; i.e. long needles with a flat plate. Also any change in emitter to extractor distance z_0 or tip (needle outer) radius r_e leads to a change of the cone half angle defined by the hyperbola. Consequently when $z_0 >> r_e$, the geometry resembles a slender emitter, but when $z_0 \sim r_e$ the geometry little resembles a needle of a certain radius, as the hyperbola is considerably fatter.

Various attempts to revise the calculation of the onset voltage have been attempted[13,45,46]. Regele *et al.* and Quang Tran Si *et al.* extended the analytical V_{on} model to take into account the effect of multiple emitters relatively close to each other. As the emitter to emitter distance was decreased the onset voltage increased, up to a point where the field of an emitter interacted with its neighbour, at which point V_{on} decreased.

Krpoun *et al.* used a Finite Element Method (FEM) to calculate the electric field at the tip of an emitter, by applying multiple sharpening conic geometries to the emitter tip, until a Taylor cone is accurately reproduced[13]. The resulting electric field is equal to the Taylor cone electric field (as with the analytical method), and the onset voltage could be calculated for varying apex radii. Below a certain radii, approximately equal to the radius of the emitter, the predicted onset voltage reached an asymptote. This numerical onset voltage compared favourably with the experimental values reported, demonstrating better accuracy than the theoretical approach outlined above.

As the electric field scales as $\gamma^{1/2}$, for some electrospraying liquids electrical breakdown occurs before the cone-jet onset voltage[31], with the situation worse for an electrospray of negatively charged, rather than positively charged, particles. This breakdown or discharging can be mitigated by the use of an ‘electron scavenging’ gas (i.e. oxygen), or by spraying at high or low pressures[7].

The cone-jet onset voltage is a measure of the voltage at which a constant and stable cone-jet structure first appears as the applied voltage is increased. However, as the voltage is decreased from operating in cone-jet mode the point at which the cone-jet system becomes unstable (typically called the cone-jet mode extinction voltage) is often found to be significantly lower than the onset voltage[17,37,47]. The reason for this 'voltage hysteresis' remains unclear, although it has been suggested that it is a result of varying cone meniscus shape with voltage[7].

2.3.3. Jet formation and break up

Once the cone-jet onset voltage has been applied a stable cone-jet fluid meniscus occurs, as illustrated in Figure 2.1 and 2.4. It has been hypothesized that the transition from the cone to a jet takes place at the point where the electrical relaxation time is equal to the dynamic time[30]. At this point the charge convection (the flow of charges within a liquid) is overwhelmed by flow of charges towards the cone surface, resulting in a non-equipotential surface and the formation of a jet[7].
Mathematically the liquid (hydrodynamic) residence time and the electrical relaxation time are respectively[30],

$$\tau_{res} \approx \frac{r^3}{Q}, \qquad \tau_{rel} = \frac{\varepsilon_r \varepsilon_0}{K}. \tag{2.27}$$

Where r is as defined in Figure 2.6, ε_r the relative electrical permittivity, and K is the fluid conductivity. When the two time constants are equal the relaxation length r^* is defined[30];

$$\begin{aligned} &\frac{r^3}{Q} = \frac{\varepsilon_r \varepsilon_0}{K} \\ &\therefore r^* = \left(\frac{\varepsilon_r \varepsilon_0 Q}{K} \right)^{\frac{1}{3}}. \end{aligned} \tag{2.28}$$

This length parameter has been compared with the jet diameter[7],

$$d_{jet} = G(\varepsilon_r) r^* \tag{2.29}$$

where $G(\varepsilon_r)$ is a function of the relative permittivity.

The implementation of equation (2.29) to estimate the jet size is complicated by the thinning of the jet from the cone-jet transition point to the jet break up, and this has led to a range of functions for $G(\varepsilon_r)$[7].

The jet break up further down downstream can occur in a variety of different ways, with Hartman *et al.* suggesting that as the ratio between the electric stress and the surface tension stress increases the mode of the jet breakup changes[1]. Three modes were identified by Hartman, as illustrated in Figure 2.9. At relatively low ratios Rayleigh like varicose instabilities occurred; increasing the ratio resulted in a kink instability; and at the highest ratio values a ramified jet instability occurred. The primary droplet diameter were found to decrease with each jet regime, whilst the secondary droplet diameter increased. The kink and ramified jet were found to be non-axisymmetric[1].

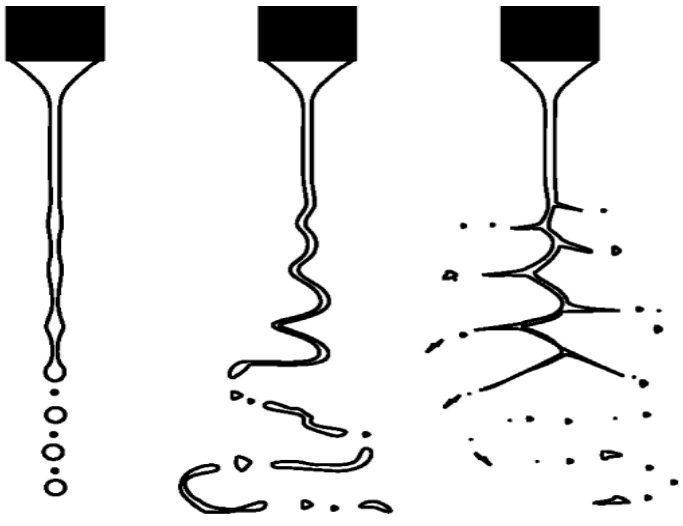

Figure 2.9. The different types of jet break-up, as identified by Hartman[1]. From left to right; the axisymmetric varicose break-up, the lateral kink break-up, and the ramified jet break-up.

Hohman *et al.* found similar results within the application of electrospinning, with the jet becoming non-axisymmetric as the electric field increased[48,49]. Only one non-axisymmetric mode was identified, a whipping regime, with two axisymmetric modes, one Rayleigh instability induced, and the second electrically induced. Indeed within the parameter space that creates the long jet needed for electrospinning the whipping instability naturally occurred[50].

At some point the jet breaks up into droplets. Classically the break-up of a non-charged jet is described by the Rayleigh-Taylor stability theory [51],

$$d_{droplet} = 1.89 d_{jet}, \tag{2.30}$$

where $d_{droplet}$ is the diameter of the drop. This theory though is for an un-charged capillary jet – in actuality the charge carried by the jet has an effect, as demonstrated by the variation of the jet stability and droplet size with the electric stress as found by Hartman[1] and Hohman[49].

The maximum charge possible on a spherical droplet of radius $r_{droplet}$ is commonly labelled the Rayleigh limit,

$$q_{\max} = 8\pi(\varepsilon_0 \gamma)^{1/2} r_{droplet}^{3/2}. \tag{2.31}$$

In reality any variation away from a spherical shape results in a non-uniform division of the droplet[34], with the actual charge on the droplet falling within $1/2\, q_{\max} < q < q_{\max}$.

The situation is further complicated with volatile liquids, as evaporation results in Coulombic explosions[52]. This situation occurs repeatedly to the point at which ion evaporation from sub micron droplets occurs, and is the established methodology for extracting ions in Electrospray Mass Spectrometry.

2.3.4. Scaling of current with parameters

The current carried along the surface of the cone (the radially rotated cone generatrix) can be given by[34];

$$I_s = 2\pi(r\sin\alpha)\rho_s u \tag{2.32}$$

with u the radial velocity of the fluid and arbitrary length r, and where $\rho_s = \varepsilon_0 E_n$, with the normal electric field given by equation (2.3).

The fluid velocity is given by $Q = uA$ where A is the area of the cones spherical cap, as outlined in Figure 2.10.The surface current is consequently,

$$I_s = \frac{Q}{r^{3/2}}\sqrt{\frac{2\gamma\varepsilon_0 \sin\alpha_T \cos\alpha_T}{(1-\cos\alpha_T)^2}} \tag{2.33}$$

Over most of the cone this surface charge is negligible[34], as can be intuited by the negative power of r. The total current is the sum of the surface and ohmic bulk conduction current;

$$I_{Total} = KE_r A + I_s\,. \tag{2.34}$$

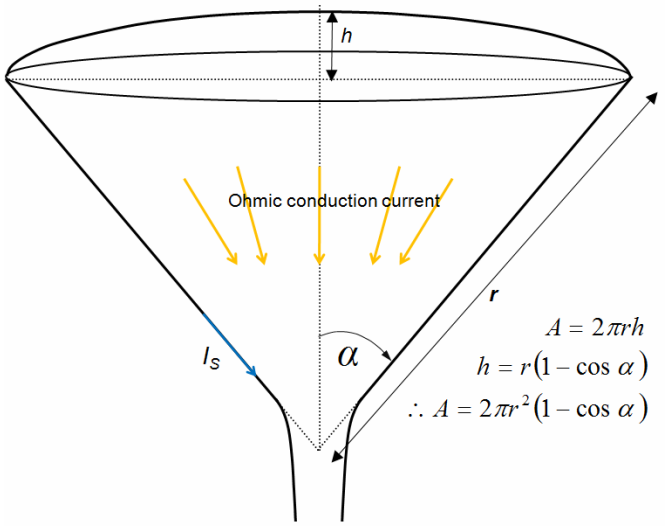

Figure 2.10. Geometry of cone with spherical cap.

Within the cone tip-jet region (as defined by equation (2.28)) it is assumed that surface charge convection becomes the main charge transport mechanism, significantly larger than bulk conduction, which dominates in most of the cone[30]. This is justified as the radial electric field (associated with the bulk conduction current)

$$E_r = \frac{I_c}{AK} = \frac{I_c}{2\pi(1-\cos\alpha_T)Kr^2} \tag{2.35}$$

decreases with r to the power negative two whilst the normal electric field (equation (2.3) – associated with the surface current since it attracts the charges to the surface) decreases with r to the power of a negative a half.

Substituting the relaxation length r^* (equation (2.28)) into (2.23), under the assumption that the majority of the current at the transition region is on the surface, gives a relationship for the scaling of current[53];

$$I = \sqrt{\frac{\sin 2\alpha_T}{(1-\cos\alpha_T)^2}\frac{\gamma KQ}{\varepsilon_r}} \quad . \tag{2.36}$$

Fernández de la Mora and Loscertales[30] introduced a similar theoretical approach for estimating the current. Assuming sink flow resulted in the equation

$$I = f(\varepsilon_r)\sqrt{\frac{\gamma KQ}{\varepsilon_r}}\,, \tag{2.37}$$

which is very similar to equation (2.36), with the exception of an empirical function of the relative permittivity. This function $f(\varepsilon_r)$ was found to vary from approximately 8 to 20. Fernández de la Mora compared Equation (2.37) with experimental results from six different fluids over a wide range of flow rates[30]. Defining non-dimensional groups,

$$\xi = \frac{I}{\gamma(\varepsilon_0/\rho)^{1/2}}\,, \quad \eta = \sqrt{\frac{\rho KQ}{\gamma\varepsilon_r\varepsilon_0}}\,, \tag{2.38a, b}$$

it was found experimental and theoretical results agreed very well[30], as reproduced in Figure 2.11. Of note though is the necessary division of ξ by $f(\varepsilon_r)$ – when not included the data collapse is not as good.

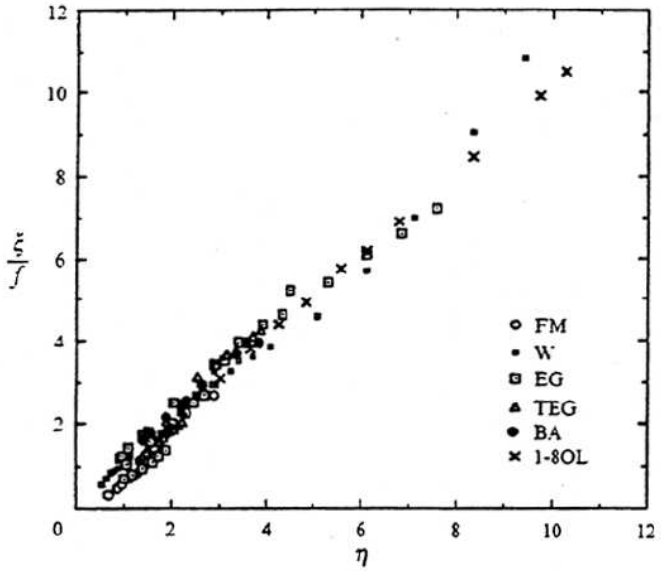

Figure 2.11. Correlation between current dimensionless group and theoretical flow rate dimensionless group[30].

Various other studies have put forward scaling laws for the current, producing somewhat varying equations[54-57]. To generalize, for higher conductivity fluids the same $I \propto \sqrt{\gamma KQ}$ relationship has been found. There are suggestions that under different parametric ranges (for example inertia or surface tension dominated situations) other current scaling laws may apply[58].

There is also some suggestion that the relationship contained by Equation (2.37) is incomplete, solely a good first approximation[59]. Smith *et al.* found that although Fernández de la Mora's current scaling provided a reasonable fit over all data, when each experimental data set was separated a considerable deviation from theory was clear[59]. The exponent *n* of the current scaling relationship, defined as $I \propto Q^n$, was found to vary from 0.41 to 0.65 (compared to $n = 0.5$ in equation (2.37)), with this variation affected by the molar conductivity in a logarithmic fashion[59]. A relationship $n = 0.051\ln(\Lambda_m) + 0.41$ between exponent and molar conductivity Λ_m (in units S·cm^2/mol) was found, with an R^2 fitting of 0.911[59].

2.3.5. The minimum flow rate

In some situations, a minimum flow rate has been noted, below which a stable cone-jet mode electrospray is not possible[30,57,60]. This disruption of the Taylor cone would seem to occur when the dimensionless group η (equation 2.38 (b)) is less than a lower limit, of the order unity. This defines the minimum flow rate Q_{min};

$$Q_{\min} = \frac{\gamma \varepsilon_r \varepsilon_0}{\rho K}. \tag{2.39}$$

This limit upon the stability of a cone-jet is of some importance as it defines the smallest jet possible for a particular liquid (via equation (2.29)), and hence the size of the droplets. There is though no rigorous explanation of this theoretical limit.

Some attempts at an explanation for Q_{min} have been attempted[7,57]. The maximum current possible under experimental conditions is when full charge separation occurs[7],

$$I < I_{Max} = zeQ \tag{2.40}$$

where z is the ion concentration, and e the elementary charge. This provides an extreme limit, where there are solely ions of one sign in the electrospray particles produced; in reality this is probably an unattainable situation except perhaps when using ionic liquids. In some experimental studies the experimental value for Q_{min} is not near the charge separation limit[7], suggesting another explanation is needed.

Currently no clear explanation of minimum flow rate would seem to be available. Part of the problem arises from the ambiguity of some experimental studies. An in depth study of Q_{min} using various solvents with different properties would be enlightening.

As well as a minimum flow rate for stable cone-jet mode electrospray, there has been some suggestion that there is also a maximum[7,57]. Beyond a certain flow rate the cone is no longer stable and pulses. This Q_{max} may be due to an upper limit to the amount of charge that can be passed across the dielectric emitter to extractor electrode region (as charged droplets)[7], and may depend on the electrode configuration[30].

2.3.6. Numerical models

Due to the complexity of the creation of a charged jet and its subsequent breakdown during the electrospray process, simulations of the situation are illuminating, especially of the cone-jet system. An early model of the electrospray process was completed by Hartman *et al.*[29,61]. Using the basic equations of the Taylor Melcher Leaky Dielectric model as described by Saville[62], and an Finite Element Method to model the electric field, Hartman was able to simulate the cone-jet structure to within a reasonable degree of accuracy, and found the same relationship of current to flow rate as found by Fernández de la Mora *et al.*[30].

The electrospray process is though difficult to simulate, thanks to the order of magnitude size differences between the diameter of the emitter needle and the jet, creating a very stiff set of equations. Even so, since Hartman's studies in the late 1990's, modelling studies of the cone-jet and the subsequent break-up have improved. One of the more complete models, incorporating detailed analysis of the cone structure and comparisons to experimental parameters, was created by Carretero-Benignos[63,64]. Using the Leaky Dielectric model, including conservation of charge energy and mass, it demonstrated reasonable accuracy to experimental results. Yan *et al.* followed a very similar method, with approximately the same results[65].

Recently there has been some improved modeling attempts[66], many using the in-built electrohydrodynamic function of the modeling software, FLOW3D[67-70]. The software provides off-the-shelf analysis of a charged fluid interface in an electric field, again using the Taylor-Melcher model. It resulted in reasonable agreement with experiments, and the model was extended to include the creation and pulsation of a cone[68] and even multiple emitters[70].

2.4. The Effect of applied voltage in electrospray

Introduction

For the electrospray process to occur a potential difference must be applied between the emitter and the extractor electrode, as illustrated in Figure 2.1. This potential difference initiates the electrohydrodynamic processes that create the small charged droplets. From this point in the thesis onwards, for reasons of expediency this potential difference between the emitter and the electrode will be known as the applied voltage, or as simply the voltage.

As described in the introduction, the effect of this applied voltage on the flow rate and current of the electrosprayed droplets forms the majority of the experimental investigation of this thesis. The following section outlines the existing understanding of the effect of voltage, and attempts to put into context various studies. Particular emphasis is put on the investigations completed by Smith *et al.* [9,12,71,72] (which this study extends upon) , with an attempt to relate these findings to previous results.

2.5. The effect of the applied voltage on the electrospray flow rate

The effect of the applied voltage on the flow rate of emitted droplets within cone-jet electrospray is difficult to measure due to the low flow rates involved, of the order of nano-litres per second (nLs^{-1}).

Studies have employed various methods to measure this extremely low flow rate. The most commonly applied involve measuring the pressure at two points; at one point upstream of the cone, and a second point within the electrospraying chamber. The pressure difference is calculated, from which the flow rate is derived using the Poiseuille equation[30,56,73]. The system is calibrated using flow visualisation; a bubble or small

particle is introduced within the fluid line and its velocity is measured, from which the flow rate may be calculated[30,53].

There are though some errors involved with this method. The assumption that the bubble is travelling at a speed comparable to the fluid velocity may be simplistic, and the bubble can reach and disturb the cone meniscus, making the application of the calibration method difficult when the apparatus is online.

Perhaps though the largest error involved is the lack of accounting for the change in pressure across the cone-jet meniscus. The determination of the pressure at only one point upstream ignores any effect of a change in cone-jet geometry on the pressure. This problem has in the past been avoided by the varying of the applied voltage to keep the cone-jet geometry constant[74], or making its effect small compared to the total pressure difference between a point upstream of the emitter and the electrospraying chamber, by increasing the hydraulic resistance[75].

Despite the difficulties in measurement, various studies have found a relationship of flow rate to the applied voltage[9,10,47,71,72,76-78], although in most studies the effect is no more than partially investigated.

Yahiku *et al.*, early pioneers of electrospray colloid propulsion, used time of flight techniques to calculate the mass flow rate of an annular colloid electrospray thruster[77]. An annular thruster consists of two concentric rings, with the propellant being fed between the annular gap[77]. Taylor cones formed in the gap once a suitable voltage was applied, with a linear relationship between the voltage and mass flow rate emanating from the annular thruster found.

Mutoh *et al.* demonstrate a similarly strong relationship of flow rate to voltage, that could be approximated as linear[78]. In this case doped Xylene was tested using a simple electrospray setup.

An interesting note on the effect of the voltage was made by Hartman[61]. Hartman produced a model of electrohydrodynamic atomization but did not investigate the effect of applied potential in detail, justifying the decision with;

If the potential difference over the electrodes increases and the supply of liquid to the cone remains the same, then the liquid flow rate into the jet will increase, and the liquid cone will become smaller. As a result, the increased electric field will be reduced again to values just above its original value, and the flow rate will decrease again until a stable jet with the appropriate flow rate into the jet is formed. This adjustment of the cone size reduces the effect of the increase in potential difference.

Hence Hartman attributes the small flow rate-voltage sensitivity to changes in cone meniscus geometry, in a feedback-like mechanism process. He does not though test this hypothesis.

Lenggoro *et al*. mention the increase of current with voltage, and attempt to explain the phenomena by attributing it to solvent evaporation from the cone meniscus[47]. With a solution conductivity of 5.62×10^{-3} Sm^{-1}, whilst operating in cone-jet mode the results showed the current increased with voltage. The relationship was attributed to fluid evaporation from the cone. The flow rate through the jet (~proportional to the current in this case as the current is measured at a droplet collector electrode downstream) is;

$$Q_{jet} = Q_{feed} - Q_{evap} \tag{2.41}$$

where Q_{feed} is the flow rate through the capillary, and Q_{evap} the flow rate due to evaporation. From previous studies it was well established that the axial cone length decreased with voltage[61,74], hence the area and the evaporation flow rate decreased with voltage, and from above Q_{jet} (and therefore the current) increased. Lenggoro's hypothesis seems correct when current is measured from the charged droplets, but would not be if the *I(V)* relationship occurred when measuring current at the emitter.

An unambiguous demonstration of the flow rate-voltage relationship in cone-jet mode electrospray was realised by K. Smith *et al*[10,71]. The design and then implementation of an ultra-accurate flow rate measurement device[10] allowed the measurement of the

volumetric flow rate Q to an unprecedented flow rate resolution of 10^{-12} Ls $^{-1}$. In comparison to other flow measurement devices used, this is a generation jump in flow measurement at the minuscule level.

Smith measured the volumetric flow rate from the pressure difference ΔP between two points in the fluid line upstream from the electrospray nozzle. This method is similar to that used by other studies[30,56,73], but with the addition of another pressure measurement point upstream to account for changes in pressure from the variation of the cone geometry with the applied voltage.

The pressure at these two points is calculated from the stress applied to two quartz pressure transducers situated a distance L apart within the fluid pipe system. Assuming a laminar flow, Poiseuille's law gives

$$\frac{\dot{m}}{\rho} = Q = \frac{\Delta P \pi R_i^4}{8 \mu L} \tag{2.42}$$

where $\dot{m}$ is the mass flow rate, ρ the density of the fluid, R_i is the internal radius of the pipe, and μ the dynamic fluid viscosity. The volumetric flow rate Q (m^3s^{-1}) can then be obtained (after some suitable calibration of the system).

Following directly from the implementation of this high fidelity flow meter was the finding that the applied voltage can significantly affect the flow rate of the electrospray system[9]. A typical flow rate-to-voltage ($Q(V)$) dependency can be seen in Figure 2.12, courtesy of Smith *et al.*[9]. The liquid used was Ethylene Glycol, doped with Sodium iodide (NaI) to increase the conductivity to 0.0029 Sm^{-1}.

Before applying a voltage a back pressure resulted in a nominal flow rate, termed Q_{nom}. Then as the voltage between the extractor grid and the capillary was applied and then increased the spray went through various modes, until obtaining cone-jet mode at V_{on}, at a flow rate of Q_{on}. Once cone-jet mode was established the rate increased as the voltage was increased, and conversely as the voltage decreased the flow rate decreased.

A significant effect was found, demonstrating a linear relationship between the flow rate and the applied voltage. There was an approximate 45% change in flow rate over the 1.5kV cone-jet range[9], with the linear flow rate-to-voltage ($Q(V)$) relationship having a gradient of ~2.6 $nLs^{-1}kV^{-1}$.

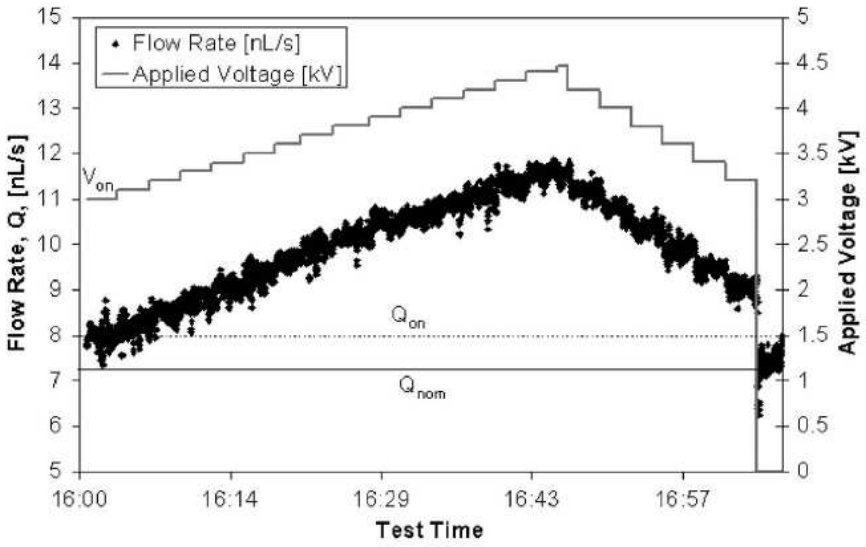

Figure 2.12. Illustration of the flow rate-voltage relationship[9].

Explanations of the *Q(V)* phenomena have been attempted[71], with varied conclusions. Lenggoro *et al.* suggested evaporation of the solvent from the liquid meniscus as a mechanism for the variation of flow rate with voltage[47], as described by equation 2.41. For the solvent evaporation hypothesis to be valid then evaporation must increase with voltage. But as the area of the cone decreases with increases in voltage (as the cone length generally decreases with voltage in cone-jet mode[10]), the evaporative flow rate would decrease with voltage - the opposite to what might have been an explanation to the *Q(V)* relationship. A *Q*(*V*) analysis by Smith *et al.* investigated the evaporative flux hypothesis in detail, and concluded that it has an insignificant effect[71]. For a non-volatile electrosprayed solution evaporative flux was shown to only account for approximately 0.1 - 1% of the total flow rate, too small a fraction to explain the *Q(V)* relationship found experimentally.

The effect of the surface tension pressure was also suggested as a possible cause of the *Q(V)* dependence[71]. The pressure due to the surface tension is given by;

$$P_\gamma = \gamma\left(1/R_{c1} + 1/R_{c2} \right) \tag{2.43}$$

where R_{c1} and R_{c2} are the principal radius of curvatures. When the liquid forms a spherical cap $R_{c1} = R_{c2}$, and hence $P_\gamma = 2\gamma/R_c$. For a parabola shaped cone, the mean curvature at a particular point is given by [10,79];

$$M_{\mathrm{K}} = \frac{\left(1+f_y^2\right)f_{xx} - 2f_x f_y f_{xy} + \left(1+f_x^2\right)f_{yy}}{2\left(1+f_x^2+f_y^2\right)^{3/2}}, \tag{2.44}$$

with f the profile curve as a function of x and y , and the subscripts denoting differentiation with respect to x or y. The surface tension pressure is the product of the above equation with twice the surface tension. By solving this equation, the change in surface tension pressure from changes in the cone geometry as the voltage is increased can be calculated (by fitting a curve to experimental photos at each voltage), and compared with actual changes in flow rate. Following this analysis smith *et al.* found changes in surface tension pressure due to changes in shape as the voltage was increased resulted in an increased flow rate. But the increase was deemed too large, and non-linear, and could not describe the $Q(V)$ phenomenon[10]. From the results of this analysis, Smith comes to the conclusion that changes in pressure due to changes in cone curvature cannot account for voltage modulation of flow rate.

2.6. The flow rate –voltage relationship in detail

2.6.1. The effect of hydraulic resistance and emitter geometry

Smith demonstrated that the *Q(V)* dependence occurred consistently within cone-jet mode electrospray, and that neither the conductivity nor the cone-jet onset flow rate had an effect on the flow rate sensitivity to voltage[9]. The conductivity was tested in the range 0.0025 - 0.23 S/m.

Given that the observations by Smith provided a linear relationship between voltage and flow rate for it is possible to write this as

$$m_Q = \frac{dQ}{dV_{app}} \tag{2.45}$$

with m_Q constant for a particular configuration. For different liquids m_Q varies, with this change attributable to the varying hydraulic resistance of the fluid system as a result of the differing viscosities and internal diameters of the fluid system[9]. From the Poiseuille equation (2.42) the hydraulic resistance of the system R_T is given by $8\mu L/\pi r^4$. The pressure difference can be rewritten to consist of two parts[72],

$$QR_T = P_T = P_D + P_e \tag{2.46}$$

where P_T is the total pressure difference, P_D is the driving pressure drop due to the head of the fluid reservoir, whilst P_e is the electric pressure drop which results from the Maxwell stress tensor term relating to pressure. Differentiating with respect to the applied voltage V_{app}, and assuming that the driving pressure remains constant due to constant hydrostatic conditions (i.e. $dP_D/dV_{app} = 0$), gives[72];

$$\frac{dP_e}{dV_{app}} = \frac{dQ}{dV_{app}} R_T = m_Q R_T = m_{pe}. \tag{2.47}$$

Hence m_{pe} is the sensitivity of the "electric pressure" to voltage - it is the sensitivity of flow rate to voltage m_Q once the effect of the hydraulic resistance is removed. The units of m_{pe} are Pascals/Volt, equivalent to the volumetric charge density (charge per metre cubed).

The value of the "electric pressure sensitivity" to the applied voltage, m_{pe}, was calculated by Smith *et al.* for emitters of different diameters, as shown in Figure 2.13. The emitter inner diameter was varied from 50 – 305 μm, whilst the outer diameter varied from 115 – 560 μm. Shown are results using three different liquids of varying viscosities.

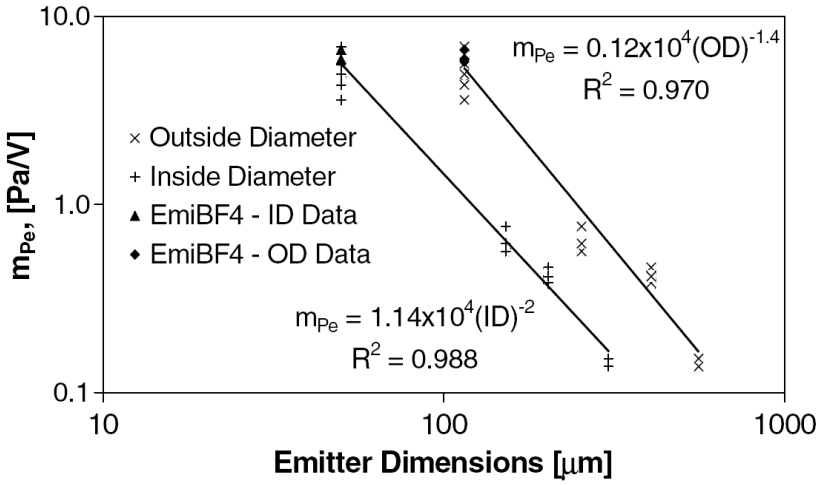

Figure 2.13. Comparison of m_{pe} variations for ethylene glycol (EG), triethylene glycol (TEG) solutions (data for both liquids is contained within '+' and '×' points), and ionic liquid $EmiBF_4$ for various emitter geometries[72].

The plot of m_Q versus emitter diameter for these differing fluids did not follow one trend line[72], but once the effect of hydraulic resistance was removed the points fell on one trend line.

From Figure 2.13, the effect of the voltage on the electric pressure was found to decrease as the emitter diameter decreased. m_{pe} would seem to be proportional to the reciprocal of the square of the inner diameter or the reciprocal of the outer diameter to the three halves, although the results are ambiguous as to whether it is the outer or inner dimensions of the emitter that affects the electric pressure sensitivity[9,12]. For all the emitters tested the outer diameter scaled with the inner diameter, and consequently it was not possible for the authors to distinguish the underlying dependence.

If the electric pressure is sensitive to the inner and not the outer diameter, there are two competing effects as the inner diameter is varied; the hydraulic resistance and the electric pressure change with voltage. Consequently there will be a peak in the value of the m_Q, as can be seen in Figure 2.14[72]. The capillary conductance is the reciprocal of the hydraulic resistance, whilst the driving parameter of the electric pressure is taken to be the inner diameter of the emitter. It should be noted though that if the electric pressure variation with voltage is not a function of inner diameter (instead being a function of outer diameter), a peak will not occur.

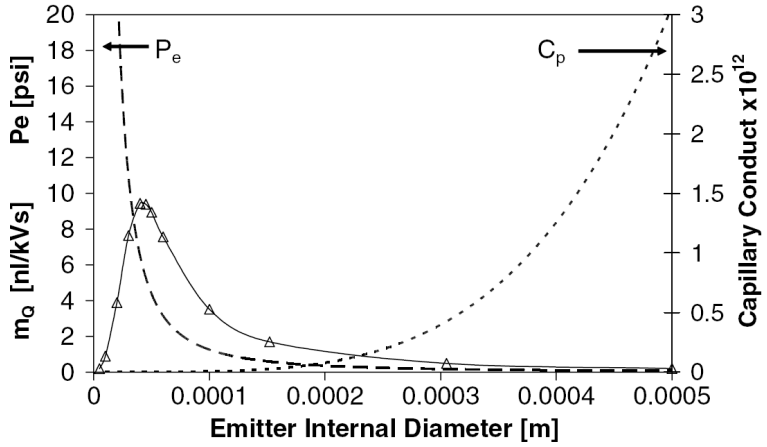

Figure 2.14. Example of m_Q optimization for $EmiBF_4$[72].

2.6.2. The *Q*(*V*) relationship using ionic liquids

The field of electrospray colloid thrusters, a form of low-thrust spacecraft propulsion that uses the electrospray technique, has experienced a resurgence, partly due to the use of ionic liquids as the propellant. These have the advantage over previous propellants in that they can produce ions[80]. These ions can be accelerated to a greater exhaust velocity, which through the Tsiolkovsky equation[81], results in less propellant mass needed to obtain a certain change in velocity of the spacecraft. Also as ionic liquids have zero vapour pressure (the ions are held in the liquid by the ionic forces and can't evaporate) they will not be affected by the vacuum space environment.

As Figure 2.13 illustrates, experiments have revealed that ionic liquids have a similar flow rate dependence upon voltage as the organic liquids tested. When the voltage was increased the flow rate of the ionic liquid markedly increased[72]. The finding that ionic liquids do follow the same trends as organic solvents is remarkable, as the two liquid types differ considerably.

The ionic liquid tested (1-ethyl-3-methyl imidazolium tetrafluoroborate ($EmiBF_4$)) has a high enough conductivity (1.3 Sm^{-1}) to emit ions directly from its meniscus. No direct evidence that the system was working in the ionic regime whilst demonstrating the *Q*(*V*) relationship was found by the previous studies though[72]; as a result further investigation

is required to ascertain whether the flow rate-voltage relationship is unchanged when emitting ions.

Ionic liquids have negligible vapour pressure, and so evaporation is minute (or may simply not occur). However the similar $Q(V)$ relationship for both ionic liquids and organic solvents reinforces the earlier observation by Smith that the effect cannot be generally attributed to evaporation from the meniscus, as suggested previously[47].

2.6.3. Application of voltage modulation of flow rate to colloid thrusters

The electrospray process can be used in spacecraft propulsion where the charged droplets and/or ions produced are accelerated, and provide the thrust for the propulsive device[34,82]. This type of device has been termed a colloid thruster. Colloid thrusters are particularly useful in fine attitude control, as a result of their high exhaust velocity and efficiency. Also they may have an application in nano-satellites primary propulsion[53].

The variation of flow rate with voltage can be applied to electrospray colloid thrusters, as it can be used to vary the delivered thrust[72]. The thrust can be estimated from;

$$T = \rho Q\left(2V_{acc}\, q/m\right)^{0.5} \tag{2.48}$$

where ρ is the density of the sprayed liquid, V_{acc} the acceleration voltage on the acceleration grid further downstream (taken to be constant). The specific charge q/m is

$$\frac{q}{m} = \frac{I}{Q\rho}. \tag{2.49}$$

The specific impulse, a parameter that helps to characterise propulsion systems, is given by:

$$I_{sp} = v_e / g_0 = \frac{1}{g_0}\left(2V_{acc}\, q/m\right)^{0.5}. \tag{2.50}$$

g_0 is the value of gravitation acceleration at the Earth's surface. When combined with Fernández de la Mora's current scaling law (equation 2.37), the following relationships are found;

$$T \propto Q^{3/4}$$
$$I_{sp} \propto Q^{-1/4} \tag{2.51}$$

with the flow rate proportional to the voltage applied to the extractor electrode. Note that these relationships are approximate, partly as Fernández de la Mora's scaling law half power is often deemed to be inexact[59], and also since there will be various efficiency losses[83]. The assumption that voltage does not greatly affect the spray current is also made; a situation found previously[10,56], although this is challenged by other studies[10] (the $I(V)$ relationship is discussed further in the next section). Nevertheless these simplified relationships for thrust and specific impulse do demonstrate that by changing one parameter (the extraction voltage) it is possible to change the performance of a colloid thruster. The thrust increases with the extraction voltage whilst the specific impulse decreases.

Specific impulse is often the defining factor for the use of a propulsion system, with a high specific impulse reducing the amount of propellant needed for the completion of a particular mission. For a colloid thruster the highest specific impulse is given at the lowest flow rate possible; this will be at the point of transition from pulsed to cone-jet mode, the minimum flow rate as defined in equation (2.39). At this low flow rate the voltage modulation on the flow rate relationship will have the greatest effect. For a TEG solution the percentage increase in Q from Q_{min} per kV is calculated to be ~103%, whilst for $EmiBF_4$, with its lower Q_{min} (but similar flow rate sensitivity), there is an approximate 23 fold increase per kV increase of extractor voltage[72]. This 23 fold increase will result in a ~9 fold increase in thrust, but a significant decrease in specific impulse.

2.7. The effect of voltage on the electrospray current

The most frequently measured parameter in electrospray systems is the current – the charge streaming from the cone tip per unit time[30]. This is understandable as it displays some important electrospray characteristics - i.e. mode, occurrence of spraying, stability -

and (using a potential divider system or a low current ammeter) is easily readable. Consequently it is often the case that an effect of voltage on current is found, rather than an effect of voltage on flow rate. It is this current dependence on voltage (normally in cone-jet mode), rather than the $Q(V)$ dependence, that is more often concluded to be minimal.

Many studies have noted an effect of voltage on current in cone-jet mode electrospray[12,30,37,56,60,75,82,84-91], and on occasion more detailed findings have been presented[10,92-94]. Some studies found a significant variation of I with V [10,12,37,75,90-92,94], whilst other studies described a minimal *I(V)* relationship[30,56].

Fernández de la Mora *et al.* found the current I follows the approximate relationship $I \propto Q^{1/2}$ within cone-jet mode electrospraying[30]. Electrostatic parameters like the extractor voltage or geometry of the emitter were not included in the current relationship, with their omission justified since at high conductivity the dimensions of the emitter are considerably larger than the jet radius. With this disparity in size the sensitivity of I to geometry or applied potential difference is described as likely to disappear[30]. The study's experimental results seemed to verify this conclusion.

Gañán-Calvo *et al.*[56] also found a weak relationship between the current and the applied voltage. The results (illustrated in Figure 2.15) show the voltage having a "6-7% effect" on the current, in a linear fashion. Although the current does increase with voltage, the increase is small compared to the cone-jet mode onset current. Gañán-Calvo sets aside the *I(V)* effect as too small to be of importance, a justifiable action considering his experimental results.

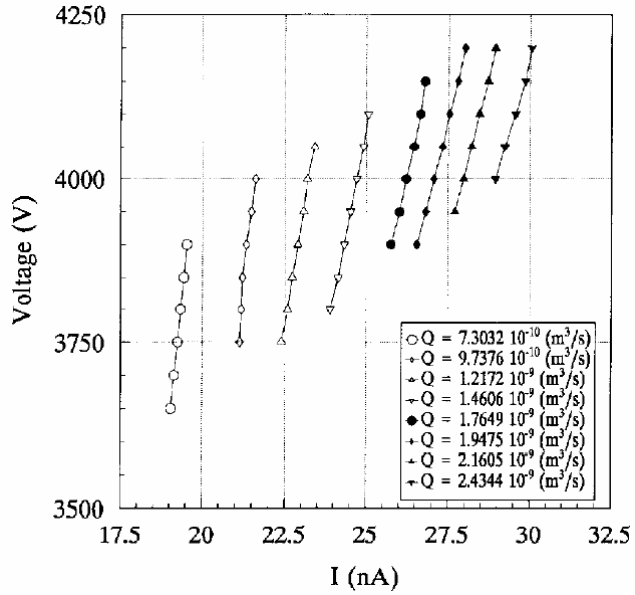

Figure 2.15. The effect of voltage on the current in cone-jet mode, as found by Gañán-Calvo *et al*[56].

Other studies also found the effect of voltage on current to be slight[75]. Rosell states that in some studies the current is observed to have a stronger relationship to voltage; "*It appears that for those particular cases the flow rate was sensitive to V*"[75]. This is expected to occur when the electric field 'suction' reduces the hydrostatic pressure by a non-negligible fraction of the pressure drop along the liquid supply line Δp[75]. In general Rosell finds current more sensitive to voltage than found by Fernández de la Mora[30], although he agrees that it becomes less sensitive as the ratio d_{jet}/r_e decreases (which corresponds to the flow rate decreasing).

Ku *et al.*[92] mention a current-voltage relationship, stating that the spray current depends on the voltage. The explanation is offered that at some critical voltage the electric field is large enough to allow for ion evaporation from the cone meniscus, hence above this critical voltage the current consists of charged droplets from jet breakdown and ions from direct evaporation, allowing for an increase in current. This hypothesis needs further investigation before acceptance, and seems unlikely to result in a linear *I(V)* relationship.

Marginean *et al.* completed a thorough investigation of how the current changes over and within different regimes, investigating the effect of distance, back flow rate, and breakdown discharges[93]. The results show the current is affected by voltage not only in the cone-jet regime, but also within other electrospray regimes. Within the cone-jet regime the effect is small and approximately linear.

Wilm and Mann noticed a significant dependence of current on voltage, with an approximate 50% change of current in some cases[94]. An equation was derived to describe the *I(V)* dependence;

$$I = 6\left(\frac{\pi^2}{\rho}\right)^{2/5} \frac{c}{R_T^{1/5}}\left[\gamma \tan\left(\frac{\pi}{2} - \vartheta\right)\right]^{3/5}\left\{\left(\frac{U_a}{U_T}\right)^2 - 1\right\}^{3/5}, \qquad (2.52)$$

where ρ is the density of the spraying liquid, c is the surface charge density on an emitted droplet, R_T is the total hydraulic resistance, ϑ the liquid cone angle, U_a the applied voltage and U_T the threshold voltage (the cone-jet mode onset voltage). This equation fits their results well, producing a close to linear line. Also, as the hydraulic resistance is included in the above relationship, this agrees with the results found for the flow rate variation with voltage[72].

Smith investigated current-voltage effects, finding as the voltage is increased the current linearly increased, a phenomena analogous to the *Q(V)* effect[10].

If current is proportional to flow rate to the half (from equation (2.37)) the conclusion that Q is proportional to the applied voltage, would seem to lead to $I \propto V^{1/2}$, but this was not found[10].

The conductivity of the liquid tested by Smith *et al.* was 0.01 Sm^{-1}, greater than the conductivity limit of 10^{-4} S m^{-1} above which de la Mora[30] states that the voltage had no effect. Smith also noted that the *I(V)* dependence was sensitive to the volumetric flow rate[10] - an effect noticed before[56,75,92].

In a related study, Alexander *et al.* commented on the linearity of the $I(V)$ relationship[12], with regard to colloid electrospray thruster experiments.

Smith also found the *I(V)* relationship to be sensitive to the conductivity[10], with the slope of the current-voltage relationship increasing with conductivity. This effect has also been found previously[17], but is in conflict with Fernández de la Mora's finding that the *I*(*V*) dependence is insignificant above a certain conductivity.

2.7.1. Modelling the current - voltage dependence

There have been several attempts to model electrospray physics by numerical integration of a coupled ordinary or partial differential equation system. Of these models some have mentioned the effect of the voltage on spray parameters[29,63,68,69].

Carretero-Benignos modeled the electrospray cone-jet by mass, charge, and momentum conservation, assuming a pressure balance across the liquid surface, with the Laplace equation solved using a boundary element method. He shows a "slight (approximately linear) dependence" of current to applied voltage[63] (author's parentheses).

During his simulation efforts, Hartman found a similar result to Carretero-Benignos, however with the current proportional to a power law dependence with voltage[29],

$$I/I_0 = \left(V/V_0\right)^{a_v}, \tag{2.53}$$

where I_0 is the starting simulation current, and V_0 is the starting simulation voltage. a_v is found from simulations to have a value of 0.6.

Hartman also found the diameter of the emitter nozzle had an effect on the current – voltage relationship, a finding similar to that of Alexander *et al.*[72]. This is analogous to the *Q*(*V*) relationship, where the diameter of the nozzle also has an effect (see Figure 2.13). Hartman states that "scaling laws that do not take the nozzle diameter into account can never be very accurate", as the observed current was 15% greater with an emitter with an outer diameter of 1mm compared to an emitter with an outer diameter of 8mm.

Recently there has been some significant improvement in electrospray models based upon the CFD software FLOW3D [67-70], with the most recent studies reporting on the

effect of voltage on current[69]. Using the same Taylor-Melcher Leaky Dielectric Model as applied previously by Hartman, combined with the Navier-Stokes equation, Sen *et al.* find reasonable agreement between the simulated $I(V)$ relationship and experimental results[69]. The relationship is described as a power law similar to Equation (2.53) with a_v = 0.86. Senn *et al.* consistently found the current from simulations to be greater than the experimental result, and postulated that this could be due to unaccounted-for space charge effects (the charged droplets between the emitter and extractor electrode reducing the potential difference seen at the emitter).

2.8. Voltage modulation of parameters in related fields

2.8.1. LMIS

A field with similarities to electrospray is that of Liquid Metal Ion Sources (LMIS)[95]. LMIS use a liquid metal (for example Gallium, that has a conductivity of $1\times10^6\ \mathrm{Sm^{-1}}$) contained at the tip of an emitter, and subjects it to a strong electric field. The metal coats the tip of the needle and the electric field drives the formation of a Taylor cone at the tip of the needle.

LMIS has some physical similarities with electrosprays, the most evident being that it would seem to involve the same balance of electric pressure to capillary pressure over the majority of its cone – i.e. the cone is generally equipotential. Hence Taylor's explanation[15] of a cone protrusion could be correct. The major difference is that as a result of the far greater conductivity of the liquid metal the LMIS cone is more equipotential than in an electrospray process.

A strong relationship between the current and the voltage (the relationship between flow rate and voltage in LMIS has not been investigated as the flow rate is tiny ($\sim10^{-15}\ \mathrm{m^3s^{-1}}$) and rarely measured) has been found in LMIS. The current I has been found to have a linear relationship to voltage[96]

$$I = a\left(V/V_{ext} - 1\right) \tag{2.54}$$

where a is a constant that depends on the system geometry and source material, and V_{ext} is the 'extinction voltage', the voltage at which the cone-jet mode turns off (different from the onset voltage due to hysteresis). This 'extinction voltage' is a function of the geometry. Mair[96] derives the constant a to be,

$$a = \left\{3\pi\gamma\left(2e/m\right)^{1/2}\right\}V_{ext}^{-1/2}R_b\cos\alpha_T \tag{2.55}$$

where e is the elementary positive charge, m the mass of an atom of the sprayed liquid metal, R_b is the base radius of the Taylor cone, and α_T is the Taylor angle. The derivation of this equation is described in full by Forbes[97].

From Forbes[95], it is shown that the voltage is proportional to the current, and Mair[98] demonstrates that there is good correlation between experiments and the theory. The theory used takes into account the space charge effects of the spray, and Forbes states that:

> *It seems that the space-charge behaves in such a fashion as to "nearly cancel out" any increase in the total force on the emitter when voltage is increased. Some small increase in total force is needed to increase the flow rate and hence the emission current, but this is a second-order effect*[95].

Therefore like Hartman[61] a feedback system is used to account for the smaller than expected *I(V)* relationship[29]. Hartman though describes this feedback as a lack of change in electric field due to changes in geometry, whilst Mair describes the space charge increasing with voltage and canceling out any extra force from increases in voltage. For LMIS, with its high current, the space charge hypothesis would seem possible, but at lower conductivity electrospray space charge does not seem to be a driving process that defines the output parameters.

Further work is necessary to decide whether space charge has any great effect within electrospray. One indication that it perhaps does not is that the electrospray simulations described above found a relationship between current and voltage that approximately matches the experimental work, yet did not include space charge in the models[69]. Drawing any strong conclusions from a comparison between LMIS and electrospray is

difficult though as different driving forces are involved. Due to the far higher conductivity of a liquid metal than a typical electrospray solvent, the cone is considerably more equipotential in LMIS. This results in Maxwell normal stresses dominating in LMIS, whilst tangential stresses dominate in electrospray[95].

2.8.2. Nanoelectrospray

Nanoelectrospray differs from conventional electrospray by using emitters with very small tip diameters (1-2 μm), and very low flow rates of ~0.3 nL/s, without the use of pumping – i.e. the flow rate is not forced[99]. Instead the flow rate results from the application of a potential difference to the emitter.

Nanoelectrospray has shown that it is possible to initiate spraying from an increase in voltage, without the application of back pressure. This is often used in Electrospray Mass Spectrometry (ESMS) where a small emitter (often a drawn and metal-coated glass capillary) is filled with the analyte, which is held within the emitter by capillary action. The potential difference is then applied between the emitter and an opposing electrode, drawing out the liquid and resulting in an electrospray. Consequently the effect of voltage on flow rate is of fundamental importance to nanoelectrospray.

To illustrate the effect voltage has on nanoelectrospray a new term has been coined; Voltage Modulated Nanoelectrospray (VMES)[100]. By analyzing the high frequency oscillations within pulsed mode, Alexander *et al.*, characterized different modes within the pulsed regime that occurred at differing voltages, as described in Section 2.2.2. The authors were able to measure the current and flow rate across these subset modes, finding both increased with voltage within these regimes, with the exception of the Axial IIB mode where current decreased.

2.9. Conclusions – voltage effects in electrospray

Many studies have found an effect of the extractor voltage on the current and flow rate, although the magnitude of the relationship varies significantly.

In the most comprehensive study Smith *et al.* found the flow rate to have a linear relationship with voltage within cone-jet mode electrospray, and this relationship not to be affected by the conductivity of the solution or the starting flow rate[9]. Also ionic liquids were found to follow the same $Q(V)$ relationships as organic liquids.

The *Q(V)* dependence is affected by the inner diameter of the liquid, in a relationship that seems to be dependent on the hydraulic resistance. This effect can be removed by calculating the product of the gradient of the *Q(V)* relationship and the hydraulic resistance, giving the 'electric pressure sensitivity'. The *Q(V)* relationship seems though to have a second relationship to the emitter geometry although whether this is a result of the variation of the emitter inner or outer diameter remains undetermined.

The voltage modulation of flow rate has significant consequences for the operation of a colloid spacecraft propulsion system. It would seem to have opposing effects on the specific impulse and the thrust, allowing for variable performance.

Current also would seem to increase linearly with voltage, but unlike the *Q(V)* relationship the dependence is affected by the starting flow rate and conductivity. Also it would seem to be affected by the hydraulic resistance and the outer diameter of the emitter, in a manner very similar to the *Q(V)* effect.

This dependence of the *I(V)* relationship to various parameters, more parameters than the *Q(V)* relationship, probably results in the large variation of *I(V)* relationships found throughout the electrospray literature.

Various computational simulations of electrospray have demonstrated a possible linear current-to-voltage relationship. Although they agree reasonably with experimental results, it seems no attempt was made to provide a qualitative reason for the findings.

The voltage is a major factor in the physics of electrospray. The understanding of its relationship to other variables is not complete, but important insights have been found. More work is necessary to gain a greater understanding of the relationships.

Chapter 3

3. Experimental procedure

3.1. Methodology

This study has the aim to characterize the relationship between flow rate and the applied voltage within cone-jet mode electrospray. This has been extended to include enhanced dripping, pulsed and multi-jet modes. This was completed simply by running a typical experiment over a greater voltage range.

As described in the literature review, previous studies have discovered that the geometry of the emitter has an effect on the magnitude of the *Q(V)* relationship within cone-jet mode[9,72]. This research also focuses on these geometric issues, further investigating the geometrical dependence.

Initial experiments investigated the effect of emitter inner and outer diameter on the flow rate to voltage relationship, as these have previously been found to have an effect on the *Q(V)* relationship[9] (see Figure 2.13).

Secondly the effect of the emitter tip to extractor distance on the flow rate to voltage sensitivity was investigated. This was completed by using a translation stage to move the emitter perpendicular to the extraction electrode.

Thirdly the effect of the emitter length on the flow rate sensitivity to voltage was investigated. This was completed by varying the length of the emitter by adjusting a movable plate along the emitter length.

Finally some brief experiments were completed investigating the effect on the *Q*(*V*) relationship of the diameter of the aperture in the extractor electrode.

The flow rate was measured during the experiments by a high fidelity inline flow rate measurement system, whilst the current was measured by a potential divider system,

except for a few cases where a fast amplifier and oscilloscope were used. A known voltage was applied to the extractor electrode.

The experiments were completed at atmospheric pressure, rather than within a vacuum system with a pressure of fractions of a millibar. It has previously been established that the air pressure has little effect on the $Q(V)$ relationship[10], so it was deemed simpler to complete the experiments in an atmospheric system. Further, the highly accurate flow meter (previously used by smith[9,10,71]) which is integral to the study, is considerably more difficult to operate in a vacuum system (due to minute bubbles in the flow meter piping expanding under a strong vacuum[10]).

Running the experiments at atmospheric pressure does though make the results less directly applicable to colloid electrospray thrusters. The first aim of this study was though to investigate the effect of voltage on flow rate in a general electrospray system, and to relate the experimental work to an analytical model. This analytical model and experimental work then has significant repercussions on the applicability of the $Q(V)$ relationship to colloid thrusters.

To investigate the flow rate-to-voltage dependence with ease, a low viscosity solvent was chosen, since the magnitude of the $Q(V)$ relationship would seem to be dependent on the hydraulic resistance[9] (and hence viscosity). Low viscosity solvents though generally have a higher vapour pressure, and are thus less applicable to colloid electrospray thrusters. But the aim of this thesis was to investigate the general $Q(V)$ relationship, with the intention of an analytical application of the effect to a colloid thruster system, and experimental thruster work to be completed at a later date. It was deemed more important to collect excellent quality $Q(V)$ dependence data, with a simple system, rather than using a more complicated vacuum system.

3.2. Experimental System

A schematic of the experimental setup is illustrated in Figure 3.1, with the main components of the rig being the spray emitter, an extraction and collector electrode, a high voltage power supply, a flow measurement system, a camera, a voltmeter, and a PC. The emitter needle was held in a stainless steel bulkhead union by a vespel ferrule. For experiments varying the emitter outer and inner diameter, the union was held in place within a cage mount, and the cage mount was attached to four vertical poles that formed part of the stand (two are shown in figure 3.1). A wire was attached to the union, leading to a 1 $M\Omega$ resistor, and then to ground. The voltage drop across the large resistor was measured, forming the potential divider current measurement system.

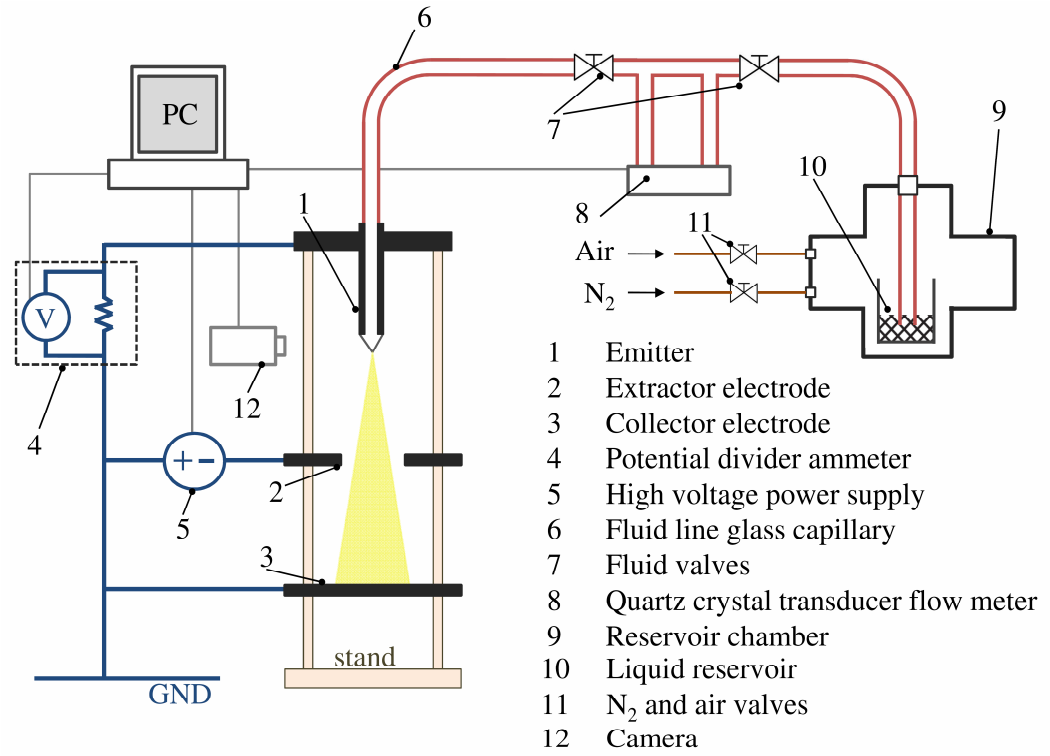

Figure 3.1. Experimental set-up.

Below the emitter another cage mount was attached to the four poles. This held the high voltage stainless steel extractor electrode, which was insulated by a PEEK holder. The extractor electrode was 20mm diameter, with generally a 6mm diam. aperture to allow the sprayed fluid to continue to the collector electrode below it.

On the underside of the extractor electrode the high voltage wire was attached. For the emitter outer diameter and inner diameter (o.d., i.d.), emitter length, and electrode aperture size experiments an emitter to extractor distance (z_0) of 3mm was chosen, so as to agree with previous experiments[72].

A fluid collector electrode, consisting of a small aluminium bowl with angled holes through to its underside, was positioned ~30 mm below the extractor ring electrode. The collector electrode was connected to ground.

The spraying liquid was supplied to the emitter from a solvent reservoir upstream by a glass capillary with an i.d. of 0.53mm. The fluid reservoir consisted of a glass beaker positioned within an X-piece stainless steel chamber. This insulated the reservoir from atmospheric effects, and allowed for nitrogen to be supplied to increase the pressure head. In all sprays conducted though, the pressure head was gravity driven, with nitrogen used only to fill the fluid lines.

In the capillary fluid line between the reservoir and emitter a highly accurate flow rate measurement system was attached, as described in Section 3.4.

The change in pressure as the reservoir drained was insignificant, as each spray used at most 0.5 millilitres of solvent, which resulted in a change in height of ~1.2 mm in the size of the reservoir used. This is small compared with the height difference between reservoir and emitter needed for a low nominal flow rate, of the order of 50 mm. In reality the change in height due to reservoir draining was less at low nominal flow rates, and thus the actual change in height was probably even smaller than this estimate predicts.

3.3. Experimental geometry

3.3.1. Choice of emitters

As shown in Table 3.1, two groups of emitter needles were tested; those with an approximately constant outer diameter of 800 μm and those with an approximately constant inner diameter of 100 μm. In the first set the i.d. was varied from 100 μm to 635 μm, each with an outer diameter of approximately 800 μm. In the second set the emitter outer diameter was varied from 200 to 1600 μm, with the i.d. constant at ~100 μm. All emitters tested were of length 50 mm, of which 31mm protruded from the emitter union.

Several of the emitters have large tolerances for the inner diameter, and therefore it was necessary to calculate the inner diameter. Assuming the emitter is straight with no internal protrusions, the calculated internal radius r_i is

$$r_i = \left(\bar{r}_e^2 - \frac{\overline{M}}{\rho \pi \overline{L}} \right)^{1/2} \tag{3.1}$$

where $\bar{r}_e$ the average measured external radius over ten measurements, $\overline{M}$ the average mass of the emitter over ten measurements, ρ the density of 316 stainless steel, and $\overline{L}$ the average length of the emitter, again over ten measurements. As illustrated in Table 3.1, once tolerances are taken into account the calculated inner diameters agree quite well with the manufacturers stated diameter.

The error of this internal radius calculation was sought to further corroborate the technique. Since the uncertainty of the emitter i.d. calculations depends on several variables an error propagation technique[101] was used to calculate the standard deviation of the calculated inner radius, r_i. Since $r_i = r_i\left(\bar{r}_e, \overline{M}, \overline{L}\right)$, the standard deviation is calculated by

$$\left(\sigma_{r_i}\right)^2 = \left(\sigma_{r_e}\right)^2 \left(\frac{\partial r_i}{\partial \bar{r}_e} \right)^2 + \left(\sigma_M\right)^2 \left(\frac{\partial r_i}{\partial \overline{M}} \right)^2 + \left(\sigma_L\right)^2 \left(\frac{\partial r_i}{\partial \overline{L}} \right)^2 . \tag{3.2}$$

After differentiating equation 3.1 with respect to each variable, this gives the following equation;

$$\left(\sigma_{r_i}\right)^2 = \left(\bar{r}_e^2 - \frac{\bar{M}}{\rho\pi\bar{L}}\right)^{-1}\left\{\left(\sigma_{r_e} 2\bar{r}_e\right)^2 + \left(\frac{\sigma_M}{\rho\pi\bar{L}}\right)^2 + \left(\frac{\sigma_L\bar{M}}{\rho\pi\bar{L}^2}\right)^2\right\}, \qquad (3.3)$$

where barred letters represent the mean of the variable. The standard deviations of the inner radius using this method are shown in Table 3.1. The values are generally small, demonstrating that radius estimation technique is valid, and that the emitters are well manufactured.

Table 3.1. Emitters, supplied by: [a]Upchurch Scientific, [b]Coopers Needles.

Manufacturers i.d., μm	Manufacturers i.d. Tolerence, μm		Calculated average o.d., μm	Calculated i.d., μm	Standard deviation of calculated i.d., μm
	+	-			
100[a]	50	0	818	144	17.5
150[a]	0	50	807	138	13.4
200[a]	0	50	808	184	36.2
250[a]	0	50	783	266	11.8
400[a]	0	50	814	350	14.7
450[a]	0	50	819	465	16.7
635[b]	15%	15%	806	644	6.2
101[b]	15%	15%	201	98	5.6
102[b]	15%	15%	277	107	7.5
127[b]	15%	15%	231	127	5.7
125[b]	15%	15%	1612	126	25.2
125[b]	15%	15%	517	155	5.2

3.3.2. Varying the emitter to extractor distance

The distance between the emitter tip and the electrode was varied by attaching the emitter union in an L-shaped piece of acrylic. To the vertical part of this acrylic a translation stage was attached, allowing for the variation of the emitter to extractor distance (z_0), as shown in Figure 3.2.

To calibrate the emitter tip to extractor distance a stainless steel block of known thickness was placed on the extractor electrode. Using the translation stage the emitter was moved towards the top face of the calibration block. The camera was used to visually confirm the point at which the emitter touched the block. This gave a calibration distance, and consequently it was possible to adjust the translation stage with knowledge of the emitter to extractor distance. The distance from the emitter tip (with no Taylor cone) to the electrode was varied from 0 – 13 mm, with the relative distance between the emitter and electrode measured to an accuracy of approximately 0.1 mm.

Two emitter needles were tested for the experiments investigating the effects of emitter to extractor distance– an emitter with an i.d. of 127 μm and an o.d. of 230 μm, and a second emitter with an i.d. of 155 μm and an o.d. of 510 μm. These were chosen since their different outer diameters would hopefully give considerably different values of the $Q(V)$ sensitivity at the same emitter to extractor distance, and thus highlight the $Q(V)$ sensitivity versus emitter to extractor distance trend at different magnitudes.

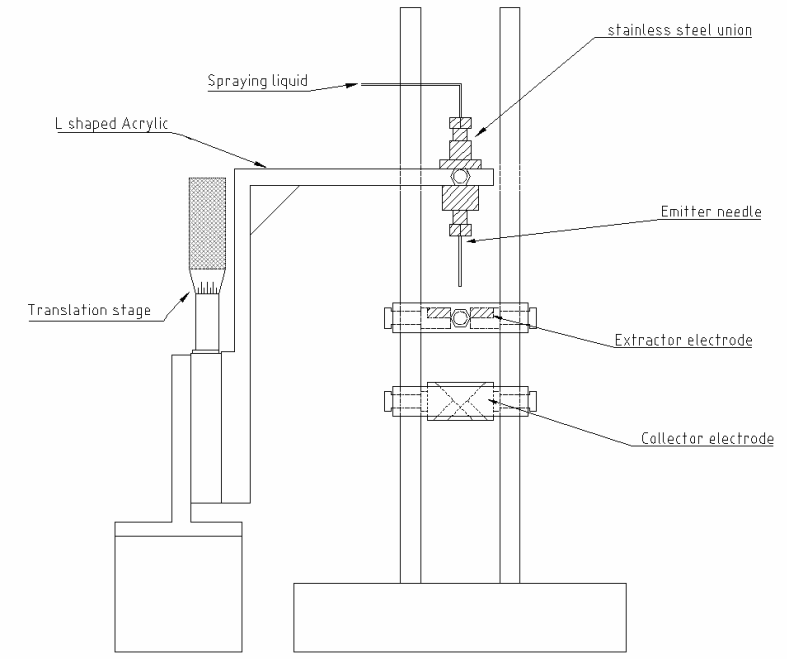

Figure 3.2. Experimental set-up for varying the emitter to extractor distance.

3.3.3. Varying the emitter length

Rather than using emitters with varying emitter lengths, the effective emitter length was varied, as shown in Figure 3.3. The emitter union and extractor electrode were held in place using the same method as the experiments investigating the effects of inner and outer diameter. An aluminium plate was attached to the underside of the horizontal part of the L-shaped acrylic piece. The aluminium plate was 20 mm wide and 64 mm long, with a thickness of two mm. The emitter was inserted through an aperture in the acrylic L-piece and the aluminium plate. The L-piece of acrylic was again attached to a translation stage, allowing for the horizontal aluminium plate to be moved vertically. Consequently the effective length of emitter seen by the extraction electrode was varied.

Varying the effective emitter length may not though be exactly the same electrostatically as varying the actual emitter length. For example, an actual 1mm long emitter would protrude from the stainless steel emitter union, which has a diameter of approximately 10mm. An emitter of effective length 1mm would protrude from a large flat conducting plate, and consequently there are significant geometrical differences from a real short

emitter. The aim here though is to demonstrate that using short emitters may have an effect on the $Q(V)$ sensitivity, and varying the effective emitter length will adequately illustrate this, whilst avoiding manufacturing issues.

The calibration of the effective emitter length was completed by adjusting the translation stage so that the emitter tip was flush with the surface of the aluminium plate. The emitter's effective length, the amount protruding from the underside of the aluminium plate, was varied incrementally from 0.5mm to 31mm, with an accuracy of approximately 0.1 mm.

The aluminium plate was electrically connected to the emitter union; therefore the aluminium plate used to vary the length the emitter and the emitter union were at ground.

The emitter used to investigate the effect of emitter length had an outer diameter of 810 μm and an inner diameter of 450 μm.

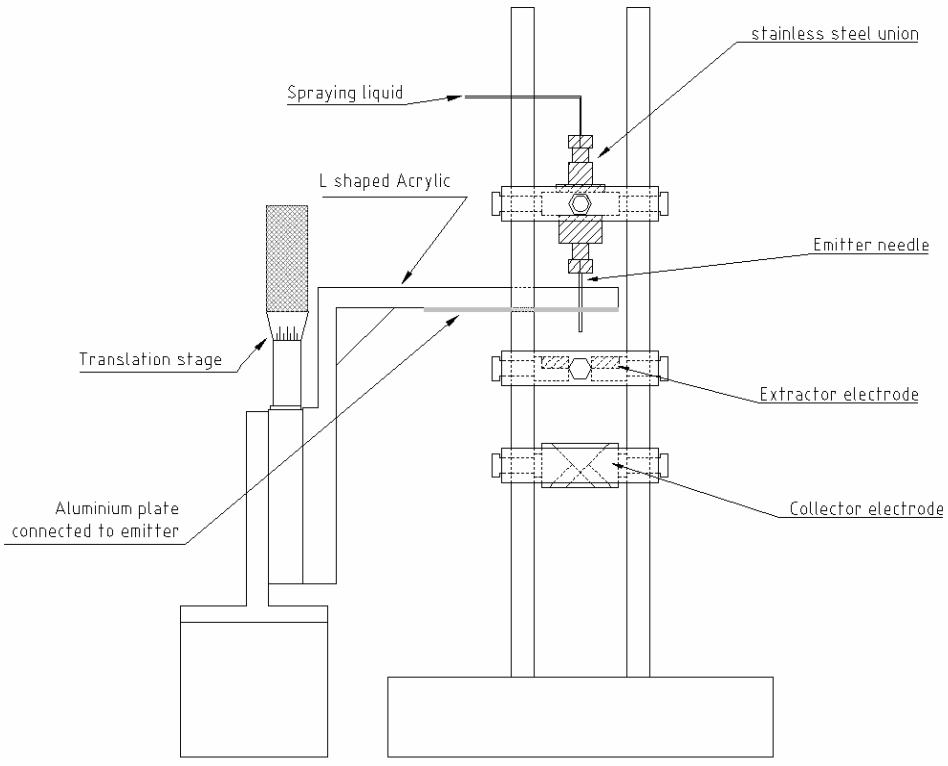

Figure 3.3. Experimental setup for varying the emitter length.

3.3.4. Varying the aperture in the extractor electrode

Some brief experiments investigating the effect of the diameter of the aperture through the extractor electrode on the various output parameters were completed. These were completed by testing four extractor electrodes, with 10, 6 (used in all other experiments), 3 and zero mm diameter apertures. All had a 20mm diameter and were 3mm thick. Two sets of tests were completed, one using a 1mm long emitter, and a second using a 10mm long emitter.

For the experiments using the extractor electrode with no aperture the sprayed solvent accumulated on the extractor electrode surface. To reduce the effect of this deposition the voltage was increased every 20 seconds, a time increment that was felt long enough to collect adequate data, but avoided significant fluid deposition.

3.3.5. Summary of geometry variations

Table 3.2 lists the various geometric variations that were tested, with the variable parameter shown in italic. For the emitter outer diameter varying experiments (geometry variation [2] in the table), there was some variation in the value of emitter inner diameter as well as outer diameter due to limitations on what emitters were available.

The emitter to extractor distance was tested twice (variation [3] and [4]), using emitters of different outer diameters. The variation of the diameter of the extractor electrode aperture (variation [6] and [7]) was also tested twice, using emitters of varying length.

Table 3.2. The geometric variations tested.

Geometric variation	Emitter inner diameter, μm	Emitter outer diameter, μm	Emitter to extractor distance, mm	Emitter length, mm	diameter of aperture in extractor electrode, mm
[1] Emitter inner diameter	*139 - 644*	810	3	31	6
[2] Emitter outer diameter	98 - 155	*200 - 1610*	3	31	6
[3] Emitter to extractor distance, 1st	125	230	*1 - 13*	31	6
[4] Emitter to extractor distance, 2nd	155	510	*0 - 15*	31	6
[5] Emitter length	465	810	3	*0.5 - 31*	6
[6] Extractor electrode aperture, 1st	465	810	3	1	*0 - 10*
[7] extractor electrode aperture, 2nd	465	810	3	10	*0 - 10*

3.4. Flow measurement System

It was anticipated that the flow rates tested would be of the order of 5-150 nLs^{-1}, and therefore a flow meter with an accuracy of greater than 0.1 nLs^{-1} was needed to read these flow rates, and the flow rate change with voltage, acceptably.

Smith *et al.* have previously designed such a high fidelity flow meter, and this measurement device was again used here for all experiments. Full details for this flow meter can be found elsewhere[10,71]; what follows is a brief overview.

The high accuracy flow meter consists of two pressure transducers positioned at two T-sections within the flow line, as shown in Figure 3.4. The Paroscientific digiquartz pressure transducers measure the pressure at two points in the fluid line, effectively measuring the pressure drop along the line connecting them. This pressure drop is proportional to the flow rate, via the Pouiselle equation, equation (2.42).

To protect the transducers, the tubing connecting them to the flow system was filled to a point below the T-sections with Dow Corning FS1265 silicone oil. For each transducer

the amount of buffer oil inline may vary slightly, resulting in each experiencing a slightly different pressure head. Also the length of vertical tubing from the transducers to the T-section may vary slightly. Therefore the Pouiselle equation is imprecise, and calibration is required. Calibration is completed by measuring the fluid mass out of the system over a certain time, and recording the difference in pressure between the two transducers. By doing this repeatedly for different reservoir head heights, a calibration line is produced, which can be used to convert pressure difference to flow rate[10].

The transducers output an RS-232 signal to a PC with a data logging program. The transducers have a total accuracy of 0.01% or better, and a maximum resolution of 1ppm at a sampling rate of ~1Hz. For details on the transducers and difficulties on filling the fluid lines, please see previous literature[10,71].

The transducers average the pressure over a certain time period, with the time period being chosen by the user. The best integration time period was found to be 0.134 seconds, with the data outputted about every 0.6 seconds, after taking into account the time for the data logging program to operate. This produced sufficient data over the time the voltage was held constant to produce an accurate average flow rate.

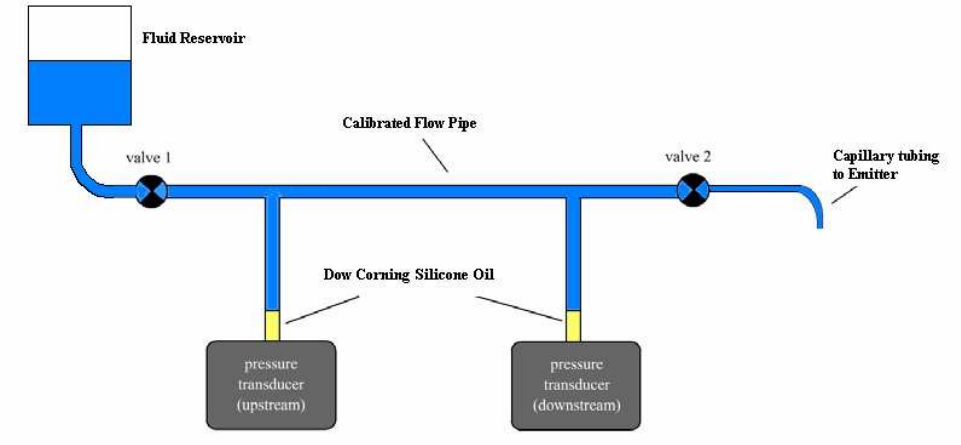

Figure 3.4. Flow rate measurement system. Courtesy of K. Smith[10].

The length and diameter of tubing between the transducers affects the resolution of the flow meter, so a careful choice of capillary must be made for this section. Although previously specially manufactured tubing had been used[10], it was found by experimentation that using a glass capillary as the calibrated flow pipe produced very acceptable results.

A smaller diameter or longer length capillary would produce greater resolution of results, but would result in a higher driving pressures being needed for a certain flow rate. This could result in the upstream transducer being over-pressurized; therefore careful selection of the tubing dimensions was needed.

The length of pipe needed can be estimated from the Poiseuille equation;

$$L = \frac{\Delta P \pi R_i^4}{8 \mu Q} \tag{3.4}$$

where ΔP can be taken to be the minimum pressure reading possible with the transducers (as stated by the manufacturer), R_i a chosen inner radius, and Q to be taken as the minimum flow rate for a particular fluid, with a certain dynamic viscosity μ. Q_{min} is the resolution flow rate, which in the case of propylene carbonate with a conductivity of 0.15S/m was calculated as 0.1nL/s. A capillary with a 0.125mm inner radius was chosen, and this resulted in a length of pipe of 0.5m.

3.5. Current measurement system

The current was measured at the emitter, to avoid complexities of measuring the current at high voltage, and to be sure that all the current was measured.

The current was measured using a potential divider system, which allowed for it to be recorded using an inexpensive and simple voltmeter. A drop in voltage due to the current of the electrospray was measured across a 1MΩ resistor. The voltmeter used was an ISO-TECH IDM 207 multimeter, chosen for its optical to RS-232 output allowing for data logging of the current to a PC. The IDM 207 has a logging period of 0.5s, and an accuracy of $\pm 0.06\%$ +2 digits. The data logging was accomplished using a program provided by the current meter manufacturer.

For some experiments involving emitters of shorter lengths, it was found that there seemed to be an effect of the pulsed mode frequency on the cone-jet mode onset voltage, which necessitated a faster current frequency measurement. The effect was investigated using a current amplifier attached to the emitter, feeding the resulting voltage signal to an oscilloscope. This system has the ability to measure the current within pulsation mode much more accurately, and importantly fast enough to measure the several 100 Hz frequency. The current amplifier used was a Femto DHPCA-100, connected to a Lecroy Wavesurfer 422 oscilloscope. This oscilloscope also has the advantage that it can complete a Fourier transform on the frequency signal, and in so doing give an immediate readout of the primary pulsation frequencies.

3.6. Camera system

The tests did not call for visual analysis of the spray; hence the camera was used only for checking the stability of the spray, and the mode at each voltage. A Navitar lens was used, whilst the camera was a JVC TK-S350 video camera.

3.7. High voltage power supply

The high voltage power supply (HVPS) used was an adapted FUG HCL 14-6500. This power unit was chosen as the high voltage output could be controlled by a small voltage input. A 0 -10 volt input to the power supply from a DAQ card corresponded to a 0 – 6.5 kV voltage output. The NI USB-6008 DAQ card was controlled by Labview through a PC.

This equipment permitted automated changing of the high voltage incrementally. It also allowed for more immediate and accurate changes in voltage than varying by hand offered. The Labview program was written so that the voltage could be changed after a certain time had passed.

The size of the voltage steps varied between 30 – 100V depending on the stable cone-jet voltage range. Each voltage was applied for between 20 seconds and 2 minutes, giving enough time to collect good flow rate data.
The high voltage applied to the ring extraction electrode was negative since it is easier to spray positive ions to a negative plate as air breaks down more easily when a positive voltage is applied to a flat plate.

3.8. Choice of electrospray fluid

It has been shown by previous electrospray studies that the voltage may only have a small effect on the current and flow rate of a system. Therefore to measure the effect of voltage requires highly accurate measurement apparatus, and these have been chosen. It has also been shown that a greater hydraulic resistance of the piping system significantly decreases the voltage effects on flow rate[9,72]. The hydraulic resistance is proportional to viscosity, so a liquid with low viscosity was chosen for these tests.
Various other fluid properties are important for choosing a liquid that would be straightforward to electrospray, and these include:

- Low surface tension is desirable as the onset voltage for spraying is proportional to surface tension (see equation 2.26). Too high a surface tension can result in a discharge voltage occurring before stable spray; this often occurs with pure water.
- The fluid should have a reasonable fluid conductivity. The minimum flow rate Q_{min} is inversely proportional to conductivity, so too high or too low conductivity would make it difficult to produce a stable spray or conversely to accurately measure the flow rate. The current is proportional to flow rate so the same rationale holds for current measurement.
- If a non-charged liquid is used then a high relative permittivity is needed. Relative permittivity is proportional to the amount of charged species a solvent can absorb, and therefore the possible conductivity range increases with a higher relative permittivity.
- Other important characteristics include the toxicity, the vapour pressure, and whether the liquid is hygroscopic.

After some consideration, propylene carbonate was chosen as the electrospraying solvent. The properties of propylene carbonate are shown in Table 3.3, with water and triethylene glycol (TEG) properties shown for comparison.

Propylene carbonate is a reasonably common solvent, used in lithium batteries, the cosmetic industry, and adhesives, amongst other applications. It has low viscosity, is non toxic but a mild skin irritant, classified as stable, decomposing to propylene glycol and CO_2 in the presence of an acid, base or metal oxide[102].

Different amounts of the salt Sodium Iodide (NaI) were added to propylene carbonate to investigate its conductivity range. The conductivity was measured using a Horiba B-173 conductivity meter, with an accuracy of ±2% full scale ±1 digit, and a range 1 to 199 μSm^{-1}. Figure 3.5 illustrates the conductivity of the solution varying with salt concentration, and shows that the solvent becomes saturated above a concentration of ~80gL^{-1}. It also shows that propylene carbonate has a large range of possible conductivities, with the pure solvent having a conductivity of around 10^{-6} Sm^{-1}.

After some initial testing, a concentration of 0.1 gL^{-1} of NaI in propylene carbonate was chosen for all experiments. This corresponds to a conductivity of 2.6×10^{-3} Sm^{-1}, which resulted in a stable cone-jet mode, with Q_{min} ~7.4 nLs^{-1}.

Table 3.3. Properties of solvents. Properties from reference [103] unless marked. 'a' – [102]. 'b' – [104].

Solvent	viscosity, cP	Relative permittivity	surface tension, Nm^{-1}
Propylene Carbonate	2.76[a]	63[a]	0.0452[b]
TEG	49.00	23.69	0.0452
Water	1.00	80.103	0.0726

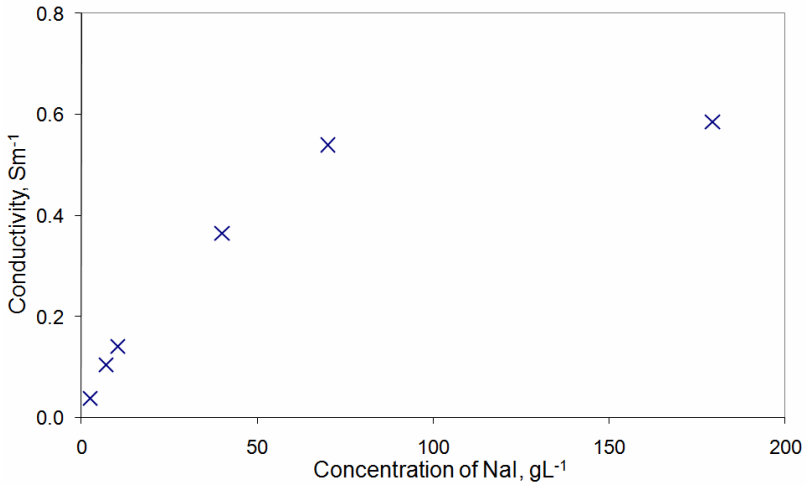

Figure 3.5. Conductivity of propylene carbonate with varying amounts of NaI.

3.9. Experimental method

For each electrospray experiment a gravitational pressure was chosen to obtain a certain flow rate. The pressure head was created from the height difference between the needle exit and the reservoir fluid level.

The valves in the fluid flow line were opened, and a flow rate reading was taken with no voltage applied to the extractor electrode, to identify the nominal flow rate, Q_{nom}. The voltage was then switched on, and the current logging started.

The voltage was increased incrementally using the Labview software, starting from enhanced dripping or pulsed mode, through the cone-jet onset voltage, and into multi-jet mode. For experiments investigating the effects of emitter inner and outer diameter, once multi-jet mode was reached the voltage was then decreased incrementally until pulsed mode was again observed.

Finally when the experiment was finished the voltage was turned off and the flow rate was measured again, to identify the finishing flow rate and any gravitational pressure drop that occurred during the experiment run.

Chapter 4

4. The effect of voltage on flow rate within cone-jet mode electrospray

Some of the results discussed in this chapter have been published in a peer reviewed journal[11]. This publication is included as Appendix A.

4.1. The sensitivity of flow rate to voltage whilst electrospraying

Previous studies have found a variation of the flow rate with the voltage in cone-jet mode[9,10,71,72]. This thesis, along with analysing the effect of geometry on the $Q(V)$ relationship, attempts to extend this analysis across the most common modes of electrospray; enhanced dripping, pulsed, cone-jet, and multi-jet modes. Figure 4.1 illustrates a typical trend of flow rate against voltage across these four modes of spraying.

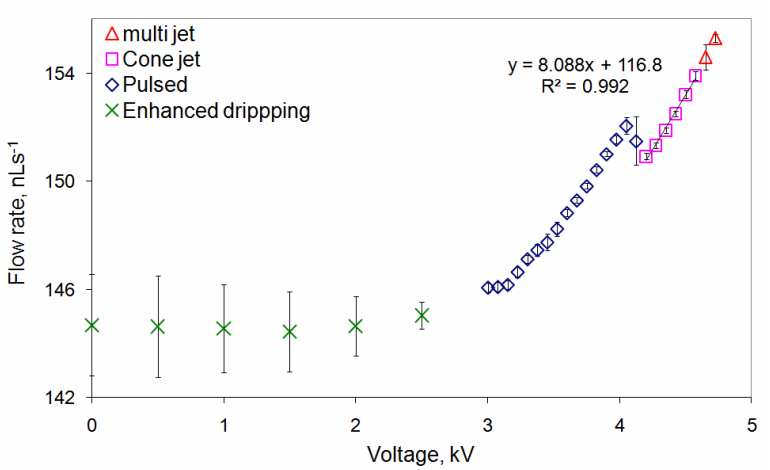

Figure 4.1. Average flow rate against voltage across whole range. Liquid sprayed propylene carbonate, $K = 2.6 \times 10^{-3}$ Sm^{-1}, $Q_{nom} = 144.7$ nLs^{-1}.

The average flow rate at each voltage increment has been calculated, whilst the error bars are the standard deviation of this mean.

From the figure there are evidently some differing relationships of flow rate to voltage across the four different modes. This chapter though deals solely with the effect of voltage on flow rate within cone-jet mode, and its variation with geometry. The remaining three modes (enhanced dripping, pulsed, and multi-jet), and the changes across the different modes, are described in detail in Chapter 6.

4.2. The effect of voltage on flow rate within cone-jet mode

Figure 4.2 illustrates a typical flow rate voltage relationship found whilst in the cone-jet mode of operation. The flow rate from the electrospray emitter increases with the voltage applied to the electrode. The effect very closely approximates linearity, demonstrating an *R*-squared value of greater than 0.99. The liquid electrosprayed was propylene carbonate doped with sodium iodide to a conductivity of $\sim 2.6\times10^{-3}$ S/m, as described in Chapter 3. The nominal flow rate (the flow rate occurring with zero voltage) was approximately 84 nLs^{-1}, whilst the '200' μm inner diameter emitter was used, as listed in Table 3.1 (the inner diameter was calculated to be 184 μm).

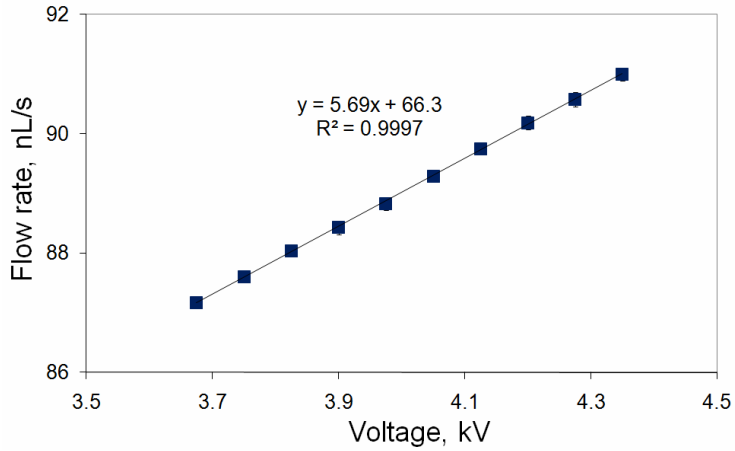

Figure 4.2. Effect of voltage on flow rate for Propylene carbonate + NaI.

Figure 4.2 was found to be typical of the effect of voltage on flow rate within cone-jet mode, illustrating a highly linear relationship. Over the several hundred experiments that were completed during this research the strong linearity was found repeatedly, and is in agreement with the linear relationship found previously[9,10,71].

The value of the gradient in Figure 4.2 is termed m_Q, the change in flow rate with voltage in cone-jet mode, with units nanolitres per kilovolt, chosen because of their unity-sized values. Prior to this research 2.64 $nLs^{-1}kV^{-1}$ was the largest value reported for m_Q[9]. But due to the lower viscosity of the solvent chosen for this work m_Q would be expected to be greater (because of its dependence on hydraulic resistance found previously[9]) and Figure 4.2 illustrates this, with a flow rate sensitivity to voltage of approximately 5.7 $nLs^{-1}kV^{-1}$, more than twice the previous maximum found.

4.2.1. Effect of nominal flow rate on m_Q

It is possible to spray in cone-jet mode over a large variation of flow rates solely resulting from fluid back pressure and with no voltage applied, termed nominal flow rates (Q_{nom}). Smith *et al.* found the cone-jet mode onset flow rate (which is proportional to Q_{nom} but slightly larger as shown in Figure 4.1) had no effect on m_Q, so it seems likely that the nominal flow rate has no effect on the flow rate sensitivity.

The effect of the nominal flow rate Q_{nom} on m_Q for the solvent propylene carbonate is illustrated in Figure 4.3, for an emitter with a '200' μm inner diameter. The *R*-squared value for the linear fitting of m_Q is at least 0.99 for all of the results shown, and the error bars representing the standard deviation for each linear regression line.

Although Figure 4.3 would not seem to show any trend of m_Q varying with Q_{nom}, a statistical method can be used to determine whether the nominal flow rate affects the $Q(V)$ sensitivity. To analyse whether the gradient of the line of best fit of Figure 4.3 is significantly different from zero, the test statistic t of the slope is calculated and compared to a critical value of the test statistic[105]. The test statistic is given by;

$$t = \frac{m - M_0}{\sigma_m} \tag{4.1}$$

where m is the experimental value of the slope, M_0 the hypothesized slope value, and σ_m the standard error of m. Assuming the theoretical gradient is zero ($M_0 = 0$) results in

$$t = \frac{m}{\sigma_m}. \tag{4.2}$$

For the data in Figure 4.3, m = -0.0032 and $\sigma_m = 0.0024$, which gives t = -1.32. Now if $|t| < t_{crit}$ then it can be said that the experimental slope is not significantly different from zero, and no significant slope is in evidence. For a two tailed test at level of significance α = 0.05, with eight degrees of freedom[105], t_{crit} = 2.306. Consequently in this case it can be concluded that m_Q does not depend on the nominal flow rate.
This method of statistical analysis of the effect of Q_{nom} on m_Q was repeated for other emitters of varying inner and outer diameter, with all demonstrating that the slope is not significantly different from zero. Consequently these experiments provide good evidence that there is no relationship between nominal flow rate and *Q(V)* sensitivity.

Figure 4.3 does though illustrate some considerable spread of results from experiment to experiment. This leads to the average m_Q (5.39 $nLs^{-1}kV^{-1}$) having a large standard deviation of 0.34 $nLs^{-1}kV^{-1}$. This deviation of flow rate sensitivity to voltage over multiple experiments is much larger than previously found[71,72], and could be a outcome of the lower viscosity of propylene carbonate resulting in small fluctuations in flow stability having greater effect.

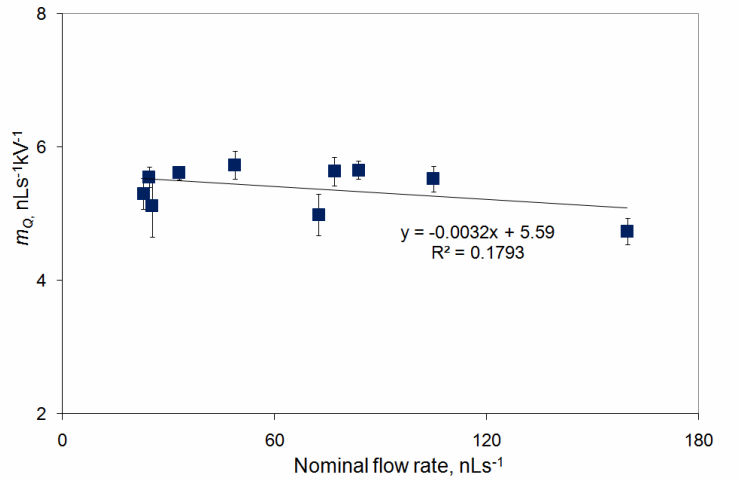

Figure 4.3. Variation of flow rate sensitivity with nominal flow rate, for emitter of inner diameter '200' μm.

4.3. Effect of inner diameter on m_Q

It has been previously established that the pipe system hydraulic resistance R_T affects the flow rate sensitivity to voltage[9,72]. The system hydraulic resistance consists of the summation of the hydraulic resistances from all differing sections of the piping;

$$R_T = R_1 + R_2 + R_3 + \ldots R_n. \tag{4.3}$$

Whilst the hydraulic resistance is given by;

$$R_n = \frac{8\mu L}{\pi r_i^4} \tag{4.4}$$

with units Nsm^{-5}. For the experiments completed only the emitter needle was changed, with the remainder of the pipe system's hydraulic resistance remaining constant.

Keeping the emitter outer diameter constant the effect of inner diameter was explored, as shown in Figure 4.4. The data used represents the average change in flow rate with voltage for each emitter, with an experimental sample of at least eight experiments for each emitter. The error bars represent the standard deviation of the m_Q value, over the

experiments completed for each emitter. The emitters used had outer diameters of approximately 800 μm (as described previously in Table 3.1 and illustrated here again in Table 4.1), and the values for inner diameter (i.d.) calculated in the manner described in Section 3.3.1.

Table 4.1. Emitter Geometries with varying inner diameter (i.d.).

Manufacturers i.d., μm	Calculated average o.d., μm	Calculated i.d., μm	Standard deviation of calculated i.d., μm
100	818	144	17.5
150	807	138	13.4
200	808	184	36.2
250	783	266	11.8
400	814	350	14.7
450	819	465	16.7
635	806	644	6.2

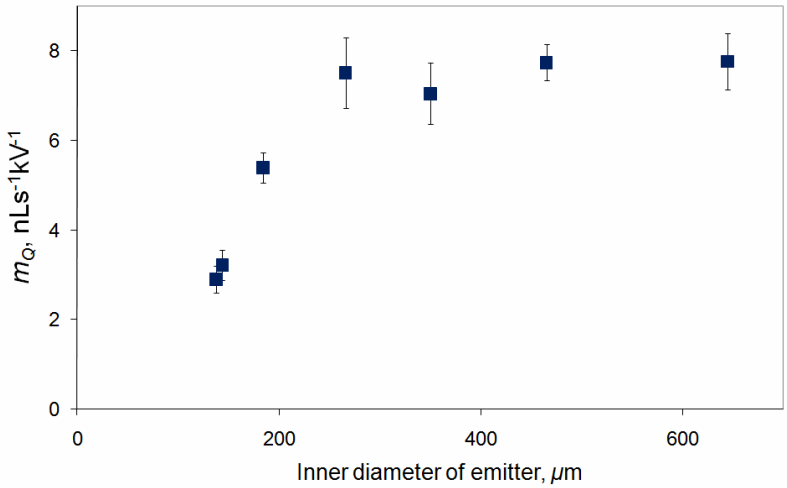

Figure 4.4. Variation of flow rate sensitivity with inner diameter of emitter.

The rate of change of flow rate with voltage does not appear to vary significantly until the inner diameter of the emitter is small. This is also the case for the total system hydraulic resistance, for as the emitter i.d. decreases its resistance becomes a larger part of the total piping system hydraulic resistance, whilst for a large i.d. emitter its resistance is insignificant compared to the upstream piping resistance. This strongly suggests that the change of m_Q with inner diameter is directly attributable to variations of the total system hydraulic resistance.

As described in Section 2.6.1 it is possible to remove the effect of the hydraulic resistance by determining the change of electric pressure with voltage, m_{pe}

$$m_{pe} = m_Q R_T, \tag{4.5}$$

which has units PaV^{-1}. The average m_{pe} against emitter inner diameter is plotted in Figure 4.5, with the errors bars on representing the standard deviation of the average value of m_{pe}.

The figure demonstrates an approximately constant value of m_{pe} for different inner diameters. A slight decreasing trend is noticeable for smaller inner diameters, but it seems likely this is a result of errors in the hydraulic resistance calculations when the average i.d. is small.

To attempt to confirm there is not a trend between m_{pe} and emitter i.d. the same t statistic method used for m_Q against Q_{nom} was again applied. It was found that the test statistic had a value of 2.26, whilst for a two tailed test at level of significance $\alpha = 0.05$ with five degrees of freedom the critical test statistic was 2.57. Therefore $|t| < t_{crit}$, and the gradient is not significantly different from zero. Consequently it can be concluded that the variation of the flow rate sensitivity to voltage with emitter inner diameter is predominantly a result of the varying hydraulic resistance.

This effect of hydraulic resistance on flow rate sensitivity may go some way to explain why changes in flow rate are often found to be marginal. It is conceivable that some previous studies have used systems with high hydraulic resistance, and consequently found little change of flow rate with voltage.

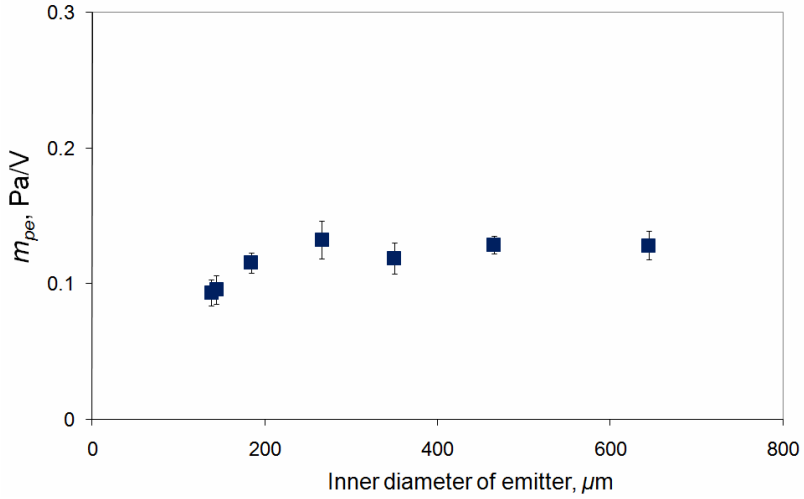

Figure 4.5. Effect of inner diameter on electric pressure sensitivity.

4.4. Effect of outer diameter on m_Q

Smith *et al.* found a strong dependence of flow rate sensitivity to voltage with the emitter diameter, but could not discern between the effect of the emitter inner and outer diameter due to the emitters i.d. and o.d. scaling with each other[72]. In the experiments conducted here, by keeping the emitter inner diameter approximately constant it was anticipated that a clear distinction could be made between the effect of the inner and outer diameter.

Using emitters listed in Table 3.1, reproduced here as Table 4.2, the emitter i.d. was kept at approximately 100 μm, whilst varying the outer diameter (o.d.) from 200 to 1600 μm. Again, it was found that the nominal flow rate did not influence the flow rate dependence on voltage, and as a result it was possible to calculate an average m_Q for each emitter. The variation of this average with emitter o.d. is illustrated in Figure 4.6, with the error bars the standard deviation of the average m_Q. Again all the m_Q values included had an *R*-squared regression fitting of at least 0.99.

Table 4.2. Emitter Geometries for emitter outer diameter (o.d.) varying experiments.

Manufacturers inner diameter, μm	Calculated average outer diameter, μm	Calculated inner diameter, μm	Standard deviation of calculated i.d., μm
100	818	144	17.5
150	807	138	13.4
101	201	98	5.6
102	277	107	7.5
127	231	127	5.7
125	1612	126	25.2
125	517	155	5.2

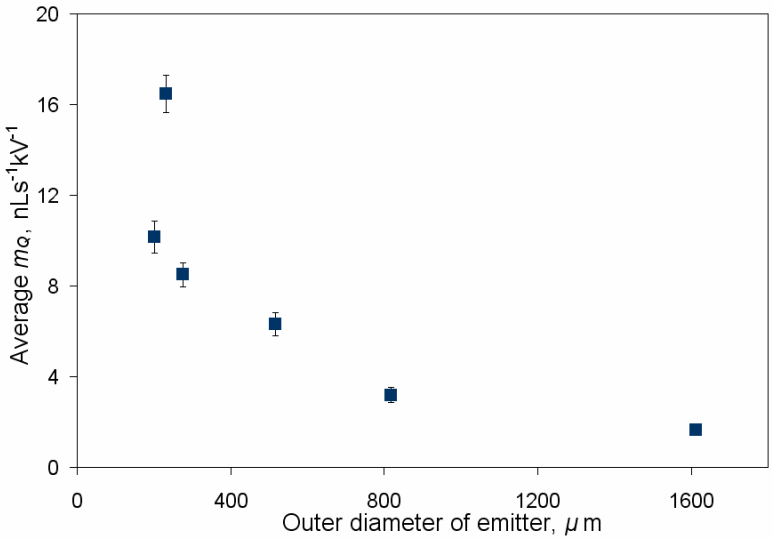

Figure 4.6. Effect of emitter outer diameter on flow rate sensitivity to voltage.

There is an apparent increase of the sensitivity of flow rate to voltage as the emitter outer diameter decreases, but also a seemingly anomalous result is evident. This inconsistent data point occurred with the emitter of 127μm i.d. and 231μm o.d., giving a mean value of m_Q = 16.8 ± 0.6 nLs^{-1}kV^{-1}. This possibly erroneous result gave the largest value of m_Q found so far, over six times greater than the largest value from preceding studies.

Closer analysis has revealed the anomalous point is in fact consistent with the other results. The emitter in question had a somewhat greater inner diameter than other emitters with similar outer diameters. The two other emitters with outer diameters of the order 200 μm, 201 and 277 μm respectively, were found to have inner diameters of 98 and 107 μm respectively. These inner diameters are ~20 μm smaller than the 231 μm o.d. emitter. Since the hydraulic resistance varies greatly when the inner diameter is small, this slight variation of inner diameter has a large effect on the flow rate dependence to voltage.

Once the electric pressure sensitivity m_{pe} is calculated and the effect of hydraulic resistance removed, as shown on Figure 4.7, the anomalous point collapses on to the experimental best-fit line, and a distinct trend is shown. The error bars illustrate the standard deviation of the average value of m_{pe}. Also shown is the regression fit line from Alexander *et al.*[72], where m_{pe} was found to vary with emitter outer diameter to the power -1.4. Theses previous results agree well with the experimental results found here.

Figure 4.7 demonstrates there is a convincing relationship between m_{pe} (or m_Q) and the outer diameter of the emitter.

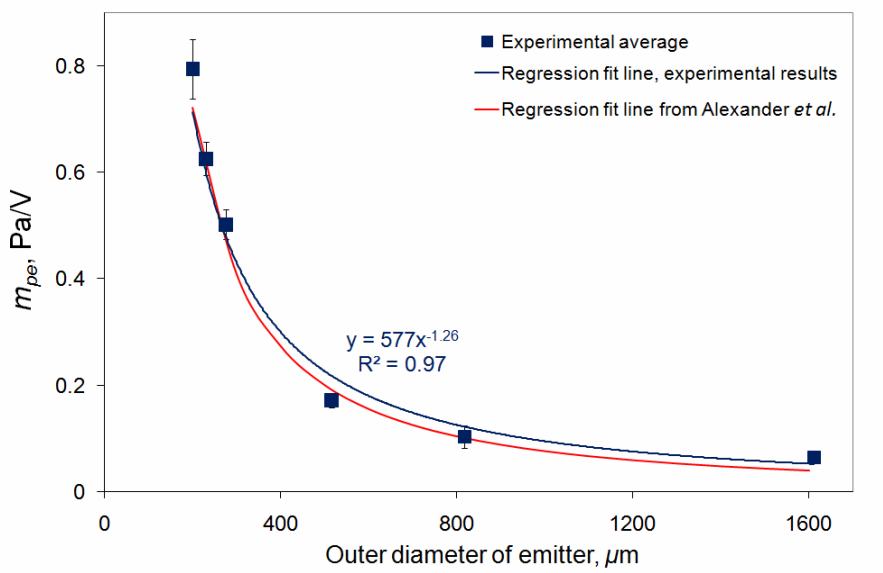

Figure 4.7. Effect of outer diameter on electric pressure sensitivity to voltage.

4.5. Theoretical variation of m_{pe} with outer diameter of emitter

As it is the sensitivity of electric pressure that varies with geometry, it would seem likely that the $Q(V)$ relationship is driven by the electric field; hence electrostatics may be able to provide an explanation of the dependence. As derived in Section 2.3.2 a simplified equation for the electric field at the emitter tip is

$$E_0 = -\frac{\phi_0}{A_1 r_e \ln\left(4z_0 / r_e\right)}, \tag{4.6}$$

where A_1 is a constant of the order unity, ϕ_0 is the potential difference between the emitter needle and the plate electrode, z_0 is the distance between an emitter tip and the extractor plate (the emitter to extractor distance), and r_e is the outer radius. Different authors have derived different values for A_1; Loeb[43] finds a value of 0.707, whilst Jones[44] derives 0.5, and others have found analytical functions of z_0 and r_e amongst other parameters[106]. Here we will allow A_1 to be adjusted to fit theoretical to experimental data, as done previously when comparing theoretical to experimental cone-jet onset voltages[37]. If one assumes a perfectly conducting liquid it is possible to ignore tangential stress terms, and the electric stress can be given by

$$\begin{aligned} P_e &= \tfrac{1}{2}\varepsilon_0 E_0^2 \\ &= \tfrac{1}{2}\varepsilon_0 \left(\frac{\phi_0}{A_1 r_e \ln\left(4z_0 / r_e\right)} \right)^2 . \end{aligned} \tag{4.7}$$

Differentiating with respect to ϕ_0 gives

$$\frac{dP_e}{d\phi_0} = \frac{\varepsilon_0 \phi_0}{\left(A_1 r_e \ln\left(4z_0 / r_e\right)\right)^2} . \tag{4.8}$$

This can be thought of as the variation of theoretical electric pressure with voltage, and may be compared to m_{pe}. Both this analytical value and the experimental values for m_{pe} are plotted on Figure 4.8, and demonstrate similar trends. Here A_1 is set to a value 0.5, and ϕ_0 is taken to be the onset voltage, measured experimentally for each different o.d. emitter.

The analytical (theoretical) values of the electric pressure sensitivity resulting from equation (4.8) are dependent on the constant A_1. The least squares best fit of theoretical to experimental results occurs when $A_1 \approx 0.37$, as also shown in Figure 4.8. This is within the range for A_1 calculated by Pantano *et al.*[106]. Once A_1 is adjusted in this way a very good correlation is demonstrated, suggesting that the underlying sensitivity for m_{pe} (or m_Q) is as characterised by this simple analytical approach. This, as far as the author knows, is the first time that a reason for the variation of the $Q(V)$ sensitivity with outer diameter has been demonstrated, and forms a part of a peer reviewed paper[11].

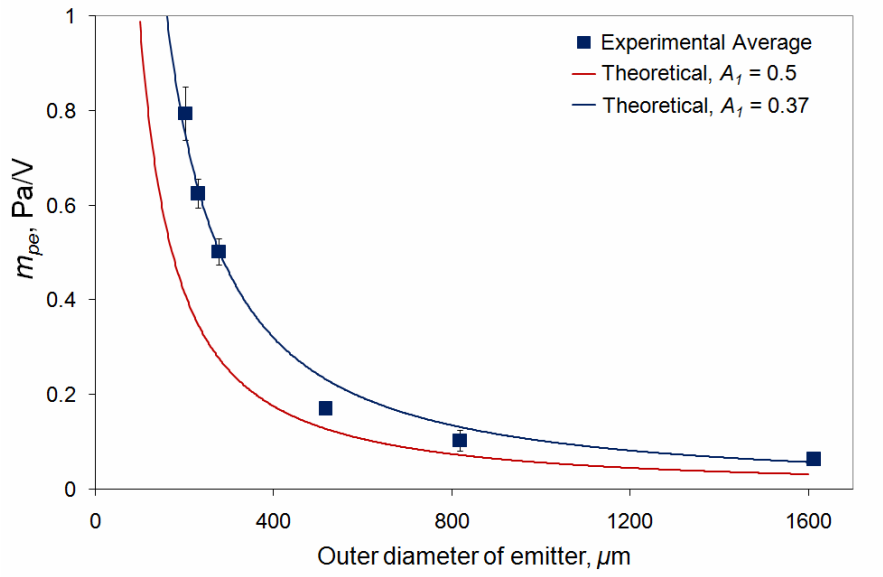

Figure 4.8. Variation of the electric pressure with voltage, as the emitter outer diameter changes: comparison between theoretical and experimental results.

A question however still remains regarding the validity of varying A_1, required as a disposable parameter to fit the experimental observations. It is worthwhile noting that although Jones[44] and Loeb[43] use different initial assumptions of the emitter shape (Jones starts with a simple line of charge, whilst Loeb assumes a hyperboloid), they derive the same electric field equation with the exception of the value of A_1. This suggests that A_1 may be a corrective factor that can partially take into account the shape of the tip.
It should be noted that equation (4.7) is solely used as an intermediary to calculate the change in electric stress with voltage, and not to calculate the liquid pressure in the liquid meniscus, as this is invalid without an analysis of the cone shape. There will be an influence of meniscus shape on the overall pressure, and as the cone shape was found to vary with voltage (as found by other studies[10]), also on the change in overall pressure with voltage. For a full description this must be taken into account. Presented here is only a first order analysis of the change of pressure with voltage, which fits remarkably well with experimental results.

Equation (4.8) is further complicated by the use of the onset voltage within it. This varies considerably for varying emitter outer diameters, as illustrated in Figure 4.9 (this experimental data was used in the theoretical calculation).
The onset voltage can be kept constant across the emitters with differing outer diameters, as demonstrated in Figure 4.10. The onset voltage is kept constant with two different values, corresponding to the highest and lowest experimental onset voltages found, illustrated. There is little difference between these two trend lines, which suggests that the onset voltage does have a noticeable effect but it is marginal compared to the overall trend.

The variation of the onset voltage with geometry is described in more detail in the next chapter of this thesis.

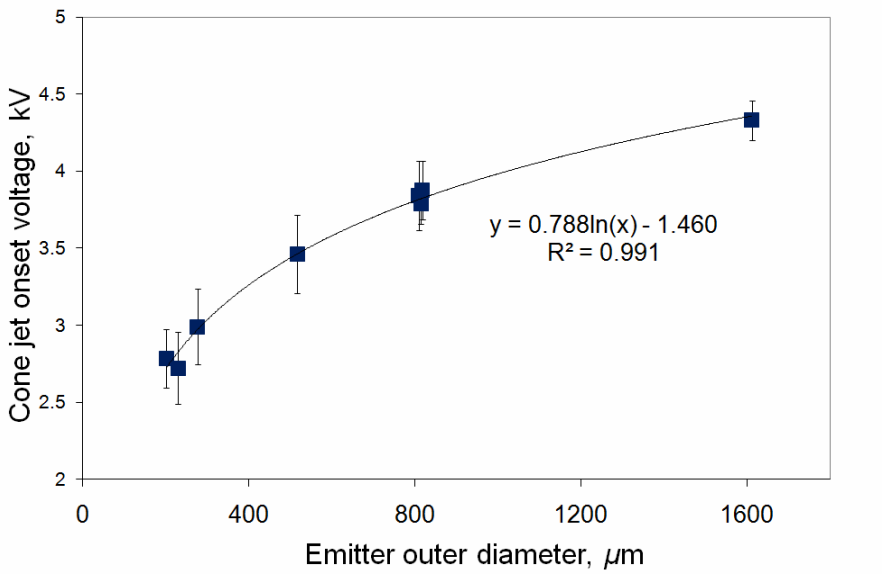

Figure 4.9. Variation of cone-jet onset voltage with emitter outer diameter.

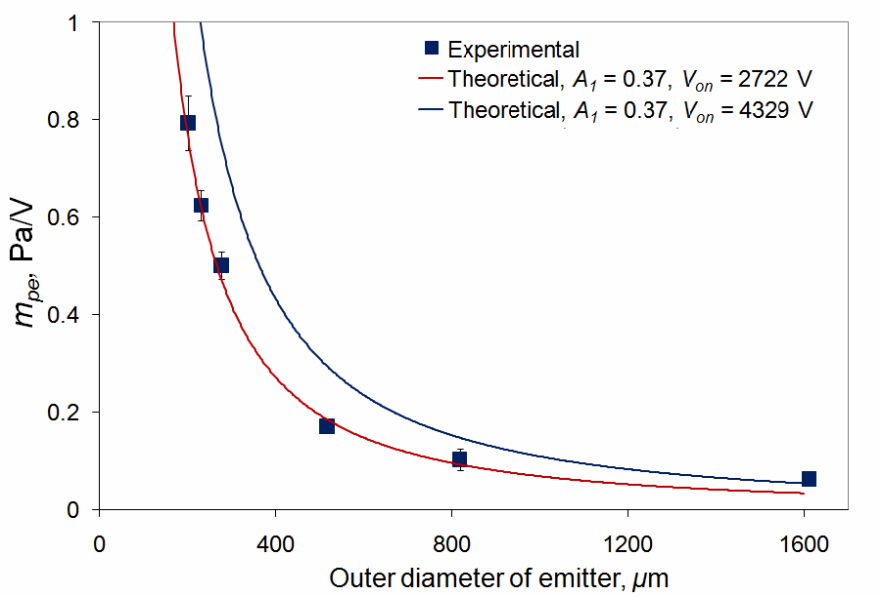

Figure 4.10. Variation of experimental and theoretical m_{pe} with emitter o.d. Two theoretical lines are shown; with constant V_{on} = 2722 V, and 4329 V.

Various other limitations on the experimental to theoretical comparison also exist.
To avoid the accumulation of the sprayed solvent on the electrode the experiments used an extractor electrode with a 6mm diameter aperture. The theoretical evaluations on the other hand are based upon a simple infinite flat electrode. Intuitively it would seem that an aperture in the electrode would reduce the effect of changes in voltage on the electric field (as the unipotential lines can bulge out more though the aperture, spreading out and therefore reducing the electric field), although this cannot be resolved without the use of finite element analysis software to model the field in detail. Experiments investigating the effect of differing sized electrode apertures have been completed, and are described in Section 4.10.

Also the effect of the charged droplets between the emitter and extractor electrode (space charge) has not been considered. Although space charge will have an effect, especially for highly conductive fluids, in this initial analysis it is assumed to be secondary.

There is some question as to how accurately equation (4.6) describes the electric field for certain emitter geometries[107], as it is a simplification of a more complex equation under the assumption that $z_0 >> r_e$ (see Section 2.3.2). Alternatively the more complex electric field equation (2.23) can be used to calculate the change in electric pressure with voltage, resulting in

$$\frac{dP_e}{d\phi_0} = \frac{\varepsilon_0 \phi_0 \left(1 + r_e / z_0\right)}{\left(A_1 r_e \ln\left[\frac{r_e + 2z_0 + 2\sqrt{z_0\left(z_0 + r_e\right)}}{r_e} \right] \right)^2} . \tag{4.9}$$

A comparison between equations (4.9) and (4.8) is shown in Figure 4.11, with the two equations predicting almost the same result. Experimentally the emitter to extractor distance (z_0) was kept constant at 3mm, whilst the largest emitter tested had a radius of 0.806 mm. So although z_0 was always greater than r_e, with the largest emitter it was only

approximately three times greater, so the assumption that $z_0 >> r_e$ is incorrect. Therefore it is a little surprising that equations (4.8) and (4.9) agree so well.

There is also another reason why equation (4.9) should produce more accurate results for when z_0 is greater than r_e. As a result of both z_0 and r_e defining the hyperboloid coordinate η (as in equation 2.20 (b), Section 2.3.2), the hyperboloid surface more resembles a sharp long emitter when z_0 is considerably greater than r_e[107].

These complications in comparing experimental and theoretical results do not influence the basic argument of the theory - the variation of the flow rate sensitivity to voltage with outer diameter results from variations in the electric field sensitivity to voltage, with outer diameter. Very good agreement is found between experiments and theory, strongly suggesting that the theory is valid.

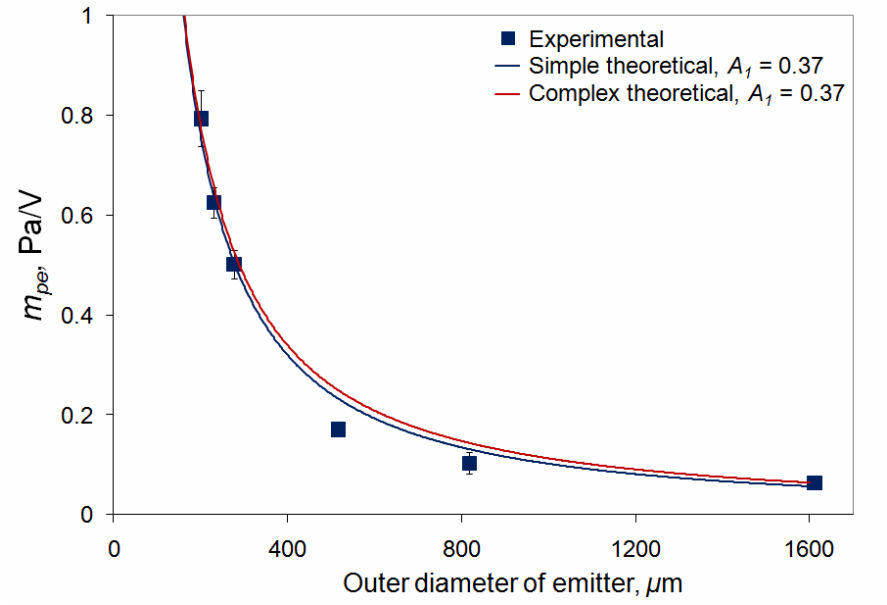

Figure 4.11. m_{pe} against emitter outer diameter. Comparison between experimental and the two theoretical results.

4.6. The effect of emitter to extractor distance on m_Q

Equations (4.8) and (4.9) imply that that the emitter tip to extractor electrode distance z_0 may also influence the flow rate sensitivity to voltage, with sensitivity increasing with decreasing distance. Further experiments have been completed to investigate whether this predicted effect occurs, and are described in this section.

The effect of electrode to emitter distance on m_Q is illustrated in Figure 4.12 and Figure 4.13. Two emitters were tested, one with 230 μm outer diameter, and a second with a 510 μm outer diameter. Both emitters were 31mm in length, with the geometry variation described in Table 3.2 as numbers [3] and [4]. The emitter to extractor distance was varied by the use of a vertical translation attached to the emitter, as described in section 3.3.2, with the distance measured from the tip of the emitter to the extractor electrode, ignoring the Taylor cone meniscus. For the emitter with a 510 μm outer diameter experiments were completed with an emitter to extractor distance of zero; this was possible as the extractor electrode had a 6mm aperture (see Table 3.2).

The same effect was in evidence for both emitters; as the distance from the emitter tip to the electrode decreases, the flow rate sensitivity to voltage increases. The 230 μm outer diameter emitter demonstrated an asymptotic behaviour at greater electrode to emitter distances, and the second larger emitter also suggests a levelling out of the relationship. As far as the author is aware, this is the first time that the emitter to extractor distance has been shown to have an effect on the Q(V) relationship.
At an emitter to extractor distance of 1mm, the 230 μm outer diameter emitter had an average m_Q of 19.5 ± 0.8 $nLs^{-1}kV^{-1}$, the largest value for m_Q found.

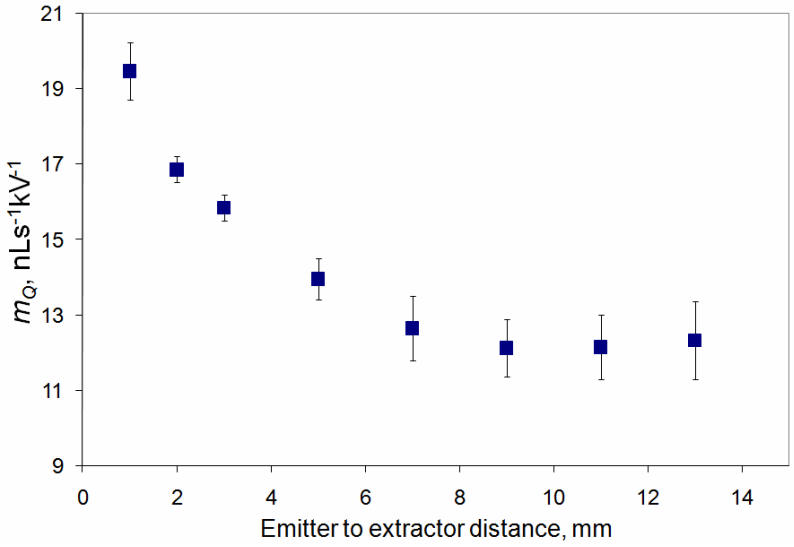

Figure 4.12. Variation of m_Q with electrode to emitter distance, for emitter of inner diameter 127 μm, and outer diameter 230 μm.

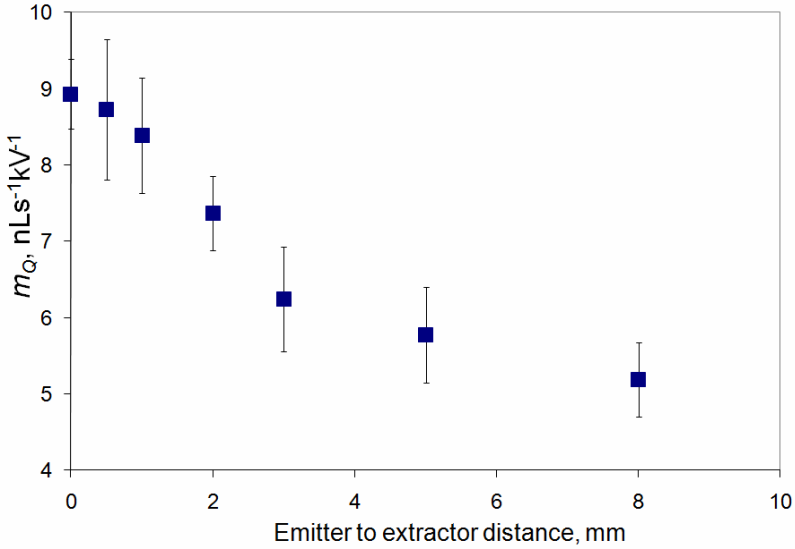

Figure 4.13. Variation of m_Q with electrode to emitter distance, for emitter of inner diameter 155 μm, and outer diameter 510 μm.

4.7. Effect of emitter to extractor distance on m_{pe}

The experimental value for the change in electric pressure with voltage (m_{pe}) can be compared to the theoretical value as the emitter to extractor distance varies. The simplified version of the theoretical result, equation (4.8), was used, and the results for the two emitter to extractor distance (z_0) varying experiments are illustrated in Figure 4.14 and Figure 4.15. A_1 was adjusted to give the smallest sum of the squares of the residuals of the difference between the theoretical and experimental results for both z_0 varying experiments and r_e (outer diameter) varying experiments. The best value found was A_1 = 0.41, which compares well with the value found for solely r_e varying experiments, A_1 = 0.37.

Within equation (4.8) ϕ_0 was again taken to be cone-jet onset voltage, estimated from experimental results.

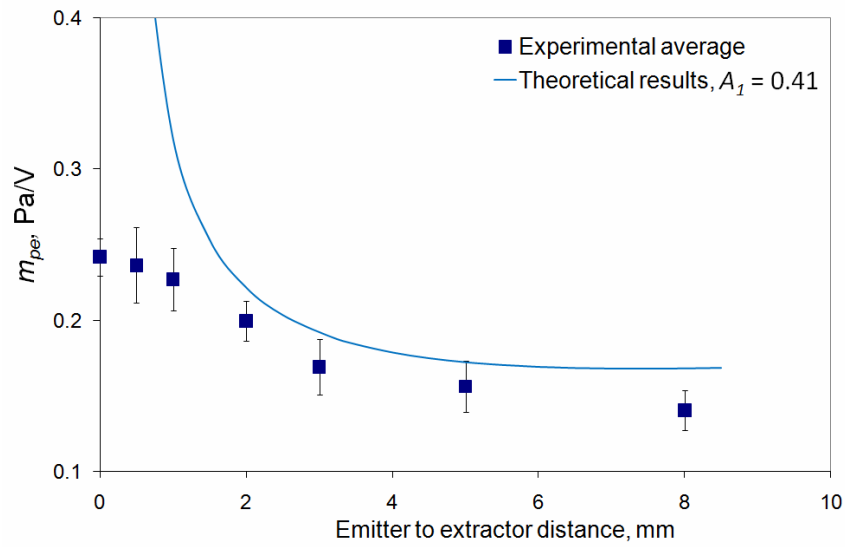

Figure 4.14. Variation of experimental and theoretical m_{pe} with emitter to extractor distance for emitter of outer diameter 510 μm, and inner diameter 155 μm.

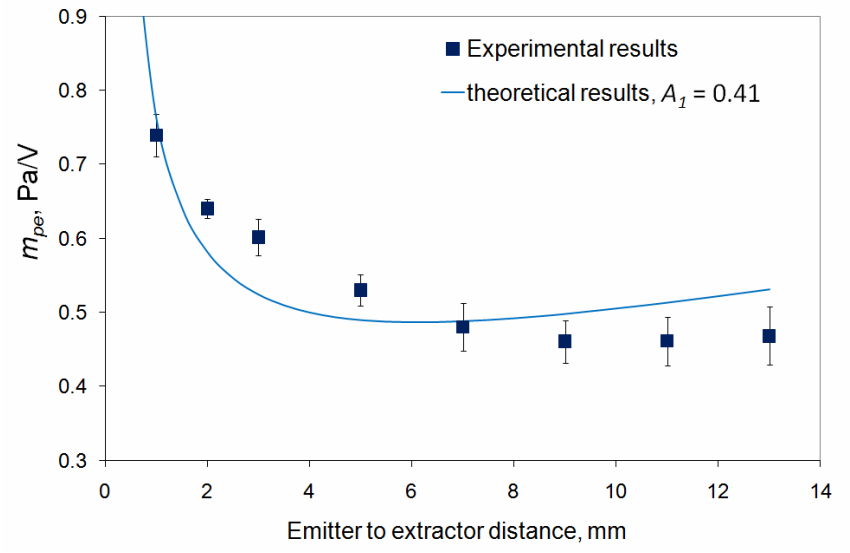

Figure 4.15. Variation of experimental and theoretical m_{pe} with emitter to extractor distance, for emitter of outer diameter 230 μm, and inner diameter 125 μm.

Figure 4.14 and Figure 4.15 illustrate the theoretical solution is not as accurate when calculating the variation of m_{pe} with z_0 as it was for varying emitter outer diameter. The general trend is though correct, with both the theoretical and experimental m_{pe} increasing with decreasing z_0, suggesting the theory is capturing the underlying physical mechanism.

For the experiments using an emitter with an outer diameter of 510 μm (Figure 4.14) there is considerable deviation between theoretical and experimental results as z_0 becomes smaller. This is likely a result of the theoretical equation only being applicable when $z_0 >> r_e$ (see Section 2.3.2). The theoretical and experimental results deviate for the 510 μm o.d. emitter when $z_0 < 2$ mm, giving a $r_e : z_0$ ratio of ~1:7.75. The smallest ratio for the experiments using the 230 μm o.d. emitter (Figure 4.15) is when z_0 is 1mm, giving r_e: z_0 value of 1: 8.7, and it seems clear that if z_0 had been decreased any further for this emitter then the deviation between experimental and theoretical results would be considerable.

As with the experiments involving the variation of the emitter outer diameter, there may be some effect of the cone-jet onset voltage on the theoretical value of m_{pe}. The experimental value of the onset voltage was used in the calculation of equation (4.8), with the onset voltage increasing with emitter to extractor distances, as would be expected (this is investigated more in Section 5.4 of the following chapter). The effect of using a constant cone-jet onset voltage (V_{on}) on the theoretical variation of m_{pe} with z_0 is shown in Figure 4.16 and Figure 4.17 for the two emitters tested. The simple theoretical model has been used (equation (4.8)), with A_1 adjusted to 0.41. On each chart two theoretical lines are shown, one using a constant voltage in the calculation equal to the maximum experimental cone-jet onset voltage, whilst the second uses a constant voltage equal to the minimum experimental cone-jet onset voltage.

For the experiments using an emitter with an outer diameter of 230 μm, the theoretical results (when using the experimental values of V_{on}) increased at large emitter to extractor distances, as shown in Figure 4.15. By though using a constant voltage in the theoretical calculation the theoretical result continues decreasing for higher values of z_0, as illustrated in Figure 4.17. This suggests that at greater values of z_0, the onset voltage can have a significant effect on the value of m_{pe}, and that possibly the leveling out of the experimental m_{pe} as the emitter to extractor distance increases is a consequence of the increase in V_{on} canceling out any decrease in m_{pe}.
At first glance the theoretical result would seem to have a greater dependence on the onset voltage when z_0 varies than when the emitter outer diameter varies – in Figure 4.10 there would seem to be less difference between the theoretical result when maximum and minimum onset voltages are used, than with for the z_0 varying data, Figure 4.16 and Figure 4.17. This though would seem to be an illusion resulting from the greater range of m_{pe} when the emitter outer diameter varies.

In summary the theory was correct in that it identified the emitter to extractor distance as a factor that would affect the value of m_Q. The general relationship predicted by the theory is correct, in that it predicts an increasing of m_Q as z_0 decreases. It is though not

good at predicting m_{pe} (and hence m_Q) for a certain z_0 distance, even once the A_1 value has been fitted.

The complex version of the model was also applied (equation (4.9) - data not shown), with no improvement found.

The theory would seem to be missing some detail. This could be a result of the theory breaking down if $z_0 >> r_e$, or a result of the specific cone geometry having an effect.

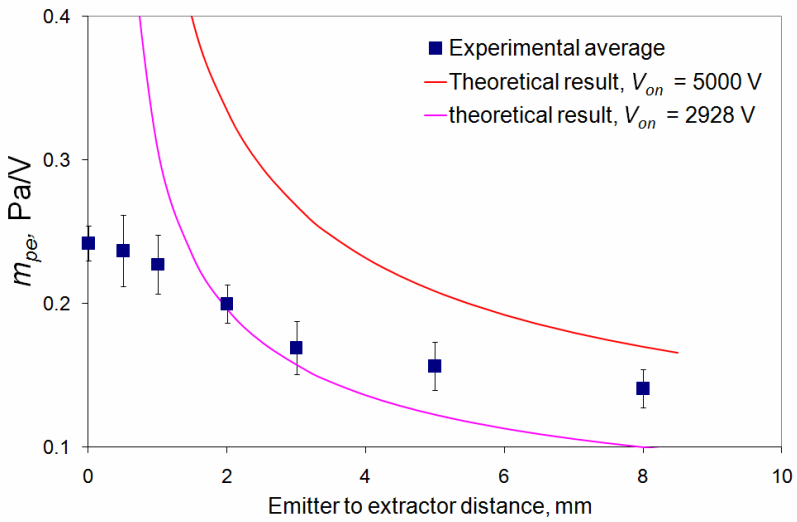

Figure 4.16. Variation of experimental and theoretical m_{pe} with emitter to extractor distance for emitter of outer diameter 510 μm. Results using maximum and minimum experimental V_{on} are plotted.

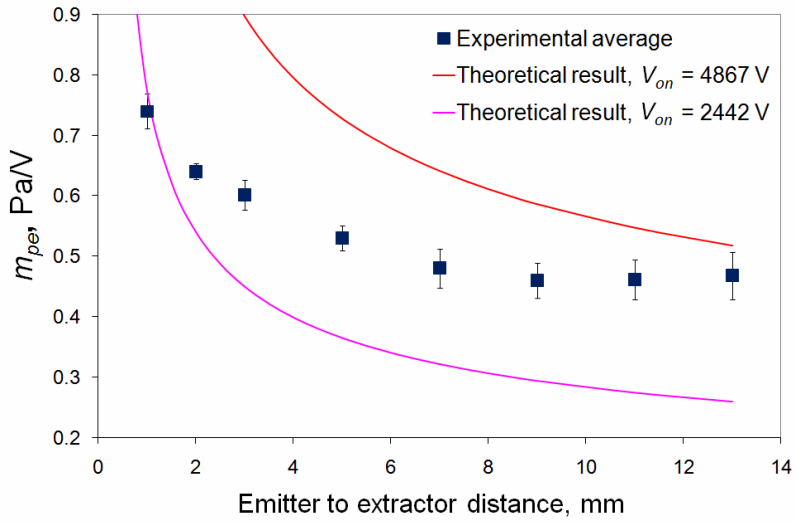

Figure 4.17. Variation of experimental and theoretical m_{pe} with emitter to extractor distance for emitter of outer diameter 230 μm. Results using maximum and minimum experimental V_{on} are plotted.

4.8. The linearity of the $Q(V)$ relationship

Within the theoretical derivation is a suggestion that the experimental results should not be linear, as equation (4.8) is differentiation of equation (4.7) where the electric pressure is proportional to the voltage squared. Consequently a linear line plotted through this V^2 dependence may not be a perfect fit. Theoretically the gradient is calculated at one point (V_{on}), whilst the experimental value is calculated from a best fit across the whole cone-jet mode range, so therefore may not be linear.

The goodness of fit of a linear line will vary with the strength of the value of m_{pe}, as for a smaller value of m_{pe} the curve of the electric pressure vs. voltage squared relationship will be shallower than for a higher value of m_{pe}.

Equation (4.7) can be divided by the hydraulic resistance to produce a theoretical chart of flow rate against voltage that demonstrates a V^2 relationship. A linear line is fitted across the stable cone-jet voltage range, with the gradient of the line corresponding to m_Q. The resulting linear line has an R-squared value of at least 0.999, independent of the geometry. The linear fitting to this theoretical V^2 relationship cannot though be perfect

and the flow rate residuals between the $Q \propto V^2$ theory and the straight line can be plotted, as illustrated in Figure 4.18. Shown is how the theoretical residuals vary across the cone-jet voltage range, for emitters of differing outer diameter (the same size emitters investigated in Section Figure 4.5).

For the larger values of m_Q there is a larger deviation from linearity, with the emitter with an outer diameter of 230 μm showing the largest residuals. The largest residuals found between the V^2 theory and the linear relationship are of the order of ~0.07 nLs^{-1}. In comparison the experimental standard deviation for the flow rate at a constant voltage was rarely lower than 0.1 nLs^{-1}. Therefore the deviation from linearity that occurs theoretically would be difficult to discern from the experimental results.

The residuals of the experimental linear $Q(V)$ relationship were investigated, and no trend was found within the residuals of the linear regression fitting.

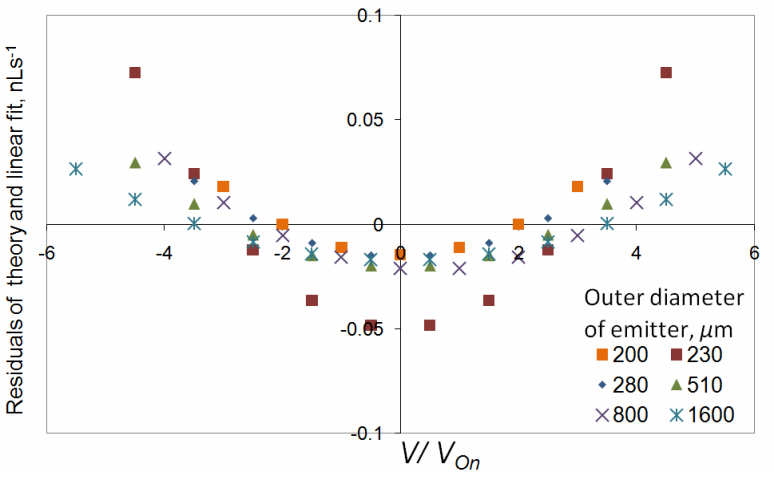

Figure 4.18. Residuals between theoretical results of Q against V and linear fitting, for emitters of differing outer diameter.

In summary, over the cone-jet mode voltage range it is not possible to distinguish between a V^2 or a linear relationship, and the theoretical results demonstrate why that is the case.

It has been suggested that to account for the linearity of the flow rate or current relationship to voltage, which should be at first glance a V^2 relationship, a feedback mechanism is present. For example (as described in Section 2.5) Hartman suggests that as the voltage increases the decreases in cone length reduces the effect of voltage on flow rate[61]. It would now seem that no feedback mechanism is needed as the non-linearity is theoretically marginal over the cone-jet voltage range.

4.9. Effect of emitter length on flow rate with voltage relationship

As two of the three geometric parameters that affect the value of m_Q (emitter o.d. and z_0) are simply a result of variations in the rate of change of the electric field, it seems reasonable that any change in geometry that affects the electric field at the emitter tip will affect the value of m_Q.

As a result various other geometric parameters were investigated, with one of these tested being the emitter length, as described in Section 3.3.3, and summarised in Table 3.2 as geometry variation number [5]. The length of an emitter with an 800 μm outer diameter and a 450 μm inner diameter was varied from 0.5 mm to 31 mm. At least eight points were collected at each length, with an average taken. The average m_Q results are shown in Figure 4.19, with the error bars being the standard deviation.

Figure 4.19 shows that as the emitter length decreased the value of m_Q decreased. There was little effect of emitter length on m_Q when the emitter was longer than 10mm. Below 10 mm there was a dramatic decrease in the flow rate sensitivity to voltage in cone-jet mode. This (as far as the author is aware) is the first time that the emitter length has been shown to have an effect on the $Q(V)$ relationship.

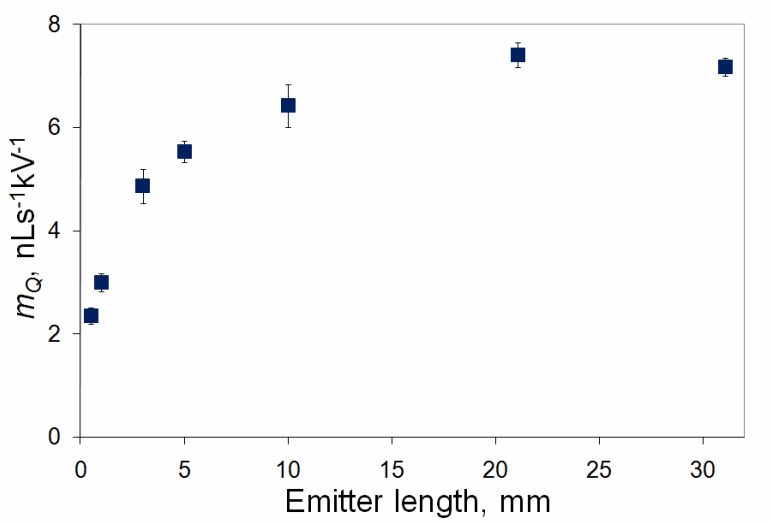

Figure 4.19. Variation of m_Q with emitter length. Emitter o.d. was 820 μm, and i.d. 465 μm. Emitter to extractor distance was 3mm for all experiments.

The parameter emitter length is not included in equation (4.8) or (4.9), but it would seem reasonable to assume that its effect is again due to variation of the sensitivity of electric field with voltage, as the geometry changes. This is analogous to the finding that any significant changes in geometry affect the onset voltage[13]. Indeed it can be hypothesised that if the onset voltage varies when the geometry is changed, then the value of m_Q will also vary.

Krpoun *et al.* extended the basic theoretical evaluation of the onset voltage (equation 2.26) to include other geometry parameters by using FEM to calculate the electric field at a certain onset voltage[13]. The same method can be applied here, to calculate the variation of electric field (and consequently electric pressure) with voltage, and this is completed in Section 4.11.

4.10. Effect of extractor aperture diameter on m_Q

Tests investigating the effect of the diameter of the extractor electrode aperture on m_Q were completed. These are described in Section 3.3.4, and as geometry variations [6] and [7] in Table 3.2. The emitter used had an i.d. of 465 μm and an o.d. of 820 μm. The emitter to extractor distance was fixed at 3mm. Two sets of data were completed using different emitter lengths, one using an emitter 1mm long, and a 2nd set using a 10mm long emitter.

For all experiments described up to this point, the same extractor electrode was used, which had an aperture through it with a diameter of 6mm. For these following experiments four situations were tested; an extractor with no aperture, and three extractors with varying aperture diameters of 3mm, 6mm, and 10mm. All these electrodes were made from a steel disc of external diameter 20mm, and thickness 3mm.

The aperture in the extractor electrode provided a path for the spray to escape to a position where it would not greatly affect the electrostatics of the system geometry. For the electrode with no aperture there is consequently an issue of fluid accumulation on the surface of the electrode. The effect of the fluid accumulation was reduced by applying only low nominal flow rates and changing the voltage every 20 seconds (instead of every minute), to minimize the amount of liquid sprayed in each experimental run. Changing the voltage every 20 s was deemed possible as the flow rate data was very stable.

For experiments using extractor electrodes with an aperture there was minimal accumulation of fluid on the electrode; consequently it was of little concern.

Figures 4.20 (a) and (b) illustrate the change in m_Q with aperture size, for the two emitter lengths tested. The value of m_Q increases as the electrode aperture diameter decreases, but the sensitivity of m_Q to electrode aperture size is small when compared to other geometric variations. There is no dramatic increase of m_Q for smaller apertures.

In Section 4.7 the theoretical value of the value of m_{pe} (or m_Q) increased much more dramatically than the experimental values as the emitter to extractor distance was decreased. This could be due to the effect of the electrode aperture reducing the

experimental value, as the theoretical value is based on a point to plane geometry. But since Figures 4.20 (a) and (b) show m_Q to not be greatly affected by aperture size, it seems likely that this hypothesis is wrong and that the variation of theory from experimental values for smaller extractor electrode to emitter distances is not explained by aperture effects.

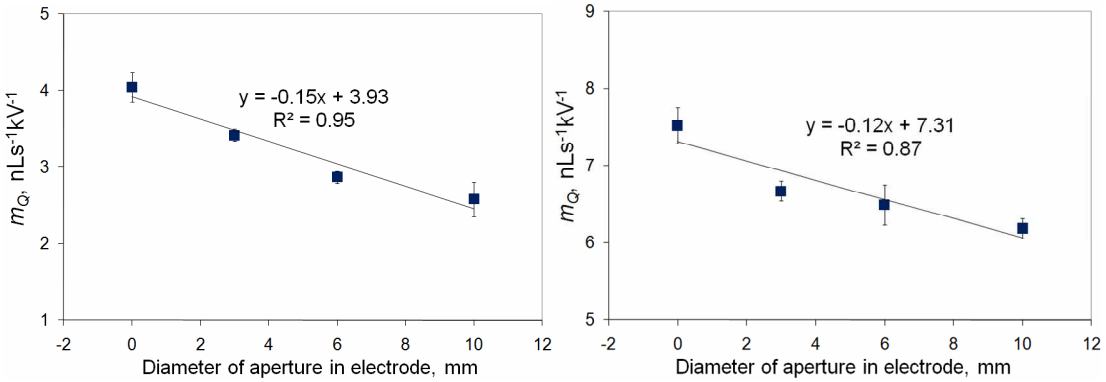

(a) (b)

Figures 4.20 (a) and **(b).** Variation of m_Q with electrode aperture diameter, for emitter of length: (a) - 1mm (geometry variation [6] in Table 3.2); (b) - 10mm (geometry variation [7] in Table 3.2).

4.11. FEM analysis of the electric pressure sensitivity to voltage

The above $Q(V)$ analysis attempts to calculate the electric field from theoretical principles, and as described results in various limitations. An alternative method is to model the electrode emitter geometry using a Finite Element Method (FEM). Simulating the variation of electric field with geometry changes has greater flexibility, enabling the inclusion of geometric parameters that are ignored theoretically.

Here the same method used by R. Krpoun *et al.* to numerically calculate the onset voltage[13,107] is used to give an estimate of the electric field at the tip of the emitter.

Krpoun *et al.* modelled a small slice of the axisymmetric emitter-extractor tip geometry using ANSYS. Bernstein-Bézier curves were attached to the emitter tip in an attempt to model the changing surface geometry in pulsed mode as the voltage is increased towards the onset of cone-jet mode. The electric field variation with voltage was found for each different emitter tip Bernstein-Bézier curve (with the remainder of the geometry constant), with each curve having a different tip radius.

For Krpoun *et al.* this choice of tip geometry would seem justified, as there have been some suggestions that the shape of the liquid protrusion within pulsed mode does vary between conical surfaces of varying tip radii. But within cone-jet mode, at all times a jet is evident from the tip of the cone, with the shape little resembling a Bernstein-Bézier curved function. Consequently applying this particular FEM analysis to the relationship of m_Q to geometry is physically incorrect, but as a first approximation it could prove enlightening. It is worth also noting that the theoretical electric field equations (4.8) and (4.9) do not resemble a cone and jet geometry, yet do model the change in flow rate with voltage, and the onset voltage, adequately.

What follows is a brief summary of the applied FEM method; a full description has been provided by Krpoun *et al.*[13,107].

A rational Bernstein-Bézier curve between three points can be expressed mathematically as[107];

$$\vec{C}(s)=\frac{B_{0,2}(s)\vec{P}_0+B_{1,2}(s)w\vec{P}_1+B_{2,2}(s)\vec{P}_2}{B_{0,2}(s)+B_{1,2}(s)w+B_{2,2}(s)}, \tag{4.10}$$

where $B_{i,p}(s)$ are Bernstein basis functions

$$B_{i,p}(s)=\frac{p!}{i!(p-i)!}s^i(1-s)^{p-i}. \tag{4.11}$$

Parameter *w* defines the apex radius of curvature, whilst *s* is the running parameter that produces the points on the curve when varied between 0 and 0.5. Three points define the arc;

$$\vec{P}_0 = -\vec{P}_2 = \left(-r_e,\ 0\right), \qquad \vec{P}_0 = -\vec{P}_2 = \left(0,\ r_e \cot\left(\alpha_T\right)\right). \tag{4.12}$$

α_T is the cone generatrix half angle, as illustrated in Figure 4.21, taken to be 49.3°. The curve arc is always tangential to the two straight cone generatrix chords of the cone at the emitter edges, with the curve shape deviating from the cone shape at different points depending on the value of *w*. For the axisymmetric case the curve can be defined parametrically as[107]

$$\begin{aligned} x(s, w) &= \frac{(1-2s)\, r_e}{1-2s(1-s)(1-w)} \\ z(s, w) &= \frac{2(1-s)\, s\, w \cot\left(\alpha_T\right) r_e}{1-2s(1-s)(1-w)} \end{aligned} . \tag{4.13}$$

As *w* varies the type of conic geometry defined by these parametric equations varies, as illustrated in Figure 4.21. To generate a certain curve *w*, α_T, and r_e remain constant whilst the running parameter *s* is varied incrementally from 0 to 0.5. This creates a set of x and z coordinates which naturally concentrate around areas of greater curvature.

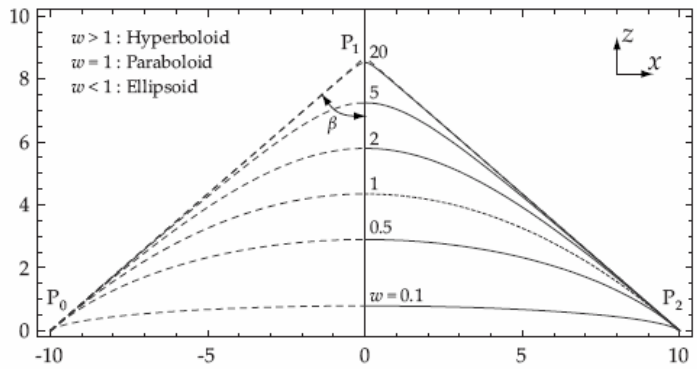

Figure 4.21. Illustration of the conic function used to model the cone structure, with r_e = 10, and $\beta = \alpha_T$ = 49.3°. Courtesy of Krpoun *et al.*[13]

The tip radius can be calculated from the above parametric equations by the differential curvature equation, which results in a simple calculation of the apex radius[107]

$$r_a = \frac{r_e}{w}\tan\alpha_T . \tag{4.14}$$

Various different tip geometries were applied to the emitter, with each having a different value of the ratio between the curve apex electric field and the applied voltage, κ,

$$E_{apex} = \kappa V_{applied} \tag{4.15}$$

κ varies with the apex radius, with the relationship $\kappa \propto r_a^{-1/2}$ found for smaller apex radii[107]. For Krpoun *et al.* this dependence of κ on r_a did not affect the onset voltage calculation, as when a balance between the electrostatic and surface tension stresses is applied the onset voltage is[107]

$$V_{on} = \frac{1}{\kappa}\sqrt{\frac{4\gamma}{\varepsilon_0 r_a}} , \tag{4.16}$$

And therefore V_{on} is independent of the tip radius r_a, since in the above equation the $\kappa \propto r_a^{-1/2}$ dependence cancels out the r_a within the square root sign.
The electric pressure can also be calculated using the FEM electric field;

$$\begin{aligned} P_e &= \tfrac{1}{2}\varepsilon_0 E_{apex}^2 \\ &= \tfrac{1}{2}\varepsilon_0 \left(\kappa V_{applied}\right)^2 . \end{aligned} \tag{4.17}$$

Consequently the electric pressure will depend on the apex radius used, as the $\kappa \propto r_a^{-1/2}$ relationship is not cancelled out.

The gradient of the electric pressure to voltage relationship across the range of voltages that cone-jet mode is stable can be compared to experimental results for m_{pe}. This differs slightly from the theoretical approach in that here the gradient is calculated graphically, rather than from a differential approach.

Figure 4.22 (a) – (c) and Figure 4.23 (a) – (c) compare the experimental and simulated m_{pe} results for all geometric variations listed in Table 3.2, except that of the emitter inner diameter as it was not affected by variations of the electric field (see Figure 4.5). The

geometric variations are the emitter outer diameter, the emitter to extractor distance, the emitter length and the extractor electrode aperture radius.

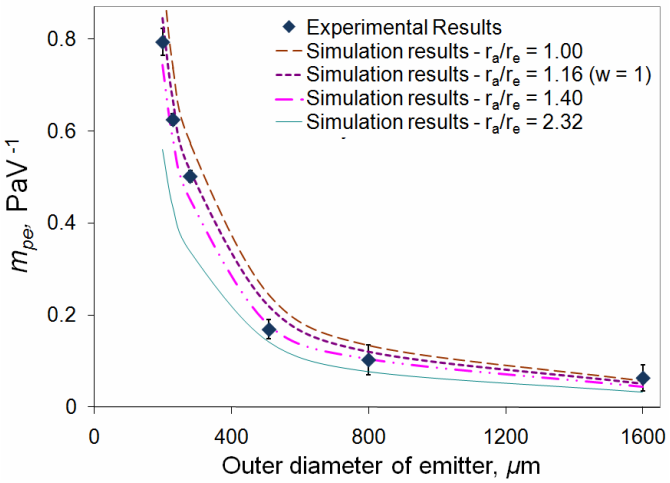

(a)

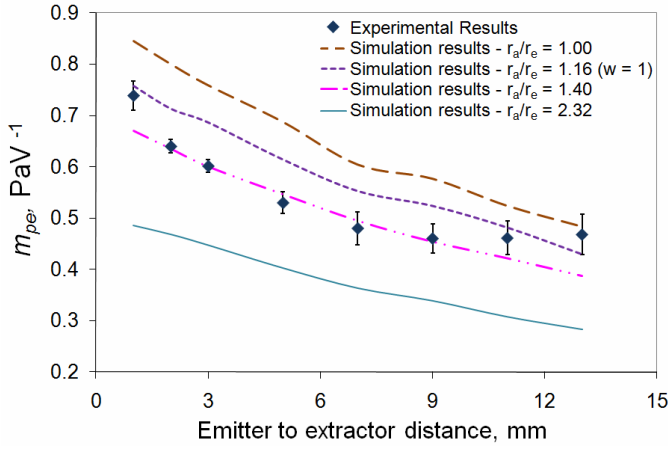

(b)

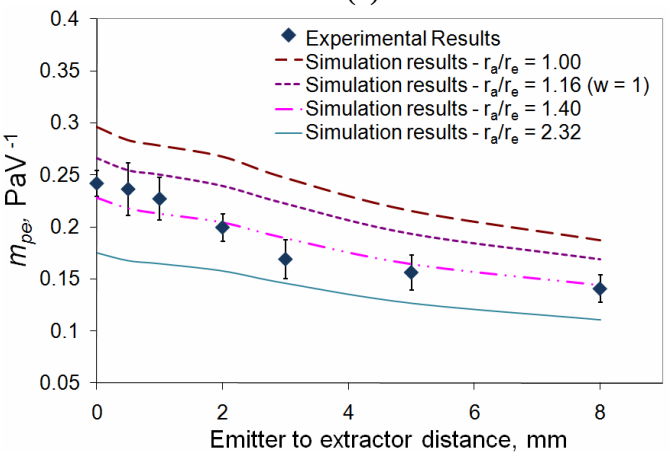

(c)

Figure 4.22 (a) – (c). Variation of m_{pe} with geometry; comparison of experimental and simulation results for different apex radii. (a) – emitter outer diameter; (b) – emitter to extractor distance using 230 μm o.d. emitter (geometry variation [3] in Table 3.2); (c) – emitter to extractor distance using 510 μm o.d. emitter (geometry variation [4]).

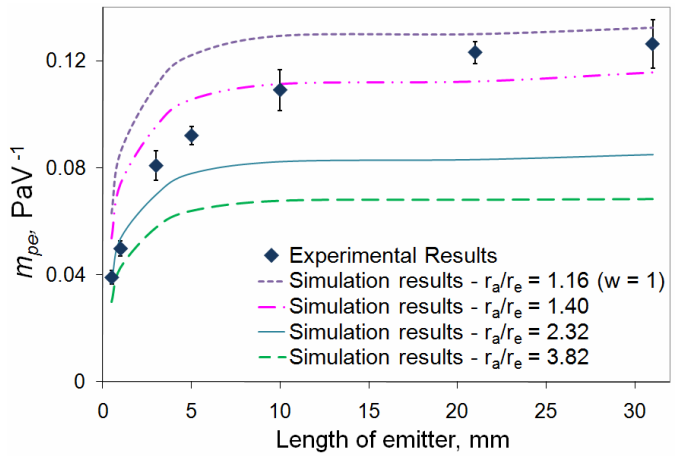

(d)

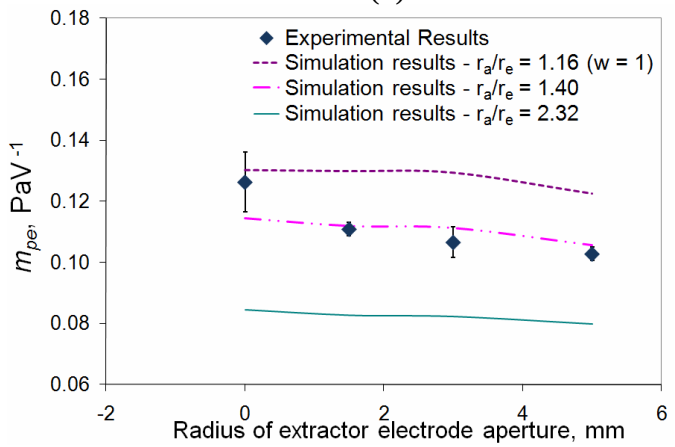

(e)

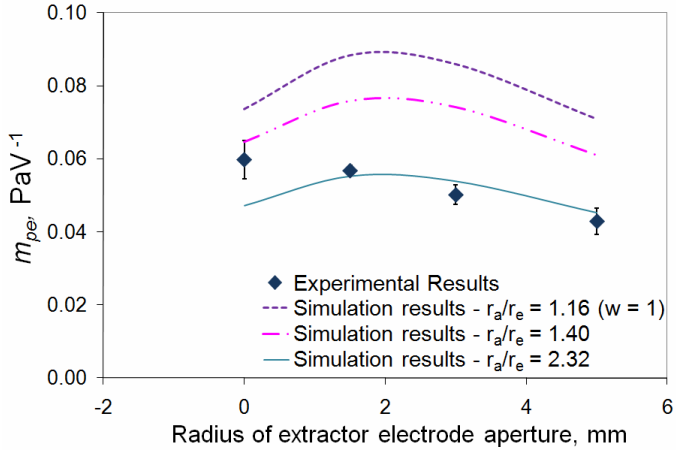

(f)

Figure 4.23 (a) – (c). Variation of m_{pe} with geometry; comparison of experimental and simulation results for different apex radii. (a) – emitter length varying (geometry variation [5] in Table 3.2); (b) – electrode aperture radius varying for emitter of length 10 mm (geometry variation [7]); (c) – electrode aperture radius varying for emitter of length 1 mm (geometry variation [6]).

The simulated results generally show the correct trend of m_{pe} varying with the geometric parameter. Various different Bernstein-Bézier curves were used in an attempt to find the best fit of experimental to FEM results, with the best agreement generally occurring for an apex to emitter radius ratio of 1.40. This is especially the case when the emitter to extractor distance is varied, with excellent agreement between simulation and experimental data for r_a/r_e = 1.40, considerably better than the theoretical comparison (compare Figure 4.14 and Figure 4.15 with Figure 4.22 (b) and (c)). In particular the two noticeable deviations of the theoretical estimate of m_{pe} with z_0 from the experimental data - the too large increase at small emitter to extractor distances, and the increase of m_{pe} at larger z_0 for the 230 μm o.d. emitter - are not present.

The variation of the simulation results with emitter length (Figure 4.23 (a)) does not agree as well with the experimental results, compared to other geometric situations. When the emitter is long the simulation geometry r_a/r_e = 1.40 provides a reasonable result, but for short emitters there is considerable deviation. But although the experimental and simulation results deviate, both show the same trend, independent of tip radius. Consequently it would seem that the variation of m_{pe} (or m_Q) with emitter length is predominately an electrostatic effect.

The simulation results for extractor aperture radius also demonstrate the lessening agreement with experimental results for shorter emitters. For electrode aperture varying experiments that used an emitter length of 10mm the simulation results agree with the experimental, with Figure 4.23 (c) showing that the electrode aperture has little effect, with a possible slight increase for smaller apertures.
But for the aperture varying experiments using the shorter 1mm long emitter, simulation and experimental results are not as comparable, with the effect of electrode aperture not as well characterised by modelling. Although the simulation results are of the right order, as illustrated in Figure 4.23 (b), they do not demonstrate the same effect as the experimental results.

For the emitter outer diameter varying (Figure 4.22 (a)), emitter to extractor distance varying (Figure 4.22 (b) and (c)), and electrode aperture varying using the 10mm long emitter (Figure 4.23 (b)), the r_a/r_e = 1.40 simulation geometry provides the best agreement with the experimental data. Why this geometry provides a good fit remains uncertain.

Figure 4.24 shows the tip geometries for the various emitter radius ratios plotted in the figures above. For comparison a tip geometry with a small apex radii is also shown. With r_a/r_e = 1.40 the emitter tip geometry does not strongly resemble a cone-like geometry. The reason why this tip ratio provides a good fit to experimental results is therefore not due to a physical resemblance. Instead when r_a/r_e = 1.40 the apex radius is close to the radius of the emitter, so perhaps this offers an explanation of its good fit – by having a large apex radius the geometry can have some significant effect on the electric field variation at the tip. But if the apex radius is the same as the emitter radius (r_a/r_e = 1) the simulation results are less comparable to the experimental, so there maybe another explanation.
Alternatively r_a/r_e = 1.40 is close to the point at which the Bernstein-Bézier curve forms a parabola, when w = 1 and r_a/r_e = 1.16, which suggests that a parabola may be the best shape for the modelled emitter tip. If though a geometry is used where w = 1, the experimental agreement is not as good, as shown in the simulated results above.

Although it is uncertain why the geometry with a tip ratio of 1.40 provides such good agreement, in general the simulated results demonstrate that the simulation approach provides a method to estimate the change in flow rate with voltage, over a greater amount of geometric variants than the theoretical approach, and with greater accuracy. The simulated results unambiguously demonstrate that the variation of the electric pressure with voltage for different geometries is predominately a result of the variation of the electric field sensitivity to voltage with geometry.

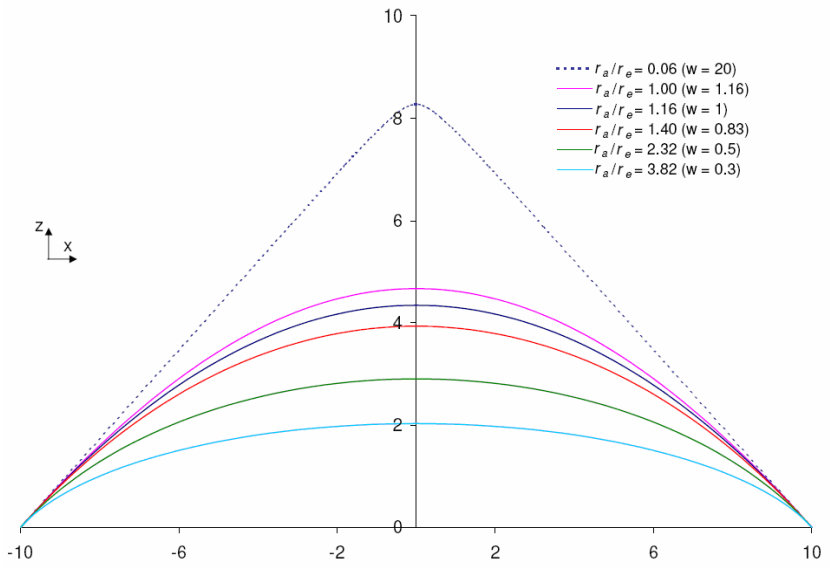

Figure 4.24. Illustration of tip geometries that provide the best fit. w = 20 geometry provided for comparison.

4.12. Effect of voltage on flow rate – repercussions for colloid electrospray thrusters

The effect of the flow rate-voltage relationship on the variability of thrust and specific impulse from a colloid thruster has been discussed previously[72], and more recently[108], and also introduced Section 2.6.3. Now using the theoretical analysis, which has been shown to adequately calculate the change of flow rate with voltage in cone-jet mode, the variation in thrust and specific impulse with changes in extractor electrode voltage can be calculated for a particular thruster geometry.

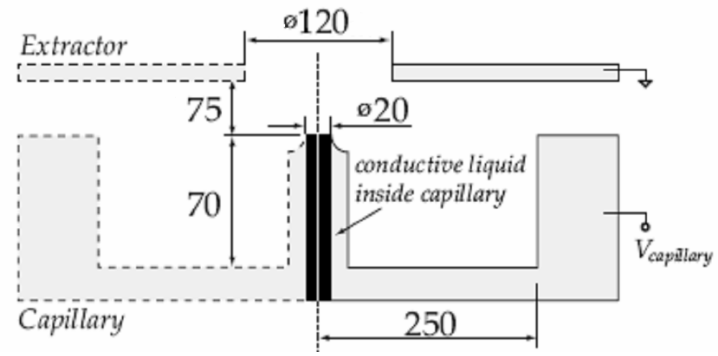

Figure 4.25. The geometry of the colloid thruster. Geometry is shown in μm. Courtesy of R. Krpoun[107].

The geometry initially investigated was that of the micro fabricated electrospray colloid thrusters manufactured and tested by Krpoun *et al.*[13,107], and illustrated in Figure 4.25. The geometry of these thrusters could be varied slightly in the manufacturing process, with the initial geometry applied outlined in Table 4.3. In general the geometry is significantly smaller than the emitters tested here, which results in a hydraulic resistance two orders of magnitude higher than conventional needles. The viscosity used in the calculation of the hydraulic resistance R_T was that of the ionic liquid $EmiBF_4$.

Using this geometry and the simplified theoretical equation (4.8) the estimate for the value of m_{pe} is 16.15 PaV^{-1}. The value of the onset voltage used is that given by Krpoun[13]. This m_{pe} value differs slightly from that published previously[108] (21.0 PaV^{-1}) as the value of A_1 has been varied from 0.36 to 0.41 to agree with experimental best fit value found during experiments.

Table 4.3. Colloid thruster geometry values[107].

Emitter i.d., μm	Emitter o.d., μm	Emitter to extractor distance, μm	Emitter length, μm	System R_T, Nsm^{-5}
24	40	75	70	1.22E+15

This m_{pe} estimate is considerably higher than the highest experimental value of approximately 0.8 PaV^{-1}, found for a 200 μm o.d. emitter (as illustrated in Figure 4.7). This greater value of m_{pe} is due to the far smaller o.d. and emitter to extractor distance of the micro fabricated colloid thruster. Its effect is partially mitigated by the higher value of hydraulic resistance, due to the smaller i.d. of the emitter. The m_Q estimate, using the hydraulic resistance value given in Table 4.3, is 13.2 $nLs^{-1}kV^{-1}$. This is a large value although it is smaller than the maximum experimental value found. Whether this value is possible is unknown, as currently no colloid thruster experiments using the in line flow meter have been completed. As the theory has predicted the experimental results reasonably well, it would seem realistic to assume that it would give a good order-of-magnitude result.

As described in Section 2.6.3, and ignoring some efficiency terms[83], the thrust T and specific impulse I_{sp} for a colloid thruster can be given by

$$T = \sqrt{2\rho QIV_{AT}}\,, \tag{4.18}$$

$$I_{sp} = T/Q\rho g\,. \tag{4.19}$$

where ρ is the density of the ionic liquid, I is the spray current, V_{AT} is the total acceleration voltage and g is the gravitational constant. The total acceleration potential is the sum of the extraction potential, $\sim V_{on}$, and the acceleration stage potential V_{acc}. There is though a loss in potential due to the cone formation process, with the assumed total acceleration potential for this case is given by

$$V_{AT} = \eta V_{on} + V_{acc}\,. \tag{4.20}$$

with the efficiency factor η taken to be 0.9[80].

The current can be estimated from the experimental $EmiBF_4$ current-flow rate relationship found previously[72], $I(nA)=1290Q^{0.42}$. The onset cone-jet flow rate is taken to be the theoretical minimum flow rate[30] for $EmiBF_4$, calculated to be 0.01 nL/s^{-1}. The acceleration voltage used is 7500V, whilst the onset voltage is the experimental value found by R. Krpoun *et al*[13] for this colloid thruster.

It has been found previously that an electrospray experiment can emit ions, if conditions are correct[80]. The point at which this change from droplet to ion mode occurs cannot currently be predicted though, and therefore the assumption is made here that the emitter is producing solely droplets.

The preceding calculations result in an estimate of the thrust and specific impulse for this colloid thruster emitter geometry over an extraction voltage range, as shown in Figure 4.27. The large theoretical value of m_Q is used, which results in the thrust increasing by nearly two orders of magnitude. This though has the considerable negative effect of the specific impulse decreasing to small values. These I_{sp} values are low, although it should though be noted that the colloid thrusters due to be tested on the LISA Pathfinder mission only requires the I_{sp} to be greater than 150 s[5].

Also it should be noted that this large variation in thrust from the large variation in flow rate does agree somewhat with the experimental findings using these emitters[107]. Experiments using these emitters were found to be difficult due to the liquid being extracted from the head by the applied voltage at too fast a rate, leading to the liquid bridging between the emitter and extractor. This agrees with the finding of a high value of m_Q for this colloid thruster. To reduce this effect, 5 μm balls were inserted into the emitter's inner core[107].

The theory outlined above allows for the variation of m_Q at the design stage. For example by increasing the hydraulic resistance, possibly by inserting 5 micrometer beads into the emitter[109], the value of m_Q can be decreased. Increasing the hydraulic resistance to $5\times10^{16}\,\mathrm{Nsm^{-5}}$, comparable to an emitter i.d. of 8 micrometer, the m_Q value would be adjusted to 0.32 $\mathrm{nLs^{-1}kV^{-1}}$. This would lead to the variation of thrust and specific impulse as shown in Figure 4.27. Here the variation of thrust is still considerable, but the change in specific impulse is more acceptable.

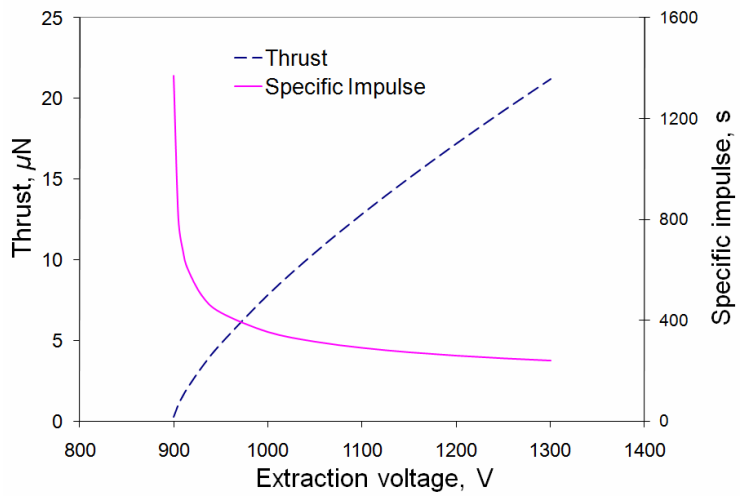

Figure 4.26. Thrust and specific impulse variation for m_Q = 13.2 nLs^{-1}kV^{-1}.

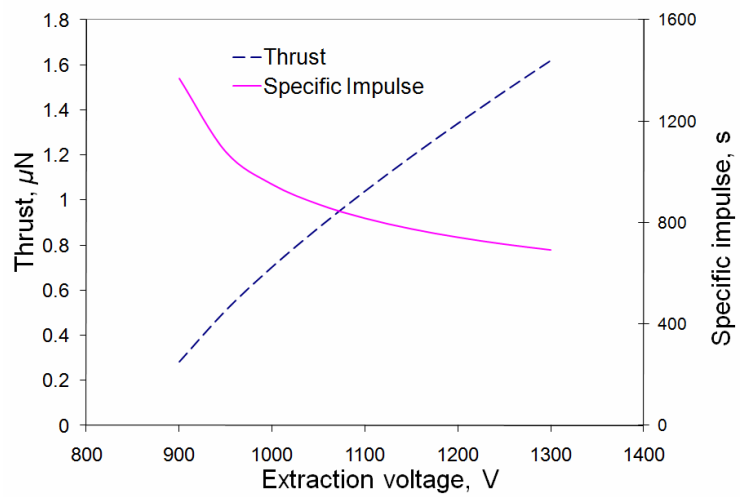

Figure 4.27. Thrust and specific impulse variation for m_Q = 0.32 nLs^{-1}kV^{-1}.

It is also possible to use FEM calculations to estimate the variation of m_{pe} for a Microelectromechanical colloid thruster with differing geometry. This is demonstrated in Figure 4.28 (a) – (d), for the same geometric parameter variations that Krpoun[107] used to estimate the onset voltages (Figure 4.6 in R. Krpoun's thesis). The geometry used for numerical calculations is that which worked best previously under most geometric cases, r_a/r_e = 1.40.

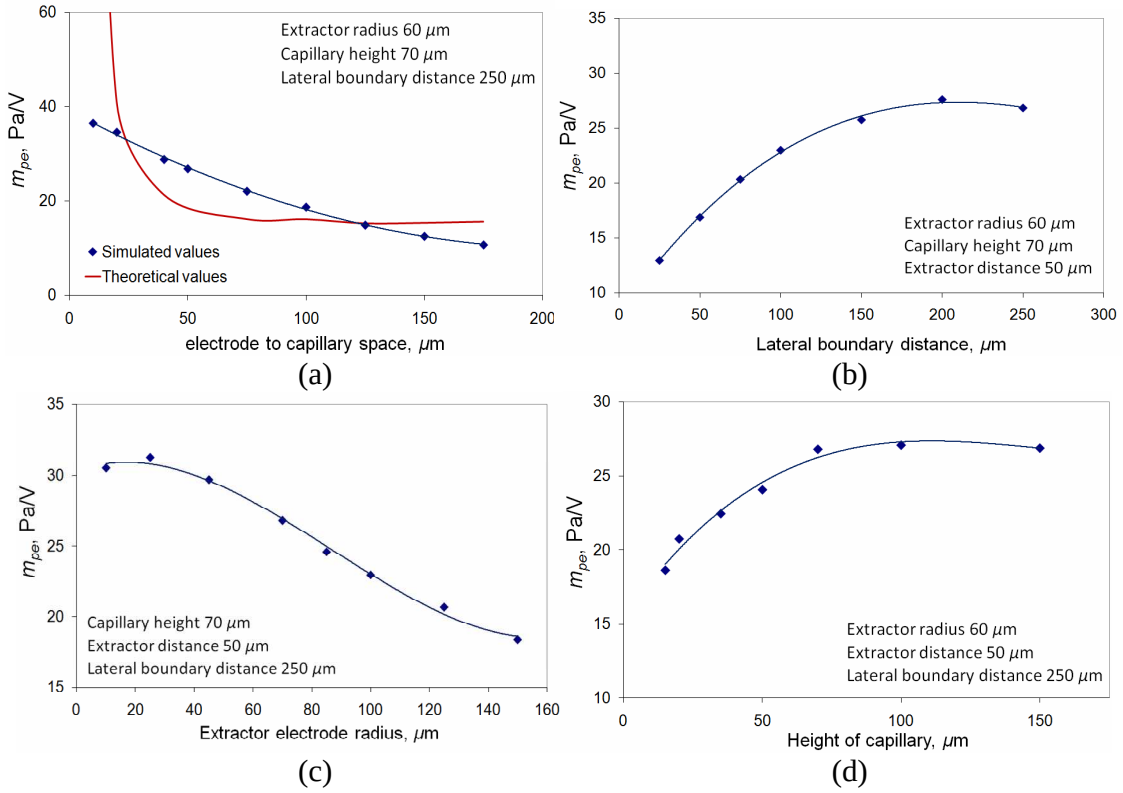

Figure 4.28. Variation of m_{pe} with colloid thruster geometry. (a) – capillary emitter to extractor distance; (b) –distance between capillary and lateral sidewall; (c) – extractor radius; (d) – height of the capillary.

There is considerable difference between the theoretical variation of m_{pe} with electrode to capillary spacing for the colloid thruster, and the numerical calculations. For z_0 = 75 μm, the m_{pe} from numerical calculations is 22.0 PaV^{-1}, giving an m_Q value of 18.0 $nLs^{-1}kV^{-1}$. This is ~36% higher than the theoretical value, but is the same order of magnitude. For the conventional macro sized emitter experiments (see Figure 4.14 and Figure 4.22 (b)), the numerical analysis provides a better fit to experimental results, and it would be reasonable to assume this is the same for the colloid thruster geometry.

Figure 4.28 (a) – (d) demonstrate that most significant changes in geometry of the colloid thruster will affect the value of m_{pe} (or m_Q) and consequently the thrust throttling of the propulsion system. To provide a more realistic estimate of the throttling for a particular geometry, FEM modeling can be done.

Various issues do exist with the overall analysis of the thrust changes with voltage, with the most important perhaps being the assumption that the onset flow rate would be close to Q_{min}. As discussed in the last chapter, there can be a significant increase in the flow rate before V_{on}, and this will adversely affect the value of specific impulse.

Overall though it would seem that the theory can allow for a better estimate of the thrust variation than previously attempted[72].However it is an estimate, with further experiments needed. It could though be possible to choose a certain change in thrust with voltage at the colloid thruster design stage, and this could be experimentally verified during testing of the colloid thruster system.

4.13. Conclusions - the effect of voltage on flow rate in cone-jet mode

An unambiguous linear increase of flow rate with voltage within cone-jet mode has been found repeatedly over approximately 600 electrospray experiments. It is found to be independent of nominal flow rate, agreeing with previous findings.

This linear increase of flow rate with voltage, termed m_Q, is found to depend on the geometry, with parameters affecting the value including the emitter inner and outer diameter, the emitter to extractor distance, the emitter length, and diameter of the aperture in the extractor electrode. Of these geometric effects, only the inner and outer diameter have been found to have an effect by previous studies[9,72], with the other geometry parameters effect being previously unestablished.

The variation of m_Q with emitter inner diameter is a result of the varying hydraulic resistance. Once the hydraulic resistance effect has been removed, there is no significant relationship between the flow rate sensitivity to voltage and the emitter inner diameter.

The variation of flow rate sensitivity to voltage with other geometric parameters is explained by the variation of the theoretical electric pressure sensitivity to voltage with

geometry. Fundamentally the electric field increases faster with voltage for an emitter with, for example, a smaller outer diameter, as the theory described above outlines.
This simple theoretical model is consistent with experimental results, acting linearly over the small cone-jet range. For the cases when other geometric parameters are important, i.e. emitter length, simulating the electric field using ANSYS provides a reasonable result, and is also an improvement on the theoretical analysis for varying emitter to extractor distances.
This analytical model and FEM analysis is the first time that a detailed explanation of the $Q(V)$ relationship in cone-jet mode electrospray has been offered, and the first time that the effect of geometry on it has been explained.

This theory can be used to calculate the change in flow rate with voltage for a colloid thruster. This can then be applied to approximate the variation of thrust and specific impulse. Consequently the variation of thrust with extraction voltage can be estimated at the design stage of a colloid thruster.

Chapter 5

5. The stability island of cone-jet mode electrospray

5.1. The stability island of cone-jet electrospray

The cone-jet mode of electrospray has often been described as an island of stability[7,17,37]. From the onset of cone-jet mode to the bifurcation of the cone into multi-jet mode, there would seem to exist a regime of stability, easily noticed visually upon commencing an electrospray experiment. This stability island is dependent upon the key parameters of flow rate and voltage[7,37], with the conductivity having a strong influence, particularly notable as it value becomes greater[7]. These three parameters *Q, V* and *K* would also seem to be interrelated – for example for a high conductivity fluid the flow rate must be extremely low for cone-jet mode to exist stably[37] (as the Q_{min} parameter described in Section 2.3.5 illustrates).

The effect of flow rate, voltage, and in addition geometry – and any interrelation between the three – on the stability island is investigated within this chapter. The effect of conductivity is not investigated as the same conductivity fluid was used throughout.

Firstly the stability of the cone-jet mode under various conditions is investigated. The results are then applied to the cone-jet onset voltage, and in particular the effect of the geometry. This is then extended to the effect on voltage hysteresis and the cone-jet mode voltage range.

Finally the *I*(*V*) relationship in cone-jet mode electrospray is investigated, with its dependence on various parameters demonstrated.

The parameter that best characterises whether the electrohydrodynamic process is stable is the current, as this has the ability to react within a short period of time. Figure 5.1 illustrates a typical variation of current with voltage found during these experiments. The voltage is increased in large steps up to the point at which a noticeable current is produced. This marks the beginning of pulsed mode, confirmed visually. This pulsed mode often exhibits a non-linear relationship of current to voltage, and this is the case in Figure 5.1. There is also an indication of two subset modes occurring within pulsed mode, suggested by the changing variation of the current.

A large jump in current marks the beginning of cone-jet mode. The current becomes a great deal more stable, and there is a seemingly linear relationship of current with voltage (this is discussed in detail in Section 5.6). Once in cone-jet mode each voltage increase results in a spike in the current, an occurrence previously discussed[10].

Another large increase in current indicates the beginning of multi-jet mode, and the end of the cone-jet mode stability island. Like cone-jet mode, multi-jet mode demonstrates stable current values but is characterised by small voltage ranges per each increase in the number of cone-jets evident. This is illustrated in Figure 5.1 by only two voltage increments occurring within 2-cone multi-jet mode, before another large increase in current marks the beginning of 3-cone multi-jet mode. This small voltage range across which each subset of multi-jet mode exists leads to it being described as unstable[16].

It would seem therefore that cone-jet mode can be described as being sandwiched between two modes of greater instability – pulsed mode due to its natural oscillations and various subset modes, and multi-jet mode, with its small voltage ranges per number of cone-jets produced.

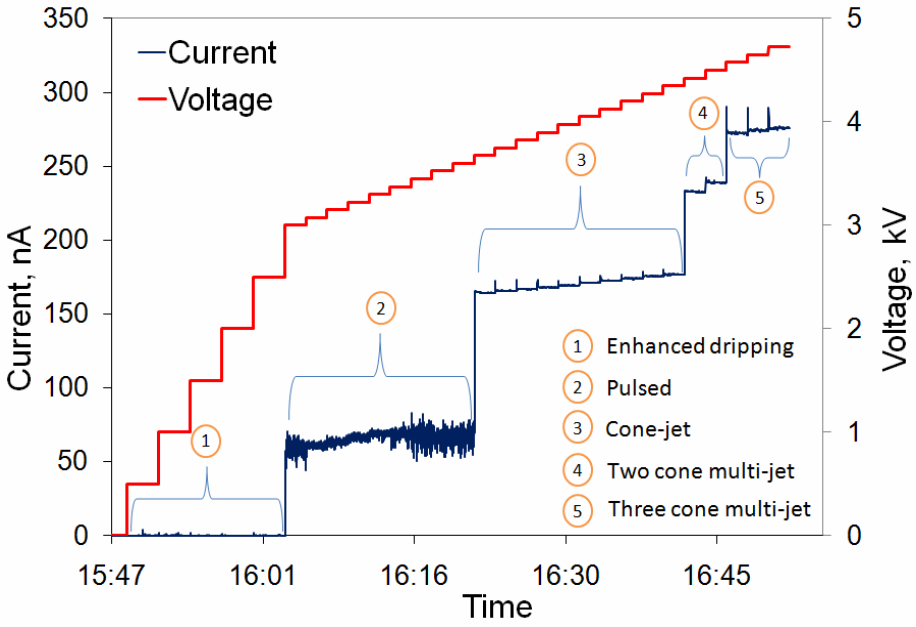

Figure 5.1. Variation of current with voltage.

5.2. The variation of the cone-jet mode stability island with nominal flow rate

Figure 5.2 illustrates various current voltage plots for a number of experiments at different nominal flow rates. The data sets all used an 800 μm outer diameter emitter. The three dimensional chart is similar to those Marginean *et al.*[93] used to characterize current versus voltage curves within electrospray.

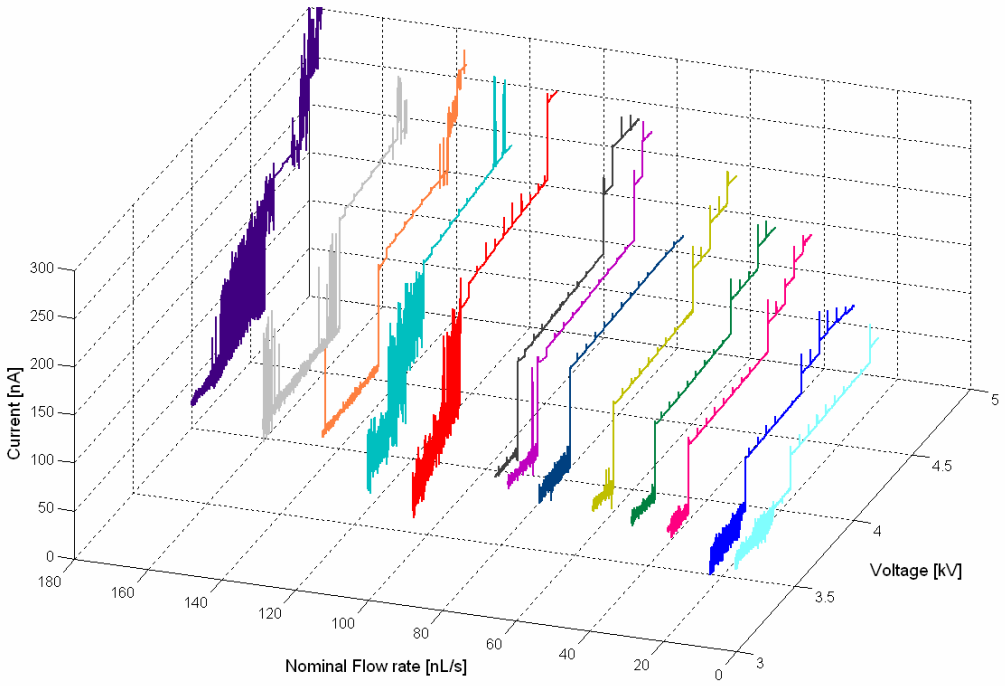

Figure 5.2. Variation of current with voltage at various nominal flow rates. Experiments used a 800 μm o.d. emitter.

At lower nominal flow rates the $I(V)$ data plot starts within pulsed mode, with a large clear jump in current occurring at the beginning of cone-jet mode, as in Figure 5.1. But as the nominal flow rate is increased this jump of current into cone-jet mode becomes less well defined. The increase of current into multi-jet mode, which at lower nominal flow rates is clearly defined, also becomes more variables as the flow rate is increased.

Both these greater variations of current at the transitions into and out of cone-jet mode can be described as greater instabilities. Stability can be defined as a continuous process, whether it is cyclic or constant, which shows no variation in a steady or a periodic function. This can describe cone-jet mode and also at times pulsed mode where the periodic function is of constant shape. Therefore as the flow rate is increased these stable modes become less apparent. Instabilities – seemingly random variations in current - begin to dominate at the transition from pulsed to cone-jet mode, and at the transition from cone-jet to multi-jet mode.

Both these instabilities encroach upon the stability island of cone-jet mode, until at approximately 180 nLs^{-1} the cone-jet mode is only stable across a few hundred volts. This decrease in the stable cone-jet mode voltage range, or stability island size, as the flow rate is increased has been described in previous studies[7,17,93], and attributed to various different effects including the increasing size of an astable transition regime before cone-jet mode[93], or the surrounding gas being unable to pass the increasing amount of charged droplets[7]. Marginean *et al.*[110] describe an astable transition region as a "transition between a limit cycle (pulsating regime) and a fixed point (cone-jet regime) in a subcritical Andronov-Hopf bifurcation due to small external perturbations (noise)". Put differently the electrospray follows an astable path that flip-flops between pulsating and cone-jetting modes. This agrees with the results presented in Figure 5.2 – at higher nominal flow rates the current demonstrated a switching between values suggestive of pulsed and then cone-jet modes. Visually this could at times be confirmed, with a cone-jet forming and then collapsing into a pulsed mode cycle after a short period of time. As this switching or flip-flopping occurs to a greater extent at higher flow rates, here it would seem clear that the existence of a Q_{max} value, beyond which the cone-jet regime is unstable, is a result of the increasing size of an astable regime between pulsed and cone-jet modes.

5.2.1. The effect of outer diameter on the sensitivity of the stability island to nominal flow rate

Figures 5.3 to 5.5 illustrate the effect of nominal flow rate on cone-jet mode stability, for emitters of differing outer diameters. These are the same emitters (and experiments) used for the m_Q analysis in the previous chapter, and were described as geometry variation [2] in Table 3.2. They illustrate the results for the emitters of outer diameter 1610, 510 and 200 μm respectively.

At low flow rates, where the data is clearer, a variable pulsation regime is followed by a jump of current into cone-jet mode, and a greater stability. Another large increase marks the beginning of multi-jet mode.
For some emitters the variation of nominal flow rate was not incremental, consequently for some of the charts the $I(V)$ data plots are non-uniformly positioned along the nominal flow rate axis. Although this complicates the data analysis, it would still seem possible to come to some conclusions.

All the emitters demonstrate an increasingly large astable regime as the flow rate is increased, both at the transition from pulsed to cone-jet mode, and cone-jet mode to multi-jet mode. For the 200 μm o.d. emitter (Figure 5.5) the transition from cone-jet mode to multi-jet mode was often characterised by a drop in the current measured at higher nominal flow rates. This compares to what would normally be an increase in current at this point, but for this particular case at higher Q_{nom} values the multi-jet mode was particularly unstable, with the cones flickering intermittently, and this seems to be a probable cause of the drop in current.

There are some differences for the different o.d. emitters. For example the pulsation mode for the two larger emitters is easily identifiable by the current's greater variability, but for the smaller o.d. emitters the current is considerably more stable in pulsed mode, or at least seemed to be with the potential divider system used (the system was only able to record 2 current data points per second). Visually though it was clear that a pulsating cone was evident. This difference in current variability is possibly due to variations in the frequency of the pulsating current.

Perhaps the biggest difference between the four three dimensional charts (including Figure 5.2) is the varying Q_{max} value, the approximate maximum nominal flow rate at which a stable cone-jet mode still occurs. For the emitter with outer diameter of 1600 μm a stable cone-jet mode is evident up to at least 300 nLs^{-1}, whilst the 800 μm o.d. emitter is stable up to ~150nLs^{-1} (see Figure 5.2), the 510 μm outer diameter emitter to ~80 nLs^{-1}, and the 200 μm o.d. emitter up to approximately 40 nLs^{-1}. Therefore the Q_{max} value

increased by an order of magnitude as the emitter outer diameter increased from 200 to 1600 μm.

It would seem that the larger o.d. emitters demonstrate a stable cone-jet mode at higher nominal flow rates, with at least a 250 nLs^{-1} difference between the approximate Q_{max} values as the outer diameter of the emitter was increased. This result, that the outer diameter of the emitter can affect the flow rate stability, would seem to be original. Marginean *et al.* reported more astabilities at higher flow rates[93], but did not investigate the effect of emitter outer diameter, and little other work has been completed on the maximum stable flow rate.

This Q_{max} variation could simply be due to the considerably larger stable cone-jet voltage range of the larger o.d. emitters. For example the 1600 μm o.d. emitter was found to have a stable cone-jet voltage range of ~1.1kV, compared to a 0.375kV voltage range for the 200 μm o.d. emitter (this varying cone-jet voltage range with emitter outer diameter is discussed further in Section 5.5). This larger cone-jet voltage range would be less affected by the growing astable transition regimes as the flow rate was increased.

This hypothesis - that the astable regime is the same size for each emitter but has more effect with the smaller o.d. emitters because of their smaller cone-jet voltage ranges - does not though quite agree with experimental findings. For example for the emitter with an outer diameter of 510 μm there are significant astable regimes at $Q_{nom} \sim 80nLs^{-1}$ (see Figure 5.4). These encroach upon the small stable cone-jet voltage range (~0.675kV). We would expect to see the same sized astable regimes for the emitter of o.d. 1600 μm at the same nominal flow rates. But at $Q_{nom} \sim 80nLs^{-1}$ there is no evidence of an astable regime before and after cone-jet mode (see Figure 5.3). In fact for the emitter of outer diameter 1600 μm the $I(V)$ curves only begin to show astable transition regimes after 200 nLs^{-1}.

Although the varying cone-jet voltage ranges with emitter o.d. may influence the value of Q_{max}, they may not be solely responsible for the variation of Q_{max} with emitter outer diameter. Instead, it is plausible that an electrohydynamic effect is the cause of the varying stability island with emitter outer diameter. The considerably larger Taylor cone formed on the tip of an emitter with a larger outer diameter may be intrinsically more stable than that formed on an emitter with a smaller outer diameter. Why this would be the case is not though clear.

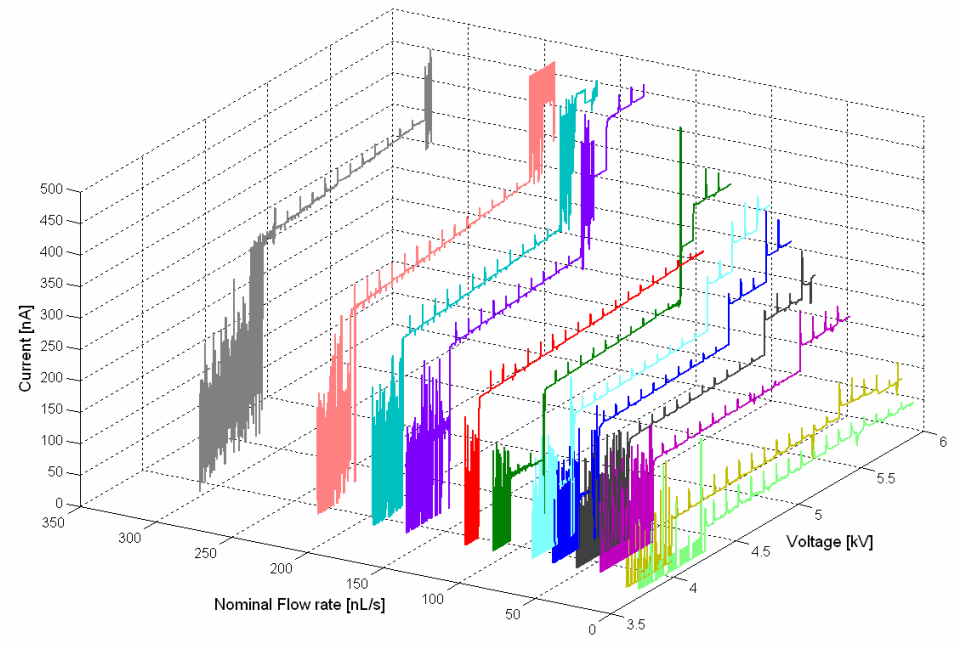

Figure 5.3. Variation of current with voltage at various nominal flow rates. Experiments used 1600-100 μm o.d. - i.d. emitter.

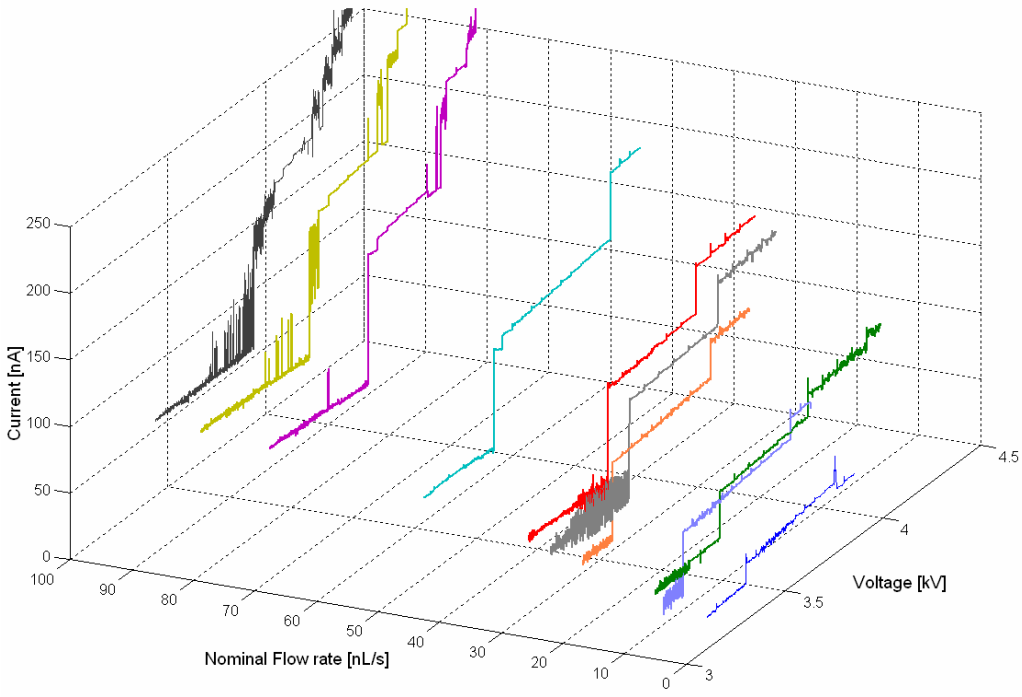

Figure 5.4. Variation of current with voltage at various nominal flow rates. Experiments used 510-100 μm o.d. - i.d. emitter.

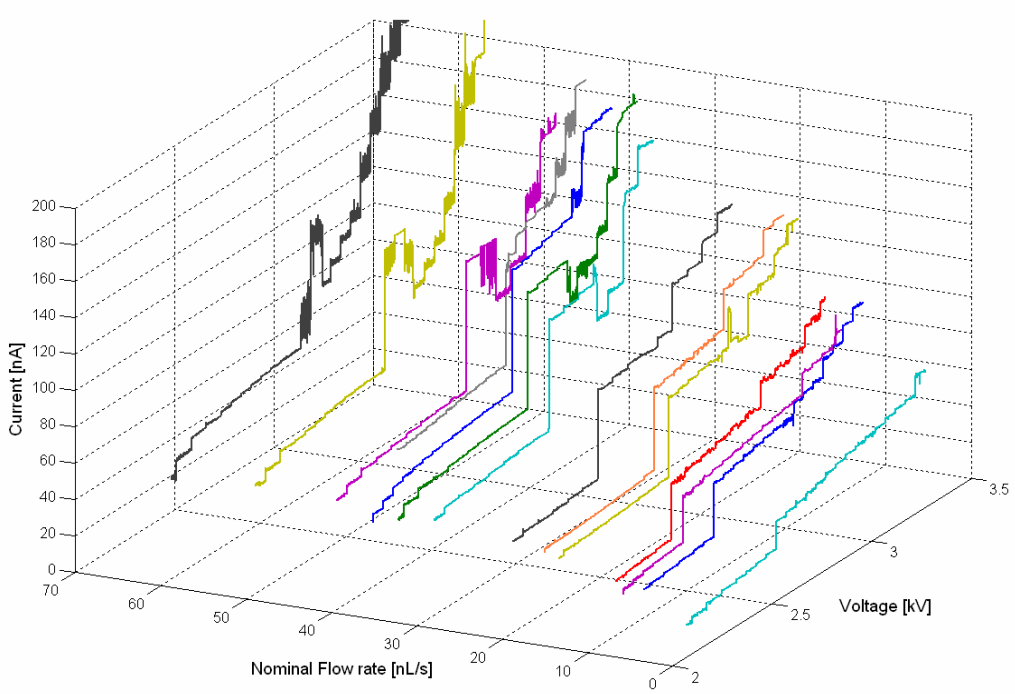

Figure 5.5. Variation of current with voltage at various nominal flow rates. Experiments used 200-100 μm o.d. - i.d. emitter.

5.2.2. Variation of cone-jet onset voltage with nominal flow rate

Let us define the cone-jet onset voltage as the voltage applied at which a stable (analysed visually and with the potential divider current meter) cone-jet mode occurs. This voltage, termed V_{on} previously, has been measured across the many experiments completed.

The effect of the emitter outer diameter on the relationship between the cone-jet onset voltage and the nominal flow rate is illustrated in Figure 5.6. Each point on the chart represents a separate experiment. For the emitters of outer diameter 510 μm and smaller, the voltage was increased in steps of 50V, for the 800 μm o.d. emitter the voltage step was 75V, whilst for 1600 μm o.d. emitter the voltage steps were 100 Volts. Therefore the error of the onset voltages will be approximately these values.

Firstly as would be expected there is considerable variation of the onset voltage for emitters of differing outer diameter – the reason for this is electrostatic, and is discussed in Section 5.4.
The emitters of smaller outer diameters do not have cone-jet onset voltages at higher nominal flow rates because of the instability of the cone-jet mode at higher Q_{nom} values, as described in the previous section.

The emitters of smaller outer diameters demonstrate an increase of the cone-jet onset voltage with nominal flow rate. For example, for the emitter shown on Figure 5.6 with a 200 μm o.d. there is an approximate 0.5kV increase of V_{on} with Q_{nom}. This would seem likely to be a result of the smaller emitters showing a larger astable transition region between pulsed and cone-jet mode than emitters with larger outer diameters, as described in the previous section. This astable transition region grows with nominal flow rate, resulting in the stable cone-jet onset voltage increasing. For larger emitters the astable region was considerably smaller, and did not grow strongly with Q_{nom}. Therefore there was little increase of V_{on} with Q_{nom}, as the data in Figure 5.6 for an emitter with an outer diameter of 1600 μm demonstrates.

Figure 5.7 illustrates the variation of the cone-jet onset voltage with nominal flow rate for experiments using emitters with varying inner diameters. The outer diameter was fixed at 800 μm. As the voltage was increased in steps of 75 Volts, the results contain an error of approximately this value. There is a slight increase of onset voltage with nominal flow rate, probably again due to an increasing astable region. The is no noticeable difference between data for emitters of varying inner diameter, as would be expected as the electric field is not affected by the emitter i.d. (see Section 4.3).
The other geometric variations (outlined in Chapter 3) followed the same trend of the cone-jet onset voltage increasing slightly with nominal flow rate, with the relationship being stronger for emitter with smaller outer diameters. This increase with nominal flow rate has been described by previous studies[10,93], although other studies have found different relationships. For example Noyer *et al.* found the cone-jet onset voltage to decrease with nominal flow rate[111], whilst Cloupeau and Prunet-Foch report a complex

relationship between flow rate and onset voltage[17]. Therefore the effect may vary, possibly due to the varying electrospray solution properties.

During these studies one exception to the effect of Q_{nom} on V_{on} was found for emitters of very short lengths, and this is outlined in the following section.

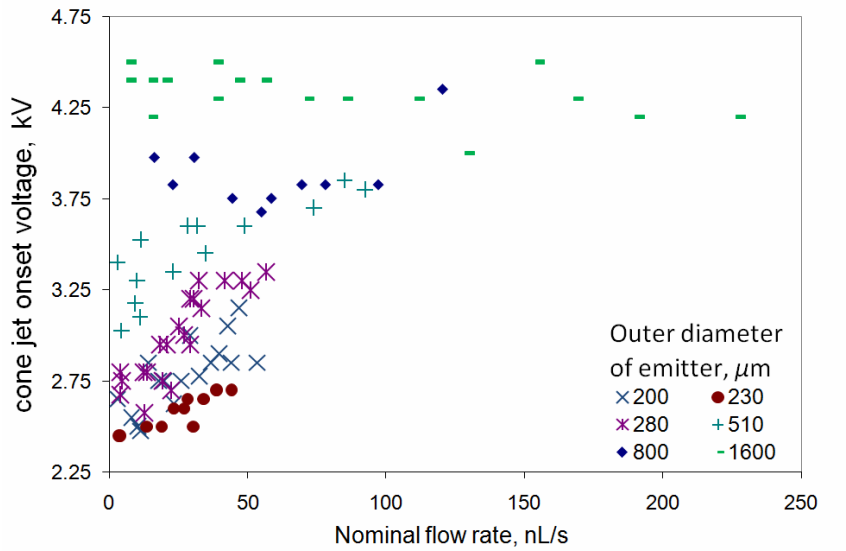

Figure 5.6. Variation of the onset voltage with nominal flow rate, for emitters of differing outer diameter. The inner diameter was constant at approximately 100 μm.

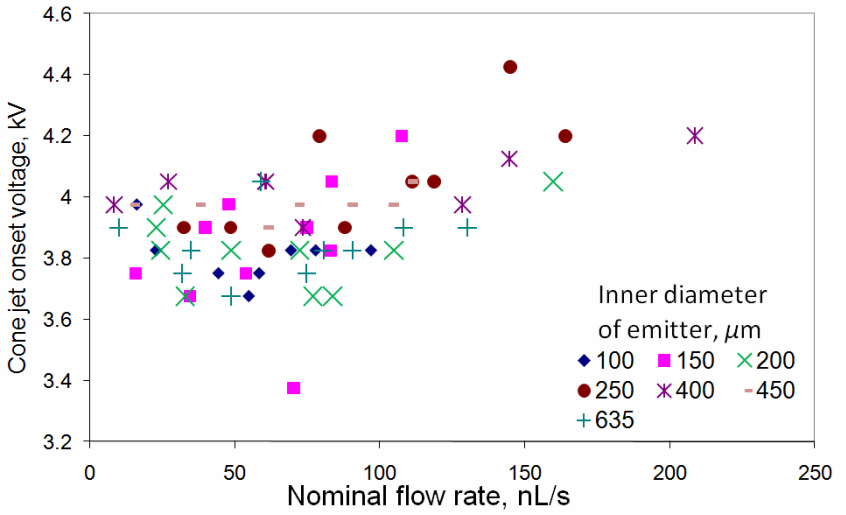

Figure 5.7. Variation of the cone-jet onset voltage with nominal flow rate, for emitters different inner diameters. The outer diameter was constant at approximately 800 μm.

5.2.3. Variation of cone-jet onset voltage with nominal flow rate for emitters of varying length

The stable cone-jet onset voltage versus Q_{nom} data for the variation of emitter length is shown in Figure 5.8. The experiments used an emitter with an outer diameter of 800 μm and an inner diameter of 450 μm. The emitter to extractor distance was kept constant at 3mm.

For most of the differing emitter lengths, there is little if any change of the onset voltage with flow rate – this is in agreement with the data in Figure 5.7 for an emitter with an outer diameter of 800 μm and an inner diameter of 450 μm.
But for the shortest emitters of length 0.5 and 1mm the cone-jet onset voltage would seem to decrease with Q_{nom}. For the 0.5 mm long emitter this is particularly clear, with different onset voltages occurring at differing nominal flow rates. This trend of V_{on} decreasing with Q_{nom} was not found using longer emitters, or indeed any other geometric variation.

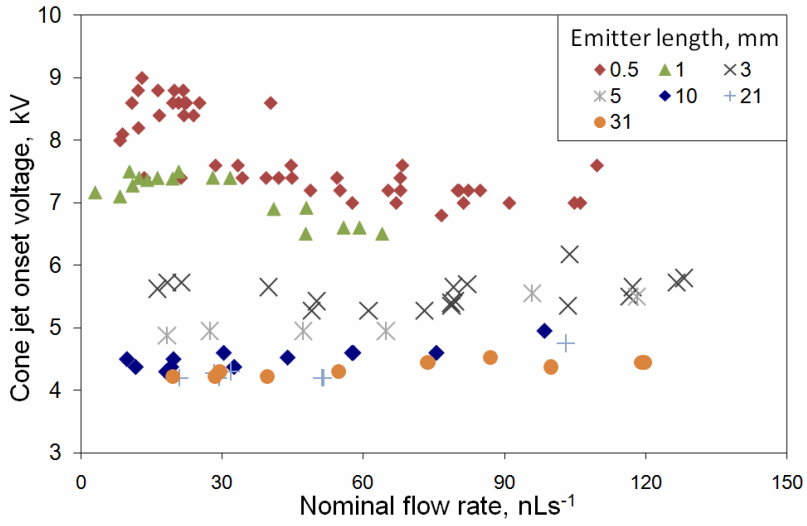

Figure 5.8. Variation of the cone-jet onset voltage with nominal flow rate, for emitter length varying experiments using an 800 μm o.d. emitter, with an inner diameter of 450 μm.

Figure 5.9 (a) and (b) illustrate the 0.5 and 1mm long emitter data sets separately. From both it seems that at lower nominal flow rates the cone-jet onset voltage tends to be higher. Focusing on the data for the 0.5mm long emitter, there are two groups of data, one with an onset voltage of ~8.5kV occurring when Q_{nom} is smaller, and a second group with an onset voltage of ~7.3kV, found to occur at higher nominal flow rates. This effect was also found to a lesser degree for the 1mm long emitter, as shown in Figure 5.9 (b). Here the lower nominal flow rates have an onset voltage of ~7.4kV, whilst at higher nominal flow rates the onset voltage drops to ~6.6kV.

The key to this V_{on} variation may lie with variations within pulsed mode, and to investigate this in more detail, it was necessary to measure the pulsation frequency. This was not possible using the potential divider system used up until this point (described in Section 3.5), as it has a maximum measurement rate of 2 Hz whilst pulsed mode pulsation frequencies are generally considerably higher[100]. To thus allow for frequency measurement a current amplifier was connected to the emitter with the signal fed into a high performance oscilloscope, as described in the experimental methods chapter (Section 3.5). This system allowed for the processing of the current oscillations within pulsed mode, just before the start of cone-jet mode. The oscilloscope performed a Fourier transform analysis of the pulsating current, and the pulsation mode frequency at a certain voltage could be calculated.

The results from this frequency analysis are shown in Figure 5.10 (a) and (b), where the frequency at the maximum point in pulsed mode is shown against nominal flow rate, for the experiments using the current amplifier and oscilloscope. It would seem that at lower nominal flow rates a higher pulsation frequency dominates, of approximately 350 – 450 Hz. At higher nominal flow rates, the frequency is two orders of magnitude smaller, at approximately 2 – 4 Hz. These greatly varying frequency values may correspond to the pulsed mode subsets axial mode I and II[26,28], which have been reported to demonstrate large differences in the pulsation frequency.

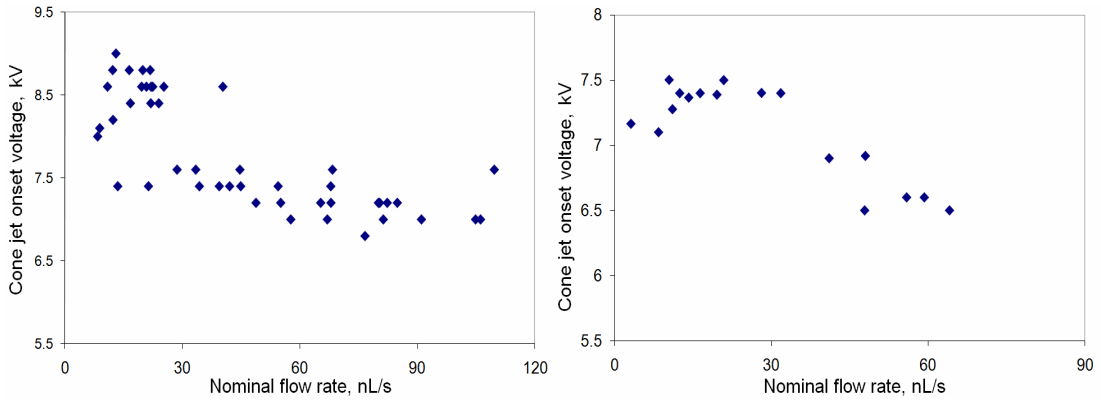

(a) (b)

Figure 5.9 (a) and **(b)**. Variation of cone-jet onset voltage with nominal flow rate, for: (a) - 0.5mm long emitter; (b) - 1mm long emitter. Using an 800 μm o.d. emitter, with an inner diameter of 450 μm.

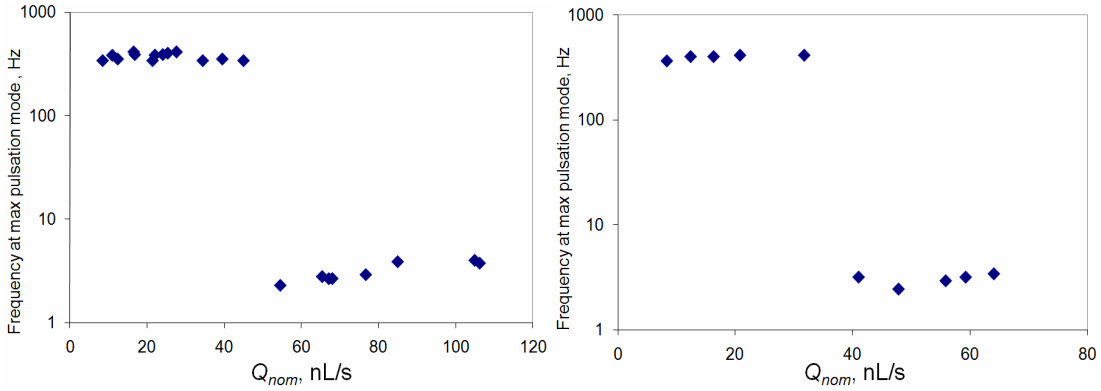

(a) (b)

Figure 5.10 (a) and **(b)**. Variation of frequency at maximum point in pulsed mode with nominal flow rate, for: (a)- 0.5mm long emitter; (b) - 1mm long emitter. Using an 800 μm o.d. emitter, with an inner diameter of 450 μm.

The onset voltage is plotted against the maximum pulsation frequency in Figure 5.11 (a) and (b). The higher pulsation frequencies demonstrate a higher cone-jet onset voltage, whilst the lower V_{on} values occur after a slower pulsation frequency in pulsed mode.

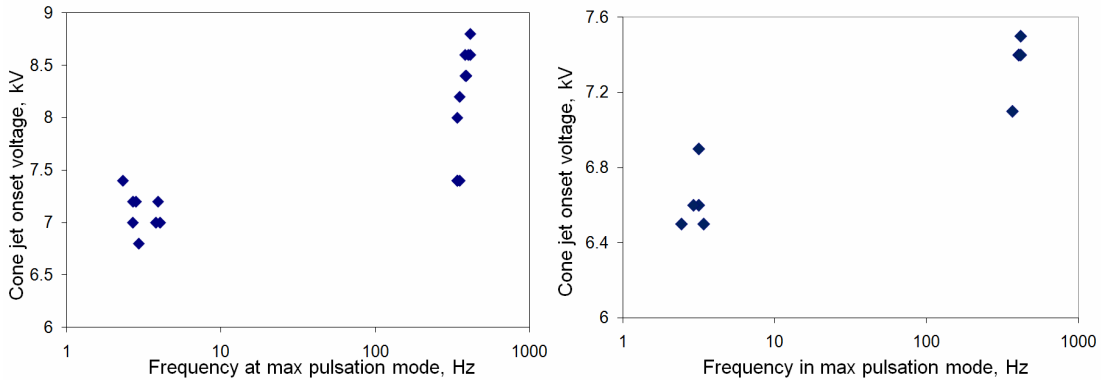

(a) (b)

Figure 5.11 (a) and **(b)**. Variation of cone-jet onset voltage with frequency at maximum point in pulsed mode, for: (a) - 0.5mm long emitter; (b) - 1mm long emitter. Using an 800 μm o.d. emitter, with an inner diameter of 450 μm.

It would seem that at lower nominal flow rates a high frequency pulsation regime dominates. This regime would seem to enable the pulsed regime to be more stable, and to delay the onset of cone-jet mode. At higher nominal flow rates the pulsed mode exhibits a much slower frequency of pulsation, and this would seem to allow for the onset of cone-jet mode at lower voltages. No sign of this effect was found when the emitter was longer, or under different geometric conditions, and further work is necessary to see whether it occurs more generally for different liquids. Why it occurs when the emitter is short could, speculatively, be because of the greater importance of the shape of the meniscus for a shorter emitter, as the meniscus constitutes a larger part of the overall emitter length. Therefore the cone shape and particularly length will have a greater effect on the electric field. As intuitively at the same nominal flow rate the slower pulsations will have a longer cone (the slower frequencies allow for a large cone to be filled), they will reach the required electric field for cone-jet mode to occur at lower voltages.

This variation of the cone-jet onset voltage with pulsation mode is (as far as the author is aware) a new finding. It could also be significant, with the 0.5mm long emitter demonstrating a 16% change in onset voltage. It is unclear though whether it is a common occurrence for short emitters, with further experimentation using an emitter with a different outer diameter needed.

As part of the study of the subsets of pulsed modes, axial mode I and II, greatly different pulsation mode frequencies have been described before[28]. There has though been no reported change of the cone-jet onset voltage between operating in axial mode I or II just before the beginning of cone-jet mode, so it is unclear whether the variation of the cone-jet onset voltage is an effect of the subset mode of operation.

If it is a more general occurrence it may have significant implications for electrospray applications where emitters of relatively low aspect ratio are used. One such field is that of Microelectromechanical Systems (MEMS) colloid thrusters, where the manufacturing process limits the value of the aspect ratio that is possible[107]. In a recent study MEMS emitters with aspect ratios for the emitter base diameter to the emitter length of 1:1.59 to 1:1.35 were tested for use as micro-colloid thrusters[107]. The data shown in Figure 5.11 used emitters with aspect ratios for the emitter outer diameter to the emitter length of between 1:0.625 to 1:1.25. This is comparable to the aspect ratio of the MEMS colloid thruster, so it may be the case that the emitter colloid thruster demonstrates onset voltage variation with pulsation frequency, although no variation was noticed during experiments using these MEMS thrusters.

The measured cone-jet onset voltage for these MEMS emitters was between 560 – 710 Volts, depending on exact emitter-electrode configuration[13,107]. 16% of these values (which is the percentage variation of V_{on} found in Figure 5.9 (a)) would be 90 – 114 volts. This is a significant variation and could lead to some ambiguity as to the exact voltage that needs to be applied to operate in cone-jet mode. Also this onset voltage will also act partly to accelerate the ions or charged droplets produced, so with a different voltage needed this would lead to a different thrust or specific impulse than that which the colloid thruster was designed for.

This possible effect on MEMS colloid thrusters is currently though only conjecture. Further tests are needed to provide evidence that the aspect ratio is the controlling parameter of the V_{on} variation, and that the MEMS colloid thruster onset voltage would vary with the pulsation mode frequency.

5.3. Cone-jet voltage hysteresis

As described in the final paragraph of Section 2.3.2, when the voltage is decreased from operating in cone-jet mode the operating voltage at which cone-jet mode ends is often lower than the point at which it begins. Consequently this cone-jet 'extinction' voltage can be lower than the cone-jet onset voltage.

Whilst investigating the effect of emitter inner and outer diameter on m_Q, the voltage was first increased and then decreased, in order to identify both the onset voltage and the extinction voltage, V_{ext}.

This extinction voltage for each inner and outer diameter varying experiment is plotted against the nominal flow rate in Figure 5.12 and Figure 5.13, respectively. For the emitter inner diameter varying chart (Figure 5.12), a logarithmic best fit line through all the data has been added, to help show the general trend.

For the emitter inner diameter varying experiments, Figure 5.12, there is a significant increase of V_{ext} with the nominal flow rate. Also, as the data for emitters of differing inner diameter falls onto the same trend line, it would seem that V_{ext} is independent of the emitter i.d. This agrees with the onset voltage results (shown in Figure 5.7) which show no discernable trend of cone-jet onset voltage varying with emitter inner diameter once the ~75V error in the values is taken into account.

There does though seem to be a change of the size of the variation with nominal flow rate between the onset voltage and the extinction voltage, for the emitter i.d. varying experiments. Across approximately 200 nLs^{-1} the cone-jet extinction voltage increased by 1.4 kV (see Figure 5.12), whilst the onset voltage increased by only approximately 0.4kV (see Figure 5.7).

For the emitter outer diameter varying experiments, Figure 5.13, there is also a significant increase of the cone-jet extinction voltage with increasing nominal flow rate. Also, as with the emitter inner diameter varying experiments described above, this variation with flow rate is more significant than that found for the onset voltage, which

was illustrated in Figure 5.6. For example, for the experiments using a 510 μm outer diameter emitter V_{on} increased by ~0.8kV with Q_{nom}, whilst V_{ext} increased by ~1.25kV. Although the finding of the cone-jet extinction voltage being smaller than the onset voltage – typically described as voltage hysteresis – has been noted before [17,37,47,60,66,93,111-113], most studies simply illustrate that hysteresis occurred, and provide little detail on the parameters that affect it's magnitude. An exception is the study of Noymer *et al.* where the extinction voltage was noted at different flow rates whilst spraying propylene glycol[111]. There was though no reported difference between the onset and extinction voltage variation with (nominal) flow rate. Consequently this study would seem to be the first time that a large decrease of the extinction voltage with decreasing nominal flow rates has been reported.

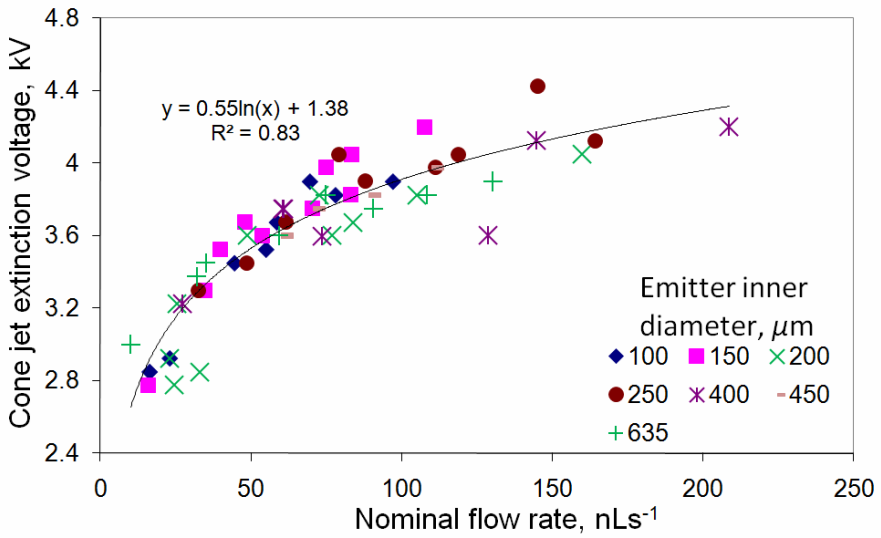

Figure 5.12. Variation of extinction voltage with nominal flow rate, for emitter inner diameter varying experiments. The outer diameter was constant at approximately 800 μm.

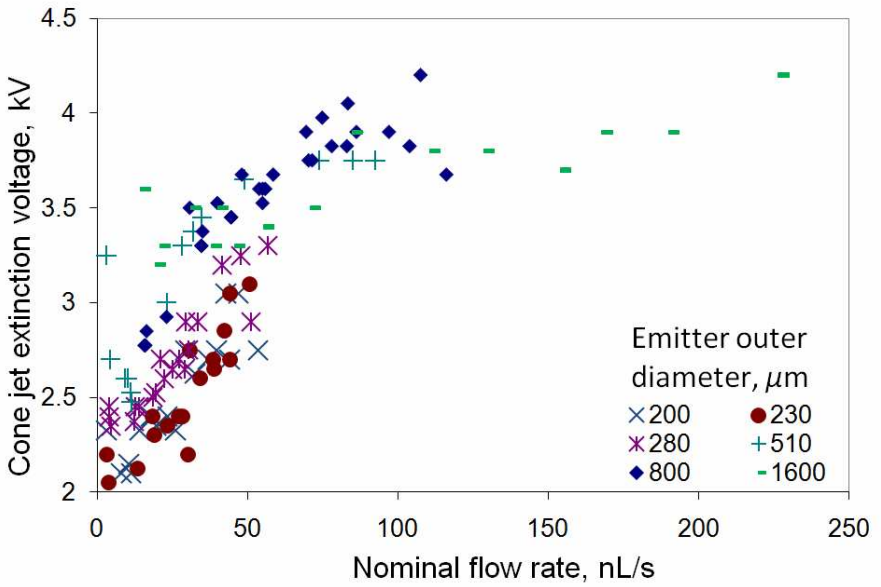

Figure 5.13. Variation of extinction voltage with nominal flow rate, for emitter outer diameter varying experiments. The inner diameter was constant at approximately 100 μm.

Why voltage hysteresis occurred more at lower flow rates remains unresolved. As outlined by Fernández de la Mora[7] voltage hysteresis itself may be a result of the varying meniscus shape with geometry, as outlined theoretically by Pantano[106]. As the voltage is decreased whilst operating in cone-jet mode the cone lengthens. Smith found that at a constant voltage the cone length was shorter with a lower nominal flow rate than a higher flow rate[10], explained by the greater dynamic pressure at higher nominal flow rates 'stretching' the cone. Assuming that there is a maximum cone length beyond which any further decreases in voltage the cone becomes pulsating, then at a lower nominal flow rates the cone will need a greater decrease in voltage to reach this maximum cone length. So therefore the extinction voltage would be lower at a lower nominal flow rate. This hypothesis, although partially supported by figure 4.12 of Smith[10], needs further experimental study for it to be proven. Namely experiments that measure cone length, and use different electrospray liquids to see if the effect occurs more generally, are needed.

To illustrate the results another way, the difference between the cone-jet onset voltage and the extinction voltage was calculated. This difference was termed $V_{hysteresis}$, and is plotted against Q_{nom} in Figure 5.14 (a) and (b), for the emitter inner and outer diameter varying experiments respectively. The inner diameter chart (Figure 5.14 (a)) shows all experimental data. For the outer diameter varying data (Figure 5.14 (b)), two data sets – for the 230 and 280 μm outer diameter emitter – are not shown, in an attempt to make any trends found clearer.

Since V_{ext} varies considerably more with nominal flow rate than V_{on}, it would be reasonable to expect the hysteresis voltage to decrease with nominal flow rate. This would seem to occur for all geometric variations shown on Figure 5.14 (a) and (b), although the data does show considerable experimental variation.

For the emitter inner diameter varying experimental data (Figure 5.14 (a)) there is no change in the $V_{hysteresis}$ to Q_{nom} trend for the different i.d. emitters, as would be expected from the extinction voltage analysis above.

For the emitter outer diameter varying experimental data (Figure 5.14 (b)), the different o.d. emitters illustrate differing trends of $V_{hysteresis}$ with Q_{nom}. At a constant nominal flow rate the larger outer diameter emitters (specifically the 1610 and 800 μm o.d. emitters) have larger values of $V_{hysteresis}$ than the smaller o.d. emitters. This would seem especially clear for the very largest o.d. emitter.

A possible reason for the increasing hysteresis with the outer diameter of the emitter could be that the larger o.d. emitters, with their resulting larger cones, have greater capacity to stretch out their cone as the voltage is decreased. It has been found before that as the voltage decreases, the cone increases in length[10]. This results in a self stabilising effect, as the longer cone results in a longer effective emitter length, and consequently the electric field is artificially kept high enough for cone-jet mode to continue to lower voltages. If a larger o.d. can support a greater increase in cone length, then this could explain the greater hysteresis found with larger o.d. emitters. Here though little data has been collected describing the variation in cone geometry with voltage, so this hypothesis cannot be tested.

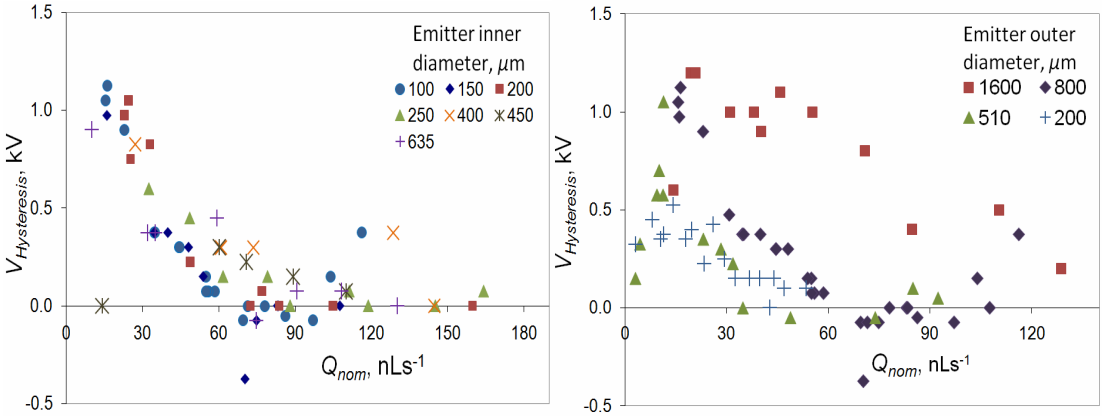

(a) (b)

Figure 5.14 (a) and **(b)**. Variation of hysteresis voltage with nominal flow rate, for; (a) – emitter i.d. varying; (b) - o.d. varying emitter experiments.

5.4. Variation of cone-jet onset voltage with geometry

As part of the analysis of the variation of the effect of voltage on flow rate in cone-jet mode electrospray, seven different geometric variations have been tested, as described in Section 3.3.5. For clarification these are again listed in. The emitter to extractor distance and the variation of the extractor electrode aperture diameter were tested twice, using slightly different geometries.

Figure 5.15 (a) – (d) and Figure 5.16 (a) – (c) illustrate the stable cone-jet onset voltage variation with the seven different geometric parameters described in. Some of the charts were shown in Chapter 4 as part of the m_{pe} analysis.

The charts show both the individual experimental results in addition to the overall average values for each data set. The individual results are all the results, across the whole flow rate range tested, whilst the experimental average was calculated using all data for each geometric configuration. This averaging process was felt justified, since as discussed in Section 5.2.2 the nominal flow rate was found to have only a slight effect on the cone-jet onset voltage, even for emitters with smaller outer diameters.

For the experiments using a 0.5 and 1mm long emitter – which was shown in the Section 5.2.3 to demonstrate two different onset voltages - the average is still taken across all data, as the size of this V_{on} variation with nominal flow rate is relatively small compared to the variation with geometry (as shown on Figure 5.16 (a)).

The errors bars for the average results are the standard deviation across all points. For some of the data, a linear or logarithmic best fit line has been added through the experimental average, to help highlight statistically significant trends.

Table 5.1. The geometric variations tested.

Geometric variation	Emitter inner diameter, μm	Emitter outer diameter, μm	Emitter to extractor distance, mm	Emitter length, mm	Diameter of aperture in extractor electrode, mm	Figure
[1] Emitter inner diameter	*139 - 644*	810	3	31	6	Figure 5.16 (a)
[2] Emitter outer diameter	98 - 155	*200 - 1610*	3	31	6	Figure 5.16 (b)
[3] Emitter to extractor distance, 1st	125	230	*1 - 13*	31	6	Figure 5.16 (c)
[4] Emitter to extractor distance, 2nd	155	510	*0 - 15*	31	6	Figure 5.16 (d)
[5] Emitter length	465	810	3	*0.5 - 31*	6	Figure 5.17 (a)
[6] Extractor electrode aperture, 1st	465	810	3	1	*0 - 10*	Figure 5.17 (b)
[7] Extractor electrode aperture, 2nd	465	810	3	10	*0 - 10*	Figure 5.17 (c)

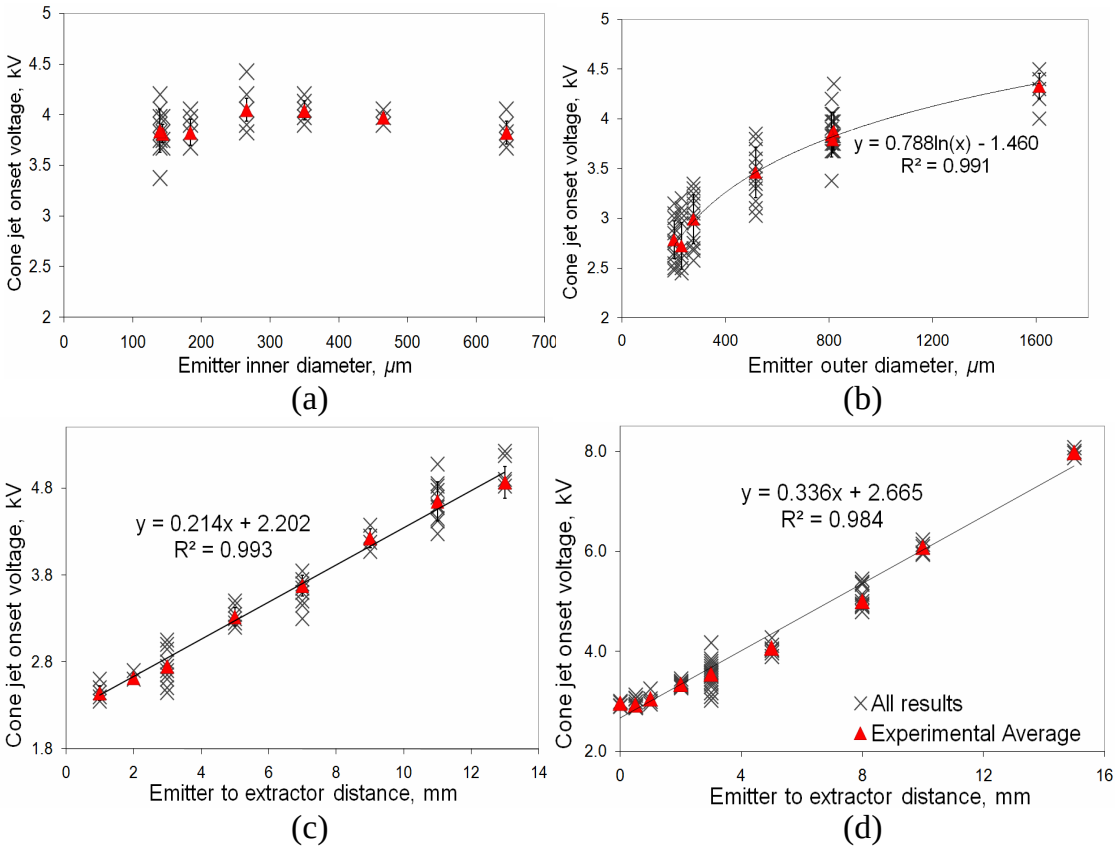

Figure 5.15 (a) – (d).Variation of cone-jet onset voltage with geometry.
(a) – inner diameter of emitter ([1] on Table 5.1);
(b) – outer diameter of emitter [2];
(c) – emitter to extractor distance for 230 μm o.d. emitter [3];
(d) – emitter to extractor distance for 510 μm o.d. emitter [4].

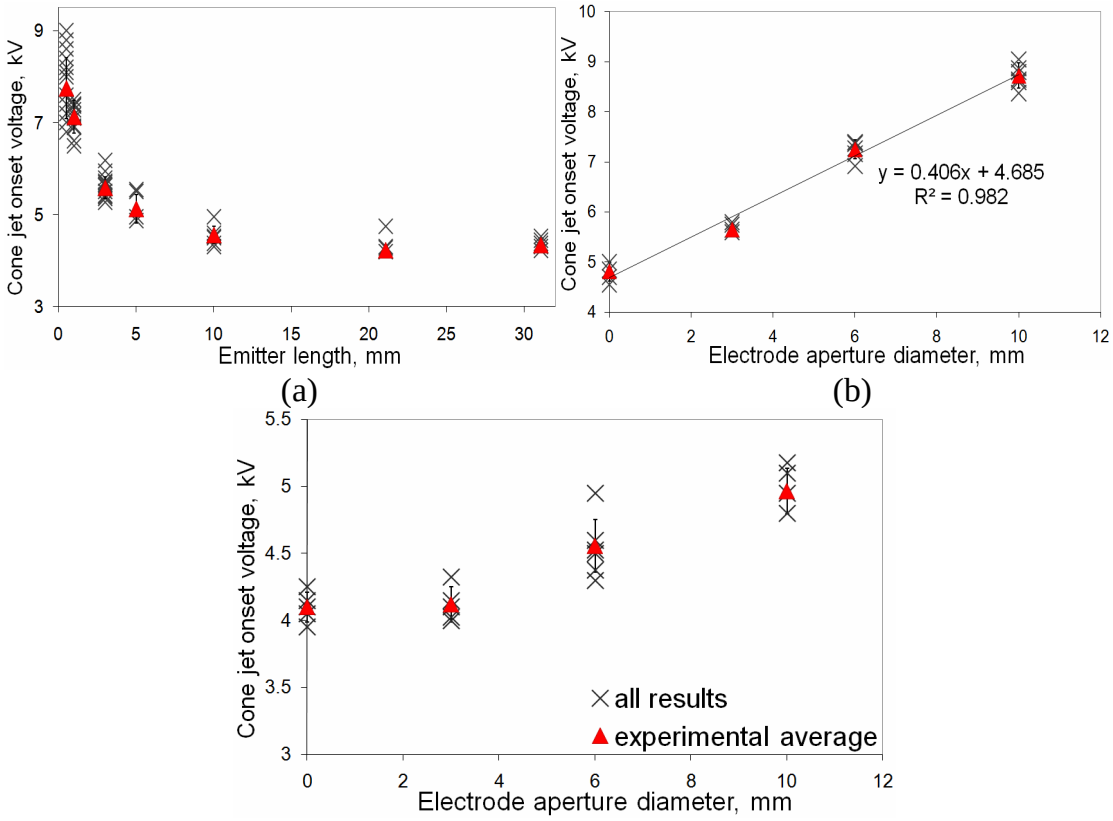

Figure 5.16 (a) – (c). Variation of onset voltage with geometry.
(a) – emitter length (geometry variation [5] on Table 5.1);
(b) – electrode aperture diameter for emitter of length 1mm [6];
(c) – electrode aperture diameter for emitter of length 10 mm [7].

The only geometric variation investigated as part of this research that showed a small effect on V_{on} was the inner diameter of the emitter. As Figure 5.15 (a) illustrates, there was little change of the onset voltage with i.d. for emitters with 800 μm outer diameters.

All other geometric variations had an effect on the cone-jet onset voltage. The largest variation occurred when varying the electrode aperture diameter of a 1mm long emitter, Figure 5.16 (b) (geometric variation [6] in Table 5.1), with an approximately 4kV increase as the counter electrode changes from a flat plate with no aperture to that of an electrode with an aperture with a diameter of 10mm. Interestingly the aperture diameter has a considerably smaller effect for the 10mm long emitter (Figure 5.16 (c), geometric variation [7]), showing only an approximate 1kV increase.

The geometry of the electrospray setup has often been found to affect the voltage at which the onset of cone-jet mode occurs[7,37,44,114-116]. As outlined in Section 2.3.2 it has been found that the o.d. of the electrospray emitter and the emitter to extractor electrode distance affect the cone-jet onset voltage[37], with a simplified equation often applied to estimate V_{on}. By the use of FEM this analysis has been further extended to include other geometric parameters, for example emitter length[107]. The size of the variation with geometry has been found to vary in significance, with it sometimes being found to be a weak logarithmic correction to the general onset voltage equation[7]. Figure 5.15 (a) – (d) though show at least a doubling of the cone-jet onset voltage with outer diameter and emitter to extractor distance, suggesting that a stronger relationship can occur. Also, with Figure 5.16 (a) – (c), other variations in geometry can have a large, if not larger, effect on the cone-jet onset voltage.

5.4.1. Theoretical analysis of cone-jet onset voltage

Equation (2.26) describes the cone-jet onset voltage to vary with the outer diameter of the emitter or the emitter to extractor distance[37];

$$V_{on} = A_1 \left[\frac{2\gamma r_e \cos\alpha_T}{\varepsilon_0} \right]^{1/2} \ln\left(4z_0 / r_e \right). \tag{5.1}$$

In the equation γ is the surface tension (for pure propylene carbonate 0.0452 Nm^{-1}), r_e the outer radius of the emitter, z_0 the emitter to extractor distance, and A_1 a variable factor of the order of unity.

The equation is geometrically dependent solely on the outer diameter of the emitter and the emitter to extractor distance; it is a simplification and so does not describe all the affecting geometric parameters. It is derived from theory such that strictly it should only be applied to long emitters and an extractor electrode with no aperture. For the majority of the experiments reported here the extractor electrode had an aperture with a diameter of 6mm, other than for those experiments that focused specifically on the effect of this

parameter. Even so a comparison between theoretical and experimental data for when o.d. and z_0 were varied can be made.

Figure 5.17 (a) – (c) compare the experimentally determined onset voltage with the theoretical values, for outer diameter varying (Figure 5.17 (a)) and emitter to extractor distance varying data (Figure 5.17 (b) for the 230 μm diameter emitter, and Figure 5.17 (c) for the 510 μm diameter emitter).

The value for A_1 has been adjusted separately for all three geometric variations, to the point where the square of the residuals between experimental and theoretical is smallest (the same method was used in Section 4.5 for the theoretical m_{pe} adjustment). The best fit value of A_1 for each chart is shown in Table 5.2, and illustrates considerable variation of the best fit A_1 value for different geometric variations.

This variation of A_1 limits the ability of the theory to predict the onset voltage *a priori*. These values for A_1 can be compared to the value found for the theoretical value of m_{pe}, described in Section 4.7. The best fit value of m_{pe} for all geometric variations was 0.41, which is considerably different to the values found from the theoretical onset voltage analysis.

Once A_1 has been varied, the theoretical V_{on} for outer diameter data (Figure 5.17 (a)) agrees well with the experiments. The agreement is excellent, although it should be noted that without the variation of A_1 the fit would not be good.

The theoretical estimates for the onset voltages as a function of emitter to extractor distance, whether it is for the 230 or 510 μm o.d. emitter (Figure 5.17 (b) or (c)), do not agree well with the experimental data. The experimental z_0 data is approximately linear, whilst the theoretical trend is indicative of a power law with an exponent less than one. This conclusion, that the theory is not good at predicting the onset voltage variation with emitter to extractor distance, disagrees with those of previous studies, where the theoretical equation did describe the experimental trend of V_{on} with z_0 well[37,44]. This suggests that the aperture in the extractor electrode is having a significant influence on the observed performance, and that the aperture results in the deviation of experimental results from the analytical model that has been found in this study.

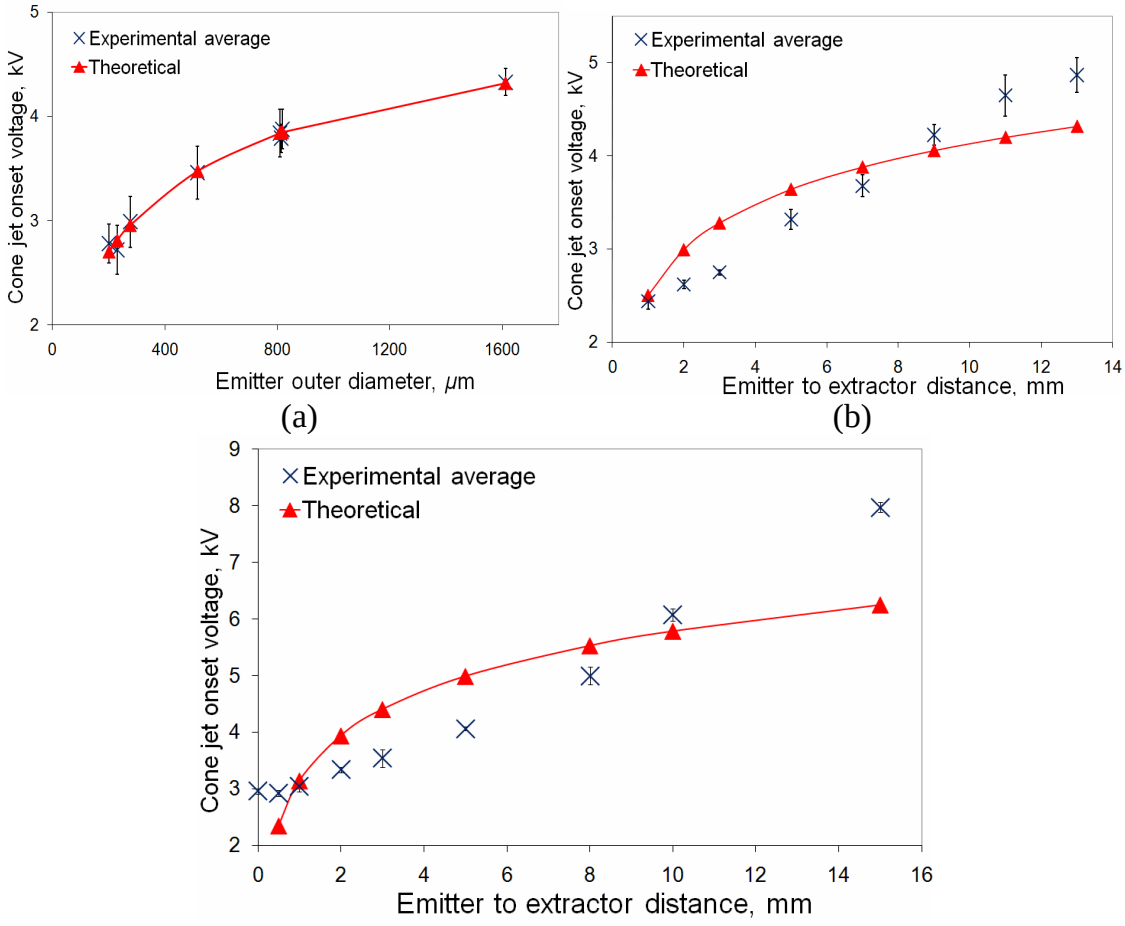

Figure 5.17 (a) – (c). comparison of experimental and theoretical onset voltages for: (a) – outer diameter varying (geometry variation [2]);
(b) – emitter to extractor distance varying for 230 μm o.d. emitter [3];
(c) – emitter to extractor distance varying for 510 μm o.d. emitter [4].

Table 5.2. Variation of best fit value of A_1 with geometric variation.

Geometric variation	Best fit value of A_1
o.d. varying	0.690
z_0 varying for 230 micron o.d. emitter	0.806
z_0 varying for 230 micron o.d. emitter	0.875

The calculation of the onset voltage uses the same electric field equation, equation 2.24 in Section 2.3.2, as the theoretical calculation of the change in electric pressure with voltage, m_{pe}. Consequently there could be some agreement for what geometric variations the experimental values of V_{on} and m_{pe} agree with the theoretical. This would seem to be approximately true, since as when the outer diameter of the emitter is varied, the theoretical values of m_{pe} (shown on Figure 4.9) or the onset voltage agree well with the experimental. But for the case when the emitter to extractor distance is varied, neither the theoretical m_{pe} (Figures 4.15 and 4.16) nor V_{on} agrees with the experimental values. They both show the correct basic trend, but diverge significantly from the experimental results.

5.4.2. FEM analysis of the cone-jet onset voltage

As discussed in Section 4.11 the cone-jet onset voltage can be modelled using FEM, by applying different cone shapes with decreasing tip radii r_a[13].

In the same way as with the theoretical V_{on} derivation, using the FEM electric field to calculate the electric pressure and equating that to the surface tension stress gives

$$V_{on} = \frac{1}{\kappa}\sqrt{\frac{4\gamma}{\varepsilon_0 r_a}}. \qquad (5.2)$$

For small apex radii the above onset voltage is independent of the apex radius, as the dependence of kappa on $r_a^{-1/2}$ cancels out the apex radius term within the square root sign (as described in Section 4.11). Consequently once the apex radius is small enough the onset voltage will reach an asymptote, and not increase or decrease further[13].

The FEM cone-jet onset voltage can be calculated and compared to the experimental results. Figure 5.18 demonstrates typical results from this analysis, showing the trend towards an asymptote as the tip radius becomes smaller (the chart is similar to Fig. 6 and 7 of Krpoun *et al.*[13]). In Figure 5.18 the modeling results agree well with the experimental data once the tip radius of the Bernstein-Bézier curve is small enough.

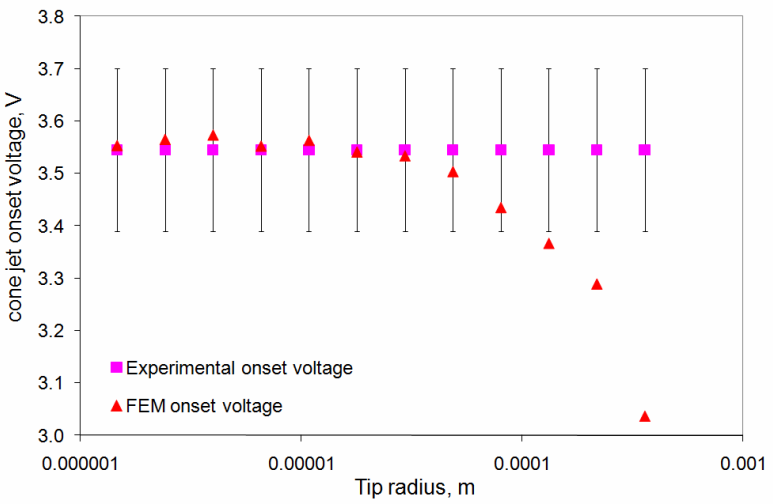

Figure 5.18. Variation of FEM onset voltage with apex radius, for emitter of o.d. 510 μm and z_0 = 3mm.

Except for the emitter inner diameter where no variation of V_{on} was found, the FEM onset voltage was calculated for all geometric changes. The apex radius was decreased to the point that the modelling estimate of the onset voltage was constant, and the average value of this asymptotic value was used. The results are shown, alongside the experimental average (and the theoretical in the o.d. and z_0 varying cases), in Figure 5.19 (a) – (f). The error bars for the experimental average are the standard deviation. For the 0.5 and 1mm long emitter results (geometric variation [5] in Table 5.1, shown in Figure 5.19 (d)), where the onset voltage varied significantly with pulsed mode pulsation frequency (see Section 5.2.3), the onset voltage is taken across all data points.

For the onset voltage data obtained by varying the outer diameter (Figure 5.19 (a)) the FEM values are in reasonable agreement with the experimental values. The FEM results do though deviate as the outer diameter becomes larger, with the theoretical values in better agreement for this data. It should be noted though that the theoretical predictions have been fitted to the experimental (by the variation of A_1), whilst the modelling requires no fitting (once a meniscus with a small enough apex radius has been applied to the emitter tip).

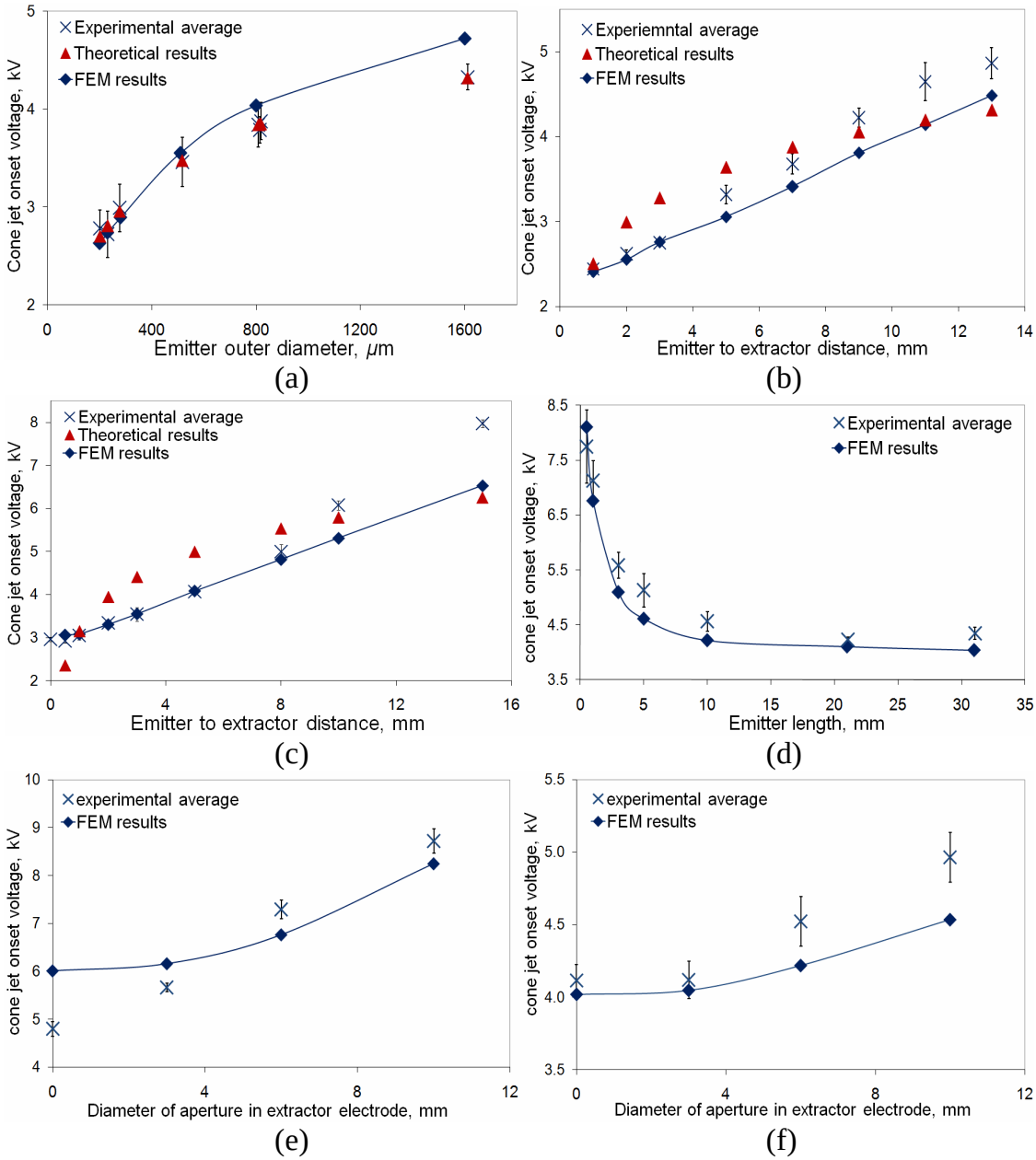

Figure 5.19 (a) – (f). Comparison of experimental, theoretical and FEM cone-jet onset voltages, for differing geometries.

(a) – emitter o.d. varying (geometry variation [2] in Table 5.1);

(b) - z_0 varying for 230 μm o.d. emitter (geometry variation [3]);

(c) - z_0 varying for 510 μm o.d. emitter [4];

(d) - emitter length varying [5];

(e) – electrode aperture diameter for emitter of length 1mm [6];

(f) – electrode aperture diameter for emitter of length 10 mm [7].

For the experiments where the emitter to extractor distance was varied (Figure 5.19 (b) and (c)) the modelled results compare well to the experimental data for small values of z_0, but deviate for larger values. Even so, the FEM results still show the overall trend better than theoretical estimate.

This deviation between FEM and experimental results at large emitter to extractor electrode distances may be a result of various effects. One such effect is that of space charge. As the distance to the extractor increases, the amount of charge contained in the volume between the emitter and extractor will increase (assuming the current is not affected by z_0). Therefore the experimental voltage would be greater than that solely resulting from the geometric variations.

Alternatively at large z_0 distances the effect of any surrounding geometry (i.e. experimental apparatus not included in the geometry that was meshed) may become significant, and this could increase the onset voltage. In the case of the z_0 varying experiments the geometry modelled consisted of a 31 mm long emitter (of either 230 or 510 μm o.d.) protruding from an infinite plate. In reality the 31 mm long emitter protruded from a stainless steel union of approximately 6 mm diameter. Therefore the geometry modelled deviated from the experimental geometry, with it being plausible that this wrong modelled geometry would only have an effect at large emitter to extractor distances.

For the emitter length varying results,Figure 5.19 (d), the FEM model follows the same trend as the experimental results. For the 0.5mm and 1mm long emitters, the onset voltage was found to vary significantly with pulsation mode (described in Section 5.2.2). Here the experimental average includes all data, and the modelled results are within the (large) error bars.

For the variation of the electrode aperture diameter (Figure 5.19 (e) for the 1mm long emitter and Figure 5.19 (f) for the 10mm long emitter) the FEM onset voltages agree approximately with the experimental results, showing the correct basic trend. It should be noted that the two charts show significantly different variations of onset voltage with the aperture in the extractor electrode. For the 1mm long emitter (geometry variation [6] in

Table 5.1) V_{on} varies by ~4kV with electrode aperture, whilst for the 10mm long emitter (geometry variation [7]) the increase is only ~1kV. The FEM onset voltage captures these differing trends well, although modelled results do deviate from the experimental for some cases.

In summary the modelling of the cone-jet onset voltage works well over order of magnitude changes in geometric parameters. It can predict the cone-jet onset voltage with outer diameter, z_0, emitter length, and electrode aperture diameter adequately, and in some case very well. It is a distinct improvement on the theoretical estimate, offering a far more adaptable cone-jet onset voltage estimate.

There were though some problems with the simulation of the onset voltage. The FEM method relies upon the modelling program's ability (ANSYS was used) to mesh a certain geometry and then solve the Laplace equation for a particular geometry. As the apex radius of the chosen cone shape must be small to best match the onset voltage, there can be a large variation in the size of the meshing element sizes involved. This can lead to difficulties with the meshing and solving of the ANSYS code. The problem is exacerbated by the long length of the emitters used during most of these experiments. In one case – for geometry variation [4] with z_0 = 0 mm – it was not possible to solve the ANSYS simulation (as shown on Figure 5.19(c)), as the volume meshing of the simulation could be completed.

The modelling of the onset voltage offers the possibility of giving a good estimate of the start of cone-jet mode, regardless of whether the geometry is simple or complex. The FEM simulation need only be run once, with a cone section that has a suitably small apex radius, so need not be laborious for the user. Currently though the modelling struggles with geometry that has greatly varying lengths. For the model to be more generally and easily applicable this would need to be solved. As currently the FEM simulation uses the rather basic ANSYS program, this could be completed by using a more advanced FEM program that has greater ability to produce and then solve an FEM mesh with large variation in element size.

5.5. Cone-jet mode voltage range

Throughout these experiments the voltage has been varied from within enhanced dripping or pulsed mode, through cone-jet mode, and into multi-jet mode. Consequently the full cone-jet voltage range (V_{range}) has been measured over several hundred experiments, and can be calculated from V_{on} to the maximum voltage at which a stable cone-jet mode occurred.

Figure 5.20 (a) to (f) illustrate the variation of the average stable cone-jet voltage range for the various different geometric parameters tested. The stable cone-jet voltage range was calculated for all experimental runs completed. The average was then calculated for experiments having the same geometry, which was over the approximately eight experiments at different nominal flow rates. The error bars are the standard deviation of the averaged data. The data for the electrode aperture investigations using the 1mm long emitter are not included as insufficient data was collected.

There are some significant errors in the calculation of the cone-jet mode voltage range. One such error results from the voltage steps, with the error being roughly two times the voltage increment (i.e. the voltage step at the beginning and also at the end of the voltage range). To mitigate against this error, the increments of the high voltage supply were decreased for geometric situations that resulted in small cone-jet mode voltage ranges. Also as the average cone-jet voltage range was calculated this can, if calculated across enough points, increase the resolution beyond that of the voltage step.

Another error in the cone-jet voltage range results from the variation of the cone-jet onset voltage with nominal flow rate, as described in Section 5.2.2. This variation though was generally small, and only affected emitters with small outer diameters or relatively small aspect ratios. By taking an average its effect is partially alleviated.

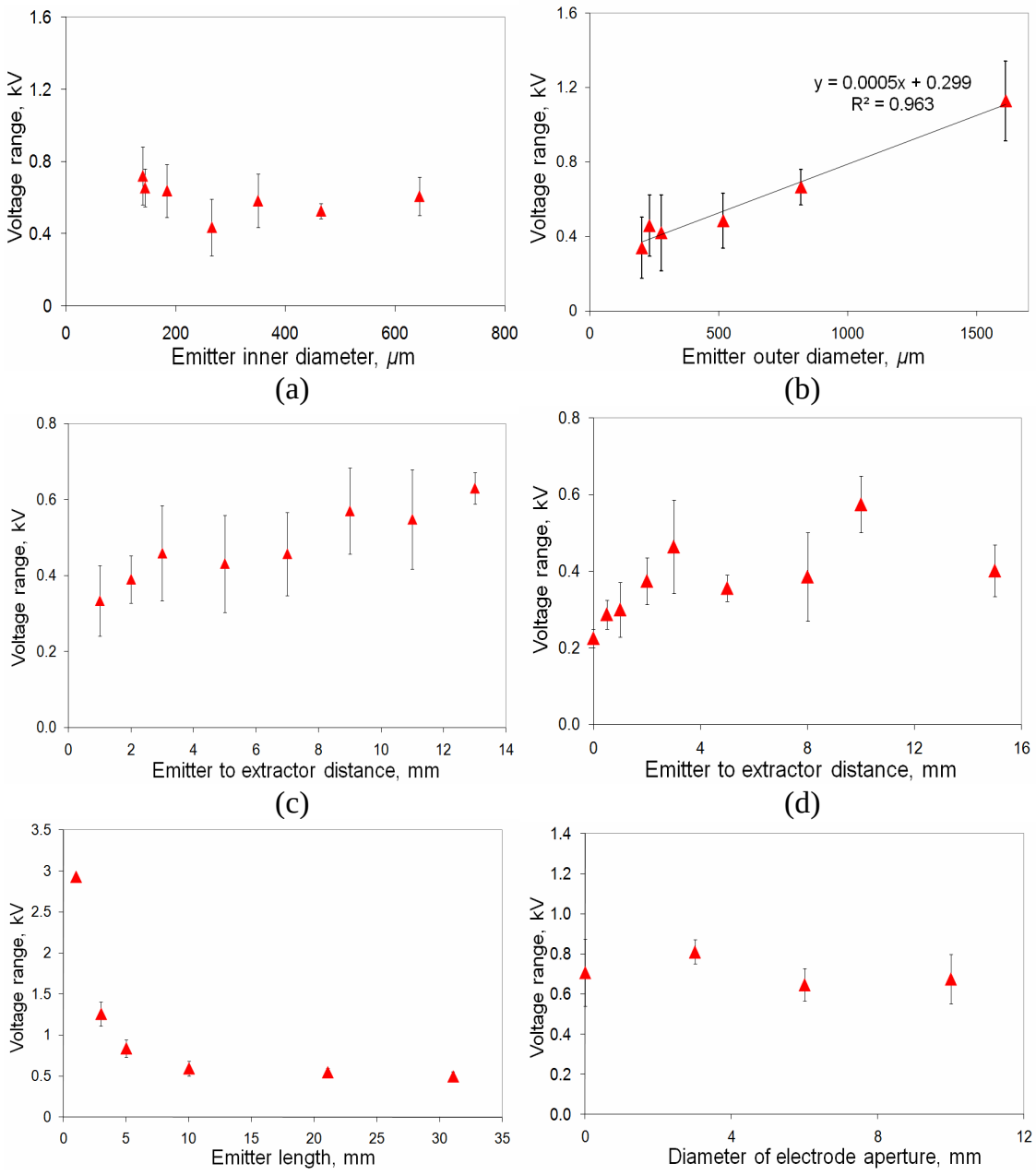

Figure 5.20 (a) – (f). Variation of cone-jet voltage range with geometry.
(a) – emitter inner diameter (geometry variation [1] in Table 5.1);
(b) – emitter outer diameter (geometry variation [2]);
(c) – emitter to extractor distance for 230 μm o.d. emitter [3];
(d) – emitter to extractor distance for 510 μm o.d. emitter [4];
(e) – emitter length [5];
(f) – electrode aperture diameter for 800 μm o.d. emitter of length 10 mm [7].

For some geometric changes little variation of voltage range was found. For example the emitter i.d. does not affect the voltage range to a great degree, as shown in Figure 5.20 (a). This agrees with the cone-jet onset voltage change with emitter inner diameter (Figure 5.15 (a)), which was found to vary only marginally with i.d.
Also for the electrode aperture o.d. using a 10 mm long emitter, Figure 5.20 (f), no significant variation of voltage range was found. This constant voltage range is likely a result of the small change in cone-jet onset voltage, as shown in Figure 5.16 (c), itself suggestive of little variation in electric field with extractor electrode aperture for this longer emitter.

For the some geometric variations there is a significant increase of the cone-jet voltage range. The variation of the emitter outer diameter (Figure 5.20 (b)), the emitter to extractor distance for the 230 μm o.d. emitter (Figure 5.20 (c)), and the emitter length (Figure 5.20 (e)), all demonstrate an effect on the cone-jet voltage range.

For the two investigations of the variation of the emitter to extractor distance (Figure 5.20 (c) and (d)), there is a slight disagreement as to whether z_0 affects V_{range}. For the 230 μm o.d. emitter (Figure 5.20 (c)) there is a trend of the range increasing with z_0. But for the 510 μm o.d. emitter (Figure 5.20 d), there is no clear trend (although there is a slight suggestion of decreasing V_{range} for small z_0 values). The reason for this disagreement is possibly due to the only slight effect (for the 230 μm o.d. emitter) of z_0 on V_{range} found. For this emitter, the voltage range increases from 333 ± 93 volts at 1mm distance, to 630 ± 41 volts at z_0 = 13 mm. This effect, although it statistically present, is small, and it is the smallness of the effect that could be why it is not as noticeable for the 510 μm o.d. emitter.

The variation of emitter length has a large effect on the stable cone-jet voltage range, as shown in Figure 5.20 (e). For an emitter of length 31 mm, the voltage range is 485 ± 118 voltage, whilst for an emitter of length 1mm the voltage range is 3028 ± 211 volts. It should be noted though that the voltage range for an emitter length of 1mm is the average of just two points, as only two experiments were completed up to multi-jet mode, as

spark discharges consistently occurred. For the even shorter 0.5mm long emitter, regular electrical breakdown resulted in no V_{range} data collected at this emitter length.
For the 1mm long emitter, if instead the average is calculated across all the experimental data for this emitter length, i.e. up to the maximum voltage tested in cone-jet mode before electrical discharges occurred, then V_{range} = 2930 ± 299 volts. This is not considerably different from the data using two points, suggesting that a very large voltage range does occur.

Another complication with this data is the variation in the cone-jet onset voltage with pulsation frequencies for short emitters, as discussed in Section 5.2.2. For the 1mm long emitter the cone-jet onset voltage varied by approximately 800 volts. Consequently the voltage range calculation for the 1mm long emitter is not accurate, but does give an indication of the seemingly exponential increase in cone-jet voltage range with decreasing emitter length.

The variation in cone-jet voltage range with geometry can be plotted against the value of m_{pe} found for each geometric case, as has been done in Figure 5.21. All six geometric variations plotted in Figure 5.20 (a) – (f) have been plotted, with y-error bars being the standard deviation of the cone-jet mode voltage range.
It would seem there is a possible relationship between the voltage range and the value of the change in electric pressure with voltage. As m_{pe} decreases the cone-jet voltage range would seem to dramatically increase.
As outlined previously in its theoretical derivation, m_{pe} can be thought of as a measure of the rate at which the electric pressure (or field) varies with voltage. Consequently, assuming that multi-jet onset occurs at the same electric field regardless of geometry, then for a smaller m_{pe} a larger voltage increase is needed to obtain the same electric field. Therefore the onset of multi-jet mode is higher, and the voltage range larger.

The change of electric field with voltage, $\Delta E/\Delta V$, can be calculated for all different geometric variations using the FEM analysis. Using the emitter tip shape that gave the closest agreement of modelled m_{pe} to theoretical m_{pe} (generally this was with a tip apex

ratio of r_a/r_e = 1.40, as outlined in Section 4.11), the change in electric field with voltage for this tip geometry can be calculated.

The cone-jet voltage range is plotted against this rate of electric field change in Figure 5.22, for all geometric variations. As would be expected it shows the same relationship as Figure 5.21, with the voltage range increasing significantly for small values of $\Delta E/\Delta V$.

The V_{range} vs. m_{pe} analysis could though be a little misleading. The cone-jet voltage range only increases rapidly once the value of m_{pe} is less than approximately 0.1 PaV^{-1}. All the experiments that had a value of m_{pe} this low used emitters with large outer diameters, either 800 μm or 1600 μm. Consequently it may be the case that the different geometric variations have similar V_{range} vs m_{pe} relationships at ~0.1 PaV^{-1} (the point at which V_{range} dramatically increases) simply because their geometry is quite similar. To establish whether the V_{range} vs m_{pe} trend is truly independent of geometry further tests need to be completed; specifically ones using a smaller outer diameter emitter (say 230 μm) that investigated emitter length would probably give values of m_{pe} of ~0.1 PaV^{-1}, that could be compared with the data shown on Figure 5.21. These experiments are though beyond the scope of the current work.

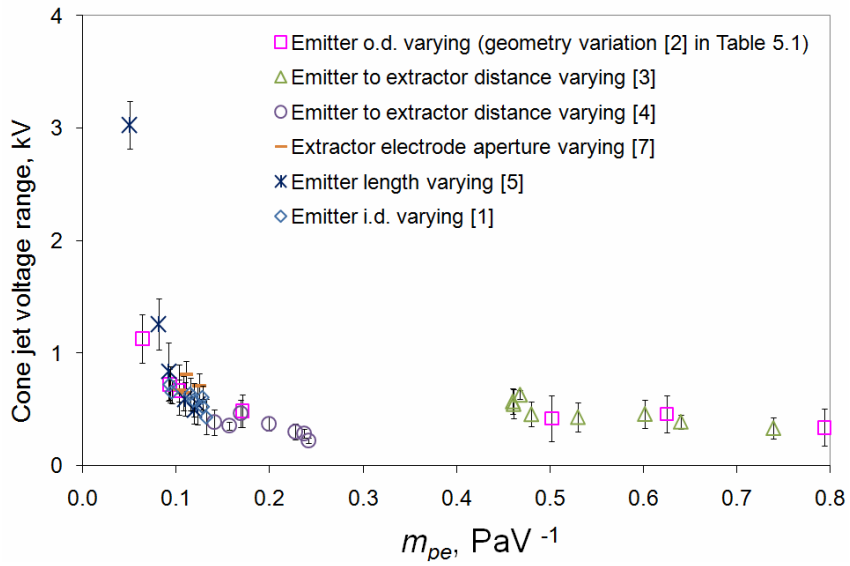

Figure 5.21. Variation of cone-jet voltage range with m_{pe}.

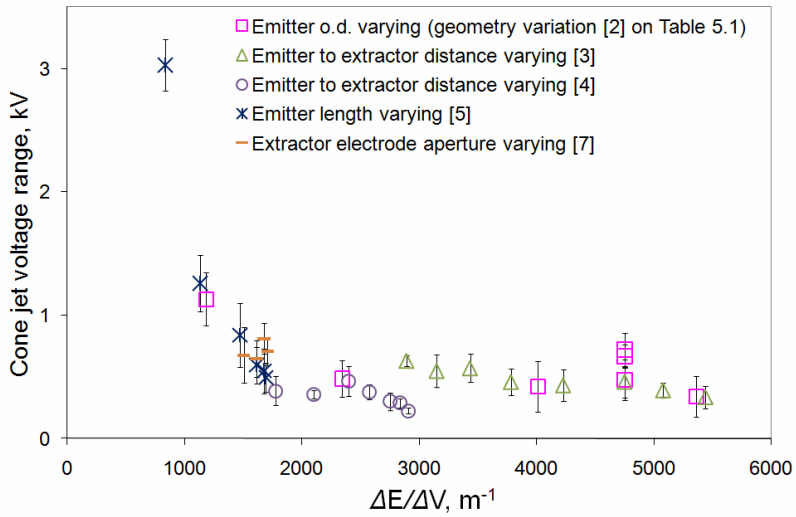

Figure 5.22. Variation of cone-jet voltage range with gradient of FEM electric field.

5.6. The effect of voltage on current in cone-jet mode electrospray

For all experiments the average current in cone-jet mode (excluding current spikes that occurred when the voltage was changed) was calculated at each voltage step. A typical plot of this average current with voltage for one experimental run is shown in Figure 5.23, where the error bars are the standard deviation of the current. In cone-jet mode the error bars are of the order 0.4nA and consequently are smaller than the data points. A linear regression line has been added to the cone-jet mode, with the line having a very good *R*-squared fitting. The gradient of the linear regression fitting, termed m_I, has a value of 18.72 nAkV $^{-1}$.

This excellent linearity of the current-to-voltage ($I(V)$) relationship within cone-jet mode occurred regularly for the experiments completed. Out of the 442 experiments with adequate data 327 have a linear *R*-squared fitting of greater than 0.99 (with at least eight data points included), with the majority of the remainder having *R*-squared values greater than 0.98. This linear relationship of current with voltage in cone-jet mode confirms the findings of previous studies[10,30], whilst disagrees with other studies[61,94], as discussed in the literature review. The results of this study suggest that a linear current-to-voltage

relationship generally occurs over the cone-jet voltage range. It may be the case though, as has been suggested with the change of flow rate with voltage in cone-jet mode (see Section 4.8), that the small cone-jet voltage range means that a non-linear relationship would be hard to distinguish. As though the linear R-squared fitting is general very good, it would seem that for a first order analysis a linear relationship assumption is more than adequate.

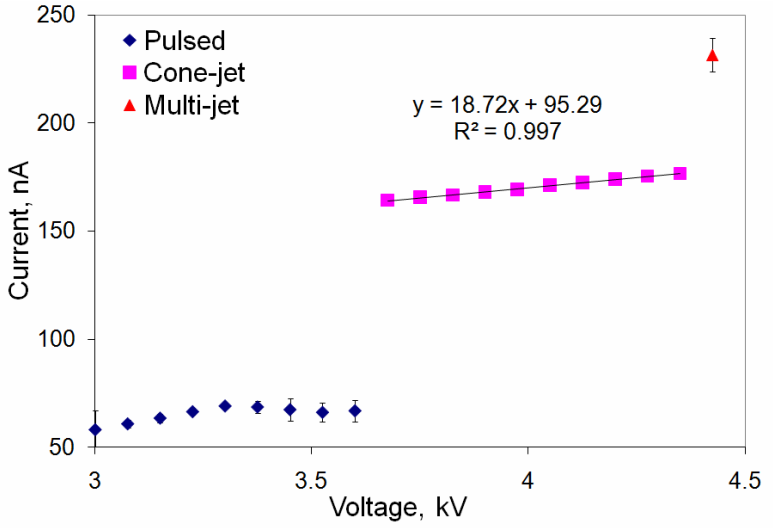

Figure 5.23. The effect of voltage on the average current.

5.6.1. Effect of nominal flow rate on m_I

Previous studies have reported that the gradient of the linear $I(V)$ relationship varies with nominal flow rate[10,56,92]. As the nominal flow rate was measured for all experiments, the same relationship can be investigated here.

Figure 5.24 and Figure 5.25 plot the gradient of the current – voltage relationship in cone-jet mode against the nominal flow rate, for emitter inner and outer diameter varying

experiments, respectively. On each chart the y-error bars correspond to the standard error of m_I.

In the case of the experiments involving the variation of emitter i.d., Figure 5.24, for all emitter inner diameters tested there is a strong trend of m_I increasing with nominal flow rate.

There is also a slight suggestion that emitters with a smaller inner diameter have a smaller value of m_I (at the same nominal flow rate) than the larger emitters. This would correspond with the hydraulic resistance affecting the value of m_I, as it was found to do so for the variation of m_Q with inner diameter.

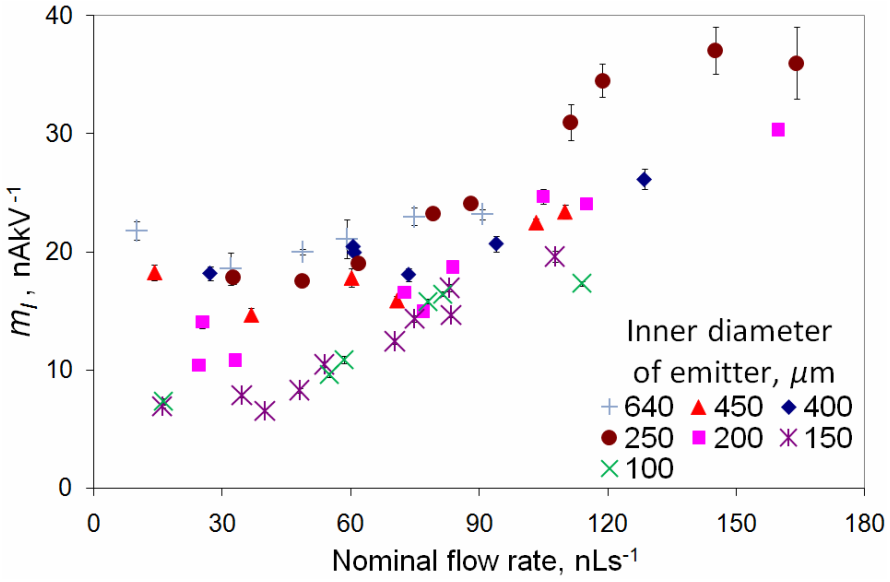

Figure 5.24. Variation of m_I with nominal flow rate, for emitter inner diameter varying experiments. Experiments used emitters with an outer diameters of ~800 μm (geometry variation [1] in Table 5.1).

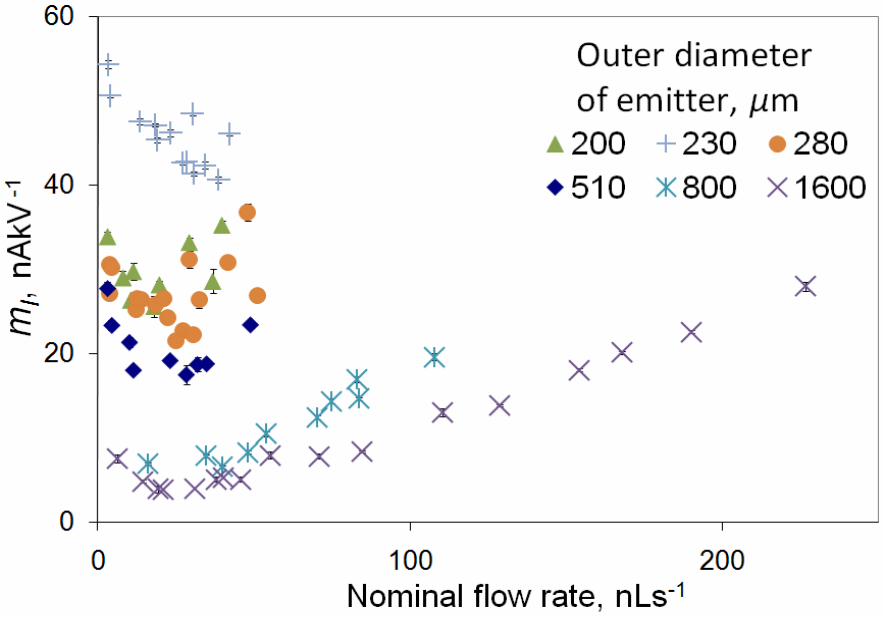

Figure 5.25. Variation of m_I with nominal flow rate, for emitter outer diameter varying experiments. Experiments used emitters with inner diameters of ~100 μm (geometry variation [2] in Table 5.1).

For the experiments involving the variation of the emitter outer diameter, Figure 5.25, the picture is considerably more complicated.

Firstly the effect of the varying cone-jet stability with the outer diameter of the emitter, as discussed in Section 5.2.1, affects the analysis. A larger emitter demonstrates a stable cone-jet mode up to much greater nominal flow rates than a smaller emitter. This has an effect on the m_I data for emitter outer diameter varying experiments as it limits the flow rates at which m_I values can be measured. For example the 230 μm o.d. emitter had a stable cone-jet mode, and therefore an m_I value), up to 50nLs^{-1}. On the other hand the emitter with an outer diameter of 1600 μm had a stable cone-jet mode up to 300nLs^{-1} and so m_I values could be obtained at these greater flow rates.

Secondly there is a clear variation of the m_I values with the outer diameter of the emitter, for the same nominal flow rate. At the same flow rate, an emitter with a smaller outer diameter has a considerably greater m_I value than a larger emitter. This strongly suggests

that m_I is affected by outer diameter in the same way as m_Q was found to be in the previous chapter.

Thirdly there is some seemingly conflicting variation of the m_I value with nominal flow rate for emitters of differing outer diameter. For the smaller o.d. emitters the value of m_I decreases with Q_{nom}, whilst the larger emitters show trends of m_I increasing with Q_{nom}. This could though be an artifact of the varying flow rate stability with emitter outer diameter, resulting in no m_I values for smaller emitters at higher nominal flow rates. If m_I values could have been obtained using smaller o.d. emitter at higher flow rates, then within the high flow rate range their m_I values may also have increased.

As mentioned above, the data in Figure 5.24 and Figure 5.25 suggests that the geometry may have an effect on the value of m_I. Figure 5.26 (a) and (b) plot the variation of the change in current with voltage in cone-jet mode with geometry. The geometry variations shown are the emitter inner and outer diameter respectively. The value of m_Q is plotted on the secondary y-axis of each chart. The m_I values plotted all have an *R*-squared value of at least 0.99.

Both charts would seem to show the same trend of m_I varying with geometry as was found for m_Q. For example the value of m_I decreases with decreasing emitter inner diameter, as shown in Figure 5.26 (a), as does the value of m_Q. The effect though is not as clear, as unlike with m_Q the nominal flow rate effects the value of the m_I gradient. Therefore there is considerable spread of results for a particular geometric configuration, and as a result the data is more difficult to interpret.

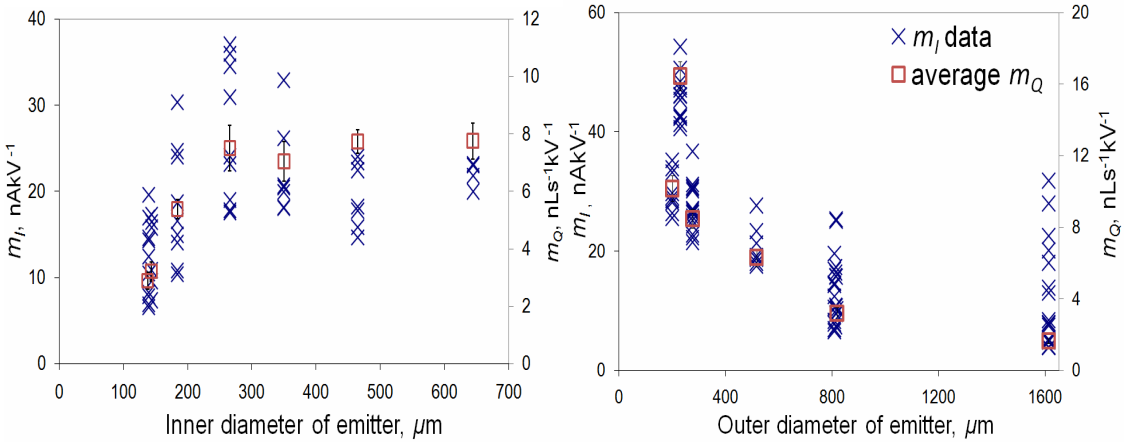

(a) (b)

Figure 5.26 (a) and **(b)**. Variation of m_I with;
(a) – inner diameter of emitter (geometry variation [1] on Table 5.1);
(b) – outer diameter of emitter (geometry variation [2]).
m_Q values are shown for comparison.

For the variation of m_Q with geometry two separate causes were found (see chapter 4); firstly the effect of the hydraulic resistance as a result of the varying emitter inner diameter, and secondly the variation of the change in electric pressure with voltage (m_{pe}) as other geometric parameters were varied. Both these effects are evident in Figure 5.26 (a) and (b). The effect of inner diameter (i.e. hydraulic resistance) can be seen in Figure 5.26 (a) as the m_I values decrease with decreasing emitter i.d, in the same way as m_Q did (see Figure 4.4). But it can also be seen in Figure 5.26 (b), since with the 230 μm o.d. emitter m_I is considerably larger than for emitters of comparable o.d. This was also found for during the m_Q analysis (see Section 4.4), and was explained by this particular emitter having a slightly larger inner diameter than emitters of similar o.d.
The second effect of geometry, the effect of m_{pe}, is shown in Figure 5.26 (b) by the increasing value of m_I with decreasing emitter outer diameter. This was found for m_{pe} also, as shown previously in Figure 4.8.

As m_I is affected by the geometry in the same manner as m_Q it should be possible to collapse the m_I versus Q_{nom} data by dividing by m_Q. Figure 5.27 and Figure 5.28 illustrate

this collapse, plotting m_I/m_Q against the nominal flow rate for the emitter inner and outer diameter varying experiments respectively.

For the emitter inner diameter varying experiments, Figure 5.27, there is a slight collapse of the data onto one line. The collapse is not that strong though, in part because there was found to be little difference between the emitters of different i.d. (as shown in Figure 5.24 and Figure 5.26 (a)).

For the emitter outer diameter experiments, Figure 5.28, the variation of m_I/m_Q with nominal flow rate for o.d. varying data shows a quite remarkable collapse, compared to Figure 5.25. For all emitter outer diameters the m_I/m_Q versus Q_{nom} data follows the same trend.

From Figure 5.28 it would seem that m_I/m_Q decreases slightly with nominal flow rate at first and then increases with flow rate once Q_{nom} is greater than approximately 25nL/s. The emitter inner diameter varying data, Figure 5.27, also seems to show the same trend, although with little data at low flow rates the slight decrease is unclear. There is though no fundamental difference between the two charts.

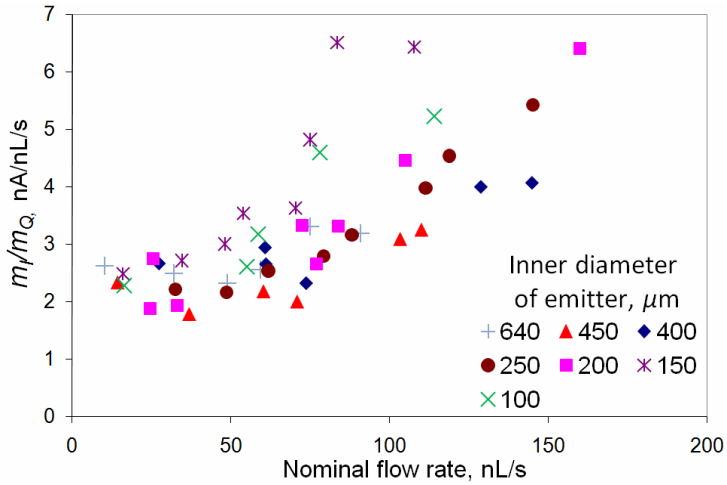

Figure 5.27. Variation of m_I/m_Q with nominal flow rate, for emitter inner diameter varying experiments.

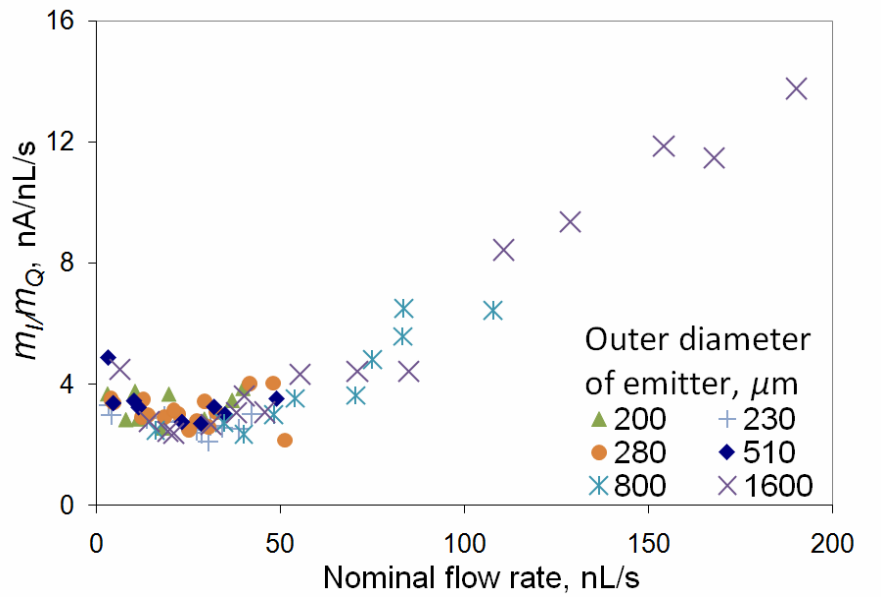

Figure 5.28. Variation of m_I/m_Q with nominal flow rate, for emitter outer diameter varying experiments.

The units used for m_I/m_Q are nA/(nL/s). Interestingly this has the fundamental units of charge/mass, or specifically $\Delta Q/\Delta M$ (as m_I and m_Q are gradients). These units, although currently it is ambiguous as to whether they have a importance, may prove enlightening upon the physics that causes m_I to vary with flow rate.

In summary there are various parameters that have found to have an effect on the value of m_I.

Firstly the hydraulic resistance has an effect on the value of m_I. This is shown most clearly by Figure 5.26 (a) and (b). It is the same variation with hydraulic resistance that was found for m_Q.

Secondly m_I is affected by the variability of m_{pe} with geometry, as illustrated in Figure 5.26 (b). It is the same variation with geometry that was found for m_Q. This effect of geometry on m_I is significant since Figure 5.25 shows an almost order of magnitude change of m_I as the emitter o.d. is varied, at a constant flow rate.

This effect of geometry on the strength of the $I(V)$ relationship in cone-jet mode has been described before[61,72,75] (as described in Section 2.7), although not in such detail, and with

little explanation. Of the previous studies, Rosell agrees most with this study, stating that the current is sensitive to voltage when "*the flow rate was sensitive to V*"[75].
As the value of m_{pe} can be calculated theoretically, the change in m_I when the geometry is varied can be calculated (as long as the value of m_I when using the first geometry setup is known).

Thirdly the nominal flow rate affects the value of m_I. This effect seems to be complex with a decrease with Q_{nom} up to approximately 25 nLs^{-1}, then an increase with Q_{nom} above this value. Why this occurs is not understood. An effect of flow rate on m_I has been noticed by previous studies[10,56], although this is the first time a minimum is reported.

Finally the value of m_I has been reported in previous literature to vary with conductivity[10]. This, combined with the variation of m_I with nominal flow rate, makes any attempt to calculate m_I by a theoretical method extremely difficult, and beyond the scope of this project. It would seem that charge transfer mechanisms are involved in determining the exact value of m_I, suggested by the variation of $\Delta Q/\Delta M$ with nominal flow rate. An electrohydynamic model may be needed to calculate m_I, as was successfully demonstrated by Sen *et al.*[69].

5.7. Conclusions - the stability island of cone-jet electrospray

As also found by previous studies[7,30,57], the stability of cone-jet mode electrospray is affected by the nominal flow rate, with a Q_{max} occurring beyond which no stable cone-jet mode is evident. This Q_{max} is dependent on the outer diameter of the emitter, with a larger emitter having a higher Q_{max}. This dependence of stability on the outer diameter has not been described previously.

The cone-jet onset voltage is dependent on all variations in geometry except the inner diameter. The cone-jet onset voltage has been predicted theoretically for some geometric variations, and for all geometric variations using an FEM model.

The theoretical predictions agree well with the experimental measurements of V_{on} for the emitters of different outer diameter (once A_1 has been varied), but does not provide a good estimate for the emitter to extractor distance varying experiments. It has no ability to predict the effect of other geometric changes, which can affected V_{on} to a greater degree than variations of emitter o.d. or changes in z_0.

The FEM model adequately predicts the V_{on} value for most cases, with the results presented being the first detailed study into the effectiveness of this method. It is a distinct improvement on the theoretical estimate, offering a far more adaptable cone-jet onset voltage estimate. Currently though the FEM calculation is somewhat unstable, but this could be solved by using software that can solve element meshes with greater element size differences.

The cone-jet voltage range varies with geometry, especially so when the emitter length is varied. It would seem to have an inverse relationship with the variation of electric pressure with voltage (m_{pe}), increasing dramatically for smaller values of m_{pe}. This would seem due to the variation of the change in electric field with voltage. This is, as far as the author is aware, the first time that an effect of geometry on the cone-jet voltage range has been reported, and may be the first systematic investigation of the voltage range. The relationship to the change in electric field with voltage may also provide an indication as to how to estimate the onset of multi-jet mode.

As long as the cone-jet mode is stable, the current increases linearly with applied voltage. This was found to occur over several hundred experiments, suggesting that the linearity may be a general occurrence, at least with this and similar solvents. This linear increase of current with voltage, termed m_I, is dependent on the nominal flow rate, the hydraulic resistance, and the value of m_{pe}, with the latter two relationships being reported for the first time. The large amount of data collected also allowed for the complex relationship of m_I to Q_{nom} to be analysed, suggesting that a minimum value occurred. Due to this added complexity of the variation of m_I with many parameters, and with the addition of the variation of m_I with conductivity reported in previous literature[10], resulted in a prediction of m_I being difficult. It is felt that an electrohydrodynamic simulation is needed to predict the value of the change of current with voltage in cone-jet mode electrospray

Chapter 6

6. The variation of flow rate with voltage across various modes of electrospray

6.1. Introduction

Chapter 4 described how voltage influences flow rate in cone-jet mode electrospray, with the flow rate increasing linearly with voltage. The following results extend the analysis to different modes, describing the effect of flow rate across dripping, pulsed, and multi-jet modes, and any noticeable effects when changing modes.

Figure 6.1 (a) illustrates a typical trend of flow rate varying with time as the voltage was increased across various modes of spraying, from enhanced dripping to multi-jet mode. For comparison the variation of current is included, Figure 6.1 (b). The experiment is the same as that shown in Figure 5.1.

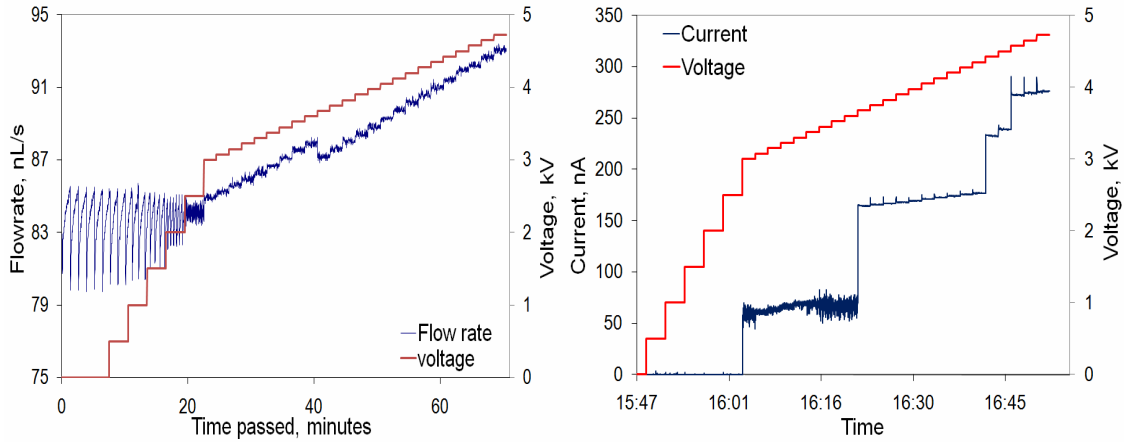

(a) (b)

Figure 6.1(a) and **(b).** Variation of flow rate and current with time, as voltage is increased. Q_{nom} = 83.8 (with a standard deviation of 1.31) nLs^{-1}.

At first the voltage was increased in large 0.5kV steps up to 3kV. Before 3kV the flow rate demonstrated a saw tooth like shape, and no current was noticed. This typified the enhanced dripping mode. As each droplet was produced the variation in the curvature of the droplet as its size increased resulted in a variation of the surface tension pressure, and therefore a variation in flow rate. This effect has been briefly measured previously whilst using the high fidelity flow meter[10]. The effect of voltage on flow rate within enhanced dripping mode is discussed more in Section 6.2.

The lower end of pulsed mode was defined by the change from producing droplets the size of the emitter to producing charged droplets considerably smaller then the emitter. Visually a clear delineation was generally possible, with an unstable cone like structure forming after the slowly pulsing dripping faucet-like situation had terminated. A jump to a measurable current also occurred. The pulsed mode is shown in Figure 6.1 (a) to be affected by voltage in an approximately linear fashion. The effect of voltage upon flow rate within pulsed mode is further investigated in Section 6.3.

At the transition from pulsed to cone-jet mode, a fall in flow rate can be seen in Figure 6.1 (a). This was a clear and repeatable effect, observed over many hundreds of experimental runs, and is further investigated (with reasons for its occurrence hypothesized) in Section 6.5.

At the highest voltages tested, multi-jet mode occurred, signified by the large current increases at high voltages shown in Figure 6.1 (b). There was found to be an effect of voltage on flow rate within multi-jet mode, as can be partially seen in Figure 6.1 (a). The $Q(V)$ relationship in multi-jet mode is though complicated by a small multi-jet stable voltage range, and the transition from two to three and more cone multi-jets. The $Q(V)$ relationship in multi-jet mode is commented upon in Section 6.4.

6.2. The effect of voltage on flow rate within enhanced dripping mode

Figure 6.2 illustrates the same data as Figure 6.1 (a), but focuses on the enhanced dripping mode. One point within pulsed mode has been included at 3kV; at this point a clear current occurred, and there was considerably less variation of the flow rate.

The variation in flow rate as each droplet is formed is clearly visible. At first the flow rate increases quickly as the capillary pressure rapidly changes with the shape variation of the relatively small droplet. This increase in flow rate tails off as the larger drop changes shape less for each extra amount of fluid added to it. Then once the capillary and frictional forces cannot withstand the gravitational and electric field forces, the droplet falls. The meniscus curvature and capillary pressure decreases, the flow rate drops instantly, and the process repeats.

Based on the flow rate measurements Figure 6.2 would seem to show the frequency of the macro-sized droplets increases with voltage, and this is confirmed in Figure 6.3, where the frequency of enhanced dripping is plotted against the applied voltage.

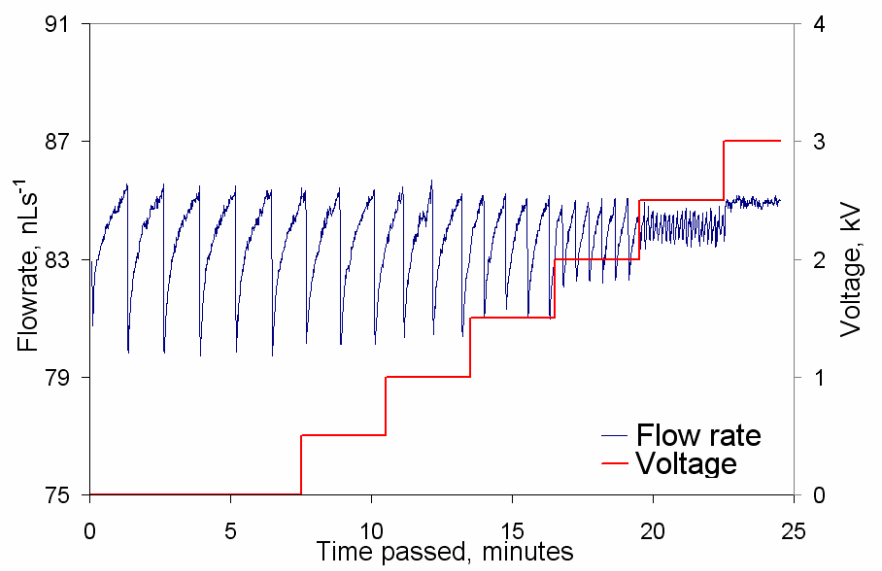

Figure 6.2. The variation of flow rate with voltage in enhanced dripping mode.

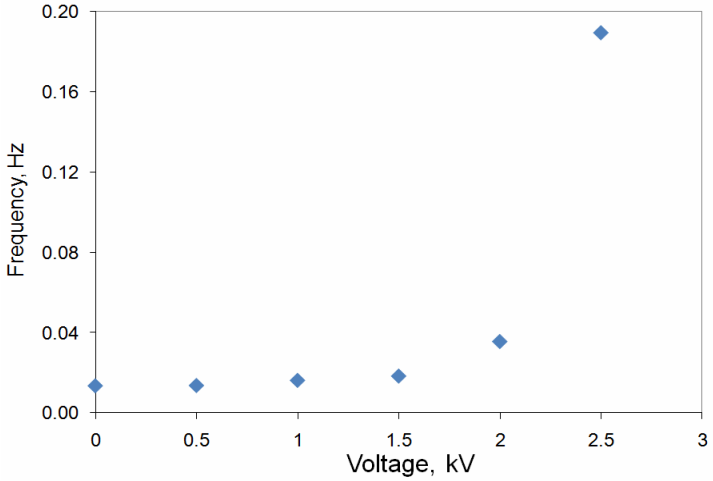

Figure 6.3. Variation of enhanced dripping mode droplet frequency with voltage.

At low voltages of the order 1kV the droplet emission period is only of the order 60 seconds. Consequently as the voltage is increased every three minutes, the frequency values are probably somewhat inaccurate.

Also the flow meter used has a maximum flow rate measurement frequency of ~2 Hz, and therefore once the droplet frequency reaches this limit there is considerable uncertainty in its value. The droplet frequencies in Figure 6.3 are though an order of magnitude smaller than 2 Hz.

Even with these associated errors, the overall trend seems clear - the frequency of the droplets does not vary until a certain voltage is applied, beyond which it increases dramatically. This relationship frequently occurred in the experiments completed, and has been found previously[21,112].

Looking carefully at the oscillations of the flow rate shown in Figure 6.2 it would seem that the difference between the maximum point of each oscillation and the minimum decreases with voltage. To investigate this further the average of the 10 minimum and the average of the 10 maximum flow rate data points can be calculated at each voltage increment. This is plotted in Figure 6.4, along with the difference between the two averages.

Whilst the maximum flow rate of the data's periodic shape does not vary the minimum increases with voltage. Physically this relates to the surface tension pressure not returning to the same point, when the capillary pressure is smallest as the radius of curvature is greatest. This occurs when the large macro-droplet has just broken from the emitter, and there is little liquid on the emitter tip. Therefore it would seem that as the voltage is increased, the droplet emission does not result in all the liquid being removed from the emitter tip every time a droplet breaks off. Consequently the droplets decrease in size with voltage, and this decrease cancels out the effect of the increasing frequency, resulting in the average flow rate being relatively constant. This reduction in the droplet volume with voltage confirms results published[21,112]. As the electric stress increases with voltage the surface tension stress must increase to balance it. This is achieved by an increase in the curvature, or in other words a decrease in the size of primary drops[22].

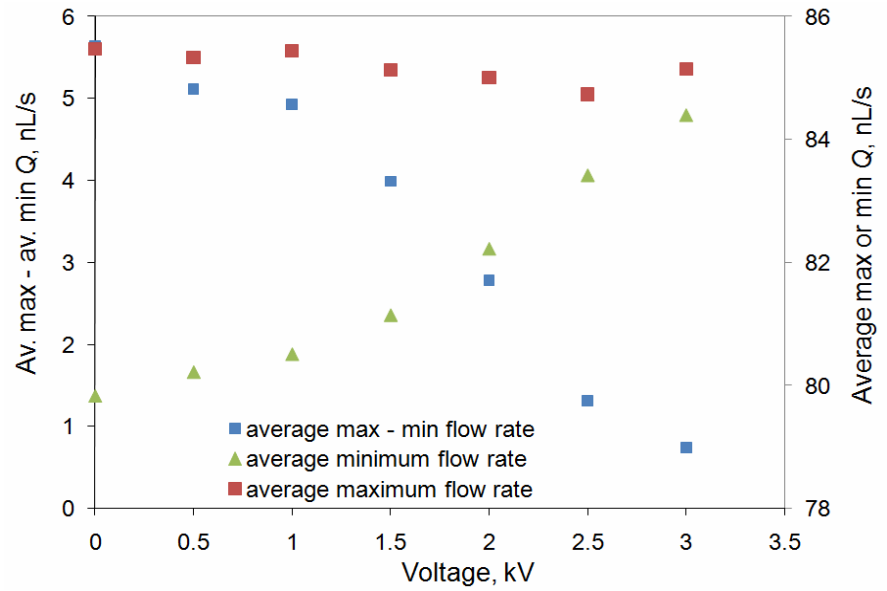

Figure 6.4. Variation of average Q_{max} and Q_{min} in enhanced dripping, and the difference between them, with voltage.

6.3. The effect of voltage on flow rate within pulsed mode

As shown in Figure 6.1 (a), there is an increase of flow rate with voltage in pulsed mode. To investigate this in more detail, the time averaged flow rate can be calculated for every voltage increment in pulsed mode. The result of this is illustrated in Figure 6.5, for the same experiment run shown in Figure 6.1. A linear regression line has been added to the points within pulsed mode, and based on the regression coefficient demonstrates a very linear trend with data.

The gradient of the $Q(V)$ relationship in pulsed mode, termed m_{pulsed}, has in this case a value of 5.03 $nls^{-1}kV^{-1}$ with a standard error of 0.09 $nls^{-1}kV^{-1}$. This is close to the value found within cone-jet mode (also shown on the chart), of 5.69 $nls^{-1}kV^{-1}$ with a standard error of 0.04 $nls^{-1}kV^{-1}$. The two gradient are though statistically different from each other (there is more than 1σ difference between them), but the actual values are reasonably close when compared to the values found for m_Q previously (from 0.4 to 20 $nls^{-1}kV^{-1}$). The differences between m_Q and m_{pulsed} are discussed further in Section 6.3.2.

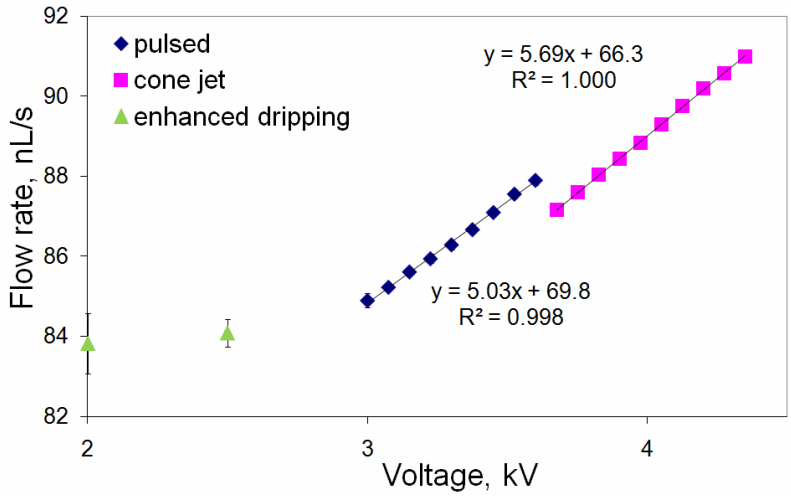

Figure 6.5. Variation of average flow rate with voltage in pulsed mode. Q_{nom} = 83.8 (with a standard deviation of 1.31) nLs^{-1}.

6.3.1. Linearity of the *Q*(*V*) effect in pulsed mode

Within cone-jet mode there was found no indication of any non-linearity of the *Q*(*V*) relationship (see Section 4.8). Within pulsed mode though this was not the case, and non-linearity was observed towards the lower end of the mode, at the transition with enhanced dripping. This non-linearity is illustrated in Figure 6.6, where it would seem that the lowest four points in pulsed mode show a deviation away from linearity.

Figure 6.7 shows the variation of the average current with voltage for the same experiment. There is a relatively constant pulsed mode current at higher pulsed mode voltages. At 3.075 kV there is a peak in the current, as the 'silver bullet' cone-jet mode occurred. This is a form of cone-jet mode that is known to occur at lower voltages, and is typically associated with a long, stretched Taylor cone that forms, and then drains itself and collapses[57]. It generally occurs when the emitter is wetted[60], and was occasionally noticed during these experiments, normally at only one voltage increment.

At lower voltages than 3.075 kV the current was unstable and decreased to the point at 2.5kV where no current was read. This transition region between the enhanced dripping and pulsed modes coincides with the non-linear results shown on Figure 6.6, suggesting that the *Q*(*V*) non-linearity occurs (at least partially) because of the transition from enhanced dripping to pulsed mode.

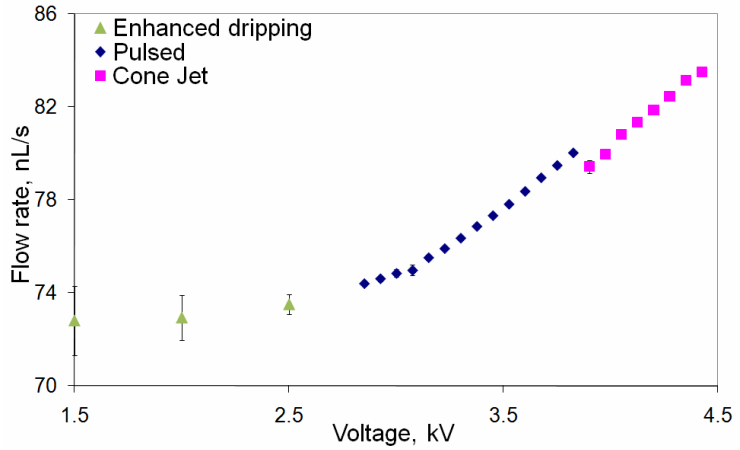

Figure 6.6. The variation of flow rate in enhanced dripping, pulsed and cone-jet modes, for an experiment showing a non-linear $Q(V)$ relationship at the lower end of pulsed mode.

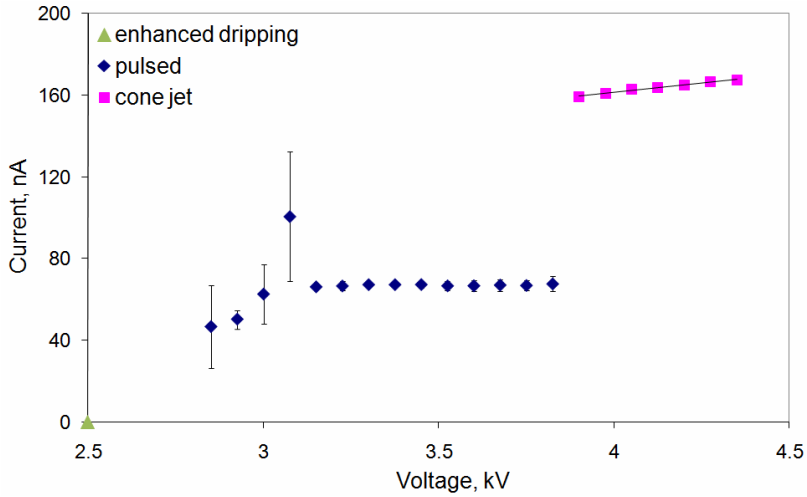

Figure 6.7. Variation of average current in pulsed mode with voltage, for the same experiment as Figure 6.6.

For all sprays with pulsed mode data a linear regression fit was applied to the flow rate – voltage measurements. To account for the non-linearity described above, this linear regression fitting was carried out only over the region where there was evident linearity. This was decided to be at the point where the *R*-squared value of the linear regression

started to drop significantly, as more data points below cone-jet mode were added. This was justified as the *R*-squared value is calculated from;

$$R^2 = 1 - \frac{SS_{err}}{SS_{tot}}, \tag{6.1}$$

where SS_{err} is the sum of squared errors and SS_{tot} is the total sum of squares;

$$SS_{err} = \sum_i (y_i - f_i)^2, \quad SS_{tot} = \sum_i (y_i - \bar{y})^2. \tag{6.2 a, b}$$

y_i are the observed values, f_i are the modelled values, and $\bar{y}$ is the mean of the observed data. Consequently the *R*-squared value decreases significantly when the observed values diverge from the modeled values (i.e. at the point where the sum of the square of the residuals (errors) between model and experimental results increase).

To calculate the point at which this deviation occurred a straight line was plotted through the maximum three points in pulsed mode (just below cone-jet mode) and the *R*-squared value was calculated. The process was repeated with the addition of the next highest pulsed mode data point, with the *R* - squared value and m_{pulsed} calculated again. A typical plot of this method is shown in Figure 6.8. With more than 12 points included in the linear regression, the value of R-squared starts to decrease, and so m_{pulsed} was taken to have the value when using 12 points. As with the data shown in Figure 6.6, this non-linearity occurred at the transition from pulsed to enhanced dripping mode, where the current values began to decrease and became unstable.

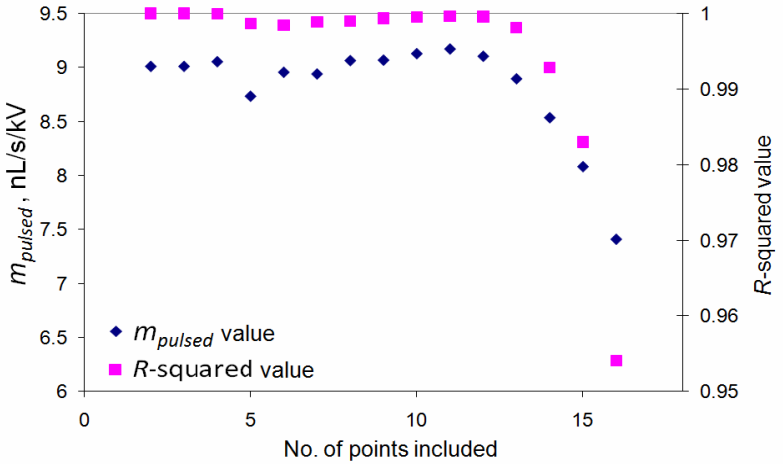

Figure 6.8. Calculation of m_{pulsed}, as length of linear line increases.

In general this method provided linear regression coefficients greater than 0.99, and more than eight data points included in the linear regression fit. As this good linearity was found across hundreds of sprays, this suggests that the linear analysis is a very good approximate estimation of the change in flow rate with voltage within a fully established pulsed mode.

Often though, since the focus of these experiments was cone-jet mode, an experiment was not initiated whilst in dripping mode. Generally the experiments started in pulsed mode, to be sure that the whole of the cone-jet mode was experimentally tabulated. Therefore some experimental runs do not have data across the whole voltage range of the pulsed mode. For the approximately 430 experimental runs with adequate data, around 130 tested the whole pulsed regime (i.e. from dripping mode into cone-jet mode in incremental voltage steps), with the remainder only partially investigating pulsed mode. The method described above though was still applied to all experiments, and no difference in the m_{pulsed} value was found between experiments investigating the whole of pulsed mode, and those investigating only the section at higher voltages.

6.3.2. Relationship between m_{pulsed} and m_Q

From Figure 6.1 (a) one could guess that there may be some similarity between the value of m_Q and m_{pulsed}. Figure 6.9 illustrates this, for different geometric configurations as described in the previous chapters. All points have an *R*-squared value in the determination of both m_Q and m_{pulsed} of at least 0.99.

The value of m_{pulsed} and m_Q are approximately the same, although there is more spread of results at higher values of m_{pulsed} and m_Q.

There is no *a priori* reason to suggest that a linear relationship exists between flow rate and voltage in pulsed mode, and that it would have the same approximate value as in cone-jet mode, since these two modes seem to behave quite differently electrohydrodynamically. It strongly suggests that the flow rate depends upon voltage in the same way, regardless of mode (with the exception of enhanced dripping mode). As cone-jet mode flow rate to voltage dependence has been shown previously to be due to the increase of electric pressure with voltage, it would seem that the same occurs in pulsed mode.

As m_{pulsed} and m_Q are similar in value, it is reasonable to assume that m_{pulsed} will follow the same trends as m_Q: varying with geometry, whilst being independent of the nominal flow rate. Figure 6.10 illustrates the variation of the value of m_{pulsed} with nominal flow rate for the emitters tested with differing outer diameters. Although there is some scatter of the value of the m_{pulsed} for each emitter, none of the emitters show a trend of m_{pulsed} varying with Q_{nom}.

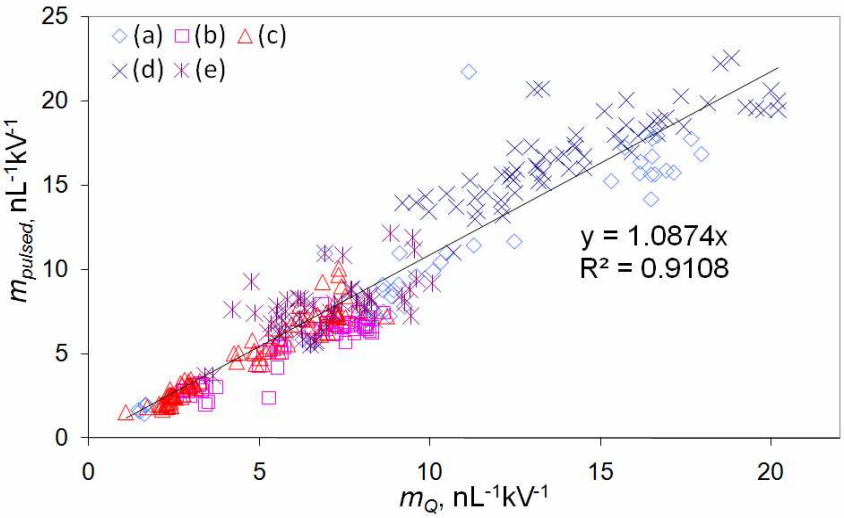

Figure 6.9. Relationship between m_{pulsed} and m_Q for different geometric investigations.
(a) – emitter outer diameter (geometry variation [2] in Table 5.1);
(b) – emitter inner diameter [1]; (c) – emitter length [5];
(d) – emitter to extractor distance for 230 μm o.d. emitter [3];
(e) – emitter to extractor distance for 510 μm o.d. emitter [4].

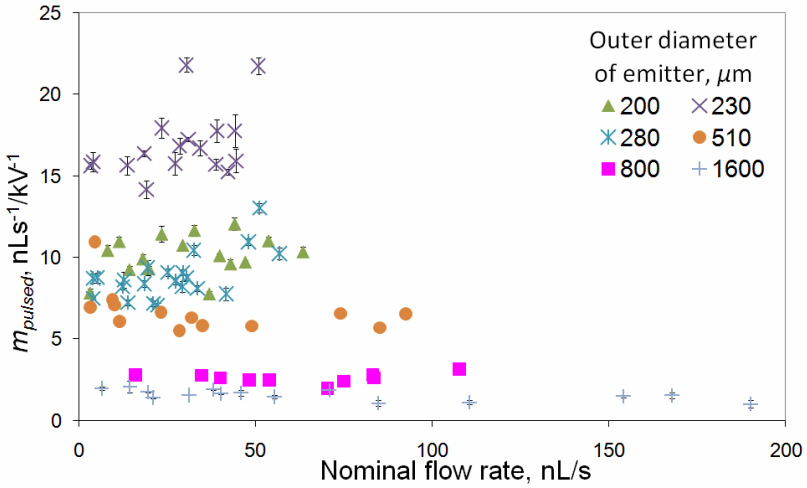

Figure 6.10. Variation of m_{pulsed} with nominal flow rate, for experiments varying the emitter outer diameter.

Figure 6.11 (a) – (e) show the variation of m_{pulsed} with geometry, with m_Q also included for comparison. The points for m_{pulsed} are the average values for results that have an *R*-squared value of greater than 0.99, and have greater than six points included in the linear line. The error bars are the standard deviation.

There would seem to be the same strong dependence of m_{pulsed} on geometry as there was with m_Q. For example m_{pulsed} decreases with both emitter inner diameter and length (Figure 6.11 (a) and (e)), as m_Q was found to. This seems to confirm that m_{pulsed} is affected by the same two parameters as m_Q; the hydraulic resistance and the variation of m_{pe} with geometry. For the emitter to extractor distance varying data, Figure 6.11 (c) and (d), whilst there are apparently individual data points showing disagreement, none of the points have a difference above 3σ, and hence it is possible to conclude both still follow the same trend.

In summary the average flow rate in a well established pulsed mode is highly linear, following the same trends and having the same approximate values as m_Q. Although a $Q(V)$ relationship within pulsed mode has been described before[100], the data set was limited to a few results for the effect of voltage on flow rate within pulsed mode. Therefore this is the first time that an unambiguous and repeatable $Q(V)$ effect in pulsed mode electrospray has been established. The effect of geometry has for the first time been demonstrated, with the relationship bearing a very close relationship to that found within cone-jet mode. Consequently for a particular geometry the effect is reasonable predictable using the analytical model outlined in Chapter 4. The effect has implications for the idea of a minimum flow rate below which no stable cone-jet mode is possible, and this is described in more detail in Section 6.6. Also it has implication for colloid thrusters, as described in Section 6.6.1, and for passively fed electrohydrodynamic processes, as described in in the conclusions of this thesis.

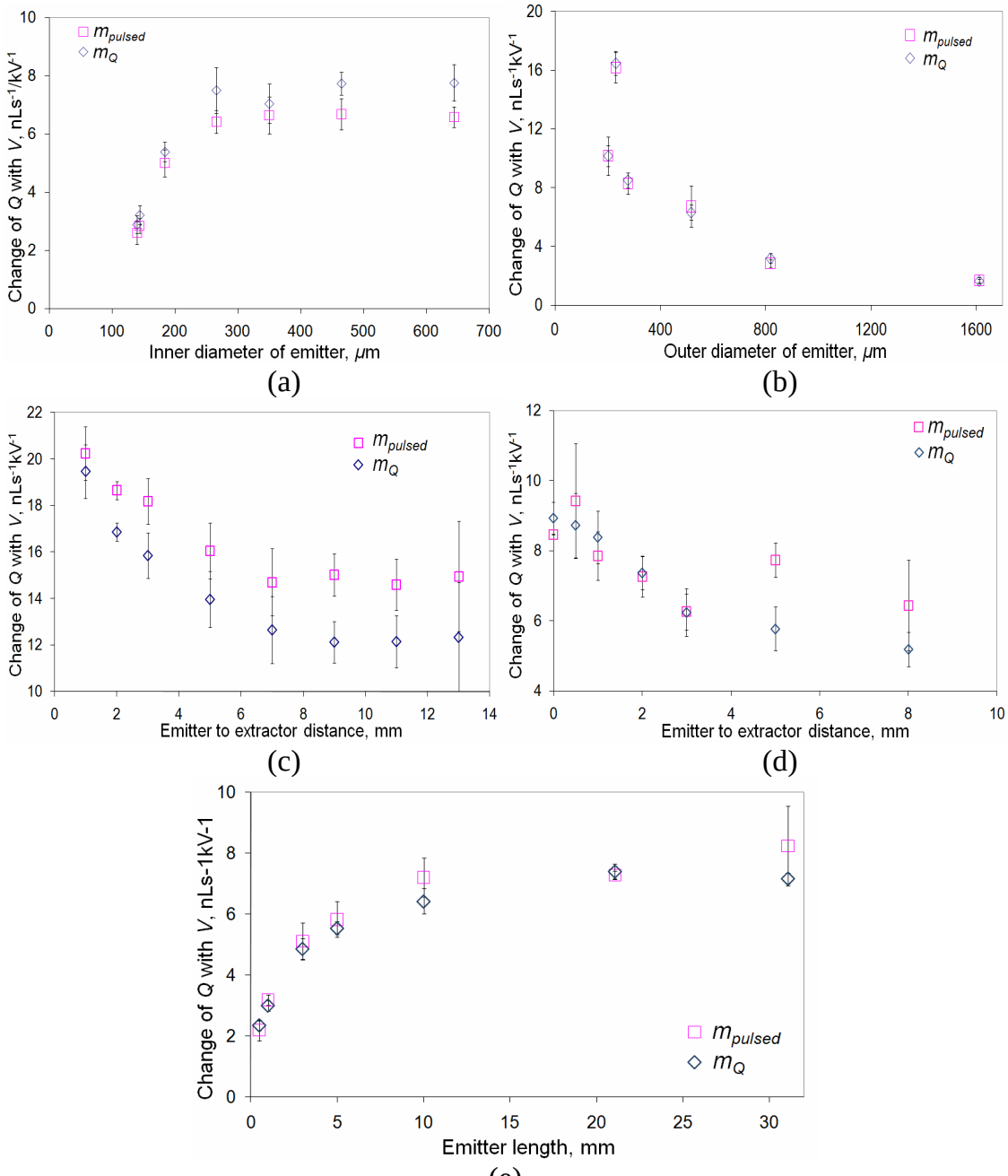

Figure 6.11 (a) – (e). Variation of m_{pulsed} with geometry, with comparison to m_Q.
(a) – inner diameter of emitter (geometry variation [1] in Table 5.1);
(b) – outer diameter of emitter (geometry variation [2]);
(c) – emitter to extractor distance for 230 μm o.d. emitter [3];
(d) – emitter to extractor distance for 230 μm o.d. emitter [4];
(e) – emitter length [5].

6.4. The effect of voltage on flow rate within multi-jet mode

Figure 6.12 illustrates a typical flow rate and current variation as the voltage is increased. Shown are the results through cone-jet and multi-jet modes. The flow rate change with voltage is plotted on the primary x and y axis, whilst the current change with time (as the voltage was increased) is plotted on the secondary axis. The changes of flow rate with voltage are discrete time-averaged data, whilst the current is continuous, non-averaged data. Plotting the current as a continuous data set was chosen so that subtle changes in the current output are more easily distinguishable.The continuous current data has been aligned to the voltages at which the data occurred.

Figure 6.12 demonstrates that multi-jet mode also showed a strong linear dependence of flow rate with voltage. The gradient of the relationship, termed m_{MJ}, has in this case a value of 22.6 $nLs^{-1}kV^{-1}$, close to the value of m_Q in the same figure.

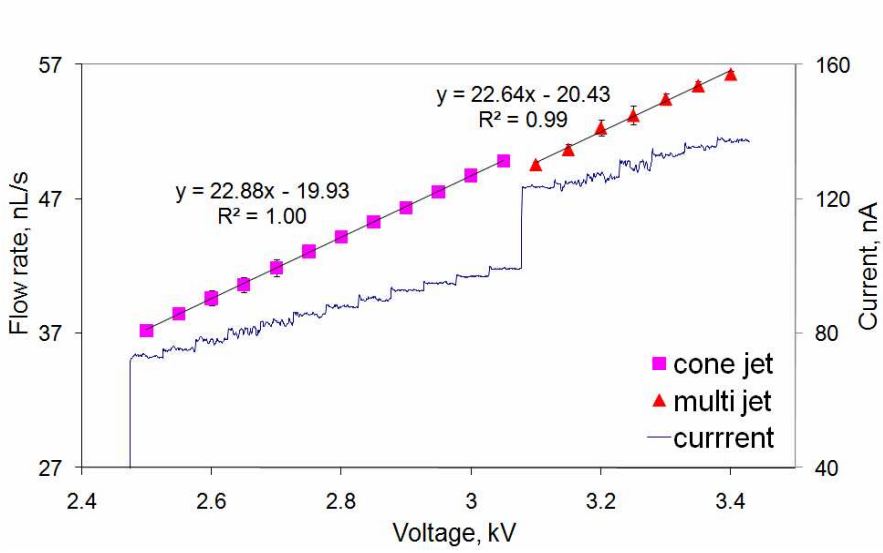

Figure 6.12. Variation of flow rate and current as voltage is increased, across cone-jet and multi-jet modes. Experiment used a 31 mm long, 230 μm outer diameter emitter. Q_{nom} = 29.5nL/s.

In general the multi-jet mode demonstrated a linear $Q(V)$ relationship, although only limited data sets were collected within this mode. In part this was a result of multi-jet mode being found to be considerably more unstable and with a smaller voltage range than cone-jet mode, and this limited the amount of $Q(V)$ data that could be collected.

Figure 6.13 illustrates an experiment where a small multi-jet voltage range was found; again the average flow rate with voltage is shown, along with continuous current data. The current increases as two-cone multi-jet mode occurs, with this two cone multi-jet mode occurring for two voltage increments, until another increase in current marks the beginning of a three-cone multi-jet mode. This change from two to three cones affects the $Q(V)$ relationship, with a slight divergence from linearity at this point. This drop in flow rate probably has some relationship to the drop found when going from pulsed to cone-jet mode, discussed in the following section. If a linear line is plotted through all five multi-jet data points the *R*-squared value is only 0.963. Consequently, because of the small voltage range for each subset of multi-jet mode, there is a difficulty in determining any $Q(V)$ relationship with any great deal of accuracy (without taking smaller voltage steps).

For many experiments the instability of multi-jet mode adversely affected the linearity of the $Q(V)$ relationship, as demonstrated in Figure 6.14. The cone-jet mode would seem to be stable, with an approximately constant current for each voltage increment. The beginning of multi-jet mode though shows a greater variation in current for the first three points, strongly suggesting an unstable transition between the two modes. This resulted in the flow rate data showing non-linearity at the start of multi-jet mode. Once a stable multi-jet mode occurred there was considerably less variation in current and the flow rate began to increase approximately linearly with voltage.

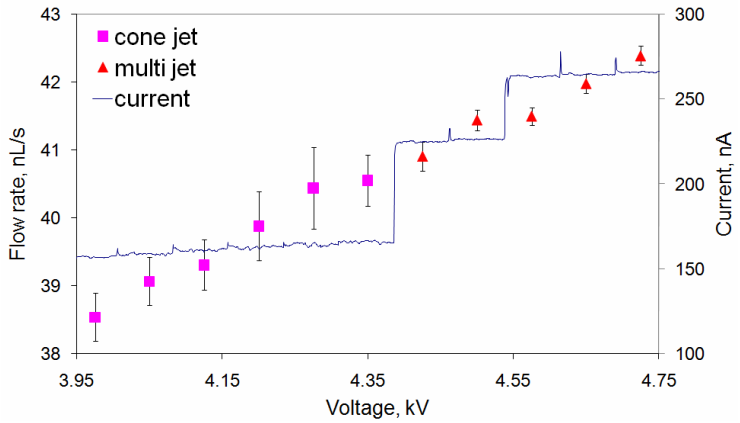

Figure 6.13. Variation of flow rate and current as voltage is increased, across cone-jet and multi-jet modes. Experiment used a 31 mm long, 510 μm outer diameter emitter, at a z_0 distance of 5mm.

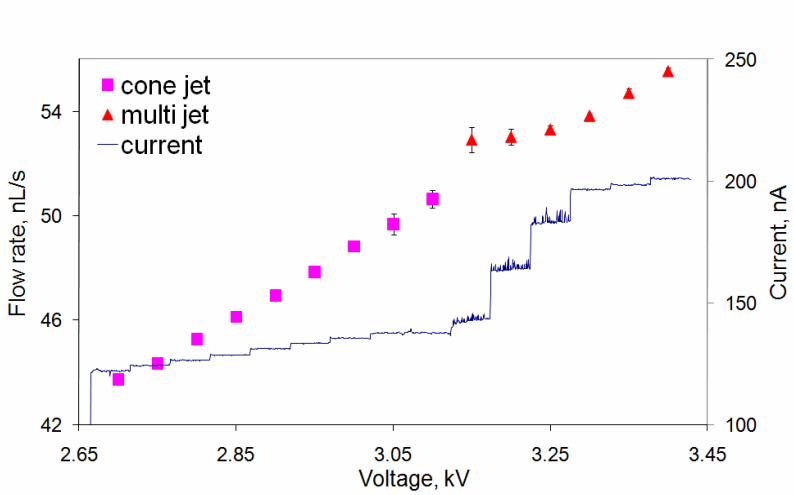

Figure 6.14. Variation of flow rate and current as voltage is increased, across cone-jet and multi-jet modes. Experiment used a 31 mm long, 230 μm outer diameter emitter, at a z_0 distance of 3mm.

It is worth noting that these changes of flow rate for when the multi-jet mode is unstable are small, and in comparison to the current - which dramatically increases - the flow rate shows little variation from cone-jet mode to multi-jet mode. This results in multi-jet mode having greater charge density on the droplets produced, possibly due to charge transfer occurring within two cones rather than one. This suggests having just one Taylor cone may limit the amount of current that can be transferred to the jet, and that multi-jet

mode offers a more efficient charge transfer regime. Noymer *et al.* found the droplet mean diameter in multi-jet mode to be a third of that in cone-jet mode[111]. This agrees with a the finding here of greater charge density in multi-jet mode, as this would encourage more Coulombic explosions of the charged droplets, reducing their diameter to a greater extent.

Even with the difficulties in producing a stable multi-jet mode with a wide voltage range, some experiments still demonstrated good $Q(V)$ linearity across a reasonable number of points in multi-jet mode, as shown by Figure 6.12.

The gradient of the $Q(V)$ relationship in multi-jet mode, termed m_{MJ}, is plotted in Figure 6.15 (a) and (b), with regard to its change with emitter inner and outer diameter. Only m_{MJ} values with R-squared results of greater than 0.98, and including more than 4 points in the linear regression, have been included. All multi-jet data is shown, rather than an average m_{MJ}, whilst the average m_Q has been included for comparison. For the other geometric variations investigated data on the multi-jet $Q(V)$ relationship was too limited for any analysis to be performed.

The two charts demonstrate that m_{MJ} again follows the same dependence on inner and outer diameter of the emitter as m_Q. It therefore seems probable that m_{MJ} is affected by the same parameters as m_Q - the hydraulic resistance and the variation of m_{pe} with geometry.

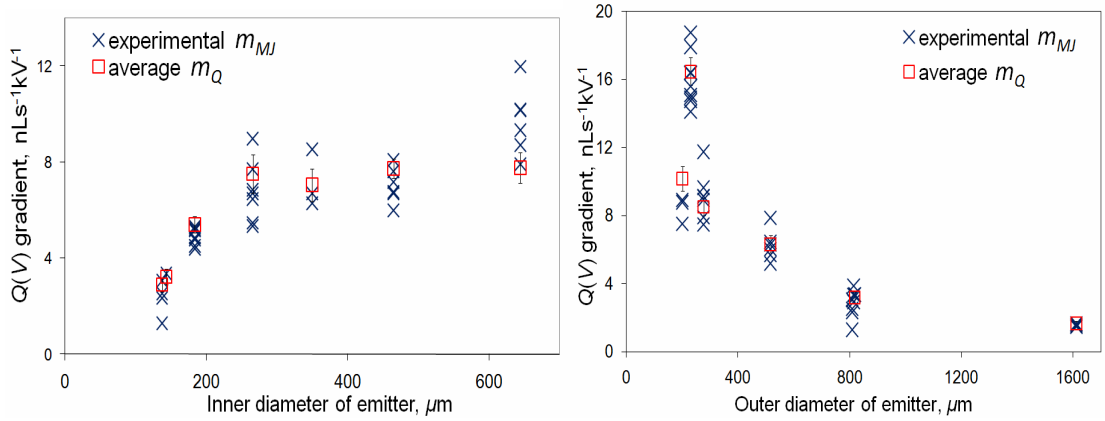

(a) (b)

Figure 6.15. (a) and (b). Variation of m_{MJ} with geometry. (a) – inner diameter of emitter; (b) – outer diameter of emitter.

6.5. The reduction in flow rate in transition from pulsed to cone-jet mode

As has been illustrated in Figure 6.1, Figure 6.5, and Figure 6.6 there is a drop in flow rate when the mode changes from pulsed electrospray to steady cone-jet mode. To quantify this reduction in flow rate a term Q_{jump} is proposed. Due to the linear dependence in both the pulsed regime and the cone-jet regime as shown by the experimental results of the preceding sections, it is possible to define Q_{jump} accurately, rather than rely upon the singular value of the last and first flow rate measurements in each mode. The calculation of Q_{jump}, as illustrated in Figure 6.16, is

$$Q_{jump} = \left[\left\{\left(V_{on} - V_{\max\ pulsed}\right)/2 + V_{\max\ pulsed}\right\} m_{pulsed} + c_{pulsed}\right] - \left[\left\{\left(V_{on} - V_{\max\ pulsed}\right)/2 + V_{\max\ pulsed}\right\} m_{Q} + c_{Q}\right] \quad (6.3)$$

$V_{max\ pulsed}$ is the maximum voltage in a stable pulsed mode, c_{pulsed} the point at which the pulsed mode linear line crosses the y axis, and c_Q the same for the cone-jet linear line. For the experiment shown in Figure 6.16, Q_{jump} has the value of 1.21 nLs^{-1}.

Also included in Figure 6.16 are curved blue lines that represent the 95% prediction intervals - i.e. the intervals in which 95% of future observations will fall within. The predictive intervals are used rather than the more common confidence intervals as the Q_{jump} calculation uses a new intermediate value of voltage, half way between the end of pulsed mode and the beginning of cone-jet mode. They differ from the confidence intervals in being generally larger as they depend on the error from the estimated model and the error associated with future observations[117].

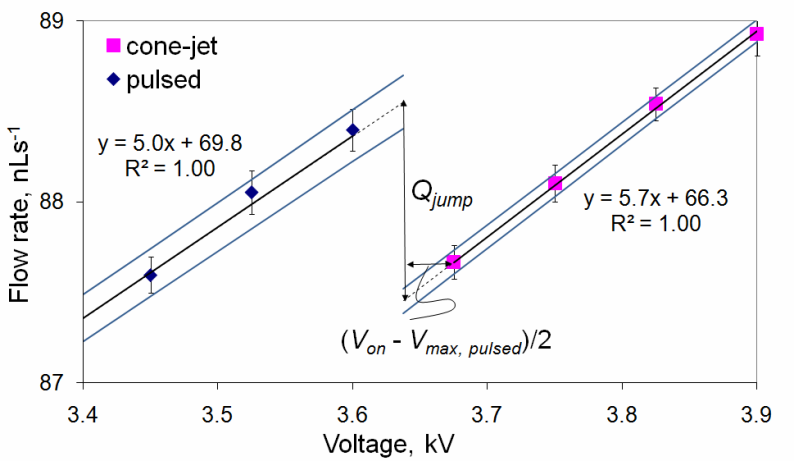

Figure 6.16. Illustration of the calculation of Q_{jump}. The blue lines represent the 95% prediction intervals.

As can be seen from Figure 6.16 the 95% prediction intervals for both linear lines are quite small, suggesting that the value of Q_{jump} is reasonably accurate. To give a qualitative value of the prediction interval for Q_{jump}, the sum of the square of both intervals at the Q_{jump} voltage can be calculated, and the result square rooted. This gives a 95% prediction interval of ±0.16 nLs^{-1} for the Q_{jump} value of 1.21 nLs^{-1}. Consequently the value of Q_{jump} seems reasonably accurate.

The magnitude of the drop in flow rate differed between experiments, and a histogram of the size of this variation is shown in Figure 6.17. Although the drop is generally small - for most experiments it has a value of less than 2 nLs^{-1} - for some experiments its value can be large, as demonstrated by the long tail of the distribution. The largest value found was 7.69 nLs^{-1}, for a nominal flow rate of 16.5nLs^{-1}, using an emitter with an outer diameter of 230 μm and at an emitter to extractor distance of 11 mm.

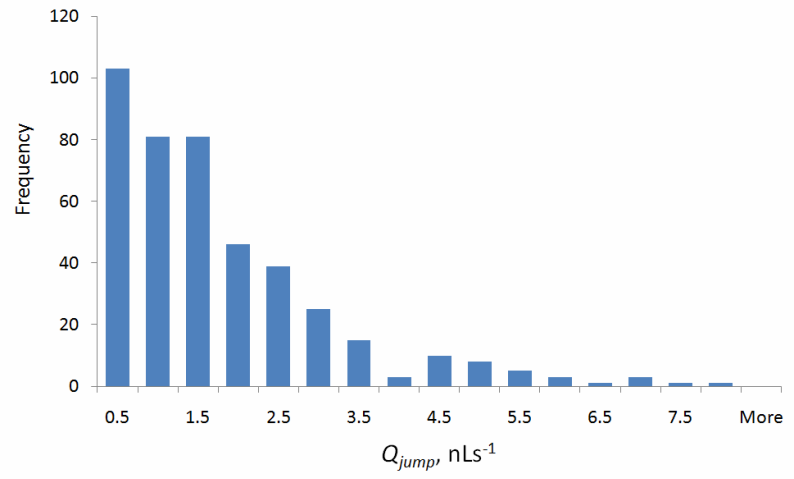

Figure 6.17. Histogram of experimental Q_{jump} values, across all experiments. x-values represent the upper limit of the bin range.

Whilst all the experiments completed here used the same liquid, propylene carbonate doped with sodium iodide, Figure 6.18 (a) and (b) (unpublished data courtesy of K. Smith[118]) illustrate $Q(V)$ data where two different liquids have been sprayed across the pulsed and cone-jet modes. The liquids are ethylene glycol doped with NaI, and 1-ethyl-3- methlyimidazolium tetrafluroborate ($EmiBF_4$). Both these liquids had considerably higher conductivity and viscosity than the solvent used during these studies experiments, as illustrated in Table 6.1.

Both fluids illustrate a similar drop in flow rate comparable to Q_{jump}. This is in spite of the two liquids having considerably different viscosity and conductivity than propylene carbonate, as illustrated in Table 6.1. This is a suggestion that Q_{jump} is a general occurrence in the electrospray process.

Table 6.1. Properties of solvents. Properties (except experimentally measured conductivity for doped solutions) from reference [103] unless marked. 'a' – [102]. b' – [104]. 'c' – [119]. 'd' – [120].

Solvent	Viscosity, cP	Conductivity, Sm^{-1}	Surface tension, Nm^{-1}
Propylene Carbonate doped with NaI	2.76[a]	0.003	0.0452[b]
TEG doped with NaI	49	0.232	0.0452
$EmiBF_4$	37[c]	1.4[d]	0.052[d]

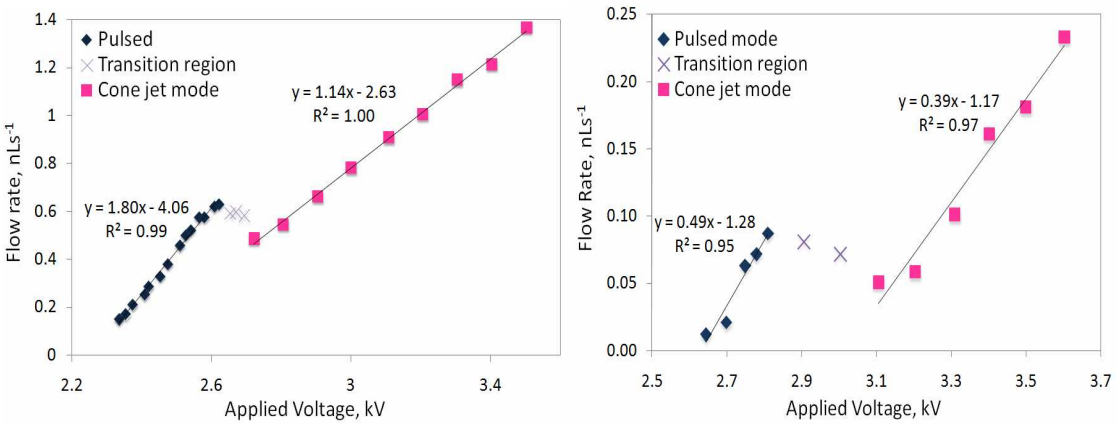

(a) (b)

Figure 6.18 (a), (b). Variation of flow rate across pulsed and cone-jet mode. (a) - Ethylene Glycol doped with NaI. (b) - 1-ethyl-3-methlyimidazolium tetrafluroborate (Emi BF_4). Courtesy of K. Smith[118].

6.5.1. Variation of Q_{jump} with geometric and flow rate conditions

The variability of the Q_{jump} value shown in Figure 6.17 suggests that it may depend upon various parameters. One such parameter was found to be the nominal flow rate, as illustrated in Figure 6.19. The data is for a 10mm long, 800 μm o.d., 450 μm i.d. emitter. The error bars are the 95% prediction interval for Q_{jump}, and only data where the *R*-squared value for both the pulsed and cone-jet mode gradients was greater than 0.99 is shown.

For this particular geometric configuration the Q_{jump} value increases with nominal flow rate, in what seems to be a power-to-a-fraction relationship.

Figure 6.20 (a) and (b) illustrate further Q_{jump} versus Q_{nom} data for emitter outer diameter varying and emitter length varying experiments respectively (geometry variations [2] and [5] as described in Tables 3.2 and 5.1). Only data with *R*-squared values greater than 0.99 for both m_{pulsed} and m_Q is shown.

There is some disagreement as to the exact relationship of Q_{jump} to the nominal flow rate, for differing geometric configurations. For example the 230 μm o.d. emitter has a considerably stronger Q_{jump} to Q_{nom} relationship than the 1600 μm o.d. emitter (see Figure 6.20 (a)). Alternatively a shorter emitter demonstrates a weaker Q_{jump} to Q_{nom} relationship than a longer emitter (Figure 6.20 (b)). This variation of the relationship suggests that there may be an effect of geometry on the value of Q_{jump}.

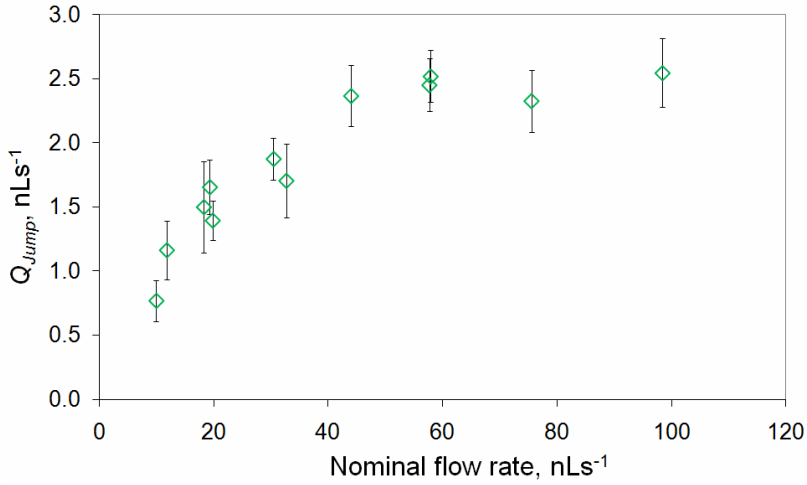

Figure 6.19. Variation of Q_{jump} with nominal flow rate. A 10 mm long, 100-800 μm inner to outer diameter emitter was used, with z_0 = 3mm.

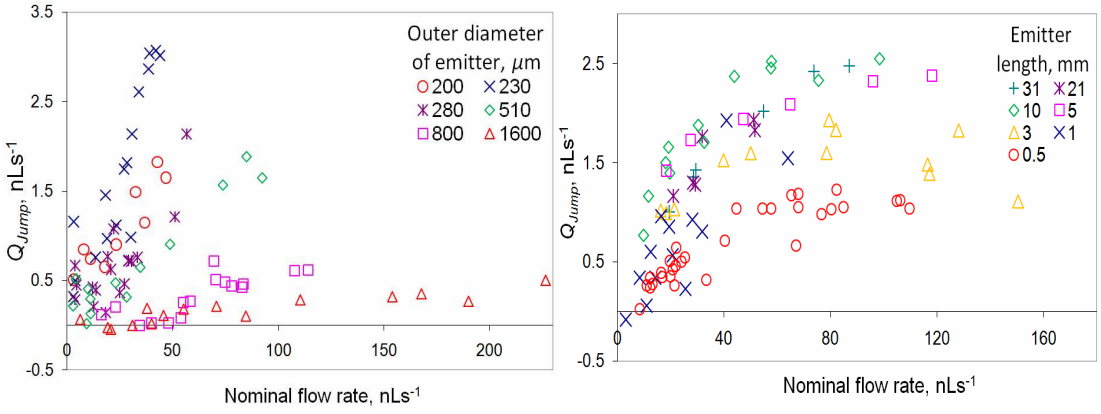

(a) (b)

Figure 6.20 (a) and **(b).** Variation of Q_{jump} with Q_{nom} under various geometric conditions. (a) – emitter inner diameter varying (geometry variation [1]); (b) – emitter length varying [5].

An alternative method to plot the Q_{jump} data is shown in Figure 6.21 (a) and (b). Here rather than plotting Q_{jump} against the nominal flow rate, the flow rate drop is plotted against the geometry parameter that has been varied. For comparison the variation of m_Q with each geometry parameter is also plotted.

There is considerable spread of results for each geometric condition, since Q_{jump} varies with nominal flow rate. Some trends though can still be seen.

Figure 6.21 (a) and (b) would seem to show that Q_{jump} varies with emitter outer diameter and emitter length in the same way as m_Q does (with the complication of the Q_{nom} variation). For example, shorter emitters have smaller Q_{jump} values than longer emitters, even accounting for the dependence on Q_{nom}.

Also the 230 μm o.d. emitter had greater Q_{jump} values than emitters of similar outer diameter (see Figure 6.21 (a)). This agrees with the results from the m_Q analysis, where it was shown that the higher value was caused by a slightly larger inner diameter than other emitters of comparable o.d. (see Section 4.4), and therefore a lower hydraulic resistance.

It is reasonable to conclude that Q_{jump} is affected by the same two parameters that had an effect on m_Q – namely the hydraulic resistance, and the variation of m_{pe} with changes of geometry.

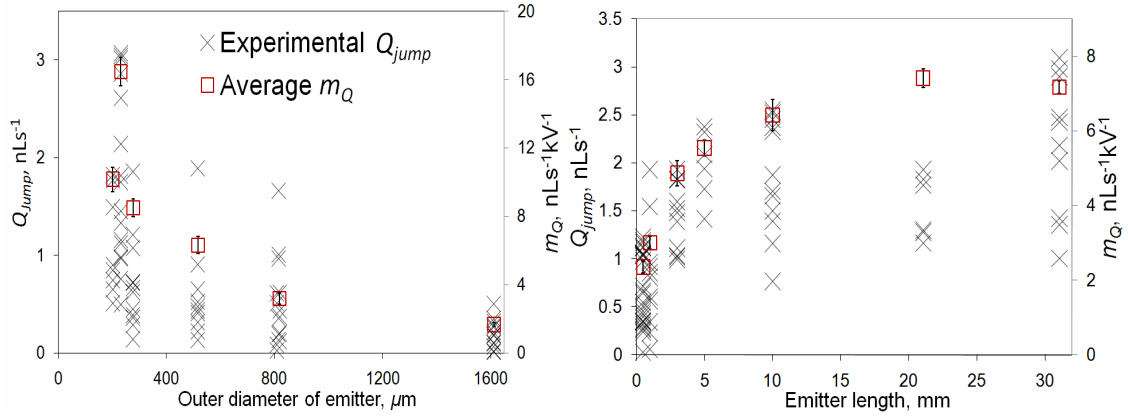

Figure 6.21 (a) and **(b).** Variation of Q_{jump} with geometric parameters.
(a) – outer diameter of emitter (geometry variation [2] on Table 5.1);
(b) – emitter length varying [5].

As the value of m_Q affects Q_{jump}, it is possible that by dividing by m_Q may remove the effect of geometry on the flow rate drop. Figure 6.22 (a) – (d) attempts to demonstrate this, by plotting Q_{jump}/m_Q against the emitter outer diameter, emitter length, and the two emitter to extractor distance varying data sets (one using a 230 μm o.d. emitter, and one using a 510 μm o.d. emitter).

In comparison to Figure 6.21, there is no variation of Q_{jump}/m_Q for the emitter outer diameter and emitter length changes (Figure 6.22 (a) and (b)). The effect of geometry has been removed, although there is still considerable spread of results because of the dependence on Q_{nom}. But for emitter to extractor distance varying experiments (Figure 6.22 (c) and (d)), the value of Q_{jump}/m_Q increases with greater emitter to extractor distances. Once the effect of m_Q has been removed Q_{jump} is affected by the emitter to extractor distance, with a dependence that is separate from the effect of m_{pe} or the hydraulic resistance.

In summary, there would seem to be three parameters that affect Q_{jump}.
Firstly Q_{jump} increases with nominal flow rate, in what would seem to be an approximate $Q_{jump} \propto Q_{nom}^{\ n}$ law, where n is a fraction.
Secondly the geometry of the emitter and extractor affect Q_{jump}, in the same way as it affects m_Q. As with m_Q the effect of geometry on Q_{jump} can be assumed to be due to two effects – the effect of varying hydraulic resistance when the emitter inner diameter is varied, and the effect of changes of m_{pe} for when other geometric parameters are varied.
Thirdly Q_{jump} would seem to increase with emitter to extractor distance, once the effect of m_Q on Q_{jump} has been removed. An explanation of why this could be the case is offered in the next section, where the origin of Q_{jump} is postulated upon.

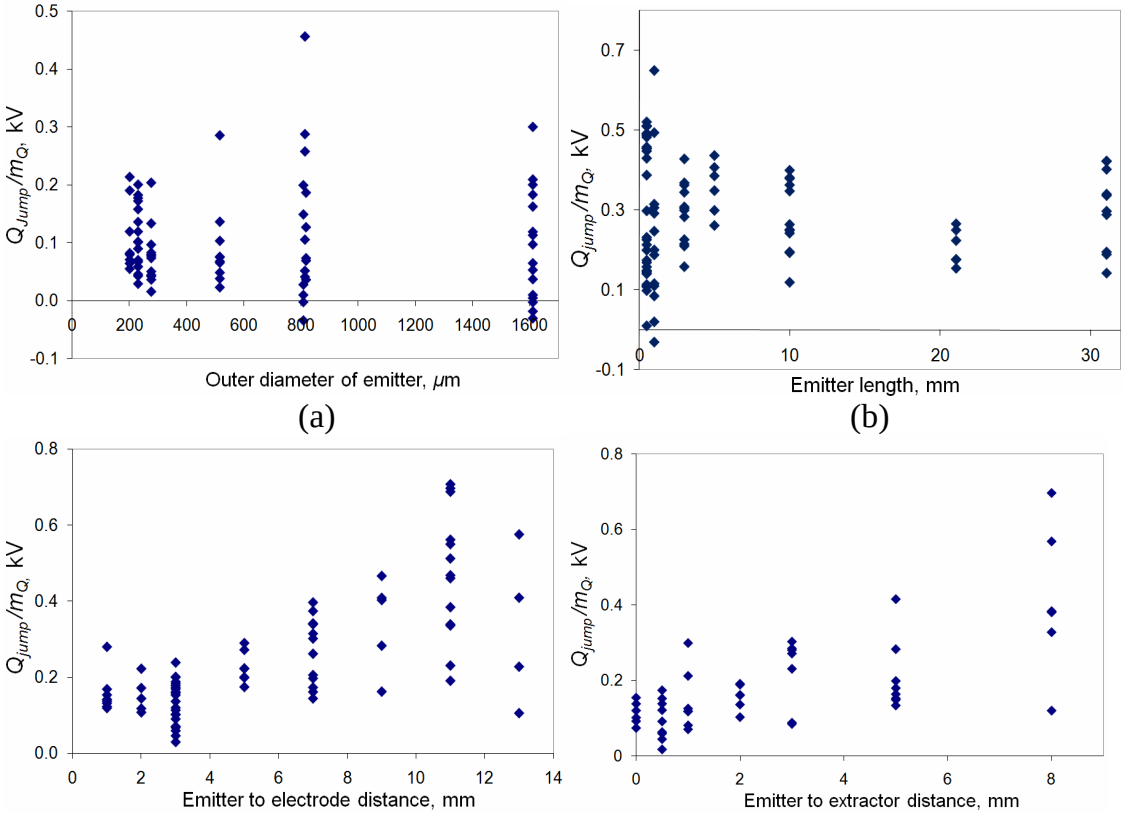

Figure 6.22 (a) – (d). Variation of Q_{jump}/m_Q with geometric parameters.
(a) – emitter outer diameter varying (geometry variation [2] in Table 3.2);
(b) – emitter length varying (geometry variation [5]);
(c) – emitter to extractor distance varying for 230 μm o.d. emitter [3];
(d) - emitter to extractor distance varying for 510 μm o.d. emitter [4].

6.5.2. Discussion of Q_{jump} and its origins

There are various possible explanations as to the origins of Q_{jump}, with perhaps the most plausible being the effect of the charged micro-sized droplets between the emitter and extractor electrode.

When cone-jet mode begins there is a large increase in the amount of current produced (see Figure 6.1). This increase results in more charged droplets (or ions for a more conductive electrospray fluid than used in these experiments) in the volume between the

emitter and extractor, and thus more space charge present. This 'space charge' will result in a decrease in the voltage seen at the emitter tip and therefore the flow rate will drop due to the observations found throughout this study of the effect of voltage on the flow rate.

Space charge is a Q_{jump} hypothesis that can intuitively explain some of its dependence on various parameters. For example the results of the previous section demonstrated that Q_{jump} increases with nominal flow rate. As the current in cone-jet mode also increases with nominal flow rate (following the $Q^{1/2}$ relationship), this can be assumed to result in an increase in the amount of charge in the volume between the emitter and extractor. Thus the amount space charge will increase with nominal flow rate, and consequently the voltage drop, and thus flow rate drop, will increase with nominal flow rate.

The space charge hypothesis can also describe the relationship of Q_{jump} to m_Q found in the previous section. The drop in flow rate Q_{jump} can be thought of as the product of m_Q and the drop in voltage as space charge increases. Consequently a larger value of m_Q will result in a larger value of Q_{jump}.

Also found in the previous section was that once the effect of geometry is removed there is a strong increase of Q_{jump} with emitter to extractor distance (see Figure 6.22 (c) and (d)). This also agrees with the hypothesis of a space charge explanation for Q_{jump}. As the emitter to extractor electrode distance is increased, the amount of space charge between the emitter tip and the extractor electrode will increase. Therefore the emitter tip will experience less voltage, and Q_{jump} will be larger.

There have been some attempts at a theoretical analysis of the effect of space charge on the electrospraying process in previous literature[96,121]. Mair, in a derivation for the theoretical determination of LMIS current (voltage) curves, provides an equation that can be used to estimate the change in electric field with and without space charge[96];

$$E_P^2 = E_L^2 - 8\left[m(2e)^{-1}\right]^{1/2} V_0^{1/2} j_0 / (3\varepsilon_0), \tag{6.4}$$

where E_P is the Poisson electric field, E_L the Laplace electric field, *m/e* the mass to charge ratio, j_0 the surface current density and ε_0 the permittivity of free space. This equation is a simplification of a more complex equation for the case of small space charge[96], originally derived by Stern *et al.*[122] under the assumption of a geometry consisting of an infinite plane electrode emitting ions. This is considerably different from a point-to-plane geometry that generally exists in electrospray systems, but Mair[96], Barbour *et a1.*[123], and Ward and Seliger[124] still find the derivation adequate for including an effect of space charge in a point to plane situation.

Inserting the above equation into a relationship for the electric pressure change (P_{change}) with and without space charge gives;

$$\begin{aligned} P_{Change} &= \tfrac{1}{2}\varepsilon_0\left(E_L^2 - E_P^2\right) \\ P_{Change} &= \tfrac{4}{3}\left[m(2e)^{-1}\right]^{1/2} V_{On}^{1/2}\, j_0 \\ Q_{Change} &= \tfrac{4}{3}\left[\rho Q_{On} / 2I_{On}\right]^{1/2} V_{On}^{1/2}\, j_0 / R_T \end{aligned} \quad . \qquad (6.5)$$

Where ρ is the density of propylene carbonate. Q_{on}, the flow rate at the onset of cone-jet mode, I_{on}, and V_{on} are given by experimental data (in SI units). j_0, the current density, ignoring spray expansion, is estimated by;

$$j_0 = I_{On} / (\pi r_e^2), \qquad (6.6)$$

where r_e is the outer radius of the emitter.

This theoretical change in flow rate due to space charge can be compared to the experimental Q_{jump}, as is shown in Figure 6.23. The data for emitter inner and outer diameter and emitter length varying experiments is used. Not included is the Q_{jump} data from varying the emitter to extractor distance, since the simplistic theory cannot take into account the varying volume of space charge between the emitter and the extractor electrode.

There would seem to be some agreement between the data, with the theoretical Q_{jump} having the correct order of magnitude as the experimental Q_{jump}. This is an indication that the simplistic theory may capture the basic parameters that affect Q_{jump}.
There is though a considerable spread of results, which would suggest that the theoretical estimate may be too simplistic. An improved estimate could be achieved by using a numerical technique to solve the Poisson equation.

In conclusion, it would seem that space charge can offer an explanation of Q_{jump}, and explain its dependence on the geometry and flow rate. The analysis though is incomplete, and the theoretical derivation inadequate for anything beyond a zeroth order estimate. A more detailed modeling of the effect of charged droplets on the potential difference seen at the emitter is required to confirm the 'space charge' hypothesis.

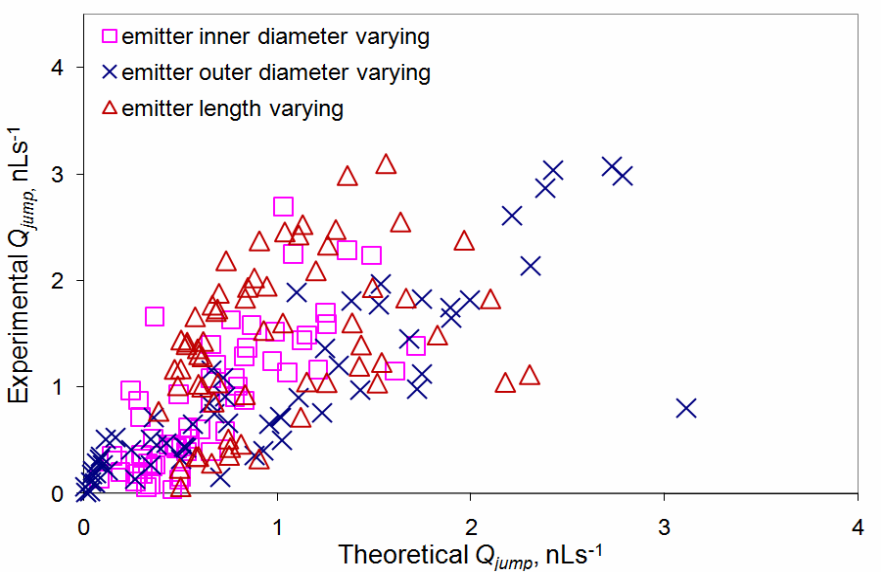

Figure 6.23. Comparison of theoretical and experimental Q_{jump}, under differing geometric conditions.

6.6. The increase in flow rate before cone-jet mode

As an effect of voltage on flow rate across pulsed mode has been found (see Section 6.3), an increase in flow rate from the nominal flow rate to the onset of cone-jet mode will occur. The total change in flow rate from the nominal flow rate (the flow rate with no applied voltage) to the onset of a stable cone-jet mode can be calculated by;

$$\Delta Q = maximum\ \ flow\ rate\ in\ \ pulsed\ \ mode - Q_{nom}\ . \tag{6.7}$$

It is the difference between the maximum flow rate found within pulsed mode (which occurs just before cone-jet mode begins) and the nominal flow rate. The maximum flow rate in pulsed mode was used, rather than the flow rate at the onset of cone-jet mode, in order to remove the effect of Q_{jump} from the calculation.

The experimental ΔQ values for the experiments involving the variation of the emitter inner diameter are shown in Figure 6.24. The average value of m_{pulsed} is also shown.

There is quite considerable variation of the value of ΔQ for any particular emitter inner diameter. This is partially due to the variation of the cone jet onset voltage with nominal flow rate, as discussed in Section 5.2.2. Also though the size of the voltage increment was 0.075kV, which would result in a 7.5% error on the approximate 1kV pulsed mode voltage range.

Even with this reasonably large variation in ΔQ it is clear that as the emitter inner diameter decreases ΔQ decreases, following the same trend as was found for m_{pulsed}. Indeed, there would seem to be a strong correlation between the value of ΔQ and m_{pulsed}, with two parameters having very similar values for the same emitter inner diameter.

Instead of calculating ΔQ from using the method in equation (6.7) it can be alternatively thought of as the product of the pulsed mode $Q(V)$ gradient and the pulsed mode voltage range, assuming there is no change in flow rate with voltage in enhanced dripping mode, and the pulsed mode has a linear $Q(V)$ relationship, which as discussed in Section 6.3.1 it

approximately does. Using this definition of ΔQ, the similarity of it to m_{pulsed} shown in Figure 6.24 suggests the voltage range of pulsed mode has a constant value of approximately 1kV, independent of the emitter inner diameter

.

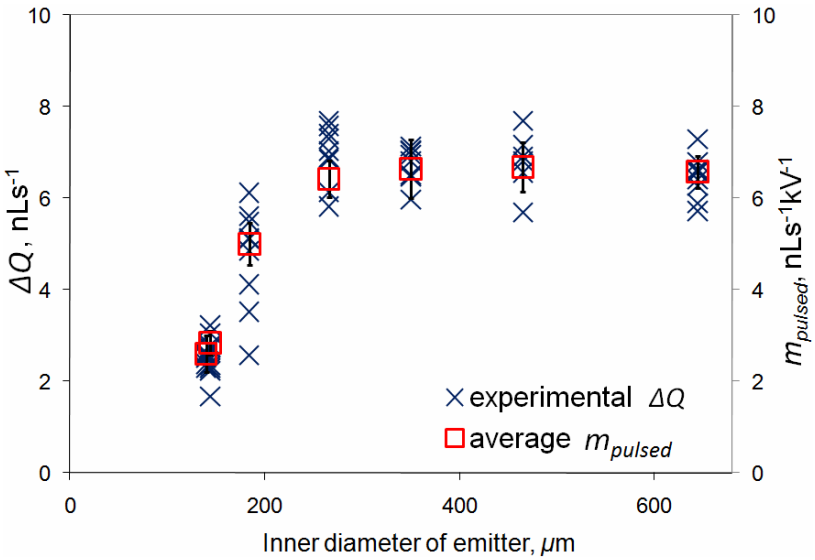

Figure 6.24. Variation of the change of flow rate before cone-jet mode with the inner diameter of the emitter. For comparison m_{pulsed} is also shown.

Both ΔQ and m_{pulsed} illustrating the same trend is a result of both being affected by the increasing hydraulic resistance as the emitter inner diameter decreases. As discussed in Section 4.5 (in relation to m_Q) when the emitter inner diameter was small, the emitter's hydraulic resistance constituted a large part of the overall piping resistance. As the emitter inner diameter increased, the hydraulic resistance of the emitter decreased, and became a smaller fraction of the total resistance (there was considerable upstream resistance from the in-line flow meter). This results in the value of m_{pulsed} reaching an asymptote for large i.d. emitters. The same is now shown to occur in Figure 6.24 for ΔQ.

If the nominal flow rate is small ΔQ can be thought of as the onset flow rate at cone-jet mode electrospray, Q_{on} (Q_{jump} can be ignored as at low flow rates its magnitude is small). Therefore under a low flow rate situation the cone-jet onset flow rate varies with emitter inner diameter.

During all these experiments the same electrospray solvent was sprayed; propylene carbonate doped with NaI to a conductivity of $\sim 2.6\times10^{-3}$ Sm^{-1}. Assuming the addition of the sodium iodide salt does not affect the value of the solvent density or surface tension (a reasonable assumption as the concentration of the salt was 0.1 gL^{-1}), equation (2.39) predicts the minimum flow rate to be 7.45 nLs^{-1}.

This minimum flow rate (Q_{min}), which is often used to define the minimum flow rate at which a stable cone-jet mode electrospray occurs[30,57,60], can be compared to the onset flow rate variation with emitter i.d. For when Q_{nom} is zero this variation of Q_{on} is shown in Figure 6.24, as with zero initial flow rate ΔQ is equal to Q_{on}. For emitters of large inner diameter, the values of Q_{on} and Q_{min} coincide. This though is a coincidence, as by decreasing the total system hydraulic resistance the value of Q_{on} would be larger for larger inner diameters (with no asymptote), and bear no relation to the value of Q_{min}.

For the emitters of smaller inner diameter, the value of Q_{on} is approximately three times smaller than Q_{min} (7.45 nLs^{-1} compared to ~2.5 nLs^{-1}). This suggests that for these experiments the minimum flow rate calculated using Equation (2.39) did not occur. Indeed during the experiments no indication of a minimum flow rate was noticed, which suggests that the idea of a minimum flow rate, at least for this particular solvent, needs some analytical improvement.

The ΔQ results involving emitters of varying outer diameter are shown in Figure 6.25, with the average m_{pulsed} again shown for comparison.

For emitters with a smaller outer diameter, there is more scatter in the data of the value of ΔQ for each emitter. This could be due to the variation of the relationship between the cone-jet onset voltage and the nominal flow rate as the emitter outer diameter varied, as discussed in Section 5.2. This onset voltage variation would affect the value of ΔQ since it would vary the pulsed mode voltage range. To investigate this, Figure 6.26 plots the

variation of ΔQ with the cone-jet onset voltage, for an emitter of outer diameter 280 μm (a smaller emitter tested). The figure demonstrates an increase of the change of flow rate before cone-jet mode with cone-jet mode onset voltage, illustrating that the V_{on} variation explains some of the scatter of ΔQ. As the cone-jet onset voltage varies considerably more for the smaller o.d. emitters (due to their larger astable regime, as discussed in the previous chapter), this provides an explanation of the greater variation of ΔQ for the smaller emitters.

As the same liquid was used throughout these experiments, the same value of Q_{min} can be calculated for the emitter outer diameter experiments, 7.45 nLs^{-1}. If again ΔQ is taken to be equal to Q_{on} at zero nominal flow rates, the value of Q_{on} varies from approximately 2 to 8 nLs^{-1} with emitter outer diameter. For larger emitter outer diameters the value of Q_{on} would be consistently smaller than Q_{min}, and therefore at low flow rates stable cone-jet mode electrospray regularly occurred below the theoretical minimum. This suggests that, as with the emitter inner diameter varying experiments, the experiments are unaffected by the theoretical minimum flow rate.

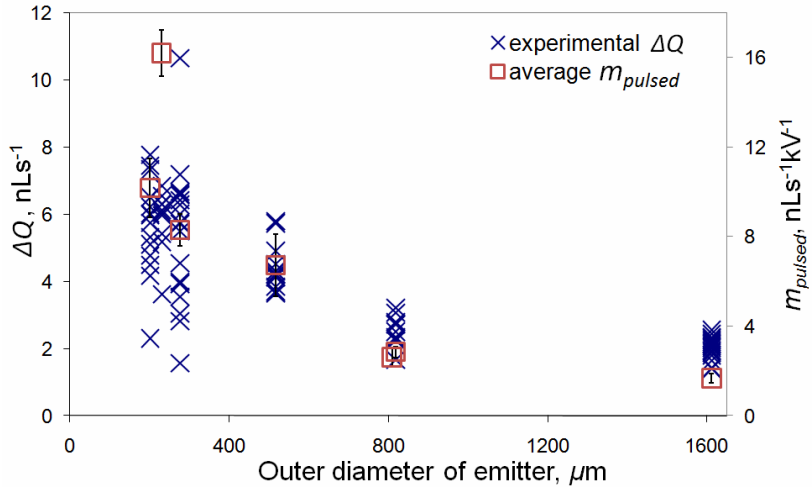

Figure 6.25. Variation of the change of flow rate before cone-jet mode with emitter outer diameter. Emitters had a fixed inner diameter of ~100μm. For comparison m_{pulsed} is also shown.

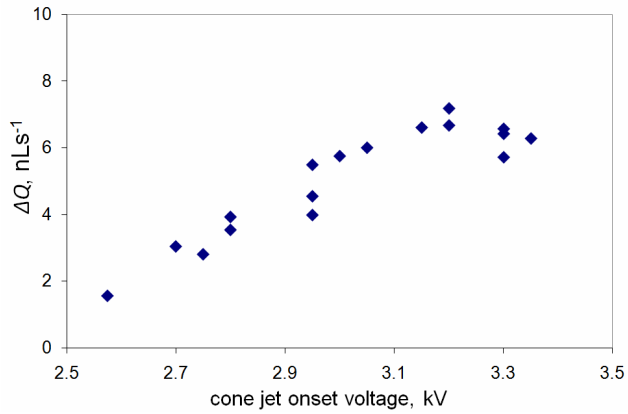

Figure 6.26. Variation of the change in flow rate before cone-jet mode with cone-jet onset voltage, for emitter with outer diameter of 280 μm.

As shown in Figure 6.25 the value of ΔQ increases as the emitter outer diameter decreases, although there is considerable scatter in the data for the reason given above. Even with the scatter though the relationship of ΔQ to emitter o.d. does not seem to be as strong as that found for m_{pulsed}. The value of m_{pulsed} is approximately eight times larger for emitters of smaller outer diameters, whilst the value of ΔQ is only three times as large for smaller o.d. emitters.

As described previously, ΔQ can be thought of as the product of m_{pulsed} and the pulsed mode voltage range. Therefore the reason for the lack of agreement between how ΔQ and m_{pulsed} vary with emitter outer diameter could be a result of a variable pulsed mode voltage range with emitter outer diameter. To test this, a hypothetical pulsed mode voltage range can be calculated (as the experimental pulsed mode voltage range is unavailable), and the product of this and m_{pulsed} found. The method used for the calculation is shown in Figure 6.27, and is

$$\Delta Q_{hyp} = m_{pulsed}\left(V_{on} - \frac{\left[Q_{nom} - c_{pulsed}\right]}{m_{pulsed}}\right). \qquad (6.8)$$

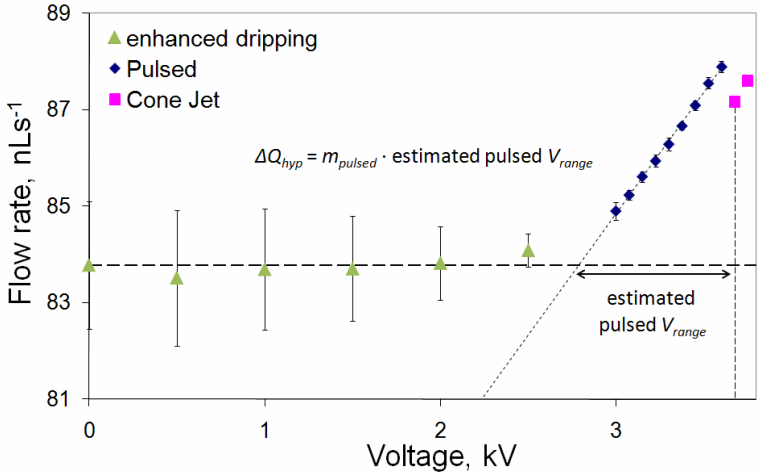

Figure 6.27. Calculation of hypothetical pulsed mode voltage range.

This hypothetical change in flow rate is calculated under the assumption that the pulsed mode is linear, and accounts for the complete change in flow rate before cone-jet mode. As discussed in Section 6.3.1 this is not quite true (there is a deviation from linearity towards the lower end of pulsed mode), but here the assumption is used as an approximation.

The variation of this hypothetical flow rate change is shown in Figure 6.28, and demonstrates the same trend as the experimental results, Figure 6.25. Therefore it would seem that the weaker effect of emitter outer diameter on ΔQ than that which was found for m_{pulsed} is a result of the increasing pulsed mode voltage range with increasing emitter outer diameter removing the effect of the decreasing value of m_{pulsed}. As the value of m_{pulsed} increases with geometry changes, the pulsed mode voltage range decreases. the two effects cancel themselves out in the calculation of ΔQ, resulting in a less strong relationship between ΔQ and the emitter outer diameter occurring.

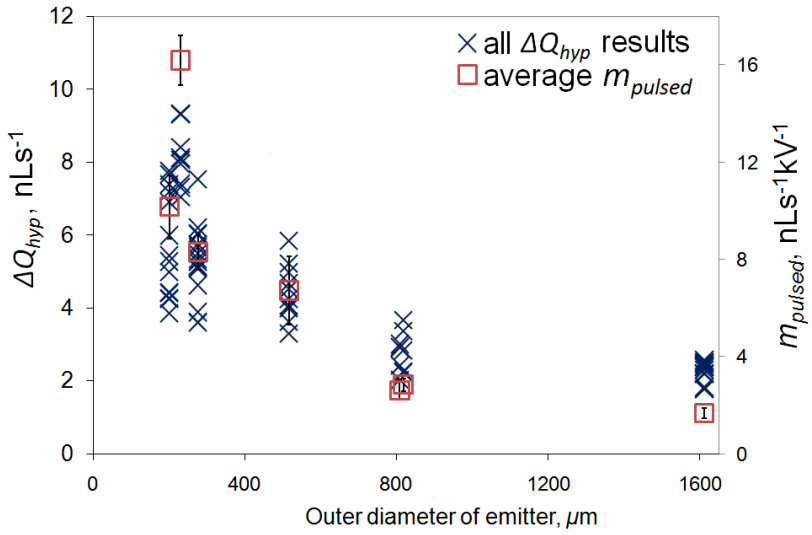

Figure 6.28. Variation of the hypothetical change of flow rate before cone-jet mode with emitter o.d. For comparison m_{pulsed} is also shown.

In summary, there is a considerable amount of variation of ΔQ for a constant geometry – an unsurprising situation given its dependence on many variables (cone-jet onset voltage, Q_{nom}, m_{pulsed}). Even so the conclusion can be drawn that the opposing variation of firstly the pulsed mode voltage range and secondly m_{pulsed} with geometry acts to partially cancel out the effect of emitter outer diameter on ΔQ. The exception to this is the variation of the emitter inner diameter, as the pulsed mode voltage range is independent of emitter i.d.

6.6.1. Effect of ΔQ on the applicability of the $Q(V)$ effect for throttling colloid thrusters

Section 4.12 described the possible use of the $Q(V)$ effect to vary the thrust in an electrospray based spacecraft thruster by changing the voltage applied to the extractor electrode. This is though accompanied by a significant decrease in specific impulse, although under some situations this decrease in I_{sp} would possibly be acceptable.

With the now added knowledge of the variation of flow before cone-jet mode, the situation becomes more complex. The previous analysis[108] assumed that the cone-jet onset flow rate was equal to the minimum flow rate. For a highly conductive ionic liquid

that would typically be used for as a colloid thruster propellant[83] the Q_{min} value would be fractions of a nLs^{-1}. The previous section described significant increases in the flow rate before the onset of cone-jet mode, which suggests that using the theoretical minimum flow rate as the onset flow rate may be incorrect.

There will though be some differences in using an ionic liquid as the electrosprayed fluid, rather than the solvent propylene carbonate used in these studies. Although no method has been found that can estimate the change in flow rate before cone-jet mode (ΔQ), an estimate can be found if the geometry of the emitter and extractor is assumed the same as that of an experiment completed during these studies. The change of liquid will then only change the hydraulic resistance of the system.

For example, for an 800 μm o.d. emitter with an approximately 150 μm inner diameter, the value of m_Q when spraying propylene carbonate was found to be 2.9 $nLs^{-1}kV^{-1}$, whilst the value of ΔQ was 2.5 nLs^{-1}. $EmiBF_4$ (a typical ionic liquid colloid thruster propellant) has a viscosity 13.4 times greater than propylene carbonate, and since both m_Q and ΔQ are dependent on the hydraulic resistance (see Figure 4.4 and Figure 6.24), their values would be 13.4 times smaller (assuming the same hydraulic resistance upstream of the emitter). This gives values for m_Q and ΔQ of 0.22 $nLs^{-1}kV^{-1}$ and 0.19 nLs^{-1} respectively when using $EmiBF_4$. Now the change in thrust and specific impulse as the flow rate changes with the applied voltage can be estimated, using the same method as described in Section 4.12, except now the estimated value of ΔQ can be used as the onset flow rate, rather than the minimum flow rate.

The results of this analysis are shown in Figure 6.29, where the specific impulse and thrust have been estimated using the simple equations given in Section 4.12. Again an acceleration grid with a potential of 7500V is used, whilst solely droplets are assumed to be emitted. Figure 6.29 demonstrates an approximate doubling of the thrust, with only a slight decrease of the specific impulse. The extractor voltage applied using an emitter with this outer diameter is though quite large, but this could be mitigated against by decreasing the emitter to extractor distance or the emitter outer diameter.

In conclusion, the increase of flow rate with voltage before cone-jet mode, although it has a slightly detrimental effect on the use of the Q(V) effect for the throttling of a colloid thruster, it does not rule out using the relationship for this application. This though is only an initial analysis, and a detailed study – looking specifically at the mission analysis and thrust requirements typically needed from colloid thrusters – needs to be completed.

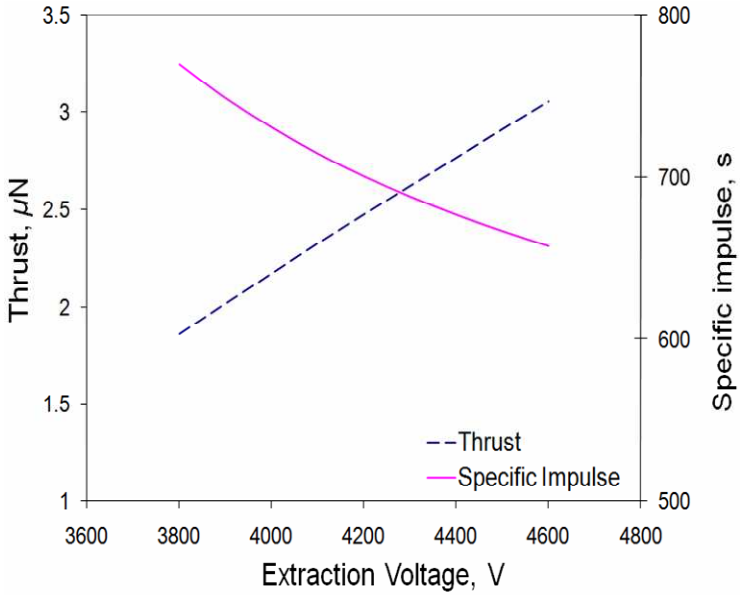

Figure 6.29. The variation of thrust and specific impulse with extraction voltage, for emitter of outer diameter 800 μm, and inner diameter 150 μm, and using $EMiBF_4$ as propellant.

6.7. Conclusions - variation of flow rate with voltage across various modes of electrospray

This chapter has discussed the effect of voltage across and within the four modes of electrospray operation commonly found during these experiments; enhanced dripping, pulsed, cone-jet and multi-jet modes.

Within enhanced dripping mode there is no net increase of flow rate with voltage. This would seem to be a result of the decreasing size of the droplets emitted cancelling out the greater frequency as the voltage was increased.

Within pulsed mode there is a linear increase of the average flow rate with voltage, once a stable pulsed mode has been established, as illustrated by a reasonable charge flux. This increase, termed m_{pulsed}, is independent of Q_{nom}, but is dependent on geometry in the same way as m_Q was found to be. The analysis presented is the first time that the effect of applied voltage on the flow rate within pulsed mode electrospray has evaluated in detail, and presents the effect of geometry on the relationship for the first time.

Within multi-jet mode there is a linear increase of Q with V, but the results are complicated by the greater instability of multi-jet mode compared to the other modes that were investigated. There is though still a strong suggestion that the change of flow rate with voltage in multi-jet mode is affected by geometry. The effect of voltage on flow rate in multi-jet mode electrospray has not previously been observed.

A significant drop in flow rate is observed when going the voltage is increased from pulsed into cone-jet mode electrospray. This effect has not been seen before in published literature, with it only being noticed previously in unpublished data from Queen Mary University (some of which is illustrated in Figure 6.18). This though is the first time that the magnitude of this effect has been shown to be variable, and is seen to depend upon the nominal flow rate, the geometry of the emitter and extractor, and separately the distance from the emitter to the extractor electrode.

A probable reason for Q_{jump} to occur would be the large increase in current when going from pulsed to cone-jet mode. This increase in current would result in an increase in the

amount of charged droplets downstream from the spraying site, a decrease in voltage seen at the emitter, and therefore a decrease in flow rate. The simplified analysis presented is consistent with this explanation for Q_{jump}.

Up to the beginning of cone-jet mode there is a total increase of flow rate, termed ΔQ. This flow rate increase is dependent on the emitter inner diameter, again as a result of the hydraulic resistance. But the effect of other geometric parameters is partially removed by the varying pulsed mode voltage range.

The variation of flow rate with voltage before cone-jet mode does not negate using the $Q(V)$ effect in colloid thrusters, with the change in thrust still being reasonable, whilst the specific impulse is acceptable. Considerable further work is necessary though to fully understand whether it is applicable for specific missions.

Chapter 7

7. Conclusions and future work

7.1. Conclusions

The effect of applied voltage on the flow rate

A large amount of experiments investigating the effect of the applied potential difference between the emitter and extractor electrode on the flow rate of sprayed liquid through the emitter have been completed. Initially these experiments concentrated on the effect within cone-jet mode electrospray. Results demonstrated that the cone-jet mode flow rate relationship to the applied voltage is linear, agreeing with previous studies at Queen Mary University[9,10,71]. For the first time though it was unambiguously demonstrated that the magnitude of the $Q(V)$ dependence is a function of the geometry of the electrospray configuration, with the effect varying with all geometric parameters tested.

Using an original analytical model this dependence was shown to result from two effects. Firstly the effect of hydraulic resistance (by varying the emitter inner diameter) was illustrated, a finding that agreed with previous studies[9,72].

Secondly, using the novel analytical model, it was demonstrated that all other geometry changes that affect the $Q(V)$ relationship can be explained by the variation electric pressure with voltage, a term that can be calculated *a priori*. This simple analytical model was at first based upon an electric field equation used commonly in the estimation of the cone-jet onset voltage. The resulting theory though is too simple to describe all changes of electric pressure with voltage. Consequently a numerical analysis of the electric pressure change with voltage was completed, which agreed remarkably well with the experimental results once a meniscus apex radius of the order of the emitter radius had been chosen.

After initial results were collected, the studies were extended to investigate the effect of voltage on the flow rate in the other modes of electrospray that typically occur; enhanced dripping, pulsed, and multi-jet modes. In the latter of these two regimes, a linear relationship of flow rate to voltage was again demonstrated to transpire.

In further original work, these $Q(V)$ relationships were shown to be affected by geometry in the same manner as was the case in cone-jet mode. This is remarkable, as pulsed and multi-jet mode would seem to be very different visually and electrohydrodynamically.

When changing from pulsed to cone-jet mode, a drop in flow rate has been found, and is dependent on the flow rate and the geometry, in a complex manner. It is suggested that this drop can be explained by an increase of charge between the emitter and extractor reducing the potential difference at the emitter. The analysis though is not conclusive, and another hypothesis could offer an explanation.

In summary, it would seem that under some situations the flow rate can be significantly affected by the applied voltage, in both pulsed, cone-jet, and multi-jet mode electrospray. Although at times, and often justifiably, disregarded in electrospray analyses, there are some electrospray-involving techniques where the applied potential difference is undeniably a controlling parameter. One such field is nano-electrospray mass spectrometry, where the electric field itself is used to initiate the flow rate from a small unattached emitter filled with spraying solution. This leads to a cone-jet mode with no applied back pressure[99,125], with the resulting charged droplets are fed into a mass spectrometer which can analyze the sprayed molecules. It seems likely that the results published here are directly applicable to this field. Currently the effect of voltage within nanoelectrospray is unresolved and little understood. It is thought that the inner and outer diameter of the emitter has an effect on the current in nanoelectrospray[94], and a previous investigation at Queen Mary has demonstrated that the flow rate in nanoelectrospray is affected by the applied voltage[28], regardless of whether it is operating in cone-jet or pulsed mode. Combined with the theoretical evaluation described here, it may now be possible to estimate the flow rate from a nanoelectrospray source. The analytical model outlined above may allow for the flow rate to be known *a priori*. With the efficiency of nano-electrospray ionization found to increase as the flow rate decreases[126], and a

generally drive towards greater flow rates through the emitters[125], it may be possible to optimize the flow rate to produce the desired increased resolution of the spectrometric signal.

Another electrohydrodynamic method that is on occasion passively fed is electrospinning. In some cases the spun fibre is formed directly from a sample situated on the tip of a large pole, or from wires cyclically dipped into a electrospray solution bath. A potential difference is applied, and at high enough voltage the liquid forms a Taylor cone directly from the wetted wires or isolated droplet. It seems likely that in this passively fed case the flow rate of spun material is a result of the voltage. Therefore it may be that the flow rate is related to the voltage by the analytical model described here. The effect of voltage on the fluid throughput in electrospinning remains unclear[127] but the results here may be applicable to this process.

The variation of the flow rate with applied extraction voltage within cone-jet mode operation also has implications for spacecraft colloid thrusters, as described within this thesis. If the change in flow rate with voltage can be predicted at the design stage, this will facilitate the optimization of the variation of the thrust and specific impulse with voltage for a colloid thruster system, resulting in simple, reproducible thrust throttle control.

The effect of applied voltage on the emitted current

Once a stable cone-jet mode was formed, the current was found to increase in a highly linear fashion with the applied voltage. This was found to occur over several hundred experiments, suggesting that the linearity may be a general occurrence, at least with this and similar solvents. This linear increase of current with voltage, termed m_I, is dependent on the nominal flow rate, the hydraulic resistance, and the value of m_{pe}, with the latter two relationships being reported for the first time. The large amount of data collected also allowed for the complex relationship of m_I to Q_{nom} to be analysed, suggesting that a minimum value occurred. Due to this added complexity of the variation of m_I with many

parameters, and with the addition of the variation of m_I with conductivity reported in previous literature[10], resulted in a prediction of m_I being unobtainable at this stage. It is felt that an electrohydrodynamic simulation is needed to predict the value of the change of current with the applied voltage in cone-jet mode electrospray.

The effects of geometry on the cone-jet mode stability island

Across several hundred electrospray experiments the point at which cone-jet mode electrospray has been found to be stable has been carefully characterized.
This stability island is strongly affected by the outer diameter of the emitter, with a larger o.d. emitter demonstrating a stable cone-jet mode up to greater flow rates than a smaller o.d. emitter.

The cone-jet onset voltage is greatly dependent on the geometry, and was found to vary from 2.440kV to 8.725kV under different geometric conditions. With the exception of the emitter inner diameter, it varied with all geometric parameters tested.

A theoretical onset voltage was compared to the experimental results, agreeing well with the experimental data but the agreement was poor when the effect of varying the distance between the emitter and counter electrode was analysed. The onset voltage was also modelled using FEM, which satisfactorily modelled the onset voltage for all geometric variations.
This is the first time that the cone-jet onset voltage has been measured systematically over a large variation in flow rates and geometry. It provides important insights for new studies as to when cone-jet mode electrospray is stable and is likely to occur.

The cone-jet voltage range varies with geometry. It would seem to dramatically increase for smaller values of m_{pe}. As m_{pe} can be predicted this could provide a first order approximation of the cone-jet mode voltage range, and also the onset voltage of multi-jet mode. This, when combined with the cone-jet onset voltage estimation, provides an estimate of the cone-jet mode window.

7.2. Future work

The implications of the variation of the change of flow rate with voltage (m_Q) with geometry for colloid thrusters have been investigated briefly as part of this study. The study though is only at a preliminary stage, with a more thorough study looking in depth at the feasibility of using the $Q(V)$ relationship for thrust throttling needed. Now that the $Q(V)$ relationship stands on a surer footing, and the change of flow rate with voltage can be predicted, this would seem possible. It would need to include an analysis of the effect of flow rate on voltage before cone-jet mode, the effect of the $I(V)$ dependence, and an attempt to tailor the effect for a particular colloid thruster design or spacecraft mission. This analysis would need to be supported by some significant experimental work, probably applying microfabricated silicon emitters.

Further, current colloid electrospray thrusters use ionic liquids to spray ions directly from the liquid meniscus. This direct extraction of ions from the meniscus may have some effect on the flow rate relationship to voltage, be it through space charge or some other means. Ionic mode operation would therefore also have to be included as part of any colloid thruster $Q(V)$ analysis.

The implications of the variation of the flow rate with the voltage for other electrospray techniques needs to be examined in greater detail. A study on the effect in the field of nanoelectrospray has been previously completed[28], but the study was only at an initial stage, and with no investigation of the effect of geometry. It would be enlightening to continue these studies using the highly accurate flow meter, to see if the analytical model applied here can be used in predicting the $Q(V)$ effect in a nanoelectrospray device.

The same can also be said within the field of passive electrospinning, where as described in the conclusions above the applied potential difference initiates Taylor cone and the electrospinning of a small thread. Here the effect of applied voltage on the mass throughput of the thread is again incompletely understood, and a study using the high fidelity flow meter would be enlightening.

This study has included an in depth simulation of the electric field at the tip of the emitter meniscus. It would be interesting to extend this model into a full electrohydrodynamic simulation. This may help explain the varying shape of the cone meniscus, as the voltage was changed, and also the variation of current with the applied voltage. Modeling of electrosprays using the Taylor-Melcher leaky dielectric model in the Flow3D software, as described in Sections 2.36 and 2.71, has improved in recent years, so this may not be as great a task as it has been viewed previously.

Appendix A

Copy of paper published in Journal of Physics D:Applied Physics, Volume 42, 155504, 2009. Contains some of the work described in chapter 4.

Effect of emitter geometry on flow rate sensitivity to voltage in cone jet mode electrospray

C N Ryan, K L Smith, M S Alexander and J P W Stark

Queen Mary University of London, London E1 4NS, United Kingdom

Received 2 March 2009, in final form 8 June 2009
Published 10 July 2009
Online at stacks.iop.org/JPhysD/42/155504

The effect of voltage on flow rate within cone jet mode electrospraying has been investigated, with particular emphasis on the effect of emitter geometry. A set of experiments investigated the effect of the outer and inner diameter on the flow rate relationship to voltage, in cone jet mode electrospray. This was accomplished by the use of a high fidelity flow meter, capable of measuring changes in flow rate to a fraction of a nano-Litre per second.

It has been previously demonstrated that there are two separate parameters that influence the flow rate sensitivity to voltage; the hydraulic resistance of the flow system, and the outer diameter of the emitter. By a simple derivation, the second of these two is explained by the variation of theoretical electric pressure with voltage, as the outer diameter is varied.

Good agreement is found between experimental and theoretical results, suggesting the simple theory explains reasonably the physics of the situation.

As well as elucidating upon the physics involved in electrospray - suggesting the electric field is an important controlling parameter within cone jet mode electrospray - the theoretical and experimental agreement has important implications for variable throttling of thrust in colloid thrusters, and could bring about better optimization of performance in other electrospray-employing fields.

PACS: 47.61.Fg, 47.65.-d, 47.57.-s

1. Introduction

If a sufficiently large electric field is applied at the interface of a conductive liquid and an insulator, the conductive liquid forms a cone like shape, with a jet emanating from the apex of the cone. Due to varicose wave instabilities on its surface, the jet subsequently breaks down into a monodisperse spray that consists of micro to nano-metre sized charged droplets.

This method of creating ultra-fine charged droplets, commonly called cone-jet electrospray, has developed into a widely employed experimental technique, particularly within Electrospray Mass Spectrometry (ESMS) [1, 2]. However although the technique is used extensively the theoretical understanding of electrospray is only partially complete [3, 4].

An explanation that has proved generally successful at describing the scaling of the current with various parameters was found by Fernàndez de la Mora [5] and Gañán-Calvo [6]. The current was found to depend upon the flow rate and various solution parameters, with some parameters demonstrating a stronger effect than others. One of the parameters found to have marginal effect was the applied voltage, although it should be noted de la Mora and Gañán-Calvo worked in a fixed flow rate (rather than pressure) mode, which may reduce the effect of applied voltage on current.

This finding that applied voltage has little effect on the spray properties is often reported. For example Gañán-Calvo found a small 6-7% change in current with applied voltage [7]. In general applied voltage is found to have a marginal effect on current, although various studies have described a stronger effect [8 -12].

The finding that the current does not significantly depend upon the applied voltage can be thought of resulting from the situation often found experimentally that the change in current in cone jet mode with voltage is small compared to the cone jet mode onset current [7]. Consequently the change in current with voltage can be disregarded when compared to the onset current.

The situation can be different when describing flow rate dependence on applied voltage. Electrospray cone jet mode is often thought to initiate at Q_{min} [5];

$$Q_{\min} = \frac{\gamma \varepsilon_r \varepsilon_0}{\rho K} \tag{1}$$

where γ is the surface tension of the liquid, ε_r the relative permittivity (dielectric constant) of the solvent, ε_r the permittivity of a vacuum, ρ the density of the solvent, and K the conductivity of the electrospraying solution. When the conductivity of the electrospraying solution is large, Q_{min} is a fraction of nano-Litre/s. Consequently, for a high conductivity fluid the onset flow rate is indistinguishable from zero, and thus any change in flow rate with voltage in cone jet mode can be significant.

However to measure the flow rate at this pico to nano-L/s scale is very demanding. With many flow rate measurement methods involving indirect and possibly inaccurate procedures, a clear and repeatable effect of voltage on flow rate had not been found.

By using a highly accurate flow measurement device, studies have begun investigating the sensitivity of flow rate to voltage in detail [13]. Using a pair of in flow-line pressure transducers,

and a flow system using a fixed pressure, the change in flow rate with voltage was accurately measured and a clear dependence between the two found. When a small initial flow rate is applied, the change in flow rate with voltage in cone jet mode can be as great as 45% of Q_{On} [14], where Q_{On} is the onset flow rate of cone jet mode. In the course of numerous experiments within cone jet mode, an unambiguous linear response of flow rate with voltage was found.

It was further established that the linear change in flow rate with voltage within cone jet mode, m_Q, is independent of the nominal flow rate (the flow rate when no voltage is applied) and the conductivity of the electrosprayed solution [14]. Also a dependence of the flow rate sensitivity to voltage on the emitter geometry was observed, with the outer and inner diameter of the emitter needle affecting the flow rate dependence [14, 15]. However it was not possible to distinguish between the ID and OD dependence, although it seems likely that the ID dependence is due to the varying hydraulic resistance [15].

Using the same high fidelity flow measurement device this paper seeks to establish the effect of the emitter geometry in greater detail, establishing the parameters that influence the flow rate change with voltage, m_Q. Specifically the effect of the outer and inner diameter is experimentally tested, and a simple theory is put forward to explain the effect of the emitter diameter on m_Q. This theory is shown to agree well with experimental results.

2. Experimental Details

2.1. Experimental Arrangement

The experimental system is shown in figure 1. The emitter needle was held in a 1/16 in. stainless steel bulkhead union by a vespel ferrule, with 34mm of the emitter protruding from the steel union. The emitter tip was optically aligned 3mm above an extractor electrode, consisting of a 20 mm diameter stainless steel disk, with a 6mm diameter aperture. A second collector electrode was positioned below the extractor electrode, and both the collector electrode and emitter union were connected to ground, with the extractor electrode at high voltage.

The current was determined by measuring the voltage drop across a 10 $M\Omega$ resistor. An ISO-TECH IDM 207 voltmeter logged the voltage to a PC at a frequency of 2Hz.

A negative voltage was applied to the extractor electrode, using a FUG HCL 14-6500 high voltage power supply, with the output controlled by LabView software, via an NI USB-6008 DAQ card.

The electrospray fluid was supplied to the emitter union from a fluid reservoir. All the experiments were completed at atmospheric conditions at both the emitter tip and reservoir, with any initial (nominal) flow rate being gravity fed. As a result the experiments were completed in a fixed pressure (rather than flow rate regime). The change in pressure as the reservoir drained was insignificant, as each spray used at most 0.5 mL, which resulted in a change in height of ~1.2mm. This is small compared to the height difference of the order of 50mm, needed for a low nominal flow rate. In reality the change in height due to draining was less at a low nominal flow rate, and thus the change in height was even less significant than this estimate predicts.

The tests did not call for visual analysis of the spray; however a CCD camera and lens were used to identify stable cone jet mode.

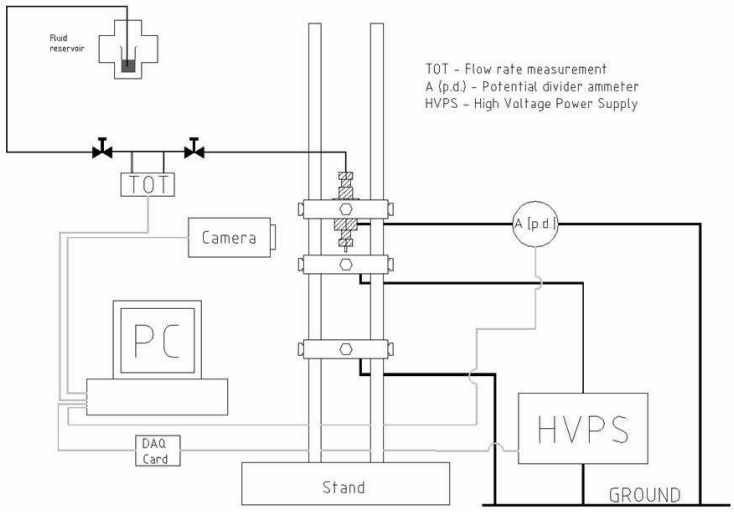

Figure 1. Electrospray experimental arrangement.

2.2. Emitter geometric properties

As shown in table 1, two groups of emitter needles were tested; those with approximately constant outer diameter and those with approximately constant inner diameter. Several of these emitters were quoted by the manufacturer to have large tolerance variation for the ID, consequently the inner diameter was calculated using;

$$r_i = \left(\bar{r}_e^{\,2} - \frac{\bar{M}}{\rho \pi \bar{L}} \right)^{1/2} \tag{2}$$

where r_i is the calculated internal radius, $\bar{r}_e$ the average measured external radius over repeated measurements, $\bar{M}$ the average mass of the emitter, ρ the density of 316 stainless steel, and $\bar{L}$ the average length of the emitter. The calculated IDs agree well with the manufacturers IDs $\pm$ tolerances. All emitters tested were of length 50 mm.

Table 1. Emitter Geometries.

Manufacturers ID (micron)	Manufacturers ID tolerence (micron)		Mean OD (micron)	Calculated ID (micron)
	+	-		
100[a]	50	0	818	144
150[a]	0	50	809	140
200[a]	0	50	808	184
250[a]	0	50	783	266
400[a]	0	50	814	350
450[a]	0	50	819	465
635[b]	15%	15%	806	644
101[b]	15%	15%	201	98
102[b]	15%	15%	277	107
127[b]	15%	15%	231	127
125[b]	15%	15%	1612	127
125[b]	15%	15%	517	155

Supplied by: [a]Upchurch Scientific, [b]Coopers Needle Works.

2.3. Choice of Electrospray fluid

Smith *et al.* found the value of flow rate change with voltage in cone jet mode, m_Q, to be proportional to the viscosity of the sprayed liquid, via the hydraulic resistance of the pipe system [14]. Consequently, to produce relatively high values for m_Q necessary for unambiguous analysis, a low viscosity liquid was needed, and Propylene carbonate was chosen. Its properties are described in table 2. Sodium iodide was added as a dopant, resulting in a conductivity of 2.6×10^{-3} S/m for all experiments. As the concentration of the salt in solution was low (~0.1 g/L), it was assumed the physical properties were that of the base solution.

Table 2. Properties of Propylene Carbonate.

Solvent	viscosity (cP)	Relative permittivity	surface tension (N/m)	Density (kg/m^3)
Propylene Carbonate	2.76[a]	63[a]	0.0452[b]	1206.9[a]

Values from: [a][16], [b][17].

2.4. Flow Measurement system

The same flow measurement system conceived by Smith *et al.* was utilized. A complete description can be found elsewhere [13, 18], with what follows a brief overview.

Two Paroscientific digiquartz 740-23A quartz crystal pressure transducers measured the pressure at two points in the fluid line, effectively calculating the pressure drop across the tubing between them. This pressure drop is proportional to the flow rate by means of the Poiseuille equation;

$$Q = \frac{\Delta P \pi r_i^4}{8 \mu L} \tag{3}$$

where ΔP is the pressure drop, L the length of pipe between the two transducers, r_i the internal radius of the pipe, and μ the dynamic fluid viscosity.

By choosing the length and ID for a desired flow rate sensitivity, the tubing measurement section could be adjusted to suit the needs of the experiments. In these experiments, a measurement section with a 0.125mm internal radius and length 0.5m was chosen, resulting in a flow rate resolution of 0.1nL/s. The flow rate was calibrated using the method used previously [13, 18], where the mass output was collected over a certain period of time, with the pressure difference across the two transducers measured. After a suitable number of repetitions, this produced an excellent linear relationship of flow rate to pressure, with an R-squared value of at least 0.99.

2.5. Experimental Procedure

For each experiment, a nominal flow rate was set by varying the reservoir height. The cone jet onset voltage was found and data logging begun. The high voltage was varied by the PC controlled power supply, increasing incrementally from the onset of cone jet mode to the onset of multi jet mode, with the size of the voltage steps varied between 50 – 100V depending on cone jet voltage range. The voltage was increased every two minutes.

Each emitter was sprayed multiple times, at different starting nominal flow rates. Visual and current analysis confirmed the spray mode. The flow rate was recorded at a frequency of 1.67 Hz giving 200 data points within the two minute constant voltage window.

3. Experimental Results

It has been reported that in cone jet mode a linear relationship of flow rate with voltage occurs [13]. Figure 2 illustrates this linearity once more, using the new solvent propylene carbonate, and over the full cone jet voltage range. The ‘200’ micron i.d. emitter, as described in table 1, was used at a nominal (zero voltage) flow rate of ~84 nL/s. The error bars represent the standard deviation of the flow rate over the two minutes of constant voltage.

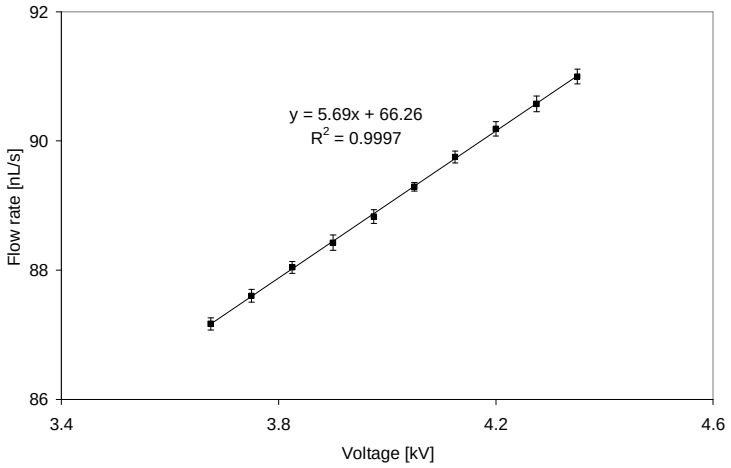

Figure 2. Effect of voltage on flow rate for Propylene carbonate + NaI.

The value of the gradient in figure 2 has been termed m_Q, the change in flow rate with voltage in cone jet mode, with the largest value for m_Q reported up to this point being 2.64 $nLs^{-1}kV^{-1}$ [14]. Thanks to the lower viscosity of propylene carbonate m_Q is expected to be greater and figure 2 illustrates this, with a flow rate sensitivity to voltage of approximately 5.7$nLs^{-1}kV^{-1}$, more than twice the previous maximum.

3.1. Effect of nominal Flow rate for variable internal Diameter Emitters

It is possible to spray in cone jet mode over a large variation of nominal flow rate Q_{nom}, i.e. the flow rate with no voltage applied. Smith *et al.* found the onset flow rate of cone jet mode does not affect the flow rate sensitivity to voltage, m_Q [14], and since the nominal flow rate is directly proportional to the onset flow rate (it is perhaps not the same since a change in flow rate with voltage before cone jet mode has been reported [14, figure 2]), it seems likely the nominal flow rate Q_{nom} has no effect on m_Q.

The effect of the nominal flow rate Q_{nom} on m_Q for the new solvent propylene carbonate, is illustrated in figure 3, for the '200' micron ID emitter. The R-squared value for the linear fitting of m_Q is at least 0.99 for all of the results, whilst the error bars represent the standard deviation for each linear fitting.

There was found a large variation of m_Q from experiment to experiment; for example the ~200 micron ID emitter has an average m_Q of 5.39 $nLs^{-1}kV^{-1}$, with a standard deviation of 0.34 $nLs^{-1}kV^{-1}$. This deviation of flow rate sensitivity to voltage over multiple experiments is much larger than previously found [13, 15], and could be an artefact of the lower viscosity of propylene carbonate resulting in small fluctuations in flow stability having greater effect.

A statistical method to determine whether nominal flow rate effects the Q(V) sensitivity is to analyse whether the gradient of the line of best fit is significantly different from zero, by calculating the test statistic *t* of the slope and comparing it to a critical value of the test statistic [19]. The test statistic is given by;

$$t = \frac{m - M_0}{\sigma_m} \tag{4}$$

where m is the experimental value of the slope, M_0 the hypothesized slope value, and σ_m the standard error of m. Assuming that the theoretical gradient is zero, i.e. $M_0 = 0$, results in $t = m/\sigma_m$. For the data in figure 3, m = -0.0032 and $\sigma_m = 0.0024$, which gives t = -1.32. If $|t| < t_{crit}$ then it can be said that the experimental slope is not significantly different from zero, and for a two tailed test at level of significance $\alpha = 0.05$ with eight degrees of freedom, $t_{crit} = 2.306$ [19]. Consequently it can be concluded that m_Q does not depend on the nominal flow rate.

This method of statistical analysis of the effect of Q_{nom} on m_Q was repeated for other emitters, with all demonstrating that the slope is not significantly different from zero, further suggesting that there is no relationship.

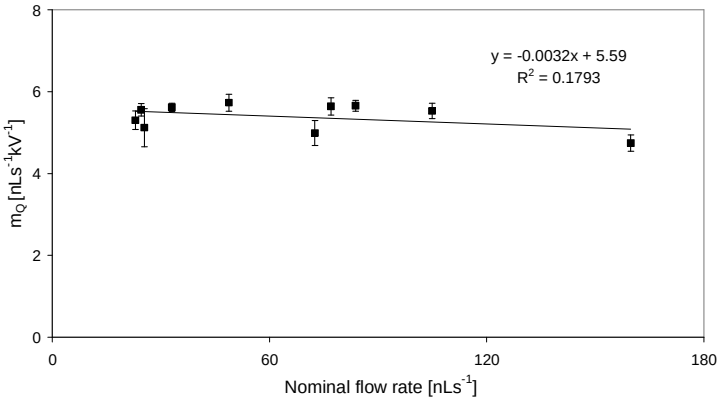

Figure 3. Variation of flow rate sensitivity with nominal flow rate, for '200' micron ID emitter.

3.2. Effect of Inner diameter on Flow rate Sensitivity to Voltage

It has been established that the system hydraulic resistance R_T affects the flow rate sensitivity to voltage [14, 15]. The system hydraulic resistance consists of the summation of the hydraulic resistances from all differing sections of the pipe system;

$$R_T = R_1 + R_2 + R_3 + \ldots R_n \tag{5}$$

The hydraulic resistance is given by;

$$R_n = \frac{8\mu L}{\pi r_i^4} \tag{6}$$

For the experiments completed only the emitter was changed, with the remainder of the pipe system's hydraulic resistance remaining constant.

Keeping the emitter outer diameter constant (on the basis that it may have an effect), the effect of inner diameter was explored, as shown in figure 4. The data used represents the average change

in flow rate with voltage for each emitter, with an experimental sample of at least eight experiments for each emitter. The emitters used have ODs of approximately 800 micron (as described in table 1), with the calculated ID used. The error bars represent the standard deviation of the m_Q value, over the experiments completed for each emitter.

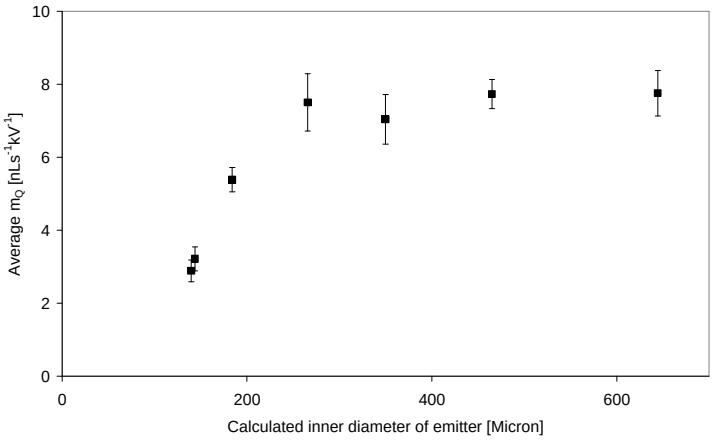

Figure 4. Variation of flow rate sensitivity with inner diameter of emitter.

The change of flow rate with voltage does not vary until the inner diameter of the emitter is small. This is also the case for the total system hydraulic resistance, for as the emitter ID decreases its resistance becomes a larger part of the total piping system hydraulic resistance. This strongly suggests that the changes of m_Q with ID are directly attributable to variations of the total system hydraulic resistance.

It is possible remove the effect of the hydraulic resistance by determining the change of electric pressure with voltage, m_{pe} [14];

$$m_{pe} = m_Q R_T \tag{7}$$

The average m_{pe} is plotted in figure 5, and demonstrates an approximately constant value for different inner diameters. The errors bars on figure 5 represent the standard deviation of the average value of m_{pe}. A slight decreasing trend is noticeable for smaller ID's, but it seems likely this is a result of inexact hydraulic resistance when the average ID is small. To confirm there is not a trend between m_{pe} and ID the same t statistic method used for m_Q against Q_{nom} was again applied. It was found that $|t| < t_{crit}$, therefore the gradient is not significantly different from zero, and it can be concluded that the variation of the flow rate sensitivity to voltage with emitter inner diameter is predominantly and most likely solely a result of the varying hydraulic resistance.

This effect of hydraulic resistance on flow rate sensitivity may go some way to explain why change in flow rate are often found to be marginal. It is conceivable that some previous studies have used a high hydraulic resistance, and consequently found little change of flow rate with voltage.

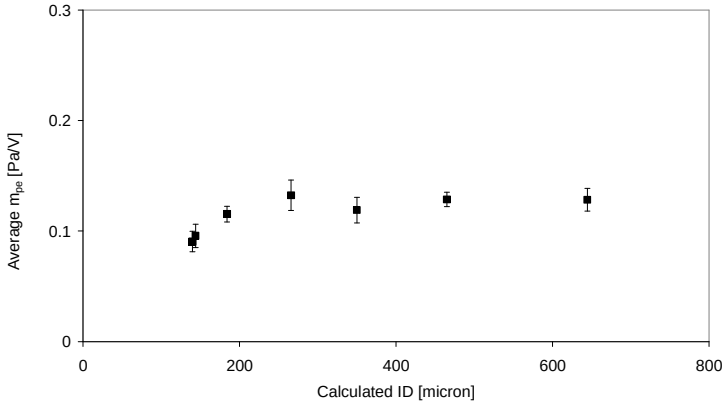

Figure 5. Effect of inner diameter on electric pressure sensitivity.

3.3. Effect of Outer diameter on Flow rate Sensitivity to Voltage

Smith *et al.* found a strong dependence of flow rate sensitivity to voltage with the emitter geometry, but could not discern between the effect of the inner and outer diameter, due to the emitters ID and OD scaling with each other [15]. In these experiments, by keeping emitter ID approximately constant it was anticipated that a clear distinction could be made between the effect of the inner and outer diameter.

Using emitters listed in table 1, the ID was kept at approximately 100 micron, whilst varying the OD from 200 to 1600 micron. Again, it was found that the nominal flow rate did not influence the flow rate dependence on voltage; as a result it was possible to calculate an average m_Q for each emitter. The variation of this average with OD is illustrated in figure 6, with the error bars the standard deviation of the average m_Q.

There is an apparent increase of the sensitivity of flow rate to voltage as the emitter OD decreases, but a seemingly anomalous result is evident. This inconsistent data point occurred with the emitter of 127μm ID- 231μm OD, with a mean value of $m_Q = 16.8 \pm 0.6\,\mathrm{nLs^{-1}kV^{-1}}$. This possibly erroneous result gave the largest value of m_Q found so far, over six times greater than the largest value from preceding studies.

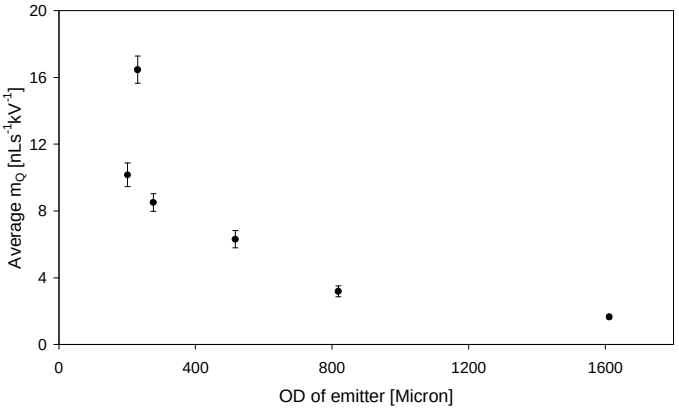

Figure 6. Effect of OD on flow rate sensitivity to voltage.

Closer analysis has revealed the anomalous point is consistent with empirical theory. The emitter producing the anomaly had a somewhat greater ID than other emitters tested, whilst also having a small OD. Since the system resistance varies greatly when the ID is small, this slight variation of R_T has a large effect on the flow rate dependence to voltage.

Once the electric pressure sensitivity is calculated and the effect of hydraulic resistance removed, as shown on figure 7, the anomalous point collapses on to the experimental best-fit line, and a distinct trend is shown. The error bars illustrate the standard deviation of the average value of the change in electric pressure with voltage. Figure 7 demonstrates there is a convincing relationship between m_Q and the outer diameter of the emitter. Also shown is the regression fit line from Ref. [15], where m_{pe} was found to vary with OD to the power -1.4.

It would seem there are two clear and separate parameters influencing the sensitivity of flow rate to voltage; firstly the inner diameter (resulting from the effect of the hydraulic resistance), and secondly the outer diameter. These are only related as a result of geometric and manufacturing constraints on the emitter.

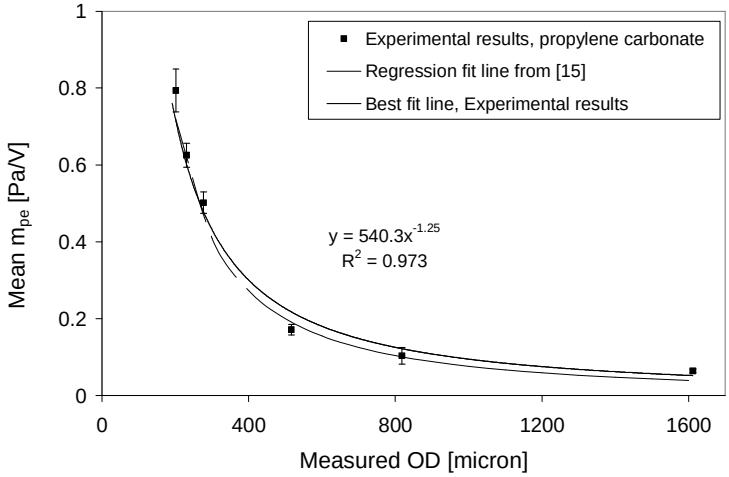

Figure 7. Effect of outer diameter on electric pressure sensitivity to voltage.

3.4. Optimization of Flow rate Sensitivity by varying emitter Geometry

Previous experiments have demonstrated m_Q is sensitive to the emitter geometry, with the two effects seemingly in conflict resulting in a maximum value of m_Q by varying the ID [15]. Earlier experiments assumed the ID influenced the value of the electric pressure sensitivity to voltage, but by keeping the OD the same it has been shown above that ID has no effect on the electric pressure sensitivity, and therefore there is no maximum value for m_Q as OD varies, when the ID is constant.

However most conventionally manufactured emitters have an approximately constant wall thickness for different size outer diameters. Consequently the hydraulic resistance would vary

with OD, and it is possible to produce a maximum value for m_Q by careful selection of emitter geometry.

This is demonstrated in figure 8, which plots the estimate of the flow rate sensitivity to voltage as OD varies, with a constant wall thickness of 50 micron. The estimate of m_Q is calculated using the line of best fit from figure 7 to calculate the electric pressure sensitivity to voltage, m_{pe}, and removing the effect of the total resistance as in Equation (7). Curves are plotted using various electrospraying solutions with differing viscosities. The viscosities are assumed to be that of the base solution with no dopant added. With the exception of the emitter the fluid piping is assumed to be the same.

The left hand side of the curves follow the same shape as the fluid conductance, the reciprocal of the resistance, a shape proportional to r_i^4. The right hand side is governed by the changes in electric pressure sensitivity with OD.

The location of the peak value of m_Q does not change with viscosity, but is considerably greater when the viscosity is small, with acetone demonstrating a theoretical peak of ~210nLs^{-1}kV^{-1}. Whether this is experimentally possible, and would result in a stable cone jet mode, is not possible to discern without further testing.

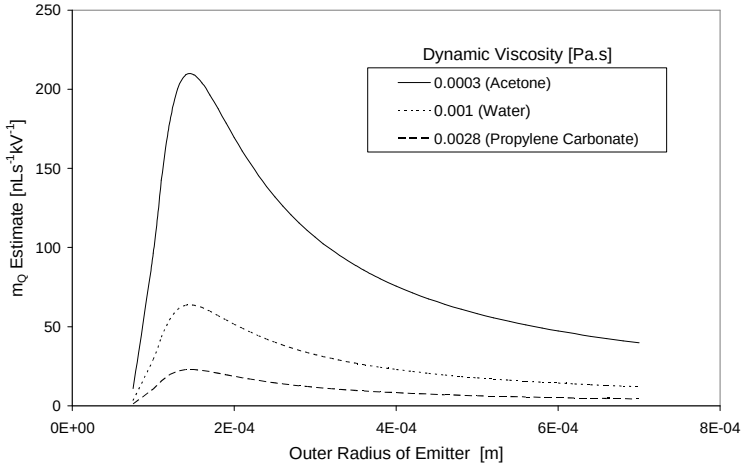

Figure 8. Estimate of m_Q with outer radius, and emitter wall thickness of 50 micron. Viscosity values from [20], except propylene carbonate [16].

4. Theoretical variation of electric pressure sensitivity to Voltage with Emitter Geometry

The electrostatics of a point-to plane system is a solved analytical problem [21], with two general methods [22]: 1) solving the Laplace equation in a suitable coordinate system; 2) use of method of images for a particular distribution of charges.

Eyring *et al.* [23] solved the Laplace equation in orthogonal coordinates, assuming the emitter was a hyperboloid, and this is the most common method, applied frequently [24, 25]. The second

technique applies the method of images and results in similar equations for the potential difference and electric field [22, 26, 27].
Once the Laplace equation is solved in orthogonal coordinates with suitable boundary conditions, the most commonly found solution for the electric field at the tip is [23 -25];

$$E_0 = -\frac{2\phi_0/a}{\left(1-\eta_0^2\right)\log\left(\frac{1+\eta_0}{1-\eta_0}\right)} \tag{8}$$

where φ_0 is the potential difference between the emitter needle and the plate electrode, η_0 the hyperboloid surface chosen to represent the emitter, and a twice the distance from the plane electrode to the focus of the hyperboloid [23, 28];

$$a = \frac{z_0}{\eta_0} \qquad \eta_0 = \frac{1}{\sqrt{1+r_e/z_0}} \tag{9a, b}$$

where z_0 is the distance between an emitter tip and the extractor plate, and r_e is the outer radius. Loeb, and separately using method of images Jones, simplified Equation (6) using the assumption $z_0 \rangle\rangle r_e$, resulting in [26, 29];

$$E_0 = -\frac{\phi_0}{A_1 r_e \ln\left(4z_0/r_e\right)} \tag{10}$$

where A_1 is a constant of the order unity. Different authors have derived different values for A_1; Loeb finds a value of 0.707, whilst Jones derives 0.5, and others have found analytical functions of z_0 and r_e amongst other parameters [30]. Here we will allow A_1 to be adjusted to fit theoretical to experimental data, as done previously when comparing theoretical to experimental cone jet onset voltages [31].
Ignoring tangential terms, the electric stress can be given by;

$$\begin{aligned} P_e &= \tfrac{1}{2}\varepsilon_0 E_0^2 \\ &= \tfrac{1}{2}\varepsilon_0\left(\frac{\phi_0}{A_1 r_e \ln\left(4z_0/r_e\right)}\right)^2 \end{aligned} \tag{11a, b}$$

Differentiating with respect to ϕ_0 gives;

$$\frac{dP_e}{d\phi_0} = \frac{\varepsilon_0\phi_0}{\left(A_1 r_e \ln\left(4z_0/r_e\right)\right)^2} \tag{12}$$

This can be thought of as the variation of theoretical electric pressure with voltage, and is comparable to m_{pe}. Both the theoretical and experimental values for m_{pe} are plotted on Figure 9,

and demonstrate similar trends. Here A_1 is set to a value 0.5, and φ_0 is taken to be the onset voltage, measured experimentally for each different OD emitter.
The theoretical values of the electric pressure sensitivity resulting from Equation (10) are dependent on the assumed constant A_1. The least squares best fit of theoretical to experimental results occurs when $A_1 \approx 0.36$, as also shown in figure 9, and this is within the range for A_1 calculated by Pantano *et al.* [30]. Once A_1 is adjusted a very good correlation is demonstrated, suggesting that the underlying sensitivity for m_{pe} is as characterised by this simple theoretical approach.

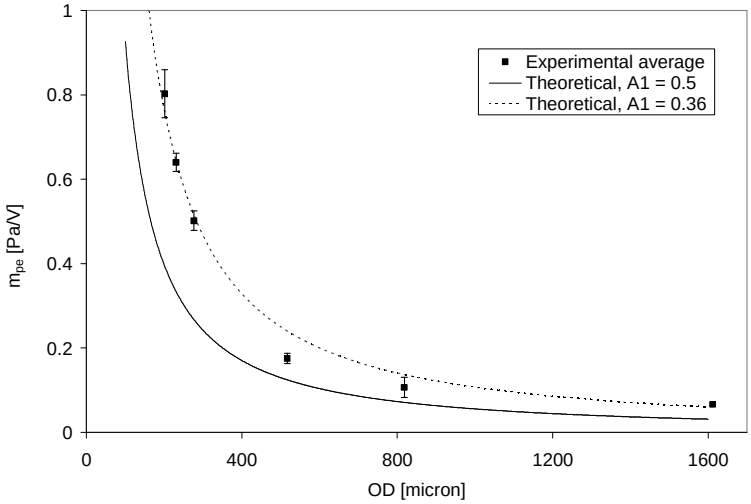

Figure 9. Variation of the electric pressure with voltage, as the OD changes: comparison between theoretical and experimental results.

A question however still remains regarding the validity of varying A_1, required as a disposable parameter to fit the experimental observations. It is worthwhile noting that although Jones and Loeb use different initial assumptions of the emitter shape (Jones starts with a simple line of charge, whilst Loeb assumes a hyperboloid) [26, 29], they derive the same electric field equation with the exception of the value of A_1. This suggests that A_1 may be a corrective factor that can partially take into account the shape of the tip.
It should be noted that Equations (11a, b) are solely used as intermediaries to calculate the change in electric stress with voltage, and not to calculate the liquid pressure in the liquid meniscus, as this is invalid without an analysis of the cone shape. There will be an influence of meniscus shape on the overall pressure, and, as the cone shape does vary with voltage [18], also on the change in overall pressure with voltage. For a full description this must be taken into account. Presented here is only a first order analysis of the change of pressure with voltage, which fits remarkably well with experimental results.

Various other limitations on the experimental to theoretical comparison also exist. The experiments used an extractor electrode with a 6mm diameter aperture (to avoid the accumulation

of the sprayed solvent on the electrode), whilst the theoretical evaluations are based upon a simple infinite flat electrode. Intuitively it would seem that an aperture in the electrode would reduce the effect of the changes in voltage on the electric field, although this can't seem to be resolved without the use of finite element analysis software.
Also the Laplace equation was solved rather than the Poisson Equation; space charge was not considered. Although space charge will have an effect, especially for highly conductive fluids, in this initial analysis it is assumed to be secondary.
These complications in comparing experimental and theoretical results do not influence the basic argument of the theory - the variation of the flow rate sensitivity to voltage with outer diameter results from variations in the electric field sensitivity to voltage, with outer diameter.

Finally, Equation (12) implies that that the emitter tip to extractor electrode distance, z_0, may also influence the flow rate sensitivity to voltage, with sensitivity increasing with decreasing distance. Further experiments are to be completed to investigate whether this predicted effect occurs. It would seem though that as the emitter to electrode distance is reduced, equation (10) becomes less valid [32], suggesting that the effect may not be entirely as has been theoretically described.

5. Conclusions

By the application of a high accuracy inline flow rate measurement system the sensitivity of flow rate to voltage within cone jet mode electrospray has been found for a previously untested liquid, propylene carbonate. The sensitivity of flow rate to voltage is found to be independent of nominal flow rate, agreeing with previous results.
Additional experimental data reported and analysed here reveals the variation of m_Q with internal diameter is solely a result of differing hydraulic resistance. Once the differing hydraulic resistance has been removed, there is no significant relationship between the flow rate sensitivity to voltage and the emitter inner diameter.
By keeping the internal diameter approximately constant, the effect of the outer diameter was investigated. The flow rate sensitivity to voltage is found to be a function of the outer diameter, with the flow rate sensitivity increasing for smaller outer diameter emitters.
This variation of flow rate sensitivity to voltage with OD is explained by the variation of the theoretical electric pressure sensitivity to voltage, with OD. Fundamentally the electric field increases faster with voltage for an emitter with a smaller outer diameter. This simple theoretical model is consistent and in good agreement with experimental results.

The variation of the flow rate sensitivity to voltage with emitter geometry is an important finding, with implications for spacecraft colloid thrusters, as well as ESMS. It will facilitate the optimization of the variation of the thrust and specific impulse with voltage for a colloid thruster system, resulting in simple thrust throttle control [13]. The new results will also help provide additional understanding of the effect of voltage on field strength when voltage is used as the principal control parameter, for example in the nano electrospray where the electric field is used to initiate cone jet mode when zero nominal flow rate is applied.

[1] Fenn J B, Mann M, Meng C K, Wong S K and Whitehouse C M 1989 *Science* **246** 64-71
[2] Cole R B (Ed.) 1997 *Electrospray Ionization Mass Spectrometry: Fundamentals, Instrumentation, and Applications* (New York: Wiley-Interscience)
[3] Fernàndez de la Mora J 2007 *Annu. Rev. Fluid Mech.* **39** 217-43
[4] Eggers J 1997 *Rev. Mod. Phys.* **69** 865-929
[5] Fernàndez de la Mora J and Loscertales I G 1994 *J. Fluid Mech.* **260** 155-184
[6] Gañán-Calvo A M, Barrero A and Pantano-Rubiño C 1993 *J. Aerosol Sci.* **24** S19
[7] Gañán-Calvo A M and Davila J 1997 *J. Aerosol Sci.* **28** 249-275
[8] Zeleny J 1935 *J. Franklin Inst*. **219** 659
[9] Yahiku A Y, Mahoney J F, Daley H L, Perel J and Sherman A.1970 *AIAA 8th Electric Propulsion Conf.* AIAA-70-1112
[10] Wilm M S and Mann M 1994 *Int. J. Mass. Spectrom.* **136**, 167-180
[11] Ku B K and Kim S S 2003 *J. Electrostat.* **57** 109-128
[12] Hartman R P A, Brunner D J, Camelot D M A, Marijnissen J C M and Scarlett B 1999 *J. Aerosol Sci*. **30** 823 - 849
[13] Smith K L, Alexander M S and Stark J P W 2006 *J. Appl. Phys.* **99** 064909
[14] Smith K L, Alexander M S and Stark J P W 2006 *Phys. Fluids* **18** 092104
[15] Alexander M S, Smith K L, Paine M D and Stark J P W 2007 *J. Propul. Power* **23** 1042
[16] Beyer K, Bergfeld W, Berndt W, Carlton W, Hoffmann D, Schroeter A and Shank R 1987 *J. Am. Coll. Toxicol.* **6**, 23
[17] Naejus R, Lemordant D, Coudert R and Willmann P 1997 *J. of Chem. Thermodyn.* **29**, 1503
[18] Smith K L 2005 Ph.D. thesis, Queen Mary University of London
[19] Kirkup L 2002 *Data Analysis with Excel* (Cambridge University Press)
[20] Riddick J A 1970 *Organic solvents: physical properties and methods of purification* (New York: Wiley-Interscience)
[21] Lekner J 2006 *Eur. J. Phys.* **27** 87
[22] Birdseye P J and Smith D A 1970 *Surf. Sci.* **23** 198
[23] Eyring C F, Mackeown S S and Millikan R A 1928 *Phys. Rev.* **31** 900
[24] Smythe W R 1968 *Static and Dynamic Electricity* 3rd edn (New York: McGraw-Hill), section 5.28.
[25] Yarin A L, Koombhongse S and Reneker D H 2001 *J. Appl. Phys.* **90** 4836
[26] Jones A R and Thong K C 1971 *J. Phys. D: Appl. Phys.* **4** 1159
[27] Taylor G I 1969 *Proc. Roy. Soc. London A.* **3113** 453
[28] Martínez-Sánchez M 2006 MIT Space Propulsion course notes, available online
[29] Loeb L B, Kip A F, Hudson G G and Bennett W H 1941 *Phys. Rev.* **60** 714
[30] Pantano C, Gañán-Calvo A M and Barrero A 1994 *J. Aerosol Sci.* **25** 1065
[31] Smith D P H 1986 *IEEE Trans. Ind. Appl.* **IA-22** 527
[32] Krpoun R and Shea H R 2008 *J. App. Phys.* **104** 064511

References

[1] Hartman, R. P. A., Brunner, D. J., Camelot, D. M. A., Marijnissen, J. C. M., and Scarlett, B., Jet break-up in electrohydrodynamic atomization in the cone-jet mode, *Journal of Aerosol Science*, **31,** 65-95, (2000).

[2] Fenn, J., Mann, M., Meng, C., Wong, S., and Whitehouse, C., Electrospray ionization for mass spectrometry of large biomolecules, *Science*, **246,** 64-71, (1989).

[3] Cole, R. B. (Ed.), *Electrospray Ionization Mass Spectrometry: Fundamentals, Instrumentation, and Applications*, Wiley-Interscience, (1997).

[4] Li, D. and Xia, Y., Electrospinning of nanofibers: reinventing the wheel?, *Advanced Materials*, **16,** 1151-1170, (2004).

[5] Demmons, N., V. Hruby, D. Spence, T. Roy, E. Ehrbar, J. Zwahlen, Martin, R., J. Ziemer, and Randolph, T., ST7-DRS Mission Colloid Thruster Development, *in* Proc. 44th AIAA/ASME/SAE/ASEE Joint Propulsion Conference & Exhibit, Hartford, Connecticut, number AIAA 2008-4823, (2008).

[6] Ceccanti, F., Paita, L., Cesari, U., De Tata, M., Giusti, N., Balducci, P., and Del Pistoia, M., 3200 hours Endurance Testing of the Lisa Pathfinder FT-150 Thruster, *in* Proc. 31st International Electric Propulsion Conference, University of Michigan, Ann Arbor, MI, Number IEPC-2009-170, (2009).

[7] Fernández de la Mora, J., The fluid dynamics of Taylor cones, *Annual Review of Fluid Mechanics*, **39,** 217-243, (2007).

[8] Eggers, J., Nonlinear dynamics and breakup of free-surface flows, *Reviews of Modern Physics*, **69,** 865-930, (1997).

[9] Smith, K. L., Alexander, M. S., and Stark, J. P. W., The sensitivity of volumetric flow rate to applied voltage in cone-jet mode electrospray and the influence of solution properties and emitter geometry, *Physics of Fluids*, **18,** 092104, (2006).

[10] Smith, K. L., *Characterisation of electrospray properties in high vacuum: with a view to application in colloid thruster technology*, PhD thesis, Queen Mary University of London, (2005).

[11] Ryan, C. N., Smith, K. L., Alexander, M. S., and Stark, J. P. W., Effect of emitter geometry on flow rate sensitivity to voltage in cone jet mode electrospray, *Journal of Physics D: Applied Physics*, **42,** 155504, (2009).

[12] Alexander, M., S. , Stark, J. P. W., Smith, K. L., Stevens, B., and Kent, B., Electrospray performance of microfabricated colloid thruster arrays, *Journal of Propulsion and Power*, **22,** 620-627, (2006).

[13] Krpoun, R. and Shea, H. R., A method to determine the onset voltage of single and arrays of electrospray emitters, *Journal of Applied Physics*, **104,** 064511, (2008).

[14] Zeleny, J., The electrical discharge from liquid points and a hydrostatic method of measuring the electric intensity at their surfaces, *The Physical Review*, **3,** 69-91, (1914).

[15] Taylor, G., Disintegration of Water Drops in an Electric Field, *Proceedings of the Royal Society of London. Series A, Mathematical and Physical Sciences*, **280,** 383-397, (1964).

[16] Duby, M.-H., Deng, W., Kim, K., Gomez, T., and Gomez, A., Stabilization of monodisperse electrosprays in the multi-jet mode via electric field enhancement, *Journal of Aerosol Science*, **37,** 306-322, (2006).

[17] Cloupeau, M. and Prunet-Foch, B., Electrostatic spraying of liquids in cone-jet mode, *Journal of Electrostatics*, **22,** 135–159, (1989).

[18] Collins, R. T., Harris, M. T., and Basaran, O. A., Breakup of electrified jets, *Journal of Fluid Mechanics*, **588,** 75-129, (2007).

[19] Cloupeau, M. and Prunet-Foch, B., Electrostatic spraying of liquids–main functioning modes, *Journal of Electrostatics*, **25,** 165–184, (1990).

[20] Ragucci, R., Fabiani, F., Cavaliere, A., Muscetta, P., and Noviello, C., Characterization of stability regimes of electrohydrodynamically enhanced atomization, *Experimental Thermal and Fluid Science*, **21,** 156-161, (2000).

[21] Zhang, X. and Basaran, O. A., Dynamics of drop formation from a capillary in the presence of an electric field, *Journal of Fluid Mechanics*, **326,** 239-263, (1996).

[22] Notz, P. K. and Basaran, O. A., Dynamics of drop formation in an electric field, *Journal of Colloid and Interface Science*, **213,** 218-237, (1999).

[23] Rayleigh, L., On the equilibrium of liquid conducting masses charged with electricity, *Philosophical Magazine Series 5*, **14,** 184-186, (1882).

[24] Jaworek, A. and Krupa, A., Jet and drops formation in electrohydrodynamic spraying of liquids. A systematic approach, *Experiments in Fluids*, **27,** 43-52, (1999).

[25] Zeleny, J., Instability of Electrified Liquid Surfaces, *The Physical Review*, **10,** 1-6, (1917).

[26] Juraschek, R. and Röllgen, F. W., Pulsation phenomena during electrospray ionization, *International Journal of Mass Spectrometry*, **177,** 1-15, (1998).

[27] Marginean, I., Parvin, L., Heffernan, L., and Vertes, A., Flexing the Electrified Meniscus: The Birth of a Jet in Electrosprays, *Analytical Chemistry*, **76,** 4202-4207, (2004).

[28] Paine, M. D., Alexander, M. S., and Stark, J. P. W., Nozzle and liquid effects on the spray modes in nanoelectrospray, *Journal of Colloid and Interface Science*, **305,** 111-123, (2007).

[29] Hartman, R. P. A., Brunner, D. J., Camelot, D. M. A., Marijnissen, J. C. M., and Scarlett, B., Electrohydrodynamic atomization in the cone-jet mode. A physical model of the liquid cone and jet, *Journal of Aerosol Science*, **30,** 823-849, (1999).

[30] Fernández de la Mora, J. and Loscertales, I. G., The current emitted by highly conducting Taylor cones, *Journal of Fluid Mechanics*, **260,** 155-184, (1994).

[31] Zeleny, B. A., On the conditions of instability of electrified drops, with applications to the electric discharge from liquid points, *Proceedings of the Cambridge Philosophical Society*, **18,** 71–83, (1915).

[32] Kreyszig, E., *Advanced engineering mathematics*, 7th ed., Wiley, (1993).

[33] Jackson, J. D., *Classical electrodynamics*, 3rd ed., Wiley, (1999).

[34] Martinez-Sánchez, M., *MIT Space Propulsion Course Notes*, (accessed 2009).

[35] Driesel, W., Dietzsch, C., and Muhle, R., In situ observation of the tip shape of AuGe liquid alloy ion sources using a high voltage transmission electron microscope, *Journal of Vacuum Science & Technology B: Microelectronics and Nanometer Structures*, **14,** 3367-3380, (1996).

[36] Driesel, W., Dietzsch, C., and Moser, M., In situ HV TEM observation of the tip shape of lead liquid metal ion sources, *Journal of Physics D: Applied Physics*, **29,** 2492-2500, (1996).

[37] Smith, D. P. H., The electrohydrodynamic atomization of liquids, *IEEE Transactions on Industry Applications*, **IA-22,** 527-535, (1986).

[38] Abramowitz, M. and Stegun, I. A. (Ed.), *Handbook of mathematical functions with Formulas, Graphs, and Mathematical Tables*, Dover, (1964).

[39] Eyring, C. F., Mackeown, S. S., and Millikan, R. A., Fields currents from points, *Physical Review*, **31,** 900-909, (1928).

[40] Smythe, W. R., *Static and Dynamic Electricity*, section 5.28, McGraw-Hill, (1968).

[41] Yarin, A. L., Koombhongse, S., and Reneker, D. H., Taylor cone and jetting from liquid droplets in electrospinning of nanofibers, *Journal of Applied Physics*, **90,** 4836-4846, (2001).

[42] Xiong, J., Sun, D., Zhou, Z., and Zhang, W., Investigation of the onset voltage for the design of a microfabricated colloid thruster, *IEEE/ASME Transactions on Mechatronics*, **11,** 66-74, (2006).

[43] Loeb, L. B., Kip, A. F., Hudson, G. G., and Bennett, W. H., Pulses in negative point-to-plane corona, *Physical Review*, **60,** 714-722, (1941).

[44] Jones, A. R. and Thong, K. C., The production of charged monodisperse fuel droplets by electrical dispersion, *Journal of Physics D: Applied Physics*, **4,** 1159-1168, (1971).

[45] Regele, J. D., Papac, M. J., Rickard, M. J. A., and Dunn-Rankin, D., Effects of capillary spacing on EHD spraying from an array of cone jets, *Journal of Aerosol Science*, **33,** 1471-1479, (2002).

[46] Quang Tran Si, B., Byun, D., and Lee, S., Experimental and theoretical study of a cone-jet for an electrospray microthruster considering the interference effect in an array of nozzles, *Journal of Aerosol Science*, **38,** 924-934, (2007).

[47] Lenggoro, I. W., Okuyama, K., Fernández de la Mora, J., and Tohge, N., Preparation of ZnS nanoparticles by Electrospray Pyrolysis, *Journal of Aerosol Science*, **31,** 121-136, (2000).

[48] Hohman, M. M., Shin, M., Rutledge, G., and Brenner, M. P., Electrospinning and electrically forced jets. I. Stability theory, *Physics of Fluids*, **13,** 2201-2220, (2001).

[49] Hohman, M. M., Shin, M., Rutledge, G., and Brenner, M. P., Electrospinning and electrically forced jets. II. Applications, *Physics of Fluids*, **13,** 2221-2236, (2001).

[50] Shin, Y. M., Hohman, M. M., Brenner, M. P., and Rutledge, G. C., Electrospinning: A whipping fluid jet generates submicron polymer fibers, *Applied Physics Letters*, **78,** 1149-1151, (2001).

[51] Rayleigh, L., On the capillary phenomena of jets, *Proceedings of the Royal Society of London*, **29,** 71-97, (1879).

[52] Kebarle, P. and Verkerk, U. H., Electrospray: From ions in solution to ions in the gas phase, what we know now, *Mass Spectrometry Reviews*, **28,** 898-917, (2009).

[53] Lozano, P., *Studies on the ion-droplet mixed regime in colloid thrusters*, PhD thesis, MIT, (2003).

[54] Gañan-Calvo, A. M., The size and charge of droplets in the electrospraying of polar liquids in cone-jet mode, and the minimum droplet size, *Journal of Aerosol Science*, **25,** 309-310, (1994).

[55] Gañán-Calvo, A. M., Cone-jet analytical extension of Taylor's electrostatic solution and the asymptotic universal scaling laws in electrospraying, *Physical Review Letters*, **79,** 217-220, (1997).

[56] Gañán-Calvo, A. M., Dávila, J., and Barrero, A., Current and droplet size in the electrospraying of liquids. Scaling laws, *Journal of Aerosol Science*, **28,** 249-275, (1997).

[57] Chen, D.-R. and Pui, D. Y. H., Experimental investigation of scaling laws for electrospraying: dielectric constant effect, *Aerosol Science and Technology*, **27,** 367-380, (1997).

[58] Gañán-Calvo, A. M., On the general scaling theory for electrospraying, *Journal of Fluid Mechanics*, **507,** 203-212, (2004).

[59] Smith, K. L., Alexander, M. S., and Stark, J. P. W., The role of molar conductivity in electrospray cone-jet mode current scaling, *Journal of Applied Physics*, **100,** 014905, (2006).

[60] Chen, D.-R., Pui, D. Y. H., and Kaufman, S. L., Electrospraying of conducting liquids for monodisperse aerosol generation in the 4 nm to 1.8 micron diameter range, *Journal of Aerosol Science*, **26,** 963-977, (1995).

[61] Hartman, R. P. A., *Electrohydrodynamic atomization in the cone-jet mode. From physical modelling to powder production*, PhD thesis, Delft University of Technology, (1998).

[62] Saville, D. A., Electrohydrodynamics: the Taylor-Melcher leaky dielectric model, *Annual Review of Fluid Mechanics*, **29,** 27-64, (1997).

[63] Carretero-Benignos, J. A., *Numerical Simulation of a single emitter colloid thruster in pure droplet cone-jet mode*, PhD thesis, MIT, (2005).

[64] Carretero, J. and Martínez-Sánchez, M., Numerical simulation of a colloidal thruster in the droplet regime, *Computer Physics Communications, Proceedings of the 18th International Conference on the Numerical Simulation of Plasmas*, **164,** 202-208, (2004).

[65] Yan, F., Farouk, B., and Ko, F., Numerical modeling of an electrostatically driven liquid meniscus in the cone-jet mode, *Journal of Aerosol Science*, **34,** 99-116, (2003).

[66] Lastow, O. and Balachandran, W., Novel low voltage EHD spray nozzle for atomization of water in the cone jet mode, *Journal of Electrostatics*, **65,** 490-499, (2007).

[67] *FLOW3D News, Development preview: new model for electro-hydrodynamics of semi-conductive fluids,* (accessed 2009).

[68] Zeng, J., Sobek, D., and Korsmeyer, T., Electro-hydrodynamic modeling of electrospray ionization: CAD for a microfluidic device-mass spectrometer

interface, *in* Proc. 12th International Conference on transducers, solid-state sensors, actuators and microsystems, 1275-1278, (2003).

[69] Sen, A. K., Darabi, J., Knapp, D. R., and Liu, J., Modeling and characterization of a carbon fiber emitter for electrospray ionization, *Journal of Micromechanics and Microengineering*, **16,** 620–630, (2006).

[70] Sen, A., Darabi, J., and Knapp, D., Simulation and parametric study of a novel multi-spray emitter for ESIMS applications, *Microfluidics and Nanofluidics*, **3,** 283-298, (2007).

[71] Smith, K. L., Alexander, M. S., and Stark, J. P. W., Voltage effects on the volumetric flow rate in cone-jet mode electrospraying, *Journal of Applied Physics*, **99,** 064909, (2006).

[72] Alexander, M. S., Smith, K. L., Paine, M. D., and Stark, J. P. W., Voltage-modulated flow rate for precise thrust control in colloid electrospray propulsion, *Journal of Propulsion and Power*, **23,** 1042-1048, (2007).

[73] Aguirre-de-Carcer, I. and Fernández de la Mora, J., Effect of background gas on the current emitted from Taylor cones, *Journal of Colloid and Interface Science*, **171,** 512-517, (1995).

[74] Gamero-Castaño, M., Aguirre-de-Carcer, I., de Juan, L., and Fernández de la Mora, J., On the current emitted by Taylor cone-jets of electrolytes in vacuo: Implications for liquid metal ion sources, *Journal of Applied Physics*, **83,** 2428-2434, (1998).

[75] Rosell, J., *Size characterization in electrosprays of submicron droplets*, PhD thesis, Yale University, (1994).

[76] Grigoriev, D. A. and Edirisinghe, M. J., Evaporation of liquid during cone-jet mode electrospraying, *Journal of Applied Physics*, **91,** 437-439, (2002).

[77] Yahiku, A. Y., Mahoney, J. F., Daley, H. L., Perel, J., and Sherman, A., Experimental study of colloid annular thrusters, *in* Proc. AIAA 8th Electric Propulsion Conference, number AIAA 70-1112, (1970).

[78] Mutoh, M., Kaieda, S., and Kamimura, K., Convergence and disintegration of liquid jets induced by an electrostatic field, *Journal of Applied Physics*, **50,** 3174-3179, (1979).

[79] Isenberg, C., *The science of soap films and soap bubbles*, Dover, (1992).

[80] Gamero-Castaño, M. and Fernández de la Mora, J., Direct measurement of ion evaporation kinetics from electrified liquid surfaces, *The Journal of Chemical Physics*, **113,** 815-832, (2000).

[81] Sutton, G. P., *Rocket propulsion elements*, 7th ed., Wiley, (2001).

[82] Martinez-Sánchez, M., Fernández De La Mora, J., Gamero-Castaño, M., and Khayms, V., Research on colloid thrusters, *in* Proc. 26th Int. Electric Propulsion Conf., Kitakyushu, Japan, number IEPC-99-014, (1999).

[83] Ziemer, J. K., Performance of electrospray thrusters, *in* Proc. 31st International Electric Propulsion Conference, University of Michigan, Ann Arbor, Michigan, number IEPC-2009-242, (2009).

[84] Borra, J. P., Tombette, Y., and Ehouarn, P., Influence of electric field profile and polarity on the mode of EHDA related to electric discharge regimes, *Journal of Aerosol Science*, **30,** 913-925, (1999).

85 Constantopoulos, T. L., Jackson, G. S., and Enke, C. G., Challenges in achieving a fundamental model for ESI, *Analytica Chimica Acta*, **406,** 37-52, (2000).

86 English, W. N., Corona from a water drop, *Physical Review*, **74,** 179-189, (1948).

87 Ikonomou, M. G., Blades, A. T., and Kebarle, P., Electrospray-ion spray: a comparison of mechanisms and performance, *Analytical Chemistry*, **63,** 1989-1998, (2002).

88 López-Herrera, J. M., Barrero, A., Boucard, A., Loscertales, I. G., and Márquez, M., An experimental study of the electrospraying of water in air at atmospheric pressure, *Journal of the American Society for Mass Spectrometry*, **15,** 253-259, (2004).

89 Meesters, G. M. H., Vercoulen, P. H. W., Marijnissen, J. C. M., and Scarlett, B., Generation of micron-sized droplets from the Taylor Cone, *Journal of Aerosol Science*, **23,** 37-49, (1992).

90 Shorey, J. D. and Michelson, D., On the mechanism of electrospraying, *Nuclear Instruments and Methods*, **82,** 296-296, (1970).

91 Zeleny, J., The Role of surface instability in electrical discharges from drops of alcohol and water in air at atmospheric pressure, *Journal of the Franklin Institute*, **219,** 659-675, (1935).

92 Ku, B. K. and Kim, S. S., Electrohydrodynamic spraying characteristics of glycerol solutions in vacuum, *Journal of Electrostatics*, **57,** 109-128, (2003).

93 Marginean, I., Kelly, R. T., Page, J. S., Tang, K., and Smith, R. D., Electrospray characteristic curves: In pursuit of improved performance in the nanoflow regime, *Analytical Chemistry*, **79,** 8030-8036, (2007).

94 Wilm, M. S. and Mann, M., Electrospray and Taylor-Cone theory, Dole's beam of macromolecules at last?, *International Journal of Mass Spectrometry and Ion Processes*, **136,** 167-180, (1994).

95 Forbes, R. G., Liquid metal Ion Sources and electrosprays operating in cone-jet mode: Some theoretical comparisons and comments, *Journal of Aerosol Science*, **31,** 97-120, (2000).

96 Mair, G. L. R., Theoretical determination of current-voltage curves for liquid metal ion sources, *Journal of Physics D: Applied Physics*, **17,** 2323-2330, (1984).

97 Forbes, R. G., Understanding how the liquid-metal ion source works, *Vacuum*, **48,** 85-97, (1997).

98 Mair, G. L. R., Current-voltage curves in liquid metal ion sources, *Vacuum*, **36,** 847-850, (1986).

99 Wilm, M. and Mann, M., Analytical properties of the nanoelectrospray ion source, *Analytical Chemistry*, **68,** 1-8, (1996).

100 Alexander, M. S., Paine, M. D., and Stark, J. P. W., Pulsation modes and the effect of applied voltage on current and flow rate in nanoelectrospray, *Analytical Chemistry*, **78,** 2658-2664, (2006).

101 Bevington, P. R. and Robinson, D. K., *Data reduction and error analysis for the physical sciences*, McGraw-Hill, (1992).

102 Beyer, K., Bergfeld, W., Berndt, W., Carlton, W., Hoffmann, D., Schroeter, A., and Shank, R., Final Report on the Safety Assessment of Propylene Carbonate, *International Journal of Toxicology*, **6,** 23-51, (1987).

[103] Riddick, J. A., Bunger, W. B., and Sakano, T. K., *Organic solvents: physical properties and methods of purification. Fourth edition*, Wiley-Interscience, (1986).

[104] Naejus, R., Lemordant, D., Coudert, R., and Willmann, P., Excess thermodynamic properties of binary mixtures containing linear or cyclic carbonates as solvents at the temperatures 298.15 K and 315.15 K, *The Journal of Chemical Thermodynamics*, **29,** 1503-1515, (1997).

[105] Kirkup, L., *Data Analysis with Excel*, Cambridge University Press, (2002).

[106] Pantano, C., Gañán-Calvo, A. M., and Barrero, A., Zeroth-order, electrohydrostatic solution for electrospraying in cone-jet mode, *Journal of Aerosol Science*, **25,** 1065-1077, (1994).

[107] Krpoun, R., *Micromachined electrospray thrusters for spacecraft propulsion*, PhD thesis, Ecole Polytechnique Fédérale de Lausanne, (2008).

[108] Ryan, C. N., Smith, K. L., Alexander, M. S., and Stark, J. P. W., Performance modulation of colloid thrusters by the variation of flow rate with applied voltage, *in* Proc. 31st International Electric Propulsion Conference, Ann Arbor, Michigan, USA, number IEPC-2009-187, (2009).

[109] Krpoun, R., Smith, K. L., Stark, J. P. W., and Shea, H. R., Tailoring the hydraulic impedance of out-of-plane micromachined electrospray sources with integrated electrodes, *Applied Physics Letters*, **94,** 163502, (2009).

[110] Marginean, I., Nemes, P., and Vertes, A., Astable regime in electrosprays, *Physical Review E*, **76,** 026320, (2007).

[111] Noymer, P. D. and Garel, M., Stability and atomization characteristics of electrodynamic jets in the cone-jet and multi-jet modes, *Journal of Aerosol Science*, **31,** 1165-1172, (2000).

[112] Speranza, A., Ghadiri, M., Newman, M., Osseo, L. S., and Ferrari, G., Electro-spraying of a highly conductive and viscous liquid, *Journal of Electrostatics*, **51-52,** 494-501, (2001).

[113] Thompson, S. P. and Prewett, P. D., The dynamics of liquid metal ion sources, *Journal of Physics D: Applied Physics*, **17,** 2305-2321, (1984).

[114] Ieta, A., Quill, D., and Doyle, T. E., Onset characteristics of aqueous electrosprays, *in* Proc. Joint ESA/IEEE-IAS/IEJ/SFE/IEA Conference, Boston, MA, (2009).

[115] Ikonomou, M. G., Blades, A. T., and Kebarle, P., Electrospray-ion spray: a comparison of mechanisms and performance, *Analytical Chemistry*, **63,** 1989-1998, (1991).

[116] Wampler, F. M., Blades, A. T., and Kebarle, P., Negative ion electrospray mass spectrometry of nucleotides: ionization from water solution with SF6 discharge suppression, *Journal of the American Society for Mass Spectrometry*, **4,** 289-295, (1993).

[117] Hines, W. W., Montgomery, D. C., Goldsman, D. M., and Borror, C. M., *Probability and Statistics in Engineering*, 4th ed., Wiley, (2003).

[118] Smith, K. L., *Private communications*, (2010).

[119] Nishida, T., Tashiro, Y., and Yamamoto, M., Physical and electrochemical properties of 1-alkyl-3-methylimidazolium tetrafluoroborate for electrolyte,

Journal of Fluorine Chemistry: Asian Fluorine Conference for Young Chemists, **120,** 135-141, (2003).

120 Fuller, J., Carlin, R. T., and Osteryoung, R. A., The room temperature ionic liquid 1-Ethyl-3-methylimidazolium tetrafluoroborate: electrochemical couples and physical properties, *Journal of The Electrochemical Society*, **144,** 3881-3886, (1997).

121 Gamero-Castaño, M., The structure of electrospray beams in vacuum, *Journal of Fluid Mechanics*, **604,** 339-368, (2008).

122 Stern, T. E., Gossling, B. S., and Fowler, R. H., Further studies in the emission of electrons from cold metals, *Proceedings of the Royal Society of London. Series A*, **124,** 699-723, (1929).

123 Barbour, J. P., Dolan, W. W., Trolan, J. K., Martin, E. E., and Dyke, W. P., Space-charge effects in field emission, *Physical Review*, **92,** 45-51, (1953).

124 Ward, J. W. and Seliger, R. L., Trajectory calculations of the extraction region of a liquid-metal ion source, *Journal of Vacuum Science and Technology*, **19,** 1082-1086, (1981).

125 Gibson, G. T. T., Mugo, S. M., and Oleschuk, R. D., Nanoelectrospray emitters: Trends and perspective, *Mass Spectrometry Reviews*, **28,** 918-936, (2009).

126 El-Faramawy, A., Siu, K. W. M., and Thomson, B. A., Efficiency of Nano-Electrospray Ionization, *Journal of the American Society for Mass Spectrometry*, **16,** 1702-1707, (2005).

127 Bhardwaj, N. and Kundu, S. C., Electrospinning: A fascinating fiber fabrication technique, *Biotechnology Advances*, **28,** 325-347.